SUSTAINABLE MATERIALIZATION OF RESIDUES FROM THERMAL PROCESSES INTO CARBON SINKS

Rafael Mattos dos SANTOS

Members of the Examination Committee:
Prof. Y. Willems, KU Leuven, *chairman*
Prof. T. Van Gerven, KU Leuven, *promotor*
Prof. J. Elsen, KU Leuven, *co-promotor*
Prof. R. Swennen, KU Leuven, *co-promotor*
Prof. B. Blanpain, KU Leuven
Prof. K. Van Balen, KU Leuven
Prof. F. Larachi, Laval University
Prof. R. Baciocchi, University of Rome Tor Vergata

Dissertation presented in partial fulfilment of the requirements for the degree of Doctor in Engineering

December 2013

Uitgegeven in eigen beheer, Rafael Mattos dos Santos, Willem de Croylaan 46, 3001 Leuven, Belgium

ISBN 978-94-6018-751-3
D/2013/7515/136

Foreword

I decided to pursue my doctoral degree in Belgium to diversify my academic, professional and personal experiences. I endorse diversity, and diversity in experiences is a career development strategy that I have adopted since graduation from my Bachelor's program. I can happily report that during my doctoral studies I acquired a myriad of new knowledge, skills and acquaintances, so I am truly pleased with my decision to come to Leuven. I also plan to carry with pride the doctoral degree I shall earn at the KU Leuven, undoubtedly a world class research intensive university with an enviable history and a bright future.

One of the things that attracted me to join the KU Leuven was the opportunity to be one of four doctoral students under the Knowledge Platform on Sustainable Materialization of Residues from Thermal Processes into Products (SMaRT-Pro^2), led by my promotor Prof. Tom Van Gerven. I figured that the collaborative nature of the consortium, integrating several academic departments, industrial partners, and governmental institutions, would have the potential to stimulate plentiful ideas and exciting developments. SMaRT-Pro^2 was instrumental in providing me the tools and resources to carry out my doctoral research. I had the opportunity to work in, and with colleagues of, several departments of the KU Leuven Association. I would like to hereby thank all of those who helped complete my research projects.

At the Department of Chemical Engineering (CIT) I must foremost thank my promoter, Prof. Tom Van Gerven, for giving me the support, advice, freedom and encouragement to pursue my research. I am honoured to have gained Tom's trust to become his first doctoral student, and I hope to have achieved what he expected of me. I am also very thankful to all the Master's students that I had the pleasure of supervising, Ellen Vandevelde, Davy François, Pieter Ceulemans, Da Ling, Jens Van Bouwel, Wouter Verbeeck and Aldo Van Audenaerde, and to the visiting researchers from the University of Galati that I assisted, Marius Bodor, Paul Dragomir, Andreea Vraciu and Geanina Cristea. It was because of them that I could successfully carry out much of the research that I present in this thesis or that are still in the works. Also from CIT, I give special thanks to those who helped with ICP-MS measurements, among other things, Michèle Vanroelen, Bram Verbinnen and Solvita Ore, and to those who helped me in many other ways, Herman Tollet, Christine Wouters, Marc Van Overloop and Alena Vaes. Cheers to all my other friendly colleagues from ProcESS, past and present, who made my stay at the department very enjoyable.

I also spent a great deal of time at the Department of Earth and Environmental Sciences, in large part because of the array of analytical equipment I had access to, courtesy of my two co-promotors, Prof. Jan Elsen and Prof. Rudy Swennen, whom I very much thank, but also in part to the friendliness of the people there and the excellent facilities. Likewise, I thank Dr. Gilles Mertens, now at Qmineral, who greatly contributed to my rapid education on X-ray diffraction, Rietveld refinement and mineralogical analysis in general, techniques that I had not been exposed to previously and which became crucial for the majority of my work. I also appreciate the technical assistance from Dirk Stenno and Rieko Adriaens.

Next, I had the pleasure of working closely with many members of the Department of Metallurgy and Materials Engineering (MTM), most notable being Prof. Bart Blanpain, Dr. Yiannis

Pontikes, Dr. Remus Iacobescu, Dr. Muxing Guo, Dr. Lubica Kriskova and Dr. Tom Jones. Several members of the technical staff were also very helpful, including Pieter L'hoëst, Rudy de Vos, Joris Van Dyck and Marc Nolmans, who provided me assistance with first-class analytical and experimental facilities at MTM.

I had many fruitful discussions with colleagues at the Department of Civil Engineering, who also share an interest in accelerated carbonation; these were Prof. Koen Van Balen, Dr. Özlem Cizer, and fellow SMaRT-Pro^2 doctoral researcher Muhammad Salman. Another, now former, SMaRT-Pro^2 doctoral researcher I had the pleasure of working with was Dr. Maarten Dubois, who, hailing from the Faculty of Economics and Business, taught engineers like me about the financial and legislative side of waste valorization. He also showed me that growing a family does not need to get in the way of getting work done.

At the Faculty of Bioscience Engineering I thank Prof. Boudewijn Meesschaert and Prof. Johan Martens for collaborations on several projects. Prof. Meesschaert, also working out of the KHBO in Oostende, was gracious in welcoming me to his laboratories. I send kind wishes to colleagues at the KHBO, in particular Annick Monballiu and Karel Ghyselbrecht. To all other SMaRT-Pro^2 and SIM^2 academic and sounding board members who are not mentioned here for brevity, I thank you for the ideas we exchanged, the lessons you taught me, and for taking the time to attend our meetings.

Outside the KU Leuven I also received invaluable help to complete my work. I had a great time at Laval University in Canada, where Prof. Faiçal Larachi, Prof. Georges Beaudoin and Amin Sarvaramini welcomed me warmly and helped me complete my hot-carbonation work in a timely manner by providing me exclusive access to their state-of-the-art equipment. More recently, I visited the Pacific Northwest National Laboratories in the United States, where Todd Schaef and Quin Miller helped me perform in-situ X-ray diffraction studies, which adds tremendous value and uniqueness to my research.

I received funding from various sources to undertake my doctoral studies, attend conferences and have short research stays abroad, for which I am very thankful. These funding agencies are the KU Leuven's Industrial Research Fund (IOF), the Natural Sciences and Engineering Research Council of Canada (NSERC), the Research Foundation Flanders (FWO), and The Metallurgy and Materials Society (MetSoc) of the Canadian Institute of Mining, Metallurgy and Petroleum (CIM).

I also must thank those who had an indirect effect on my work. Prof. Masahiro Kawaji and Prof. Ramin Farnood, from the University of Toronto, who have continued to mentor me and provide valuable guidance and advice on my career development. My family and my fiancée's family, who have continued to encourage us to pursue our interests, even if that takes us far away from them.

Most of all, I am very thankful to my fiancée Yi Wai Chiang (PhD), affectionately Emily, who agreed to come to Belgium with me and make up the last piece of the SMaRT-Pro^2 puzzle. Just as she dedicated to me in her thesis, I can also say that "my life would be incomplete without you".

Abstract

Sustainable utilization of solid residues and carbon dioxide, the two most important waste products from thermal processes, is an urgent issue for the industries involved and society as a whole, considering the financial and environmental repercussions of their generation and disposal. An attractive option for CO_2 sequestration is by its trapping as geochemically stable solid mineral carbonates, a process known as mineral carbonation, mineral sequestration or CO_2 mineralization. Mineral carbonation is the reaction of carbon dioxide with alkaline minerals such as calcium and magnesium oxides, hydroxides or silicates. Accelerated carbonation of alkaline minerals mimics the natural alteration of calcium- and magnesium-rich rocks as they react with atmospheric CO_2 over geological timescales, but at rates that can potentially match the emissions of CO_2 from industrial sources.

Besides using natural minerals, accelerated carbonation can also be applied to thermal residues due to their inherent alkalinity. These materials offer a number of advantages compared to natural minerals: they are generated in industrial areas near large CO_2 point sources, they have low to negative market price, and they possess higher reactivity due to their inherent (geo)chemical instability and, in the case of powdery products, large specific surface area. Additionally, on top of capturing CO_2 (i.e. using the waste materials as carbon sinks) other benefits such as stabilization of leaching, basicity and structural integrity can enable further valorisation of the waste materials, either via reduced waste treatment or landfilling costs, or via the production of marketable products. The main objective of this research project was the development of carbon sinks based on the process of mineral carbonation that provides a responsible and economical outlet for these waste products.

A number of economical, political and ideological factors have delayed the large-scale implementation of mineral carbonation of industrial wastes. Several process challenges also limit the successful translation of laboratory processes to industrial applications. To achieve carbonation in an economical and net-positive sequestration manner, intensified processing routes are required. In this research, the principles of process intensification were applied to pursue this goal. On-site mineral carbonation of industrial wastes also presents opportunities for process integration that can contribute to the reduction of energy demand, processing costs and complexity; these opportunities were also herein considered.

The aim of this research was to identify the material properties and processing conditions that control the carbonation reaction rate, the sequestration capacity and the conversion efficiency, and to optimize them. Several mineral carbonation strategies were studied, including liquid-film carbonation, slurry carbonation, sonochemical carbonation, and hot-stage carbonation. For each route, processing conditions were adjusted for optimization purposes. Knowledge obtained on the effect of processing conditions was used to elucidate implementation strategies. Knowledge on the mineralogical, geochemical, and morphological properties of the fresh residues, of synthetically prepared pure minerals, and of the carbonated products, was used to understand the carbonation mechanisms and to identify potential materials applications.

A class of alkaline waste materials that has good potential to act as a carbon sink are steel slags, which were the main focus of the research presented herein. Treatment and disposal of certain types of slag can be a costly burden on steel plants. Moreover, steel production is notorious for being a major industrial contributor to CO_2 emissions. Given the high alkalinity and basicity of these slags, imparting high carbonation reactivity, the potential for valorisation owing to physical and geochemical stabilization of the waste, and the opportunities for process integration available at steelworks, an on-site mineral carbonation approach is envisaged as a possibly economically favourable solution. This research focused on three types of steel slags rich in calcium and calcium-magnesium silicates, dicalcium ferrite, free lime and periclase: Argon Oxygen Decarburization (AOD) slag, Continuous Casting (CC) slag, and Basic Oxygen Furnace (BOF) slag. Two of

these slags, AOD and CC, possessed powdery morphology, which is ideal for high carbonation yield and low processing costs. BOF slag, which is traditionally cooled into monolith-shaped, low-surface area, material, is a prime candidate for hot-stage granulation, which can impart the necessary material exposure for sufficient reactivity towards hot-stage carbonation.

An intensified approach to mineral carbonation of AOD and CC stainless steel slags was investigated, whereby sonication was used as a form of localized energy as a means to enhance mass transfer and mineral carbonation conversion. The application of ultrasound led to the abrasion of particles and to the removal of passivating layers, which helped to improve carbonation extent. Ultrasound was also combined with the addition of soluble magnesium chloride, to promote the formation of the aragonite polymorph of calcium carbonate. It was found that this novel combination allows for the production of high purity aragonite precipitates with tuned and novel crystal morphologies, at much lower temperatures than achievable with conventional processes. Magnesium chloride was also found to be an attractive additive for the purposes of carbonation intensification, since it also promotes the leaching of calcium from certain mineral phases, and possesses a self-regenerative ability. These properties were studied using several alkaline materials as a calcium source. It was found that in the case of AOD slag, the combination of magnesium chloride with sonication enhances carbonation conversion even further than with sonication alone, due to the preferential formation of acicular aragonite.

An integrated and intensified approach to mineral carbonation of BOF steel slag that takes advantage of the high temperature source of the slag was tested, wherein mineral carbonation was performed while the slag cools, but at still relatively high (optimized) temperatures, thus making use of the freely available (thermal) energy. Hot-stage processing was found to be an attractive route to the treatment of BOF slag in view of applications of the slag in building materials and civil works. The granulation processing of the slag while molten can potentially reduce the cost of generating surface area needed for carbonation. Moreover, the exposure of the freshly granulated, and still hot, slag to CO_2-containing flue gases generated in the steelworks, imparts fast reaction kinetics owing to favourable thermodynamics and enhanced solid-state diffusion. This carbonation route was found to target the free lime content of the slag; reduction in free lime can decrease the hydration-driven swelling of the slag during utilization in concrete or roadworks.

Geochemical and mineralogical mechanisms of accelerated carbonation were also investigated in greater depth, making use of the Rietveld refinement mineral quantification method applied to X-ray diffraction data. Mineralogical aspects inherent to alkaline materials can contribute to carbonation limitations; thus better understanding and predictability was achieved by studying the carbonation susceptibility of synthetically prepared constituent minerals, allowing for more detailed analysis of reaction kinetics, mineral conversions, and product properties. This enabled clarification on the relationships between carbonation conditions, mineral composition, basicity and leaching, and on the susceptibility of individual mineral phases to hydration and mineral carbonation. The influence of process parameters applied during unpressurized thin-film and pressurized slurry carbonation on the CO_2 uptake, mineral conversion, carbonate formation and geochemical properties of AOD and CC stainless steel slags were also investigated, seeking the optimal conditions that maximize the potential of these slags as carbon sinks.

The finding of this doctoral research should contribute to the advancement of accelerated mineral carbonation for the purposes of carbon capture and industrial alkaline solid waste remediation.

Samenvatting

Door de financiële en milieuhygiënische gevolgen van de productie en verwijdering van vaste afvalstoffen en koolstofdioxide, de twee belangrijkste afvalstromen van thermische processen, wordt een duurzame oplossing voor deze afvalstromen steeds belangrijker voor zowel betrokken bedrijven als de samenleving. Een interessante piste voor het vastleggen van CO_2 is minerale carbonatatie, de reactie van koolstofdioxide met alkalische mineralen zoals calcium en magnesium oxides, hydroxides of silicaten. Versnelde carbonatatie van alkalische mineralen bootst de natuurlijke verwering van calcium- en magnesiumrijke gesteenten die in contact met atmosferische CO_2 over geologische tijdsperioden plaatsvindt, maar dan met een snelheid die vergelijkbaar is met de uitstoot van CO_2 door industriële bronnen.

Naast het gebruik van natuurlijke mineralen kan versnelde carbonatatie ook toegepast worden op thermische residu's die dikwijls alkalisch van aard zijn. Deze materialen bieden een aantal voordelen in vergelijking met de natuurlijke mineralen: ze worden geproduceerd in industriële gebieden in de nabijheid van grote CO_2 puntbronnen, ze hebben een lage tot zelfs negatieve marktprijs, en ze zijn reactiever door hun inherente (geo)chemische instabiliteit en, in het geval van poedervormige materialen, grote specifieke oppervlakte. Bijkomend aan de CO_2 vastlegging kunnen andere voordelen zoals de stabilisatie van uitloging, basiciteit en structurele integriteit mogelijkheden tot valorisatie vergroten, ofwel door lagere kosten van afvalverwerking of storten, of door de productie van vermarktbare producten. De belangrijkste doelstelling van dit project was de ontwikkeling van koolstof 'sinks' gebaseerd op minerale carbonatatie als duurzame en economische oplossing voor deze afvalstoffen.

Een aantal economische, politieke en ideologische factoren hebben de grootschalige implementatie van minerale carbonatatie van afvalstoffen vertraagd. Verschillende uitdagingen in het proces beperken ook de succesvolle vertaling van labo-processen in industriële toepassingen. Om carbonatatie op een economische en netto-positieve CO_2 vastlegging uit te voeren, is een intensificatie van het proces noodzakelijk. In dit onderzoek werd daarom vertrokken van de principes van procesintensificatie. Daarnaast biedt in-situ carbonatatie ook mogelijkheden voor procesintegratie zodat de energetische en proceskosten evenals procescomplexiteit kunnen beperkt worden, en deze worden dan ook in deze studie onderzocht.

Het doel van dit onderzoek was de materiaaleigenschappen en de procescondities te onderzoeken die de snelheid van de carbonatatiereactie, de vastleggingscapaciteit en de efficientie van conversie bepalen, en ze te optimalizeren. Verschillende strategieën voor minerale carbonatatie werden bestudeerd, zoals vloeistof-film carbonatatie, suspensie carbonatatie, sonochemische carbonatatie en carbonatatie op hoge temperatuur. Voor elk van deze strategieën werden de procescondities geoptimalizeerd. Kennis over het effect van procescondities werd gebruikt om implementatiestrategieën te begrijpen. Kennis van de mineralogische , geochemische en morfologische eigenschappen van de verse residu's, de synthetisch bereide zuivere mineralen en de gecarbonateerde producten werd gebruikt om de carbonatatie-mechanismen te begrijpen en mogelijke producttoepassingen te identificeren.

Een type van alkalische afvalstoffen die zich dankbaar lenen tot minerale carbonatatie zijn de staalslakken, die dan ook in deze studie centraal staan. Het verwerken en storten van staalslakken is een kostelijke zaak voor staalbedrijven. Bovendien is de staalindustrie ook één van de grootste industriële uitstoters van koolstofdioxide. Omwille van de hoge alkaliniteit van deze slakken, met een hoge reactiviteit voor carbonatatie tot gevolg, het grote potentieel voor valorisatie van fysisch en geochemisch gestabilizeerde slakken en de mogelijkheden tot procesintegratie in staalfabrieken, wordt een in-situ minerale carbonatatie-proces onderzocht als een potentieel economisch interessante oplossing. In deze studie worden drie types van staalslakken onderzocht die rijk zijn aan calcium en calcium-magnesium silicaten, dicalcium ferrieten, vrije kalk en periclaas: Argon Oxygen Decarburization (AOD) slak, Continuous Casting (CC) slak en Basic

Oxygen Furnace (BOF) slak. Twee van deze slakken, AOD en CC, zijn poedervormig, wat hen ideaal maakt voor hoge carbonatatie opbrengst en lage proceskosten. BOF slakken koelen traditioneel af als in grote monolietvormige gesteenten met een klein specifiek oppervlak. Deze slakken zijn een goede kandidaat voor granulatie op hoge temperatuur, wat het nodige contactoppervlak oplevert voor voldoende carbonatatie bij diezelfde hoge temperatuur.

Een geïntensifieerde vorm van carbonatatie van AOD en CC roestvrij staalslakken werd onderzocht, waarbij ultrageluid gebruikt werd als gelocalizeerde energievorm om massa-overdracht en conversie in de minerale carbonatatie reactie te verhogen. Ultrageluid draagt bij aan de verkleining van partikels en de verwijdering van niet-reactieve lagen, zodat de graad van carbonatatie kan verhoogd worden. Ultrgeluid werd ook gecombineerd met de toevoeging van opgeloste magnesium chloride om de vorming van de aragoniet polymorf van calcium carbonaat te stimuleren. Deze nieuwe combinatie bleek zuivere aragoniet neerslag op te leveren met aangepaste en nieuwe kristalmorfologie, en dit bij veel lagere temperaturen dan bij conventionele processen. Magnesium chloride bleek ook een aantrekkelijke toeslagstof te zijn voor de intensificatie van de carbonatatiereactie omdat het de uitloging van calcium uit bepaalde mineralen stimuleert terwijl het zichzelf regenereert. Deze eigenschappen werden onderzocht met verschillende alkalische mineralen als calcium bron. Er werd vastgesteld dat, in het geval van AOD slakken, de combinatie van ultrageluid met de toevoeging van magnesium chloride de conversie van carbonatatie hoger is dan met enkel ultrageluid, omwille van de preferentiële vorming van naaldvormig aragoniet.

De geïntegreerde en geïntensifieerde vorm van carbonatatie van BOF slakken werd bestudeerd, waarbij minerale carbonatatie werd uitgevoerd tijdens het afkoelen van de slakken, maar toch op relatief hoge (en geoptimalizeerde) temperatuur zodat gebruik kon gemaakt worden van de beschikbare (thermische) energie. Carbonatatie op hoge temperatuur bleek een aantrekkelijke optie te zijn voor de behandeling van BOF slakken met het oog op toepassingen in bouwmaterialen. Het granuleren tijdens het afkoelen van de gesmolten slak kan mogelijk de kost beperken van het vergroten van het specifiek oppervlak van het materiaal; een eigenschap die zo belangrijk is voor minerale carbonatatie. Bovendien leidt blootstelling van vers gegranuleerde warme slak aan CO_2-houdende rookgassen van de staalfabriek tot een snelle reactie omwille van de gunstige themodynamica en verhoogde diffusie in de partikels. Deze vorm van carbonatatie verminderde de hoeveelheid vrije kalk in de slak, wat het zwellen van het materiaal door hydratatie tijdens de toepassing in beton of wegenbouw kan verminderen.

De geochemische en mineralogische mechanismen van versnelde minerale carbonatatie werden ook onderzocht door het gebruik van de Rietveld kwantificatie methode toe te passen op X-stralen diffractie resultaten. De mineralogische eigenschappen van de alkalische materialen bepalen in belangrijke mate het succes van carbonatatie. Het bestuderen van de vatbaarheid van gesynthetiseerde mineralen voor carbonatatie leidt daarom tot een beter begrip en sturing van de reactiekinetiek, conversie en producteigenschappen. Dit liet toe om de verbanden tussen procescondities, minerale compositie, basiciteit en uitloging en de vatbaarheid van individuele minerale fasen voor hydratatie en carbonatatie uit te klaren. De invloed van procesparameters tijdens atmosferische vloeistof-film carbonatatie en suspensie-carbonatatie onder druk op CO_2 vastlegging, minerale conversie, carbonaatvorming en geochemische eigenschappen van AOD en CC slakken werd ook onderzocht om zo tot de optimale condities te komen die het potentieel van deze slakken voor CO_2 captatie maximaliseert.

De resultaten van dit doctoraatsonderzoek dragen bij tot de toepassing van versnelde minerale carbonatatie met het oog op CO_2 vastlegging en hergebruik van industriële alkalische afvalstoffen.

List of abbreviations and symbols

ACEME	Accelerated Carbonation for Environmental and Materials Engineering
ACM	asbestos containing material
ACV	aggregate crushing value
ANC	acid neutralization capacity
AOD	argon oxygen decarburization
APC(r)	air pollution control (residues)
BA	bottom ashes
BET	Brunauer–Emmett–Teller
BF	blast furnace
BOF	basic oxygen furnace
BSE	backscattered electrons
C_2F	dicalcium ferrite
C_2S/C2S	dicalcium silicate
CC	continuous casting
CCS	carbon capture and storage
CEN	Comité Européen de Normalisation (European Committee for Standardization)
CFBCs	circulating fluidized bed combustors
CS	monocalcium silicate
CSH/C-S-H	calcium silicate hydrate
D.I.	deionised
DIN	Deutsches Institut für Normung (German Institute for Standardisation)
EAF	electric arc furnace
EDTA	ethylenediaminetetraacetic acid
EDX	energy dispersive x-ray spectroscopy
EN	Europäische Norm (European Standards)
FTIR	Fourier transform-infrared
ICP-MS	inductively coupled plasma mass spectroscopy
IEA	International Energy Agency
IR	infra-red
L/S	liquid-to-solid ratio
LD	laser diffraction
LM	ladle metallurgy
LOI	loss on ignition
MCR	magnesium-to-calcium ratio
MSWI	municipal solid waste incineration
N.R.	not regulated
nd	not detected
NEN	Netherlands Standardization Institute
OPC	Ordinary Portland Cement
PB	pre-breakage
PCC	precipitated calcium carbonate
PF	pulverized firing
PGM	platinum group metals
PI	process intensification
RC	relative concentration
SEM	scanning electron microscopy
SIM^2	Sustainable Inorganic Materials Management
SMaRT-Pro^2	Sustainable Materialization of Residues from Thermal Processes into Products
SS	supersaturation

TC	Technical Committee
TGA	thermogravimetric analysis/analyzer
US	ultrasound
WtE	waste-to-energy
(Q)XRD	(quantitative) X-ray diffraction
XRF	X-ray fluorescence

β	beta polymorph
γ	gamma polymorph
η	ultrasound efficiency
θ	X-ray diffraction angle (Bragg's law)
π_1	process intensification
π_2	process integration
π^2	technological leap
Φ	net power of ultrasound horn

List of publications

(Doctoral thesis context)

Articles in internationally reviewed academic journals

Santos, R.M., Bodor, M., Dragomir, P.N., Vraciu, A.G., Vlad, M., Van Gerven, T. Magnesium chloride as a leaching and aragonite-promoting self-regenerative additive for the mineral carbonation of calcium-rich materials. Minerals Engineering, DOI:10.1016/j.mineng.2013.07.020.

Santos, R.M., Mertens, G., Salman, M., Cizer, Ö., Van Gerven, T. (2013). Comparative study of ageing, heat treatment and accelerated carbonation for stabilization of municipal solid waste incineration bottom ash in view of reducing regulated heavy metal/metalloid leaching. Journal of Environmental Management, 128, 807-821.

Santos, R.M., Van Bouwel, J., Vandevelde, E., Mertens, G., Elsen, J., Van Gerven, T. (2013). Accelerated mineral carbonation of stainless steel slags for CO_2 storage and waste valorization: effect of process parameters on geochemical properties. International Journal of Greenhouse Gas Control, 17, 32-45.

Santos, R.M., François, D., Mertens, G., Elsen, J., Van Gerven, T. (2013). Ultrasound-Intensified Mineral Carbonation. Applied Thermal Engineering, 57(1-2), 154-163.

Bodor, M., **Santos, R.M.**, Chiang, Y.W., Vlad, M., Van Gerven, T. (2013). Impacts of nickel nanoparticles on mineral carbonation. The Scientific World Journal (in press).

Bodor, M., **Santos, R.M.**, Van Gerven, T., Vlad, M. (2013). Recent developments and perspectives on the treatment of industrial wastes by mineral carbonation - A review. Central European Journal of Engineering, DOI:10.2478/s13531-013-0115-8.

Bodor, M., **Santos, R.M.**, Kriskova, L., Elsen, J., Vlad, M., Van Gerven, T. (2013). Susceptibility of mineral phases of steel slags towards mineral carbonation: mineralogical, morphological and chemical assessment. European Journal of Mineralogy, DOI:10.1127/0935-1221/2013/0025-2300.

Santos, R.M., Ling, D., Sarvaramini, A., Guo, M., Elsen, J., Larachi, F., Beaudoin, G., Blanpain, B., Van Gerven, T. (2012). Stabilization of basic oxygen furnace slag by hot-stage carbonation treatment. Chemical Engineering Journal, 203, 239-250.

Santos, R.M., Ceulemans, P., Van Gerven, T. (2012). Synthesis of pure aragonite by sonochemical mineral carbonation. Chemical Engineering Research & Design, 90(6), 715-725.

Chiang, Y.W., **Santos, R.M.**, Monballiu, A., Ghyselbrecht, K., Martens, J.A., Mattos, M.L.T., Van Gerven, T., Meesschaert, B. (2012). Effects of bioleaching on the chemical, mineralogical and morphological properties of natural and waste-derived alkaline materials. Minerals Engineering, 48, 116-125.

Santos, R.M., Van Gerven, T. (2011). Process Intensification Routes for Mineral Carbonation. Greenhouse Gases: Science and Technology, 1(4), 287-293.

Papers at international scientific conferences

Santos, R.M., Bodor, M., Dragomir, P., Vraciu, A., Vlad, M., Van Gerven, T. (2013). Magnesium chloride as a leaching and aragonite-promoting additive for the mineral carbonation of calcium-rich materials. In: Proceedings of the 4th International Conference on Accelerated Carbonation for Environmental and Materials Engineering (ACEME 2013). Leuven, Belgium, 9-12 April 2013 (pp. 127-139).

Bodor, M., **Santos, R.M.**, Kriskova, L., Elsen, J., Vlad, M., Van Gerven, T. (2013). Mineralogical and morphological assessment of carbonated steel slags and synthesized minerals. In: Proceedings of the 4th International Conference on Accelerated Carbonation for Environmental and Materials Engineering (ACEME 2013). Leuven, Belgium, 9-12 April 2013 (pp. 235-244).

Chiang, Y.W., **Santos, R.M.**, Elsen, J., Meesschaert, B., Martens, J.A., Van Gerven, T. (2013). Two-way valorization of blast furnace slag into precipitated calcium carbonate and sorbent materials. In: Proceedings of the 4th International Conference on Accelerated Carbonation for Environmental and Materials Engineering (ACEME 2013). Leuven, Belgium, 9-12 April 2013 (pp. 357-367).

Bodor, M., **Santos, R.M.**, Kriskova, L., Elsen, J., Vlad, M., Van Gerven, T. (2013). Synthesis of selected mineral compounds for in-depth analysis of steel slags during carbonation. In: Proceedings of the Third International Slag Valorisation Symposium. Leuven, Belgium, 19-20 March 2013 (pp. 307-310).

Santos, R.M., Verbeeck, W., Knops, P., Rijnsburger, K., Pontikes, Y., Van Gerven, T. (2012). Integrated mineral carbonation reactor technology for sustainable carbon dioxide sequestration: 'CO_2 Energy Reactor'. In: Energy Procedia 37, 5884-5891. 11th International Conference on Greenhouse Gas Control Technologies (GHGT-11). Kyoto, Japan, 18-22 November 2012.

Chiang, Y.W., **Santos, R.M.**, Monballiu, A., Ghyselbrecht, K., Martens, J.A., Mattos, M.L.T., Van Gerven, T., Meesschaert, B. (2012). Assessment of Bacterial and Fungal Mediated Bioleaching of Alkaline Materials towards Alteration and Solubilisation of Mineral Phases. In: Proceedings of the 6th International Symposium on Biohydrometallurgy (Biohydromet '12). Falmouth, Cornwall, UK, 18-20 June 2012 (pp. 1-21).

Santos, R.M., Ling, D., Guo, M., Blanpain, B., Van Gerven, T. (2011). Valorisation of thermal residues by intensified mineral carbonation. In: Waste Processing and Recycling in Minerals Industries VI. Conference of Metallurgists (COM 2011). Montreal, Canada, 2-5 October 2011 (pp. 185-196).

Santos, R.M., Ceulemans, P., François, D., Van Gerven, T. (2011). Ultrasound-enhanced mineral carbonation. In: Proceedings of the 3rd European Process Intensification Conference (EPIC2011). Manchester, UK, 20-23 June 2011 (pp. 108-116).

Santos, R.M., François, D., Vandevelde, E., Mertens, G., Elsen, J., Van Gerven, T. (2010). Process intensification routes for mineral carbonation. In: Proceedings of the Third International Conference on Accelerated Carbonation for Environmental and Materials Engineering (ACEME10). Turku, Finland, 29 November - 1 December 2010 (pp. 13-22).

Van Gerven, T., **Santos, R.M.**, Cizer, Ö., Mertens, G., Van Balen, K., Elsen, J., Van Acker, K., Jones, P. (2010). Carbon sink as one of the research themes of SMaRT-Pro². In: Proceeding of the Third International Conference on Accelerated Carbonation for Environmental and Materials Engineering (ACEME10). Turku, Finland, 29 November - 1 December 2010 (pp. 267-274).

Santos, R.M., François, D., Vandevelde, E., Mertens, G., Elsen, J., Van Gerven, T. (2010). Intensification routes for mineral carbonation. In: Proceedings of the 19th International Congress of Chemical and Process Engineering (CHISA 2010). Prague, Czech Republic, 28 August - 01 September 2010 (n. 0339).

Table of Contents

1. Introduction, scope and outline

1.1. INTRODUCTION

This doctoral research project is part of the Knowledge Platform on Sustainable Materialization of Residues from Thermal Processes into Products (SMaRT-Pro^2) of the KU Leuven. The Platform aims at valorising thermal process wastes into high-value products by intensified processes and with clear prospects on the economic and legislative feasibility, ecological benefits and societal relevance. Four doctoral projects are simultaneously undertaken, focusing on: carbon sinks, sorbents, construction materials, and economic instruments. Each doctoral project is executed from a different university department. Presented here is the carbon sink research based at the Chemical Engineering department of the KU Leuven.

Sustainable utilization of solid residues and carbon dioxide, the two largest and most important waste products from thermal processes, is an urgent issue both for the industries involved and society as a whole, considering the financial and environmental repercussions of their production and disposal. Thermal processing is widely applied in metals and cement production, power generation, waste incineration, among other industries. Solid waste residues from these processes include slags, dusts, air pollution control residues, and combustion ashes. These materials are composed primarily of oxides of silicon, calcium, magnesium, aluminium and iron, along with other components such as heavy metals, chlorides and sulphates. Several such materials are yet to find sustainable re-utilization routes, due to their inherent toxicity, and morphological and geochemical instability. As a result, landfilling is a common, but unsustainable, disposal route.

Recently, due to rising production costs, increased regulatory pressures and growing awareness towards environmental issues, there has been a change in the perception of industrial residues. It has been realized that they can be regarded as potential products rather than simply as waste. The reduction of waste stockpiling can also result in the liberation of precious land area. This shift, however, still faces numerous challenges: unavailability of reliable low-cost remediation technologies, variability of material quality, lack of legislation, underdeveloped markets for the resulting products, and poor societal experience with closing material cycles.

Thermal processes also generate a vast amount of carbon dioxide (CO_2), which is invariably emitted to the atmosphere. Out of the estimated 40 billion tonnes (Gt) of CO_2 currently emitted per year, approximately 9 Gt originate from power generation and 11 Gt originate from other industrial activities, including steelmaking (~2.3 Gt), cement production (~2 Gt) and petrochemical

processing (~1.3 Gt).[I] Concern regarding the role of carbon dioxide as a greenhouse gas in climate change is evolving rapidly. Anthropogenic emissions of CO_2 can now be confidently linked, at least in significant part, to the rise in atmospheric levels of carbon dioxide since the start of the industrial revolution, from 280 to 390 ppm and climbing.[II] Recent studies show that co-emitted air pollutants have a strong impact on air quality and human health (mainly local and immediate), but also that climate change has an additional global and long-term impact that must be accounted for. West et al.[III] estimate that mitigation of greenhouse gases can avoid as many as 3 million annual premature deaths by 2100, and that the benefit of avoided emissions can be valued at US$50–380 per tonne of CO_2, which exceeds estimated marginal abatement costs. It is evident that CO_2 emissions will become ever more regulated and taxed in the future. In this regard, it will be of financial benefit to industry to reduce its net CO_2 emissions.

Among the more deployable options for CO_2 mitigation are an array of technologies that fall under the umbrella of Carbon Capture and Storage (CCS), which relies on capturing CO_2 from concentrated industrial sources and transporting it to a storage site for geological (underground) sequestration in depleted oil and gas reservoirs and in saline aquifers. The International Energy Agency's (IEA) CCS Technology Roadmap suggests that by the year 2030, 2 Gt,CO_2/yr should be stored by CCS, and that number may rise to 7 Gt,CO_2/yr by 2050.[IV] While plenty of capacity may exists for this type of storage, there are important concerns over leakage risks and long-term stewardship of the stored CO_2. A more attractive option from the point of view of permanent CO_2 sequestration is by its trapping as geochemically stable solid mineral carbonates, a process known as mineral carbonation, mineral sequestration or CO_2 mineralization. Mineral carbonation is the reaction of carbon dioxide with alkaline minerals such as calcium and magnesium oxides, hydroxides or silicates. Carbonation of alkaline minerals mimics the natural alteration of calcium- and magnesium-rich rocks as they react with atmospheric CO_2 over geological timescales. Typical natural materials that may be used for carbon sequestration include olivine, serpentine, basalt and wollastonite. It is estimated that the natural reserves of calcium and magnesium silicates near the Earth's surface is enough to sequester the amount of CO_2 that can be produced from all recoverable

[I] Kuramochi, T., Ramírez, A., Turkenburg, W., Faaij, A. (2012). Comparative assessment of CO_2 capture technologies for carbon-intensive industrial processes, Progress in Energy and Combustion Science 38, 87-112.

[II] National Oceanic and Atmospheric Administration (NOAA) Earth Systems Research Laboratory (ESRL), Trends in Atmospheric Carbon Dioxide [Online], Available at: http://www.esrl.noaa.gov/gmd/ccgg/trends/history.html [accessed August 7, 2013].

[III] West, J.J., Smith, S.J., Silva, R.A., Naik, V., Zhang, Y., Adelman, Z., Fry, M.M., Anenberg, S., Horowitz, L.W., Lamarque, J.-F. (2013). Co-benefits of mitigating global greenhouse gas emissions for future air quality and human health, Nature Climate Change 3, 885-889.

[IV] International Energy Agency (IEA), Technology Roadmap: Carbon Capture and Storage [Online], Available at: http://www.iea.org/publications/freepublications/publication/TechnologyRoadmapCarbonCaptureandStorage.pdf [accessed October 12, 2013].

fossil fuel reserves.[V] The reaction is also important in industry for the production of solid particles used in, for example, paper, polymer, and paint manufacturing.

Besides using natural minerals, accelerated carbonation can also be applied to a variety of industrial waste materials, including the aforementioned thermal residues, due to their inherent alkalinity. These materials offer a number of advantages compared to natural minerals: they are generated in industrial areas near large CO_2 point sources, they have low to negative market price, and they possess higher reactivity due to their inherent (geo)chemical instability and large specific surface area (in the case of powdery products). Additionally, on top of capturing CO_2 (i.e. using the waste materials as carbon sinks) other benefits such as stabilization of leaching, basicity and structural integrity can enable further valorisation of the waste materials, either via reduced waste treatment or landfilling costs, or via the production of marketable products. On-site mineral carbonation of industrial wastes also presents opportunities for process integration (such as heat utilization or recovery) that can contribute to the reduction of processing cost and energy demand. The main objective of this research project is the development of carbon sinks based on the process of mineral carbonation that provides a responsible and economical outlet for these waste products.

A critical mass of research on the carbonation of waste materials has formed in recent years by the work of several doctoral graduates, the most notable of which include T. Van Gerven (KU Leuven, 2005), W.J.J. Huijgen (Delft University of Technology, 2007), S. Monkman (McGill University, 2008), C.H. Rawlins (Missouri University of Science and Technology, 2008), S. Teir (Helsinki University of Technology, 2008), M. Uibu (Tallinn University of Technology, 2008), G. Costa (University of Rome "Tor Vergata", 2009), S. Eloneva (Aalto University, 2010), P.J. Gunning (University of Greenwich, 2011), O. Velts (Tallinn University of Technology, 2011) and D. Zingaretti (University of Rome "Tor Vergata", 2013). Yet, despite this knowledge pool, many factors continue to delay the large-scale implementation of mineral carbonation of industrial wastes. These include:

- high processing costs of methods applying complex production chains that require, for example, intense milling, heat treatment or additive regeneration/replacement;
- process-material adaptability: the composition and physical properties of waste materials varies greatly, even within the alkaline class, which means that many carbonation approaches are residue-specific, making direct adaptation to another residue difficult;
- uncertainties regarding quality and marketability of valorisable products;
- the lack of legislative mandates or market incentives in place for carbon capture and waste valorisation (e.g. the presently low market levels of CO_2 credits);
- competition with geological sequestration for attention and financing; and

[V] Lackner, K.S. (2003). A Guide to CO_2 Sequestration, Science 300(5626), 1677-1678.

- the limited CO_2 sequestration capacity of solid waste materials, due to small tonnage produced relative to global CO_2 emission volumes (e.g. approx. 0.5 Gt/y of slags are produced from iron and steel making,[VI] while its CO_2 emissions amount to approx. 2.3 Gt/y[I]).

A number of process challenges also limit the successful translation of laboratory processes to industrial scale applications. At the particle level, the three rate limiting steps are:

(i) leaching of cations;

(ii) solvation and hydration of CO_2; and

(iii) diffusion to reaction zone (carbonated shell / depleted matrix).

At the reactor level, three more limiting barriers are identified:

(a) slow kinetics/low conversions;

(b) high energy cost (milling/mixing); and

(c) large mass of solid materials for handling.

To accelerate the mineral carbonation reaction to meaningful levels, to match the rate of emissions of CO_2 from industrial sources, and to achieve carbonation in an economical and net-positive sequestration manner, intensified processing routes are required. Within the context of this doctoral research project, illustrated in Figure 1.1, it is possible to identify areas that have not yet been extensively studied, and that may provide the technological leap required to make mineral carbonation of thermal residues sustainable. One such area is exploiting the high temperature source of thermal residues. It may be possible to use the intrinsic heat/exergy content to drive the carbonation reaction, potentially contributing to high reaction rates while at the same time minimizing energy input requirements. Another area that deserves attention is the use of accelerating technologies during mineral carbonation processes, especially to overcome the formation of rate-reducing passivating layers. There may also be possibilities to improve properties of the thermal residues prior to carbonation, such as adjusting its composition to produce materials more prone to mineral carbonation (i.e. with more suitable mineralogy and morphology). In order to tackle this route, it is essential to better understand how mineralogical and morphological properties of thermal residues impact their reactivity towards mineral carbonation, and how they respond to different carbonation processes (seeing as not every process is suitable for every residue). Lastly, it is essential to think of mineral carbonation not only as a process to produce carbon sinks, but also as a way to valorise waste materials and turn them into valuable products. Consequently, two approaches should be looked at: reverse engineering, whereby processing conditions are tuned to

[VI] Van Oss, H.G. (2013). Slag—Iron and Steel [Advance Release], 2011 Minerals Yearbook, U.S. Geological Survey.

meet existing materials requirements (e.g. low and basicity leaching, good physical stability, desired particle size, etc.), or identifying new opportunities to utilize the produced carbonated materials for which specific product requirements have yet to be prescribed.

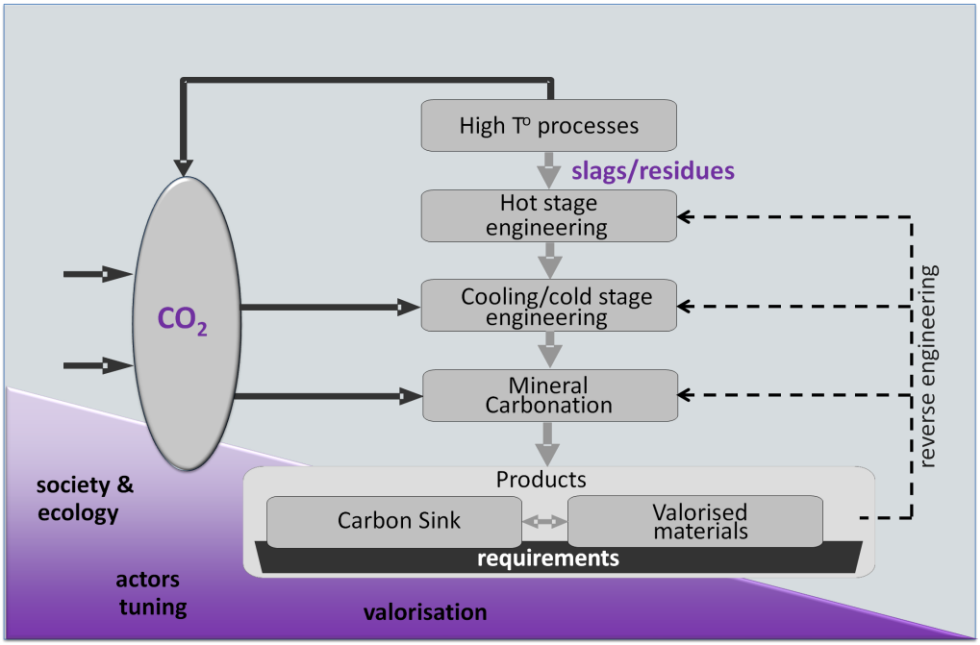

Figure 1.1. Doctoral project context.

1.2. SCOPE

The aim of this research is to identify the material properties and processing conditions that control the reaction rate, the sequestration capacity and the conversion efficiency, and to optimize them. The framework of the activities undertaken in this doctoral project is illustrated in Figure 1.2.

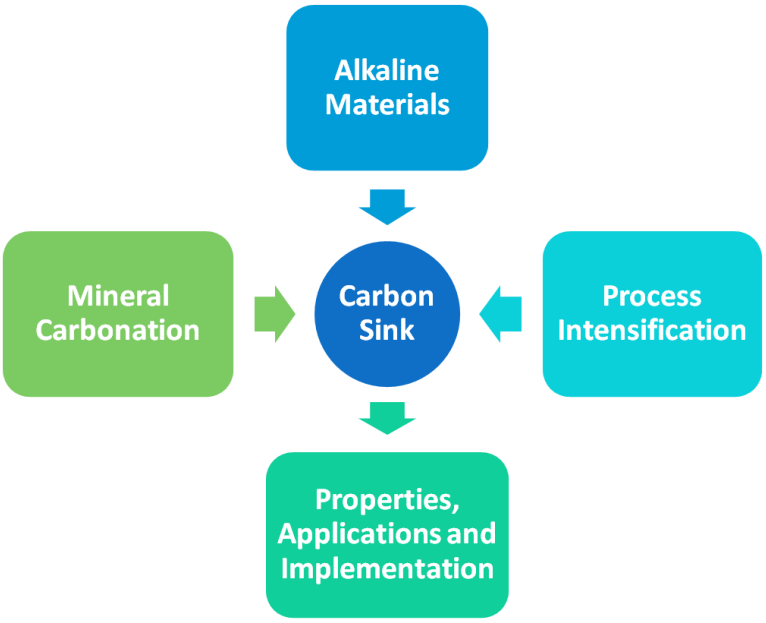

Figure 1.2. Doctoral project framework.

Several mineral carbonation strategies are studied, including liquid-film carbonation, slurry carbonation, sonochemical carbonation, and hot-stage carbonation. These different strategies are studied in order to identify which mineral carbonation process is most suitable for each material of interest. For each route, processing conditions that are adjusted for optimization purposes include: duration, temperature, pressure, CO_2 concentration, pH, liquid-to-solid ratio, leaching agents, buffering agents, particle size, and agitation. The resulting parameters monitored are: carbonation conversion (as a function of process conditions, and the limiting value), reaction kinetics, polymorph formation (e.g. calcite, aragonite and vaterite), product stability (leaching behaviour, carbon retention, and volume stability), by-product formation (minerals other than carbonates formed from solubilised elements or mineral alteration), the effect of process intensification techniques over conventional processes, and the properties of the carbonated products (looking at possible commercial applications). Knowledge obtained on the effect of processing conditions is used to elucidate implementation strategies. Knowledge on the mineralogical, geochemical, and morphological properties of the fresh residues, of synthetically prepared pure minerals, and of the carbonated products, is used to understand the carbonation mechanisms and to identify potential materials applications.

With regards to implementation and commercialization, given this doctoral work is part of the SMaRT-Pro^2 platform, market needs and opportunities as discussed with industrial partners of the platform played a role in defining possible product properties to be achieved, and hence guided to a certain extent the carbonation processes studied. Nevertheless, the main focus of the doctoral work was to produce fundamental knowledge on mineral carbonation to fill the gaps and extend the

knowledge acquired from prior literature. These included the carbonation of waste materials and synthetic minerals (that make up the waste materials) not previously studied in detail, the use of process intensification technologies not yet proven economical, the use of specialized characterization techniques, and the identification of unconventional processing and process integration opportunities (e.g. hot/cooling-stage carbonation).

A class of alkaline waste materials that has good potential to act as a carbon sink are steel slags. Treatment and disposal of certain types of slag, including Argon Oxygen Decarburization (AOD) slag, Continuous Casting (CC) slag and Basic Oxygen Furnace (BOF) slag, can be a costly burden on steel plants. Moreover, steel production is notorious for being a major industrial contributor to CO_2 emissions. Given the high alkalinity and basicity of these slags, imparting high carbonation reactivity, the potential for valorisation owing to physical and geochemical stabilization of the waste, and the opportunities for process integration available at steelworks, an on-site mineral carbonation approach is envisaged as a possibly favourable solution. As such, these slags were the main focus of the research herein presented.

Mineral carbonation routes can be classified into two branches: direct and indirect.[VII] Direct carbonation refers to processes where carbon dioxide (in the form of carbonic acid in aqueous medium or gas in dry medium) reacts directly with the alkaline material, resulting in a carbonated material of similar chemical composition to the original material, with the exception of the higher carbon content. Direct carbonation processes use stirred or fluidized reactors, spray-beds or CO_2 incubators. Indirect carbonation refers to processes where the alkaline component(s) (primarily Ca and Mg) are first extracted from the alkaline material, ideally using regenerative additives. Subsequently the leachate is reacted with CO_2, typically in conjunction with pH-neutralization or pH-swing. Solid/liquid separation after the extraction stage and prior to carbonation results in two solid products: a carbonated product containing mainly carbonate minerals, and a residual product containing the non-alkaline components of the original materials (e.g. silica, base and heavy metals). An advantage of the indirect strategy is the possibility to produce carbonate products of high purity (e.g. precipitated calcium carbonate (PCC)). Disadvantages include process complexity, especially the introduction of costly and troublesome leaching agents, and the generation of a secondary solid waste residue enriched in the non-alkaline and potentially hazardous components. Furthermore, pure carbonates may be applied commercially in products that may undergo thermal treatment in the future (e.g. incineration of PCC containing papers and plastics), thereby re-releasing the sequestered CO_2 and no longer being a carbon sink. In view of these factors and the

[VII] Bobicki, E.R., Liu, Q., Xu, Z., Zeng, H. (2012). Carbon capture and storage using alkaline industrial wastes, Progress in Energy and Combustion Science 38, 302-320.

slags utilized, which contain a multitude of regulated metals and metalloids, this work focussed on the direct accelerated mineral carbonation route.

1.3. OUTLINE

This thesis contains seven chapters that convey the main results of this doctoral project, preceded by a chapter that reviews the relevant literature background, and followed by a chapter that presents the main conclusions, perspectives and summarizes other related works concluded or in progress not included in full herein. Below is an outline of these chapters and descriptions of how they relate to each other. The relationships between the chapters and the timing of the work are illustrated in Figure 1.3.

Chapter 2: A review is made of the recent developments and perspectives on the treatment of industrial wastes by mineral carbonation. Gaps in knowledge identified from literature, as well as concepts found that are yet to be applied to mineral carbonation in general, or to the mineral carbonation of specific materials, were used to develop the research lines of this project.

Chapter 3: The principles of process intensification and process integration are discussed in the framework of accelerated mineral carbonation, and laboratory-scale strategies that combine these principles to potentially produce economically feasible and industrially acceptable technologies for large-scale implementation are introduced. This chapter was written shortly after the first year of this doctoral project, when several research lines were under way but not yet finalized, so it briefly introduces many of the concepts that are presented in more detail in the later chapters.

Chapter 4: An intensified approach to mineral carbonation of AOD and CC stainless steel slags is investigated, whereby sonication is used as a form of localized energy for abrasion of the particles in order to obtain new reaction surfaces, thus enhancing mass transfer and mineral carbonation conversion. The techniques developed here were later used in the work described in Chapter 6 to further enhance ultrasound-mediated carbonation.

Chapter 5: Ultrasound is combined with magnesium chloride to promote the formation of the aragonite polymorph of calcium carbonate, and it is found that this combination allows for the production of high purity aragonite precipitates with tuned and novel crystal morphologies at much lower bulk temperatures than achievable with conventional processes. The mechanism elucidated for magnesium chloride was used as a starting point to the work presented in Chapter 6.

Chapter 6: The calcium leaching ability of magnesium chloride, which acts as a self-regenerative additive, is studied in view of intensifying mineral carbonation of several alkaline materials, and it is found that in the case of AOD slag, the combination of this additive with sonication enhances carbonation conversion even further than with sonication alone due to the preferential formation of acicular aragonite. Concepts on the varying susceptibility of different mineral phases towards carbonation, developed in Chapter 8, were used in this work.

Chapter 7: An integrated and intensified approach to mineral carbonation of BOF steel slag that takes advantage of the high temperature source of the slag is tested, wherein mineral carbonation is performed while the slag is cooling, but at still relatively high (optimized) temperatures, thus making use of the more favourable kinetics and the freely available (thermal) energy. Hot-stage carbonation is another process that makes use of processing intensification principles (namely conducting carbonation at the right time) and also applies principles of process integration (namely combining granulation and carbonation), hence its relationship to Chapter 3.

Chapter 8: Mineralogical characteristics inherent to alkaline materials can contribute to carbonation limitations; thus better understanding and predictability is achieved by studying the carbonation susceptibility of synthetically prepared constituent minerals, allowing for more detailed analysis of reaction kinetics, mineral conversions, and product properties. This work was inspired by the preceding finding in Chapter 7 that not all mineral phases respond equally to carbonation (in that instance free lime was much more reactive than silicates and ferrites). The carbonation conditions used in this work were the optimal conditions found in the work of Chapter 9.

Chapter 9: The influence of process parameters applied during unpressurized thin-film and pressurized slurry carbonation on the CO_2 uptake, mineral conversion, carbonate formation and geochemical properties of AOD and CC stainless steel slags are investigated, seeking the optimal conditions that maximize the potential of these slags as carbon sinks. This work is a continuation of the work presented in Chapter 4, in this case applying process conditions that can improve carbonation extent and/or improve leaching stabilization and/or minimize energy intensity to reduce processing cost. This work also interacted with the work of Chapter 8 by supplying optimal carbonation conditions and making use of the mineral quantification procedure therein developed.

Chapter 10: The overall conclusions of the project are presented. Summaries of other related works conducted during this doctoral project, but not detailed herein, are provided. Perspectives on the future of accelerated mineral carbonation, in consideration of the possibilities for further development of intensified processes for the purposes of waste remediation and CO_2 sequestration, and on the valorisation of carbonated products, are discussed.

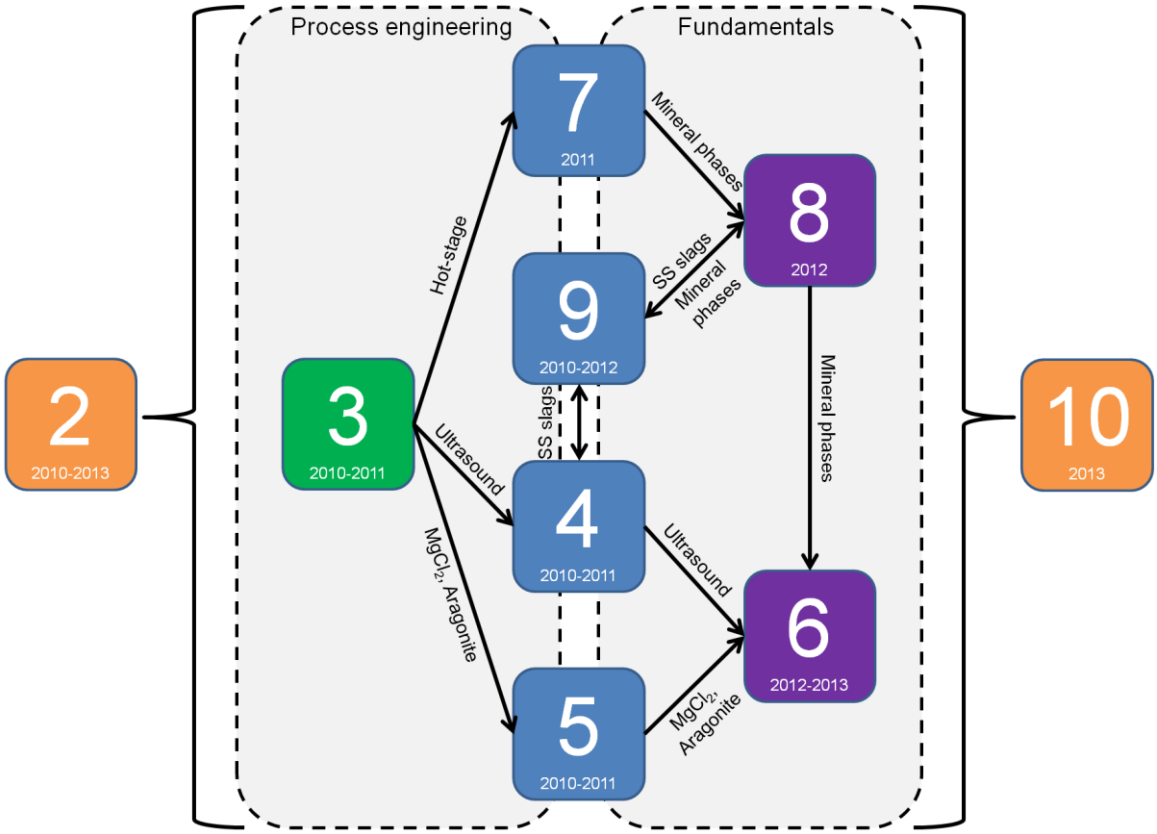

Figure 1.3. Schematic outline of thesis chapters.

2. Recent developments and perspectives on the treatment of industrial wastes by mineral carbonation – A review

ABSTRACT – Besides producing a substantial portion of anthropogenic CO_2 emissions, the industrial sector also generates significant quantities of solid residues. Mineral carbonation of alkaline wastes enables the combination of these two by-products, increasing the sustainability of industrial activities. On top of sequestering CO_2 in geochemically stable form, mineral carbonation of waste materials also brings benefits such as stabilization of leaching, basicity and structural integrity, enabling further valorization of the residues, either via reduced waste treatment or landfilling costs, or via the production of marketable products. This paper reviews the current state-of-the-art of this technology and the latest developments in this field. Focus is given to the beneficial effects of mineral carbonation when applied to metallurgical slags, incineration ashes, mining tailings, asbestos containing materials, red mud, and oil shale processing residues. Efforts to intensify the carbonation reaction rate and improve the mineral conversion via process intensification routes, such as the application of ultrasound, hot-stage processing and integrated reactor technologies, are described. Valorization opportunities closest to making the transition from laboratory research to commercial reality, particularly in the form of shaped construction materials and precipitated calcium carbonate, are highlighted. Opportunities for further intensification of mineral carbonation processes are identified and described.

Redrafted from[VIII]
M. Bodor, **R.M. Santos**, T. Van Gerven, and M. Vlad.
"Recent developments and perspectives on the treatment of industrial wastes by mineral carbonation - A review".
Central European Journal of Engineering[*], 2013, doi:10.2478/s13531-013-0115-8.
Reused with permission from Versita. License number: 3245941058319.
[*]Special Issue devoted to Chemical Engineering with focus on environmental and energy resources.

Author contributions
R.M.S. co-first authored the article.

[VIII] Parts added to this chapter, which were not included in the published article, are shown in italic font. Parts of the text that referred to the works of Santos et al. and Bodor et al. were omitted as these are presented in more detail in the subsequent chapters.

2.1. INTRODUCTION

Anthropogenic emissions of carbon dioxide (CO_2), originating mainly from the burning of fossil fuels by the transportation sector and the power generation industry, can be confidently linked, at least in significant part, to the rise in atmospheric levels of carbon dioxide since the start of the industrial revolution, from 280 to 390 ppm and climbing [1]. To avoid the potentially detrimental greenhouse gas effects of higher CO_2 levels on the climate and life on Earth, the reduction of both the emissions and the atmospheric CO_2 levels is essential. However, high availability of fossil fuels and their relatively more affordable market price in contrast with other energy sources represent some of the main reasons for which significant changes in the energetic resources domain has not yet taken place. Furthermore, it has been suggested that the continuation of carbonaceous fuels usage can be extended, beyond the timeline that otherwise would necessitate its phasing out to avoid catastrophic climate change, by the possibility to extract the CO_2 directly from atmosphere [2]. While this concept is under promising development [3-5], it is still far from large-scale implementation.

Among the more deployable options for CO_2 are an array of technologies that fall under the concept of Carbon Capture and Storage (CCS), which relies on capturing CO_2 from concentrated (typically greater than 10–20 vol%) industrial sources, wherein a purified and pressurized stream of this gas is produced, with the possibility of being easily transported to a storage site. The first method of CCS was that of geological sequestration, which came to be used on a large scale around the 1970s in the extractive industry for enhanced oil and gas recovery [6]. While plenty of capacity may exist for this type of storage [7], there are important concerns over leakage risks and long-term stewardship of the stored CO_2 [8, 9]. An alternative for CO_2 sequestration involves CO_2 injection in oceans, preferably at great depths where this gas reacts with water to form carbonic acid. However, this method lost its appeal in the last years due to uncertainties regarding environmental impact, particularly that of lowering ocean water pH and the lack of permanency of this solution [10].

A more attractive option from the point of view of permanent carbon dioxide sequestration is by its trapping as geochemically stable mineral carbonates, a process known as mineral carbonation, mineral sequestration or CO_2 mineralization, which was introduced to mainstream science by Seifritz in 1990 [11]. Carbonation of alkaline minerals mimics the natural alteration of calcium- and magnesium-rich rocks as they react with atmospheric CO_2 over geological timescales. It is estimated that the natural reserves of calcium and magnesium silicates near the Earth's surface is enough to sequester the CO_2 that can be produced from all recoverable fossil fuel reserves [7].

Besides using widely available natural minerals for carbon sequestration, mineral carbonation can also be applied to a variety of industrial waste materials. These materials are typically by-products of high temperature processes, such as slags and ashes, but can also include tailings from mineral processing operations among other suitable waste materials. These wastes are generally inorganic, alkaline, and possess a high amount of calcium (preferable for its greater reactivity) or possibly magnesium. These materials also have a number of advantages compared to natural minerals: they are generated in industrial areas near large CO_2 point sources, have low to negative market price, and have higher reactivity due to their inherent (geo)chemical instability. Additionally, on top of capturing CO_2 (i.e. using the waste materials as carbon sinks) other benefits such as stabilization of leaching, basicity and structural integrity enable further valorization of the waste materials, either via reduced waste treatment or landfilling costs, or the production of marketable products. The reduction of industrial waste stockpiling can also result in the liberation

of precious land area. A critical mass of research on these topics has formed in recent years by the work of doctoral graduates, the most notable of which include Van Gerven [12], Huijgen [13], Rawlins [14], Teir [15], Uibu [16], Costa [17], Eloneva [18], and Gunning [19], having been reported primarily in the international conferences on Accelerated Carbonation for Environmental and Materials Engineering (ACEME), held in London (2006), Rome (2008), Turku (2010) [20] and Leuven (2013) [21].

This Chapter reviews the current state-of-the-art of this technology, highlighting successful and promising routes that may eventually transition from the laboratory to the industrial scale, and identifying areas that need further research and development.

2.2. MINERAL CARBONATION APPROACHES

Mineral carbonation can be realized using one of the two main routes: direct or indirect carbonation. These methods are represented schematically in Figure 2.1:

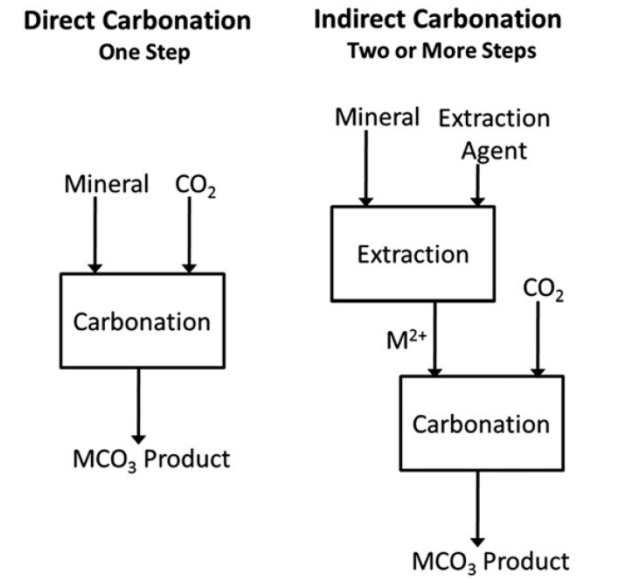

Fig. 2.1. Direct (one step) mineral carbonation (left), and indirect (two or more steps) mineral carbonation (right); M refers to either calcium or magnesium. Reprinted from Progress in Energy and Combustion Science, Vol. 38, Bobicki et al. [22], 302–320, Copyright 2011, with permission from Elsevier.

2.2.1. Direct mineral carbonation

Direct mineral carbonation is the simplest approach regarding mineral sequestration of CO_2. Its principle consists in carbonation achievement in a single reaction step, using a dry, moist or aqueous environment [10]. The resulting carbonated material consists of the precipitated carbonate and residual components of the original solid material (e.g. residual silica, iron oxides and unreacted minerals). Typically the basicity of the carbonated material is reduced in the process, becoming buffered by the pH of the carbonate phases [23]. While the technology undoubtedly works, with high degrees of carbonation being achievable in acceptable time periods, traditional processing routes (requiring energy intensive crushing/milling, mixing, pressurization, water treatment, additives use and regeneration, etc.) still prove too expensive for large-scale

implementation as a CO_2 sequestration solution (e.g. 40-80 €/t CO_2 compared with 0.4-6 €/t CO_2 for geological sequestration [24, 25]). But when applied to industrial waste materials, the valorization factor can reduce the gap between cost and benefit.

Promising results using industrial wastes were obtained by Chang et al. [26], using a slurry reactor and converter (BOF) slag with a mean particle size < 44 µm. The conversion degree was equal to 72 % at 60 °C and 1 bar (atmospheric) pressure, after 60 minutes. The same group also investigated the possibility of using residual alkaline water from industrial sources in the carbonation process, with higher CO_2 dissolution becoming possible due to the high pH of the water [27].

Another possibility for improving the carbonation process consists in applying high-power low-frequency (16–100 kHz) ultrasound. The principle lies in inducing cavitation, that is, the formation of small cavities or micro-bubbles that grow and collapse rapidly. Cavitation generates turbulence/circulation by acoustic streaming, resulting in enhanced mixing and mass transfer, including dissolution of gases such as CO_2 [28]. The collapsing micro-bubbles also produce high local temperatures, pressures and shear forces, including the formation of micro-jets. These effects cause solid surface erosion and interparticle collisions, leading to the removal of passivating layers or to the eventual breakage of particles [29].

Rao et al. [30] compared stirring versus horn ultrasonic slurry carbonation of fluidized bed combustion ashes. Conversions of CaO were reported to have increased from 23% to 62% at 15 minutes, and from 27% to 83% at 40 minutes. Particle size reduction achieved by sonication was attributed to cause the enhancement, allowing access to unreacted calcium oxide in the ash core. López-Periago et al. [31] immersed an autoclave in a sonic bath to improve the carbonation of calcium hydroxide using supercritical carbon dioxide (13 MPa). The conversion to $CaCO_3$ after 60 minutes increased from 50 wt% without agitation, to 65 wt% with mechanical stirring, and 89 wt% with sonication.

Most carbonation studies to date have aimed to achieve as high as possible CO_2 uptake, to maximize the theoretical CO_2 sequestration capacity of the materials, determined typically on the basis of the total calcium and magnesium content according to the Steinour equation [32]. Though stoichiometrically accurate, however, this prediction can be overly optimistic, causing doubts whether carbonation processes are ineffective in reaching complete conversion (due to insufficient process severity or formation of passivating layers), or if the unreacted material is inert to carbonation. Doucet [33] studied the solubility of the major silicate and ferrite minerals of BOF slag by acidification, and found that, based on the dissolved amounts of Ca and Mg in 0.5 M HNO_3, the CO_2 uptake of the slag is likely at least 25% lower than its theoretical capacity.

An alternative approach to wet carbonation is high-temperature dry carbonation, which is particularly attractive when the alkaline residues originate from high temperature (>500 °C) processes (e.g. metallurgical slags), where the required thermal energy is intrinsically contained in the system (otherwise, heating cooled products to these temperatures is not a feasible approach). High temperature carbonation is commonly applied in CO_2 capture and separation systems that utilize lime-based sorbents subject to looping carbonation/calcination cycles, which typically conduct carbonation in the flue gas temperature range of 600–700 °C at atmospheric pressure [34-36].

Prigiobbe et al. [37] tested high temperature carbonation of air pollution control residues in the temperature range of 350–500 °C, obtaining fast carbonation kinetics (50% conversion in less than 1 min) and high conversions (nearly 80%). Mikhail and Turcotte [38] were the first investigators to report carbonation of BOF slag at high temperature; while limited, their findings provided proof-of-

concept for this approach. BOF slag was carbonated at 550 °C in moist CO_2 in a thermogravimetric analyzer (TGA), and 8% mass gain was attributed to $CaCO_3$ formation. Yu and Wang [39] found BOF slag to carbonate well (up to 20% calcium utilization after 20 minutes reaction time) at temperatures between 500 and 550 °C, using CO_2 concentrations between 10-100%; however data and analyses were insufficient to provide clear insight on mineralogical effects or carbonation mechanisms and kinetics.

2.2.2. Indirect mineral carbonation

The mineral sequestration process divided into several stages is classified as indirect mineral sequestration. By this method, the reacting alkaline element (Ca, Mg, or both) is first extracted from the feedstock, and in a separate stage will react with CO_2 to form carbonates, according to Eq. (2.1) and (2.2), where wollastonite ($CaSiO_3$) and acetic acid (CH_3COOH) are used as example [15]:

dissolution: $CaSiO_3 + 2CH_3COOH \rightarrow Ca^{2+} + 2CH_3COO^{-} + H_2O + SiO_2$ (2.1)

precipitation: $Ca^{2+} + 2CH_3COO^{-} + CO_2 + H_2O \rightarrow CaCO_3 + 2CH_3COOH$ (2.2)

When the product formed is calcium carbonate, it is commonly referred to as precipitated calcium carbonate (PCC), a product that has diverse industrial applications, such as in papermaking, polymers, paint and fertilizer. An attractive feature of indirect mineral carbonation, besides the production of relatively pure carbonate products with potentially high market value, is that a major limitation of direct carbonation for achieving high conversion rates and CO_2 uptake, namely the mobility of the alkaline elements from the solids, can be more easily overcome by the use of strong acids, and also by the inherent elimination of the carbonate passivating layer that blocks access to the unreacted particle core.

As such, much research on identifying and testing suitable leaching agents, which ideally should have high extraction efficiency, but at the same time should have less affinity for the alkaline-earth elements than the carbonate ion (CO_3^{2-}) to allow for the precipitation of carbonates in the second-stage carbonation step. For instance, Bonfils et al. [40] used disodium oxalate ($Na_2(C_2O_4)$) for the extraction of magnesium from serpentine, but found that carbonation of the leachate resulted in the precipitation of magnesium oxalate dihydrate ($Mg(C_2O_4)\cdot 2H_2O$), an organic acid salt, instead of the desired magnesium carbonate.

Acetic acid (CH_3COOH) has been successfully applied for the production of PCC from steel slag [41], but after extraction it is necessary to add sodium hydroxide to neutralize the acid and promote carbonate precipitation; the formed sodium acetate can potentially be regenerated into acetic acid, but at a large processing cost. To avoid regeneration, Eloneva et al. [42] also tested the efficacy of ammonium salts (NH_4Cl, CH_3COONH_4, NH_4NO_3) and found positive results with steel converter slag, but the efficiency was poorer for blast furnace and ladle slags; this was attributed to calcium being predominantly bound as silicates in these materials (as opposed to free lime (CaO) in converter slag). The loss of ammonia (NH_3) in the off-gas also becomes an added concern when using these additives [43].

This is by no means an exhaustive review of recent works on indirect carbonation, but a general trend observed from this field of study is that, while a valuable product can be produced from waste materials, other troublesome products are also formed, including destabilized heavy-

metal containing residual solids, and salt and heavy metal laden wastewater. As such, the objective of waste treatment is not always fully realized.

2.3. TREATMENT OF INDUSTRIAL ALKALINE WASTES BY MINERAL CARBONATION

There are numerous sources of industrial wastes that can be used in the mineral carbonation processes, with varying chemical, mineralogical and morphological properties, and available in small to large quantities and in limited to wide geographical distribution. Significant amount of technological progress is still needed until widespread adoption of mineral carbonation on an industrial scale, but the body of research has already reached a level that guarantees sustained development for years to come. At this moment, the scientific literature contains an assortment of satisfactory, though preliminary, results, the most recent and relevant of which are reviewed in this section, organized by class of waste material: metallurgical slags, incineration ashes, mining tailings, asbestos containing materials, red mud, and oil shale processing residues.

2.3.1. Metallurgical slags

Steel slags, by-products of steel production processes, are a widely available class of industrial waste materials that can potentially benefit from mineral carbonation through the reduction in basicity (pH), swelling stabilization, and reduction of heavy metals leaching [23, 44]. Currently, the treatment and disposal of these slags presents a costly burden on steel plants. Moreover, their high CO_2 uptake capacities, coupled to the large on-site CO_2 emissions of steelworks, offers opportunities for carbon capture credit gains.

2.3.1.1. Carbon steel slags

Integrated carbon steel production consists of ironmaking in the Blast Furnace (BF), steelmaking in the Basic Oxygen Furnace (BOF), and continuous casting of steel billets, slabs and blooms. For over a century, with iron and steel industry booming worldwide, a vast amount of slag has been produced as an inevitable by-product of the steelmaking process. While valuable applications have been found for BF slag, mostly in the construction sector such as in cement manufacturing and as a cement replacement in concrete, much of BOF slag production, estimated at 60–120 kg/t steel presently, still ends up in landfill sites [45, 46]. The traditional use of BOF slag in road construction, as an aggregate, base or sub-base coarse, has been restricted due to the slag's undesirable expansive nature, resulting in rapid deterioration of the roads [47]. The volume expansion (up to 10% [48]) is attributed to the short term hydration and the long term carbonation of free lime (CaO) and magnesium oxide (MgO) content [38], present in significant amounts due to the high (CaO+MgO):SiO_2 ratio of the slag (Table 2.1).

Table 2.1. Example of BOF slag chemical composition, expressed as oxides [49].

Oxide	Amount (wt%)
CaO	47.7
Fe_2O_3	24.4
SiO_2	13.3
MgO	6.4
Al_2O_3	3.0
MnO	2.6
P_2O_5	1.5
TiO_2	0.7

Compared to present BOF slag treatment processes, applied in limited extent due to high processing costs and variable performance, the reaction of the alkaline oxides with CO_2, leading to the formation of geochemically stable carbonates (e.g. $CaCO_3$), is a potentially sustainable route. Besides capture of CO_2, desirable for emissions reduction, mineral carbonation also yields positive effects in terms of the leaching behavior of alkaline earth metals, heavy metals and metalloids from steel slag [44], which can lead to further valorization of the waste material. Numerous studies in recent years have assessed the potential of steel slag carbonation for storage of CO_2 utilizing a variety of direct carbonation routes, including slurry carbonation [26, 27, 50, 51], wet carbonation [52], block carbonation [53], and hot-stage carbonation [38, 39].

Huijgen et al. [50] systematically studied the effect of process variables including particle size, temperature, CO_2 partial pressure, and reaction time on the slurry carbonation extent of milled BOF slag in a stirred batch autoclave reactor. The optimal condition was found to be 30 minutes at 19 bar CO_2, 100 °C, and a particle size of < 38 μm, with which 74 % Ca-conversion was achieved. The most influential process parameters were found to be particle size (varied from < 2 mm to < 38 μm) and reaction temperature (varied from 25 to 225 °C).

Van Zomeren et al. [52] investigated accelerated BOF slag carbonation at relatively low CO_2 pressure (0.2 bar), in view of improving the environmental properties of slag (pH and leaching). Gas-solid experiments were performed in laboratory columns under water-saturated and unsaturated conditions (i.e. moist and dry gas), and temperatures between 5 and 90 °C. The major changes in the amount of sequestered CO_2 and the resulting pH reduction (~1.5 units) occurred within 24 hours, and were proportional to the free lime content of the slag, suggesting little reactivity of other mineral phases at these conditions. Also, carbonation at these conditions was found to occur predominantly at the surface of the slag grains (sieved to 2–3.3 mm in size). However, the pH reduction after carbonation led to increased vanadium leaching.

2.3.1.2. Stainless steel slags

To date, most research on single-step aqueous carbonation of steel slags have focused on Basic Oxygen Furnace (BOF) slag, and on Electric Arc Furnace (EAF) slag, originating from the first step of the stainless steel production and with results recently reported by Baciocchi et al. [23, 54]. However, a main disadvantage to the carbonation of these residues is the milling requirement to generate sufficient reactive surface area, as these slags solidify upon cooling in the form of monoliths. Two additional slags produced from the stainless steel process possess powdery morphology and can benefit in a more energy efficient manner from mineral carbonation: Argon

Oxygen Decarburization (AOD) slag, and Continuous Casting (CC) slag, also referred to as Ladle Metallurgy (LM) slag. Typical chemical composition of AOD slag is presented in Table 2.2.

Table 2.2. Typical chemical composition of AOD slag, expressed as oxides [55].

Oxide	Amount (wt%)
CaO	46-54
SiO_2	26-31
Al_2O_3	2-10
MgO	4-7
MnO	1-2
Fe	1-2
Cr	2-4

AOD slag exhibits a peculiar disintegration upon cooling due to the phase transformation of β-dicalcium silicate to the more stable, but less dense, γ-dicalcium silicate, causing detrimental expansion forces in the material [56]. The slag turns into a fine powder that causes severe dust issues during handling and storage in the steelworks; furthermore, the slag in this form cannot be readily re-utilized or valorized, and often must be landfilled [57]. Concerns regarding drainage from steel slag disposal sites, which can be extremely alkaline and a source of pollution to surface and ground waters [58], add to the disposal costs. Treatment strategies including the addition of stabilizing ions (e.g. boron), silica and rapid cooling, which aim at preventing the disintegration of the slags by hindering the expansive β- to γ- transformation of dicalcium silicate (C_2S), have been tested and, in some cases, implemented in industry [59]. However, costly and energy intensive processes, hazardous additives that introduces environmental concerns regarding leaching, and low-value final products still force the industry to search for more sustainable solutions. Furthermore, this methodology is not applied to CC slag due to process complexities, and the slag is disposed of in powdery form by landfilling. For mineral carbonation processes however, this behavior represents an advantage, as the reactive surface area is maximized; as such, some researchers have taken advantage of this to accelerate the carbonation rate and reduce processing energy expenditure.

Baciocchi et al. [23] studied the wet carbonation route with boron-free AOD slag (powder), and found maximum CO_2 uptake after 8 hours at 50 °C, 10 bar CO_2 and 0.4 liquid-to-solid (L/S) ratio. The CO_2 uptake of the aged slag, determined by calcimetry, was about 30 wt%, equivalent to 70% Ca-conversion yield. The leaching behavior of the carbonated slag was also modified, exhibiting a reduction by ~2 units from the original pH of the slag, accompanied by a decrease of Ca release and an increase of Si leaching, as a result of modified leaching-controlling phases. Vandevelde [60] studied both boron-free AOD and CC slags (fresh powders) in wet carbonation at very mild conditions. Comparison of carbonation at 30 °C and 50 °C, 0.1 and 0.2 atm. CO_2, and L/S varying from 0 to 0.5, allowed for determination of the optimum process conditions: 30 °C, 0.2 atm. CO_2, L/S = 0.3. At these conditions, over 6 days, the CO_2 uptake of AOD and CC slags were 11 and 15 wt% respectively, equivalent to 32% and 45% Ca-conversion, respectively. An attempt to realize AOD slag carbonation using higher temperatures and pressures was done by Van Bouwel [61]. Process temperature used in experiments varied between 30 and 180 °C, the CO_2 partial pressure between 2 and 30 bar, and the reaction time between 1 minute and 2 hours, with continuous agitation (1000 rpm). Best results were obtained at 90 °C, 30 bar CO_2, after one hour and with an

L/S ratio equal to 16. Using these conditions, 63% Ca-conversion of AOD slag was realized, the pH dropped from 11.7 to 9.4, and leaching of heavy metals decreased (except for V).

2.3.2. Incineration ashes

Municipal solid waste incineration (MSWI) is a waste management technology that is predominantly utilized in geopolitical regions where land availability is scarce, thereby limiting landfilling capacity, and where strict environmental regulations or tax incentives encourage incineration. The generation of energy from the combustion of the waste, termed waste-to-energy (WtE), is an additional benefit of this technology. Although incineration enables reduction in waste volume by up to 90 vol% [62], substantial amounts of residues are produced, including fly ashes and even greater amounts of bottom ashes (BA), which can reach 20–30 wt% of the original waste mass [63]. These solid residues are the final sinks for salts and numerous toxic and regulated heavy metals and metalloids, which severely limit the possibilities for valorization of these materials.

In lack of suitable valorization routes for MSWI-BA, the common industrial practice to date has been natural ageing of the material, with the aim of promoting weathering and thus reducing leaching to environmentally acceptable levels, prior to final disposal and storage in landfills. In order to accelerate and enhance the ageing mechanisms, and thus permit further valorization of the ashes, accelerated carbonation has been identified as a potential route (reviewed by Costa et al. [64]). Notable studies on accelerated carbonation of MSWI-BA include those of Van Gerven et al. [63], Arickx et al. [62], Rendek et al. [65] and Baciocchi et al. [66].

The common process methodology has been moist carbonation, whereby the solids are mixed with a limited amount of water (0.2–0.3 liquid-to-solid ratio (L/S) has been found ideal) and exposed to a CO_2-rich atmosphere (10–100 vol% CO_2) at moderate temperatures (30–50 °C) for several hours to several days (up to 7 days being common) in static condition (e.g. thinly spread layers). The general precept is to maintain the temperature low enough to maximize CO_2 solubility in the water phase, but high enough to drive the carbonation reaction kinetics. Moreover, it is desirable to use a moisture content in the mixture that provides the water required for aqueous carbonation reaction (i.e. dissolved carbonates reacting with calcium and magnesium, leached from hydrated oxides and silicates, at the reacting zone near the particle surface), but that is thin enough to limit the diffusion distance the carbonate ion has to travel to reach the reaction zone (i.e. thin-film instead of flooded sample). Rendek et al. [67] found that pressurization of the gas aids carbonation kinetics, reducing time to reaction completion from 51 to 3.5 hours, but not having a significant effect on carbonation conversion/CO_2 uptake. The aforecited studies report improvement in the leaching behavior of certain metals, especially Cu, Pb and Zn, but detrimental effect on the leaching of Cr, Mo and Sb.

Um et al. [68] subjected municipal solid waste incinerator bottom ash (MSWI-BA) with particle size < 150 μm to carbonation using 30 vol% CO_2 with 0.3 L/S at different temperatures (20–40 °C), for the purpose of studying the leaching behavior of Cr. XRD results showed that portlandite ($Ca(OH)_2$), ettringite ($Ca_6Al_2(SO_4)_3(OH)_{12}\cdot 26H_2O$) and hydrocalumite ($Ca_8Al_4(OH)_{12}(Cl,CO_3,OH)_{2-x}\cdot 4H_2O$) disappeared from the material's composition after carbonation experiments. The pH decreased from almost 12 to almost 9 after 4 hours of carbonation. Leaching of Cr registered an increase in the first minutes of the carbonation experiment (due to decomposition of ettringite and hydrocalumite) followed by a continuous

decrease after 30 minutes (due to formation of insoluble Cr-material and the adsorption effect of amorphous Al-materials having high affinity for Cr).

2.3.3. Mining tailings and asbestos containing materials

An attractive route to efficient above-ground carbon capture and storage (CCS) is the utilization of already mined and milled tailings residues, which possess high surface area and porosity, for mineral carbonation. Their large-scale availability stoichiometrically places them among the few realistic options for buffering the CO_2 emissions of today's fossil-fuel driven economy. Especially suitable are ultramafic wastes due to their high content of Mg-rich minerals (e.g. olivine ($(Mg,Fe)_2SiO_4$) and serpentine ($(Mg,Fe)_3Si_2O_5(OH)_4$)). However, these wastes can also contain abundant quantities of the hazardous asbestiform (fibrous) polymorphs, such as chrysotile ($Mg_3(Si_2O_5)(OH)_4$). For example, historical mining activities in the towns of Thetford Mines and Asbestos (Québec, Canada) have led to the accumulation of approximately 2 billion tonnes of chrysotile-rich wastes [69]. Assima et al. [70] studied the sensitivity to seasonal temperature variations (10 to 40 °C) of mineral carbonation of a saturated nickel mine residue under humid environments. The authors suggest the possibility of heat recovery by low-temperature geothermal systems, as a 4.9 °C increase in temperature is registered even for experiments at 10 °C. In addition to CO_2 capture, the asbestiform nature of the mineral can be destroyed upon carbonation [71], rendering the process also a remediation solution. This approach also has the potential to be used for treatment of asbestos wastes from the construction industry (e.g. demolition and renovation), such as cement-asbestos, as an alternative to costly thermal treatments now researched [72, 73].

Larachi et al. [74] reported that low pressure direct gas-solid carbonation of chrysotile residues led to poor conversions, at best achieving 3.3% extent after 10 hours at 375 °C, via surface impregnation of super-basic sites or amorphisation/dehydroxylation. Conversely, Larachi et al. [69] report that partial dehydroxylation and steam mediation substantially enhance conversion, reaching uptakes as high as 0.7 CO_2 moles per Mg mole at 130 °C and 3.2 MPa. Ryu et al. [75] investigated the direct aqueous carbonation of chrysotile under subcritical conditions in alkali solution. The starting material was hydrothermally treated at pH = 13, at 100 °C and CO_2 partial pressures between 0.5 and 4 MPa. As the reaction proceeded, the surface morphology of chrysotile was observed to change from acicular (needle-like) and cylindrical-like forms, to a round or oval shape initially, and later to highly crystalline magnesite. The carbonation rate increased proportionally to the applied CO_2 pressure up to 57% at 3 MPa.

Ryu et al. [76] carried out direct aqueous carbonation of tremolite ($Ca_2Mg_5Si_8O_{22}(OH)_2$), another of the six types of asbestos, at 290 °C and 5 bar CO_2. Figure 2.2 shows the evolution of the material as a function of carbonation time. A significant amount of fibrous tremolite was transformed to calcite ($CaCO_3$), which made up 60 wt% of the final material. Tremolite carbonation was coupled with a saponitization reaction, as the crystallization of calcite was systematically associated with proto-saponite ($Ca_{0.25}(Mg,Fe)_3((Si,Al)_4O_{10})(OH)_2 \cdot n(H_2O)$). Also, it was shown that the fibrous shape of tremolite transformed to a rhombohedral or round shape during the carbonation reaction, which is environmentally friendlier. Gadikota et al. [77] carbonated hazardous asbestos containing material (ACM) in various reaction fluids (D.I. water, 0.1 M Na-oxalate, and 1.0 M Na-acetate), at varying temperature (90, 125, and 185 °C), in 150 atm. CO_2, with a stirring speed of 800 rpm, for 3 hours. Despite low conversions (max. 10.2%), significant changes in the structure (particle size and pore size) were observed due to mixing and simultaneous dissolution of ACM.

Na-oxalate was found to be more effective than Na-acetate despite the lower concentration, which was attributed to it being a stronger magnesium-targeting chelating agent.

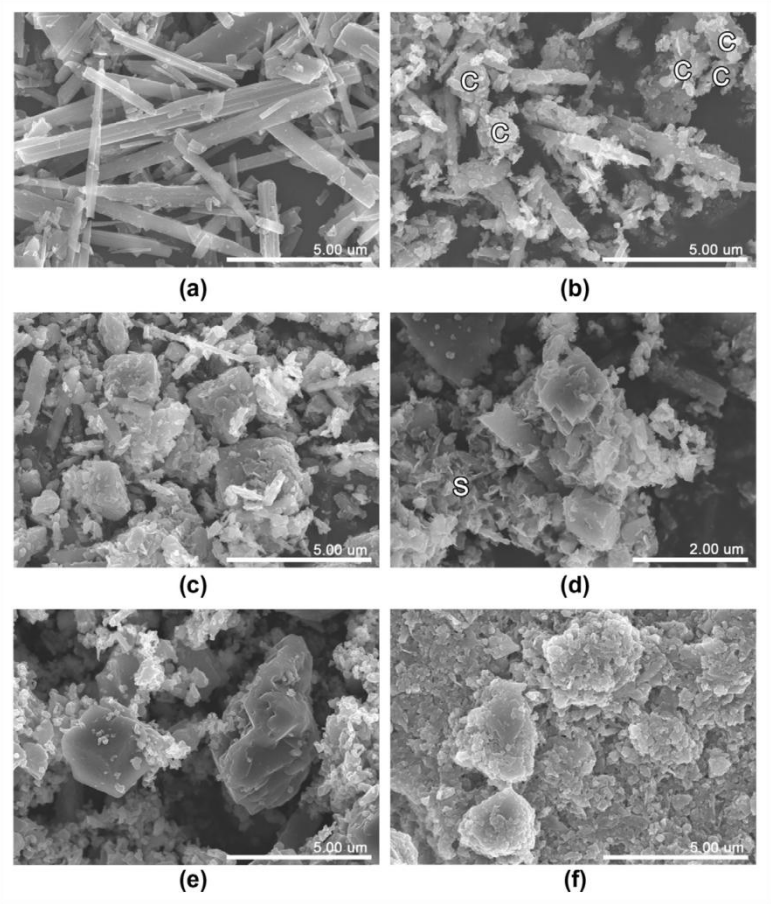

Fig. 2.2. Evolution of tremolite carbonation: (a) acicular tremolite; (b) development of <1 μm-sized calcite after 5 min of reaction; (c) image after carbonation for 15 min; (d and e) the shape of most of the tremolite grains changed to round and calcite shows euhedral morphology. (f) The edge of calcite was eroded by partial dissolution during the reaction for 5 h. 'C' and 'S' indicate calcite and saponite, respectively. Reprinted from Applied Geochemistry, Vol. 26, Ryu et al. [76], 1215–1221, Copyright 2011, with permission from Elsevier.

The tailings produced during mineral processing of non-ferrous ores, such as nickel and platinum group metals (PGM), can also contain significant amounts of magnesium silicates, and thus are potential carbon sinks. Meyer et al. [78] presented results on carbonation using the two-stage pH-swing of Mg-orthopyroxene rich tailings generated during the processing of platinum ores from South Africa. For the cation extraction, organic (oxalic and EDTA) and HCl solutions were used, followed by NaOH addition for pH adjustment before carbonation. The extraction efficiencies of Mg, Ca and Fe from the 2 M HCl was rapid for the first 30 minutes. Afterwards, the reaction slowed, and after 4 hours of reacting the dissolution of Mg and Fe reached a plateau. After 8 hours of reaction, however, Ca had not yet reached a plateau. Ca ions had the highest extraction efficiency of 31.2 %, followed by Fe at 9.1 % and Mg at 5.0 %. SEM and XRD analysis of the carbonate precipitate revealed the formation of both unstable (readily decomposing or dissolving) and stable carbonates. The unstable carbonates consisted of: trona ($Na_3(CO_3)(HCO_3)\cdot 2(H_2O)$), natrite ($Na_2CO_3$) and thermonatrite ($Na_2CO_3\cdot(H_2O)$), which formed the bulk, by weight, of the products. The stable carbonates formed were: gaylussite ($Na_2Ca(CO_3)_2\cdot 5(H_2O)$), siderite ($FeCO_3$), ankerite

($CaFe(CO_3)_2$), dolomite ($CaMg(CO_3)_2$), and hydromagnesite ($Mg_5(CO_3)_4(OH)_2{\cdot}4H_2O$). It was found that orthopyroxene, which comprises 88% of the total Mg budget in this kind of waste, remained unreacted; thus further work is needed to improve its dissolution kinetics before such mineral tailings can be considered as a viable feed stock for mineral carbonation.

2.3.4. Red mud

Red mud is a by-product of the process for obtaining alumina from bauxite ore through the Bayer process. Red mud is considered a hazardous waste, especially due to high alkalinity, and also a critical waste management issue, given the large quantities annually produced. Red mud consists of a mixture of liquid in chemical equilibrium with fine solids (20–80 wt%), the particles size of which varies between 2-100 μm, having a chemical composition typically in the range presented in Table 2.3. The pH of red mud averages at 11.3 ± 1.0, but can reach as high as 12.9. The pH is highly buffered by the presence of alkaline solids (hydroxides, carbonates and aluminates) that are formed during caustic soda (NaOH) treatment of bauxite [79]; residual NaOH in the liquid phase is also a major contributor to the high pH. The complex buffering actions of the multiple components of red mud makes it impractical to 'wash out' the alkalinity. Thus red mud is commonly stored in settling ponds, which have come to pose significant threat to neighboring populations and the environment. Yet, Si et al. [80] report that an estimated 100 million tonnes of CO_2 have been unintentionally sequestered in stored red mud worldwide by its natural weathering. Based on current production rates, about 6 million tonnes of CO_2 will be sequestered annually through atmospheric carbonation. Si et al. [80] estimate that if appropriate carbonation technologies are applied to red mud, an additional 6 million tonnes of CO_2 can be potentially captured and stored, while the hazardousness of red mud is simultaneously reduced. Since 2006, carbonation has been employed as a pre-deposition pH reduction treatment at the Kwinana refinery in Western Australia, where carbon dioxide gas is mixed with the residue slurry in pressurized vessels, after thickening of the mud to remove excess liquor [81].

Table 2.3. Average chemical composition of red mud; expressed as oxides [79].

Oxide	Amount (wt%)
Al_2O_3	2-33
Fe_2O_3	7-72
SiO_2	1-24
TiO_2	3-23
CaO	1-47
Na_2O	1-13

The carbonation of red mud implies a pre-carbonation decision: carbonate the red mud liquid-solid mixture, or the drained solids. Bonenfant et al. [82] found that pre-dried red mud suspension at a liquid-to-solid ratio of 10 kg/kg has a realizable CO_2 storage capacity of only 4.15 g CO_2/100 g red mud when carbonated at 20 °C and 15 vol% CO_2 at atmospheric pressure, which is attributed to carbonation of its Ca- and Na-(hydr)oxide contents. Yadav et al. [83] report similar CO_2 uptake (3.5 wt%) after pressurized (3.5 bar) carbonation of washed red mud solids. Bonenfant et al. [82] propose that because the red mud matrix has a great leaching capacity of Na-(hydr)oxide, the alternated carbonation of leachates separated from the leached hydrated-matrixes of red mud could

constitute a more effective method for the CO_2 sequestration than the use of aqueous red mud suspension. Sahu et al. [84] employed cyclic carbonation of red mud solids, 5 hours in duration each cycle, in aqueous slurry at atmospheric pressure. The pH, alkalinity and acid neutralization capacity (ANC) of the red mud decreased from ~11.8 to ~8.45, ~10,789 to ~178 mg/L, and ~1.3 to ~0.23 mol H^+/kg, respectively, at the end of the third cycle. The cost for sequestering a tonne of CO_2 was estimated at approximately $ 147, and the quantity of sequestered CO_2 was about 7.02 g per 100 g red mud. Khaitan et al. [85] noted that the pH of carbonated red mud rebounded to 9.9 after one day, indicating that the pH change during short-term (≤ 10 days) carbonation is due to the reaction of carbonic acid and OH^- in the pore water. Only after a longer reaction time (30 days) at 1 atm. CO_2 did tricalcium aluminate ($Ca_3Al_2O_6$) in the solid phase convert to calcite, as was observed from aged field samples that had been carbonated in air ($10^{-3.5}$ atm. CO_2) for 30 years.

Dilmore et al. [86] utilized a different route for the carbonation treatment of red mud. Instead of carbonating only the red mud, it was mixed with an industrial brine (saline wastewater) solution of low pH (~3) and rich in Ca^{2+} and Mg^{2+}. In this case, the high pH (~13) red mud actually acted as a pH buffer, to induce the carbonate formation from the brine solution constituents, while at the same time becoming neutralized itself. A bauxite residue/brine mixture of 90/10 by volume exhibited a CO_2 sequestration capacity of 9.5 g/L at 20 °C and 6.89 bar CO_2, and reached a final pH of ~7. Soong et al. [87] applied a similar process scheme, but using SO_2-containing flue gas instead of pure CO_2. They found that > 99.9% of the SO_2 was captured in the carbonated red mud/brine mixture, in the form of sulfite (SO_3^{2-}) by solubility trapping.

2.3.5. Oil-shale processing residues

A particular line of research that has been undertaken in the last few years is that of the utilization of Estonian oil-shale ashes for carbon capture [88-90]. Combustion of oil-shale by means of pulverized firing (PF) and in circulating fluidized bed combustors (CFBCs) produces ashes that contain up to 30 wt% free Ca- and Mg-oxides. Uibu et al. [88] conducted carbonation experiments using a model gas whose composition (10 wt% CO_2 and 90 wt% air) simulated the flue gases formed during oil-shale combustion. The carbonation was performed with solid/liquid ratio of 1:10 at ambient temperature and atmospheric pressure. CFBC ashes carbonated more than PF ashes: 83-98% and 48-73% conversion, respectively, equivalent to 100-160 kg CO_2/tonne binding capacity. The alkaline ash transportation water was also neutralized with CO_2, and resulted in rapid neutralization and retention of 52 kg CO_2 by the amount of alkaline wastewater used for transporting 1 tonne of ash. In Uibu and Kuusik [89], the superior carbonation performance of CFBC ashes was attributed to its more porous particle structure, which allowed better diffusion of Ca^{2+} ions into solution. In the case of PF ash, process deceleration was caused by the concurrence of two factors: low porosity of PF ash, and high concentration of dissolved salts in the liquid phase inhibiting diffusion of Ca^{2+} away from the solid surface. These factors led to the formation of insoluble layers of $CaCO_3$ and $CaSO_4$ that partially or completely prevented further dissolution of CaO. To overcome this limitation, a continuous-flow reactor was designed and tested, where the composition of the liquid phase contacting ash could be monitored and controlled. It consisted of reactor-columns working in cascade (Figure 2.3a), wherein the pH levels in the different reactors ranged from alkaline to almost neutral, thus delivering optimal conditions for lime slaking, $Ca(OH)_2$ dissociation and $CaCO_3$ precipitation. Final carbonated ashes contained 0.6-2.9 wt% of unreacted CaO and 17-20 wt% CO_2.

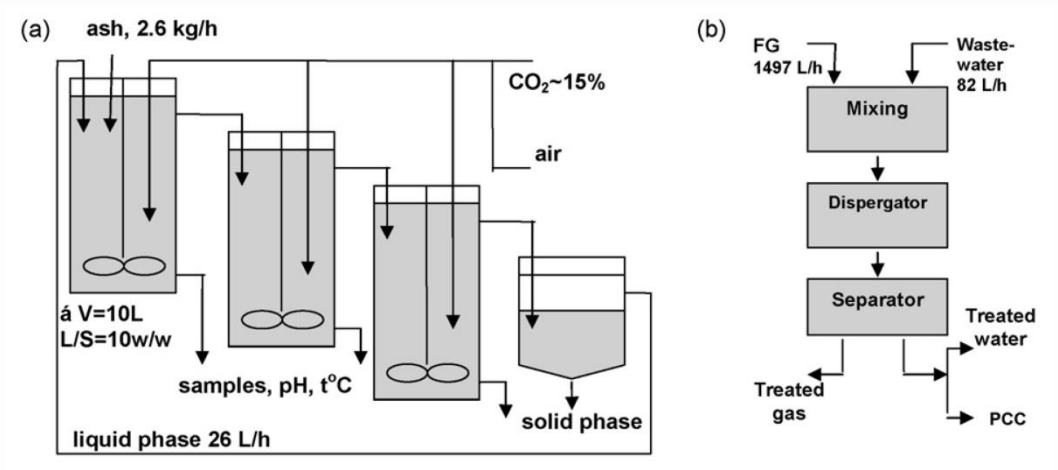

Fig. 2.3. Experimental cascading reactors for carbonation of oil-shale ash suspension (a) and alkaline wastewater (b). Reprinted from Journal of Hazardous Materials, Vol. 174, Uibu et al. [90], 209–214, Copyright 2009, with permission from Elsevier.

2.4. VALORIZATION OF TREATED INDUSTRIAL WASTES

For mineral carbonation to become economically feasible, the valorization of the resulting material could help reduce the overall cost of the process. This section outlines some of the latest developments with this objective, mainly for the production of construction materials that either contain carbonated products, or that are formed by means of carbonation.

Monkman et al. [91] studied the possibility of using carbonated ladle (BOF) steel slag as a fine aggregate in concrete. Carbonation was performed both at 500 kPa CO_2 for 2 hours and at atmospheric pressure for 56 days. The main objective was to reduce the free lime (CaO) content. Slag particles between 300-600 µm sequestered 4.2 wt% CO_2, and those smaller than 75 µm carbonated to 15.6 wt% CO_2. The extractable CaO contents were significantly reduced by carbonation treatment. The carbonated slag was then used as a fine aggregate in zero-slump press-formed compact mortar samples; similar mortars made instead with river sand as the fine aggregate were used as controls. After 28 days of moist curing, the strength of the mortars was comparable. As such, the use of carbonated ladle slag appears to be a suitable substitute as a fine aggregate in concrete.

Salman et al. [92] used continuous casting stainless steel slag with particle diameter <500 µm to fabricate cylindrical specimens of 55 mm in diameter and 75 mm in height. These specimens were then carbonated using two methods (mild conditions in an incubator, and high temperature and pressure using an autoclave reactor). While a period of 4 weeks was needed to reach the highest compressive strength (20 MPa) by incubator carbonation (5 vol% CO_2, 22 °C and 80% humidity), only 6 hours was needed to reach similar strength when using autoclave reactor carbonation at 8 bar, CO_2 and 60 °C. This compressive strength can make such materials suitable for several structural and non-structural applications.

Van Mechelen et al. [93] have worked on the upscaling of the Carbstone process, developed for the valorization of non-hydraulic slags and ashes into high quality construction materials. The process makes use of accelerated carbonation by treating various kinds of compacted slags with CO_2 at elevated pressure (5-20 bar) and temperature (up to 140 °C) without addition of binders. The carbonation process consists of three essential steps: (1) pretreatment of the slags, (2) shaping of the

building blocks by compaction, and (3) curing of the building block by CO_2. The carbonates that are produced in-situ during the carbonation reaction act as a binder, cementing the slag particles together. The carbonated materials can compete with concrete products (C35/C45), having satisfactory environmental and technical properties. Furthermore, the materials sequester 180-200 g CO_2/kg slag.

Baciocchi et al. [94] used ground basic oxygen furnace (BOF) slag (particle size < 2 mm) mixed with water to produce granulates of particle diameter up to 9 mm. This granulation was realized with and without carbonation. Leaching tests conducted after the granulation experiments indicate that select elements (e.g. K, Na and Ba) appeared to be more tightly bound to the solid matrix. The same decreasing trend was also observed for the pH and the apparent particle density. The ultimate goal of this work was the production of aggregates for use in construction works, thus aggregate crushing value (ACV) tests were performed on the granulated slag and natural gravel as a control. The results showed that the amount of fine particles (d < 2.36 mm) obtained was significantly higher (over 70 wt% of the material) than that achieved for natural gravel (20 wt%), so further optimization is required.

Gunning et al. [95] have reported the latest developments of the spin-off company Carbon8 Systems Ltd, which is developing an industrial process for the production of lightweight aggregates from waste materials via accelerated carbonation. The favored waste material is municipal solid waste incineration (MSWI) air pollution control residues (APCr), which originates from flue gas treatment where lime, carbon, and ammonia are added to neutralize pH and remove pollutants such as dioxins and volatile metals. The patented process [96] begins with APCr passing through a treatment chamber, where initial carbonation of the APCr takes place. Next it enters a batch mixer where reagents are introduced to produce a mixture that is then conveyed to the pelletizing unit. There, the materials are aggregated with further addition of CO_2, which induces chemical stabilization and solidification of the aggregate (exemplified in Figure 2.4). The aggregated product is then valorized in an on-site concrete block making process. Compliance of the aggregate product is determined based on physical properties (compressive strength, particle size and durability), and chemical characteristics (leaching of metals and anions). Specifically, to conform to End-of-Waste specifications, an average individual aggregate compressive strength of 0.1 MPa, and a maximum bulk density of 1200 kg/m^3 are required. Gunning et al. [95] shows that these requirements are consistently met (~0.28 MPa and ~1120 kg/m^3) at a full-scale facility with a production capacity of 36,000 tonne/yr.

Fig. 2.4. Pelletized lightweight aggregate product. Reprinted from Waste Management, Vol. 29, Gunning et al. [97], 2722–2728, Copyright 2009, with permission from Elsevier.

On a research sphere outside that of construction materials, Uibu et al. [90] identified a second opportunity for carbonation within oil-shale power plants, namely using the Ca^{2+}-saturated alkaline water (pH 12-13) that is recycled between the plant and sedimentation ponds for the transport of the ash to wet open-air deposits. The goal was to intensify the water neutralization process and use the wastewater as a calcium source for the production of precipitated calcium carbonate (PCC) (Figure 2.3b). The PCC formed was characterized by a regular rhombohedral structure and a homogeneous particle size (~5 μm) distribution. It was also found that to avoid agglomeration of the particles and re-dissolution of $CaCO_3$, the neutralization process should be divided into two stages: PCC precipitation and separation at high pH values in a first stage, followed by decreasing the residual alkalinity of the wastewater to acceptable disposal levels (pH ~8-8.5) in a second stage.

2.5. CONCLUSIONS[IX]

Despite the benefits of mineral carbonation of industrial waste materials identified, and the established knowledge pool, inefficiencies regarding the high overall cost of the method, uncertainties regarding quality and marketability of valorizable products, the presently low market levels of CO_2 capture credits, and the limited CO_2 sequestration capacity of these materials (due to small tonnage produced relative to CO_2 emission volumes), have delayed the large-scale implementation of mineral carbonation of industrial wastes. To accelerate the mineral carbonation reaction to meaningful levels, to match the rate of emissions of CO_2 from industrial sources, and to achieve carbonation in an economical and net-positive sequestration manner, intensified processing routes are required. Areas that deserve further research, and which were investigated in the framework of this doctoral project, include:

- *Utilization of ultrasound during the mineral carbonation of silicate-based materials, as these materials suffer appreciably from the shrinking core limitation. Sonication as a means to enhance the kinetics and ultimate mineral carbonation conversion due to the removal of mass transfer inhibiting passivating layers (precipitated carbonates and residual silica) and enhancement of micromixing shows promise. Attention should also be paid to the energy consumption of the sonication process, in order to ensure net CO_2 sequestration. Optimization strategies should be identified.*
- *Assessment if the carbonation conversion limitations could be attributable to, besides the shrinking core model, differences in the susceptibility towards mineral carbonation of individual alkaline mineral phases found in thermal residues. To this end, the synthesis and carbonation of pure mineral phases can be pursued. Furthermore, detailed mineralogical analysis by quantitative X-ray diffraction using the Rietveld refinement method can lead to a better understanding of the reactivity of the different mineral phases in the waste materials towards accelerated carbonation.*
- *In-depth investigation of the potential of hot-stage carbonation of thermal residues, in view of carbonating these materials on-site before they cool entirely. One approach is to use in-situ analytical techniques to follow the reaction kinetics and thermodynamic equilibrium at high temperatures, in order to identify the processing window that is optimal for high CO_2 uptake and waste material stabilization. It is also desirable, from an industrial scale-up and implementation perspective, to assess the effects of particle size (seeing that hot-stage*

[IX] These conclusions were re-written to reflect the omission of the results of Santos et al. and Bodor et al., and thus to serve as a preamble to the works described in detail in the following chapters.

granulation is also required to produce reactive surface area), steam addition and pressurization. Finally, it should be assessed whether hot-stage carbonation is sufficient to yield the required reduction in basicity, heavy metal leaching and volume stability that can enable valorization of the waste materials.

- *Routes that lead to dual valorization of the two products of indirect mineral carbonation should be identified, in order to symbiotically combine the benefits of CO_2 sequestration via mineral carbonation and waste stabilization/valorization. For instance, the silicon-rich solid residues from the extraction stage of alkaline components from steel slags can potentially be subjected to hydrothermal conversion for the synthesis of zeolitic materials, or be used as precursors of construction materials.*
- *The disintegration behaviour of AOD slag in the absence of boron addition (or other volumetric stabilizers) is typically undesirable due to the higher disposal costs of powdery materials. However, this behaviour can be exploited in a mineral carbonation process, given that carbonation reactivity is proportional to specific surface area. It should be investigated if the resulting particle size of AOD slag (and CC slag likewise) is sufficient, from the perspective of CO_2 uptake, to enable the use of these materials as carbon sinks. Furthermore, it should be assessed if the geochemical properties of these fine materials, which are detrimentally affected by disintegration, can be satisfactorily stabilized by mineral carbonation.*
- *A comparison of thin-film carbonation and slurry carbonation should be made to elucidate if the intensified conditions of the latter warrant the additional process complexities and associated costs of pressurized and aqueous processes. That is, is it worth it to seek maximal CO_2 uptake, mineral conversion, treatment homogeneity, and basicity and leaching stabilization, or is it sufficient to partially react the materials at mild conditions solely for the purpose of economical CO_2 sequestration?*
- *To date, several mineral carbonation and other waste stabilization methods have been tested, but seldom have they been applied to identical materials in a single study. It is thus difficult to accurately compare treatment efficiency in view of selecting the optimal one. For instance, looking at solid waste incineration bottom ashes, the performance of four different approaches for stabilization of regulated heavy metal and metalloid leaching should be assessed: (i) heap ageing, (ii) heat treatment, (iii) accelerated moist carbonation, and (iv) accelerated pressurized slurry carbonation. When evaluating these methods, it is important not only to compare them against each other, but also to compare them against regulations for the safe disposal or valorization of waste materials. National and trans-national regulations exist for composition, leaching, and other properties. These regulatory limits should be systematically applied to the results in order to assess the likelihood that any given method has of being industrially implemented.*

2.6. REFERENCES

1. NOAA ESRL, Trends in Atmospheric Carbon Dioxide [Online], Available at: http://www.esrl.noaa.gov/gmd/ccgg/trends/history.html [accessed March 4, 2013].
2. Lackner, K.S., Capture of carbon dioxide from ambient air, EUR PHYS J SPECIAL TOPICS, 2009, 176, 93-106.

3. House, K.Z., Baclig, A.C., Ranjan, M., van Nierop, E.A., et al., Economic and energetic analysis of capturing CO_2 from ambient air, PNAS, 2011, 108(51), 20428-20433.
4. Lackner, K.S., Brennan, S., Matter, J.M., Park, A.-H.A., et al., The urgency of the development of CO_2 capture from ambient air, PNAS, 2012, 109(33), 13156-13162.
5. Goeppert, A., Czaun, M., Prakash, G.K.S., Olah, G.A., Air as the renewable carbon source of the future: an overview of CO_2 capture from the atmosphere, ENERGY ENVIRON SCI., 2012, 5(7), 7833-7853.
6. Bennaceur, K., Monea, M., Sakurai, S., Gupta, N., et al., CO_2 Capture and storage - A solution within, OILFIELD REVIEW, 2004, 16, 44-61.
7. Lackner, K.S., A Guide to CO_2 Sequestration, SCIENCE, 2003, 300(5626), 1677-1678.
8. Harvey, O.R., Cantrell, K.J., Qafoku, N.P., Brown, C.F., Geochemical Implications of CO_2 Leakage Associated with Geologic Storage: A Review, Report prepared for the U.S. Department of Energy under Contract DE-AC05-76RL01830, 2012.
9. Paulley, A., Maul, P., Metcalfe, R., Scenarios for Potential Impacts from Hypothetical Leakage from Geological Storage Facilities for Carbon Dioxide, Public deliverable from the RISCS project, 2012.
10. Sipilä, J., Teir, S., Zevenhoven, R., Carbon dioxide sequestration by mineral carbonation - Literature review update 2005–2007, ISBN 978-952-12-2036-4, 2008.
11. Seifritz, W., CO_2 disposal by means of silicates, NATURE, 1990, 345(6275), 486.
12. Van Gerven, T., Leaching of Heavy Metals from Carbonated Waste-Containing Construction Material, PhD Thesis, Katholieke Universiteit Leuven, Leuven, Belgium, 2005.
13. Huijgen, W.J.J., Carbon dioxide sequestration by mineral carbonation, PhD Thesis, Technische Universiteit Delft, Delft, The Netherlands, 2007.
14. Rawlins, C.H., Geological Sequestration of Carbon Dioxide by Hydrous Carbonate Formation in Steelmaking Slag, PhD Thesis, Missouri University of Science and Technology, Rolla, Missouri, USA, 2008.
15. Teir, S., Fixation of carbon dioxide by producing carbonates from minerals and steelmaking slags, PhD Thesis, Helsinki University of Technology, Espoo, Finland, 2008.
16. Uibu, M., Abatement of CO_2 emissions in Estonian oil shale-based power production, PhD Thesis, Tallinn University of Technology, Tallinn, Estonia, 2008.
17. Costa, G., Accelerated carbonation of minerals and industrial residues for carbon dioxide storage, PhD Thesis, Università Degli Studi Di Roma "Tor Vergata", Rome, Italy, 2009.
18. Eloneva, S., Reduction of CO_2 emissions by mineral carbonation: steelmaking slags as raw material with a pure calcium carbonate end product, PhD Thesis, Aalto University, Espoo, Finland, 2010.
19. Gunning, P.J., Accelerated Carbonation of Hazardous Wastes, PhD Thesis, University of Greenwich, Chatham Maritime, United Kingdom, 2011.
20. ACEME'10, Third International Conference on Accelerated Carbonation for Environmental and Materials Engineering [Online], Available at: http://web.abo.fi/fak/tkf/vt/aceme10/ [accessed March 4, 2013].
21. ACEME'13, Fourth International Conference on Accelerated Carbonation for Environmental and Materials Engineering [Online], Available at: http://cit.kuleuven.be/aceme13/ [accessed March 4, 2013].
22. Bobicki, E.R., Liu, Q., Xu, Z., Zeng, H., Carbon capture and storage using alkaline industrial wastes, PROG ENERGY COMBUST SCI., 2012, 38, 302-320.

23. Baciocchi, R., Costa, G., Bartolomeo, E., Polettini, A., et al., Carbonation of Stainless Steel Slag as a Process for CO_2 Storage and Slag Valorization, WASTE BIOMASS VALORIZATION, 2010a, 1, 467-477.
24. IPCC, Carbon Dioxide Capture and Storage - Summary for Policymakers, ISBN 92-9169-119-4, 2005.
25. Huijgen, W.J.J., Comans, R.N.J., Witkamp, G.-J., Cost evaluation of CO_2 sequestration by aqueous mineral carbonation, ENERGY CONVERS MANAGE., 2007, 48, 1923-1935.
26. Chang, E.-E., Chen, C.-H., Chen, Y.-H., Pan, S.-Y., et al., Performance evaluation for carbonation of steel-making slags in a slurry reactor, J HAZARD MATER., 2011, 186, 558-564.
27. Chang, E.-E., Chiu, A.-C., Pan, S.-Y., Chen, Y.-H., et al., Carbonation of basic oxigen furnace slag with metalworking wastewater in a slurry reactor, INT J GREENHOUSE GAS CONTROL, 2013, 12, 382-389.
28. Gogate, P.R., Sutkar, V.S., Pandit, A.B., Sonochemical reactors: important design and scale up considerations with a special emphasis on heterogeneous systems, CHEM ENG J., 2011, 166, 1066-1082.
29. Wagterveld, R.M., Boels, L., Mayer, M.J., Witkamp, G.J., Visualization of acoustic cavitation effects on suspended calcite crystals, ULTRASON SONOCHEM., 2011, 18, 216-225.
30. Rao, A., Anthony, E.J., Jia, L., Macchi, A., Carbonation of FBC ash by sonochemical treatment, FUEL, 2007, 86, 2603-2615.
31. López-Periago, A.M., Pacciani, R., García-González, C., Vega, L.F., et al., A breakthrough technique for the preparation of high-yield precipitated calcium carbonate. J. SUPERCRIT. FLUIDS, 2010, 52, 298-305.
32. Steinour, H.H., Some effects of carbon dioxide on mortars and concrete—discussion, Concrete Briefs, J AM CONCR INST., 1959, 55, 905-907.
33. Doucet, F.J., Effective CO_2-specific sequestration capacity of steel slags and variability in their leaching behaviour in view of industrial mineral carbonation, MINER ENG., 2010, 23, 262-269.
34. Reddy, E.P., Smirniotis, P.G., High-temperature sorbents for CO_2 made of alkali metals doped on CaO supports, J PHYS CHEM B, 2004, 108, 7794-7800.
35. Blamey, J., Anthony, E.J., Wang, J., Fennell, P.S., The calcium looping cycle for large-scale CO_2 capture, PROG ENERGY COMBUST SCI., 2010, 36, 260-279.
36. Manovic, V., Anthony, E.J., Lime-based sorbents for high-temperature CO_2 capture—a review of sorbent modification methods, INT J ENVIRON RES PUBLIC HEALTH 2010, 7, 3129-3140.
37. Prigiobbe, V., Polettini, A., Baciocchi, R., Gas–solid carbonation kinetics of Air Pollution Control residues for CO_2 storage, CHEM ENG J., 2009, 148, 270-278.
38. Mikhail, S.A., Turcotte, A.M., Thermal behaviour of basic oxygen furnace waste slag, THERMOCHIM. ACTA, 1995, 263, 87-94.
39. Yu, J., Wang, K., Study on Characteristics of Steel Slag for CO_2 Capture, ENERGY FUELS, 2011, 25, 5483-5492.
40. Bonfils, B., Julcour-Lebigue, C., Guyot, F., Bodénan, F., et al., Comprehensive analysis of direct aqueous mineral carbonation using dissolution enhancing organic additives. INT J GREENHOUSE GAS CONTROL, 2012, 9, 334-346.

41. Eloneva, S., Teir, S., Salminen, J., Fogelholm, C.-J., et al., Steel Converter Slag as a Raw Material for Precipitation of Pure Calcium Carbonate, IND ENG CHEM RES., 2008, 47, 7104-7111.
42. Eloneva, S., Teir, S., Revitzer, H., Salminen, J., et al., Reduction of CO_2 Emissions from Steel Plants by Using Steelmaking Slags for Production of Marketable Calcium Carbonate, STEEL RES INT., 2009, 80(6), 415-421.
43. Eloneva, S., Mannisto, P., Said, A., Fogelholm, C.-J., et al., Ammonium salt-based steelmaking slag carbonation: Precipitation of $CaCO_3$ and ammonia losses assessment, GREENHOUSE GAS SCI TECHNOL., 2011, 1(4), 305-311.
44. Huijgen, W.J.J., Comans, R.N.J., Carbonation of Steel Slag for CO_2 Sequestration: Leaching of Products and Reaction Mechanisms, ENVIRON SCI TECHNOL., 2006, 40, 2790-2796.
45. Topkaya, Y., Sevinç, N., Günaydın, A., Slag treatment at Kardemir integrated iron and steel works, INT J MINER PROCESS., 2004, 74, 31-39.
46. Dippenaar, R., Industrial uses of slag (the use and re-use of iron and steelmaking slags), IRONMAK STEELMAK. 2005, 32, 35-46.
47. Wang, G., Wang, Y., Gao, Z., Use of steel slag as a granular material: volume expansion prediction and usability criteria, J HAZARD MATER. 2010, 184, 555-560.
48. Emery, J.J., Slag utilization in pavement construction, EXTENDING AGGR RESOUR., ASTM SPEC TECH PUBL., 1982, 774, 95-118.
49. Waligora, J., Bulteel, D., Degrugilliers, P., Damidot, D., et al., Chemical and mineralogical characterizations of LD converter steel slags: A multi-analytical techniques approach, MATER CHARACT., 2010, 61, 39-48.
50. Huijgen, W.J.J., Witkamp, G.-J., Comans, R.N.J., Mineral CO_2 Sequestration by Steel Slag Carbonation, ENVIRON SCI TECHNOL., 2005, 39, 9676-9682.
51. Chang, E.-E., Pan, S.-Y., Chen, Y.-H., Tan, C.-S., et al., Accelerated carbonation of steelmaking slags in a high-gravity rotating packed bed, J HAZARD MATER., 2012, 227-228, 97-106.
52. van Zomeren, A., van der Laan, S.R., Kobesen, H.B.A., Huijgen, W.J.J., et al., Changes in mineralogical and leaching properties of converter steel slag resulting from accelerated carbonation at low CO_2 pressure, WASTE MANAGE., 2011, 31, 2236-2244.
53. Isoo, T., Takahashi, T., Fukuhara, M., Using carbonated steelmaking slag blocks to help reduce CO_2, AM CERAM SOC BULL., 2001, 80, 73-75.
54. Baciocchi, R., Costa, G., Di Bartolomeo, E., Polettini, A., et al., Wet versus slurry carbonation of EAF steel slag, GREENHOUSE GAS SCI TECHNOL., 2011, 1, 312-319.
55. Huaiwei, H., Xin, H., An overview for the utilization of wastes from stainless steel industries, RESOUR CONSERV RECYCL., 2011, 55, 745-754.
56. Durinck, D., Engström, F., Arnout, S., Heulens, J., et al., Hot stage processing of metallurgical slags, RESOUR CONSERV RECYCL. 2008, 52, 1121-1131.
57. Domínguez, M.I., Romero-Sarria, F., Centeno, M.A., Odriozola, J.A., Physicochemical Characterization and Use of Wastes from Stainless Steel Mill, ENVIRON PROG SUSTAINABLE ENERGY 2010, 29, 471-480.
58. Mayes, W.M., Younger, P.L., Aumônier, J., Hydrogeochemistry of Alkaline Steel Slag Leachates in the UK, WATER AIR SOIL POLLUT., 2008, 195, 35–50.
59. Pontikes, Y., Jones, P.T., Geysen, D., Blanpain, B., Options to prevent dicalcium silicate-driven disintegration of stainless steel slags, ARCH METALL MATER. 2010, 55, 1167-1172.

60. Vandevelde, E., Mineral carbonation of stainless steel slag, Master's Thesis, KU Leuven, Leuven, Belgium, 2010.
61. Van Bouwel, J., Intensified aqueous mineral carbonation of alkaline industrial residues for CO_2 storage and waste remediation: effect of process parameters on carbonation conversion, leaching behavior and mineralogy, Master's Thesis, KU Leuven, Leuven, Belgium, 2012.
62. Arickx, S., Van Gerven, T., Vandecasteele, C., Accelerated carbonation for treatment of MSWI bottom ash, J HAZARD MATER. 2006, B137, 235–243.
63. Van Gerven, T., Van Keer, E., Arickx, S., Jaspers, M., et al., Carbonation of MSWI-bottom ash to decrease heavy metal leaching, in view of recycling, WASTE MANAGE., 2005, 25, 291-300.
64. Costa, G., Baciocchi, R., Polettini, A., Pomi, R., et al., Current status and perspectives of accelerated carbonation processes on municipal waste combustion residues, ENVIRON MONIT ASSESS., 2007, 135, 55–75.
65. Rendek, E., Ducom, G., Germain, P., Influence of organic matter on municipal solid waste incinerator bottom ash carbonation, CHEMOSPHERE, 2006a, 64, 1212-1218.
66. Baciocchi, R., Costa, G., Lategano, E., Marini, C., et al., Accelerated carbonation of different size fractions of bottom ash from RDF incineration, WASTE MANAGE., 2010b, 30, 1310-1317.
67. Rendek, E., Ducom, G., Germain, P., Carbon dioxide sequestration in municipal solid waste incinerator (MSWI) bottom ash, J HAZARD MATER., 2006b, B128, 73-79.
68. Um, N., Nam, S.Y., Ahn, J.W., Effect of accelerated carbonation on the leaching behavior of Cr in municipal solid waste incinerator bottom ash and the carbonation kinetics, In: Proceedings of the Fourth International Conference on Accelerated Carbonation for Environmental and Materials Engineering (April 9-12, 2013 Leuven Belgium), 2013, 529-533.
69. Larachi, F., Gravel, J.-P., Grandjean, B.P.A., Beaudoin, G., Role of steam, hydrogen and pretreatment in chrysotile gas–solid carbonation: Opportunities for pre-combustion CO_2 capture, INT J GREENHOUSE GAS CONTROL, 2012, 6, 69-76.
70. Assima, G.P., Larachi, F., Molson, J., Beaudoin, G., Assessment of the impact of seasonal temperature variations on the dynamics of CO_2 mineral sequestration by nickel mining residues, In: Proceedings of the Fourth International Conference on Accelerated Carbonation for Environmental and Materials Engineering (April 9-12, 2013 Leuven Belgium), 2013, 245-254.
71. Gerdemann, S.J., O'Connor, W.K., Dahlin, D.C., Penner, L.R., et al., Ex Situ Aqueous Mineral Carbonation, ENVIRON SCI TECHNOL., 2007, 41, 2587-2593.
72. Gualtieri, A.F., Cavenati, C., Zanatto, I., Meloni, M., et al., The transformation sequence of cement–asbestos slates up to 1200 °C and safe recycling of the reaction product in stoneware tile mixtures, J HAZARD MATER., 2008, 152, 563-570.
73. Gualtieri, A.F., Boccaletti, M., Recycling of the product of thermal inertization of cement–asbestos for the production of concrete, CONSTR BUILD MATER., 2011, 25, 3561-3569.
74. Larachi, F., Daldoul, I., Beaudoin, G., Fixation of CO_2 by chrysotile in low-pressure dry and moist carbonation: Ex-situ and in-situ characterizations, GEOCHIM COSMOCHIM ACTA, 2010, 74, 3051-3075.
75. Ryu, K.W., Chae, S.C., Jang, Y.N., Carbonation of chrysotile under subcritical conditions, MATER TRANS., 2011a, 52(10), 1983-1988.
76. Ryu, K.W., Lee, M.G., Jang, Y.N., Mechanism of tremolite carbonation, APPL GEOCHEM., 2011b, 26, 1215-1221.

77. Gadikota, G., Natali, C., Boschi, C., Park, A.-H.A., Carbonation of Asbestos for Permanent Storage of Anthropogenic CO_2, In: Proceedings of the Fourth International Conference on Accelerated Carbonation for Environmental and Materials Engineering (April 9-12, 2013 Leuven Belgium), 2013, 255-264.
78. Meyer, N.A., Vogeli, J., Becker, M., Broadhurst, J.L., et al., Mineral carbonation of PGM mine tailings for CO_2 storage in South Africa: A case study from Lonmin, In: Proceedings of the Fourth International Conference on Accelerated Carbonation for Environmental and Materials Engineering (April 9-12, 2013 Leuven Belgium), 2013, 503-507.
79. Gräfe, M. Power, G., Klauber, C., Review of bauxite residue alkalinity and associated chemistry, CSIRO Document DMR-3610, May 2009.
80. Si, C., Ma, Y., Lin, C., Red mud as a carbon sink: Variability, affecting factors and environmental significance, J HAZARD MATER., 2013, 244-245, 54-59.
81. Santini, T.C., Hinz, C., Rate, A.W., Carter, C.M., et al., In situ neutralization of uncarbonated bauxite residue mud by cross layer leaching with carbonated bauxite residue mud, J HAZARD MATER, 2011, 194, 119-127.
82. Bonenfant, D., Kharoune, L., Sauvé, S., Hausler, R., et al., CO_2 Sequestration by Aqueous Red Mud Carbonation at Ambient Pressure and Temperature, IND ENG CHEM RES., 2008, 47, 7617-7622.
83. Yadav, V.S., Prasad, M., Khan, J., Amritphale, S.S., et al., Sequestration of carbon dioxide (CO_2) using red mud, J HAZARD MATER., 2010, 176, 1044-1050.
84. Sahu, R.C., Patel, R.K., Ray, B.C., Neutralization of red mud using CO_2 sequestration cycle, J HAZARD MATER., 2010, 179, 28-34.
85. Khaitan, S., Dzombak, D.A., Lowry, G.V., Mechanisms of Neutralization of Bauxite Residue by Carbon Dioxide, J ENVIRON ENG., 2009, 135, 433-438.
86. Dilmore, R., Lu, P., Allen, D., Soong, Y., et al., Sequestration of CO_2 in Mixtures of Bauxite Residue and Saline Wastewater, ENERGY FUELS, 2008, 22, 343-353.
87. Soong, Y., Dilmore, R.M., Hedges, S.W., Howard, B.H., et al., Utilization of Multiple Waste Streams for Acid Gas Sequestration and Multi-Pollutant Control, CHEM ENG TECHNOL., 2012, 35(3), 473-481.
88. Uibu, M., Uus, M., Kuusik, R., CO_2 mineral sequestration in oil-shale wastes from Estonian power production, J ENVIRON MANAGE., 2009, 90, 1253-1260.
89. Uibu, M., Kuusik, R., Mineral trapping of CO_2 via oil shale ash aqueous carbonation: controlling mechanism of process rate and development of continuous-flow reactor system, OIL SHALE, 2009, 26(1), 40-58.
90. Uibu, M., Velts, O., Kuusik, R., Developments in CO_2 mineral carbonation of oil shale ash, J HAZARD MATER., 2010, 174, 209-214.
91. Monkman, S., Shao, Y., and Shi, C., Carbonated Ladle Slag Fines for Carbon Uptake and Sand Substitute, J MATER CIV ENG., 2009, 21(11), 657-665.
92. Salman, M., Cizer, Ö., Pontikes, Y., Vandewalle, L., et al., Carbonation potential of continuous casting stainless steel slag, In: Proceedings of the Fourth International Conference on Accelerated Carbonation for Environmental and Materials Engineering (April 9-12, 2013 Leuven Belgium), 2013, 317-327.
93. Van Mechelen, D., Quaghebeur, M., Evlard, J., Nielsen, P., et al., Development of a pilot plant for mineral carbonation of waste materials, In: Proceedings of the Fourth International Conference on Accelerated Carbonation for Environmental and Materials Engineering (April 9-12, 2013 Leuven Belgium), 2013, 509-511.

94. Baciocchi, R., Costa, G., Morone, M., Polettini, A., et al., Valorization of steel slag by a combined carbonation and granulation treatment, In: Proceedings of the Fourth International Conference on Accelerated Carbonation for Environmental and Materials Engineering (April 9-12, 2013 Leuven Belgium), 2013, 329-338.
95. Gunning, P., Hills, C.D., Carey, P.J., Commercial Application of Accelerated Carbonation: Looking Back at the First Year, In: Proceedings of the Fourth International Conference on Accelerated Carbonation for Environmental and Materials Engineering (April 9-12, 2013 Leuven Belgium), 2013, 185-192.
96. Hills, C.D., Carey, P.J., Production of secondary aggregates, US Patent Application, 2009/0104349 A1, 2009.
97. Gunning, P.J., Hills, C.D., Carey, P.J., Production of lightweight aggregate from industrial waste and carbon dioxide, WASTE MANAGE. 2009, 29, 2722-2728.

3. Process intensification routes for mineral carbonation

ABSTRACT – Mineral carbonation is a realistic route for capture and storage of carbon dioxide. The principal advantages of this approach are the chemical stability and storage safety of mineral carbonates, the opportunities for process integration available, and the potential for conversion of low-value materials into useful products. In this work the valorisation of alkaline waste materials from thermal processes by mineral carbonation utilizing intensified and integrated mineral carbonation routes is explored. Process intensification aims at providing the paradigm-shifting techniques needed to revolutionize the chemical engineering industry in the 21st century, particularly focussing on improvements towards process efficiency, yield and sustainability. The combination of process intensification and process integration strategies has the potential to produce economically feasible and industrially acceptable carbonation technologies that can soon be implemented at large-scale, several examples of which are already proven at the laboratory scale and are herein discussed.

Redrafted from[X]
R.M. Santos, and T. Van Gerven.
"Process intensification routes for mineral carbonation".
Greenhouse Gases: Science and Technology 1(4)*, 2011, 287-293.
*In Focus: Papers from ACEME10 - the Accelerated Carbonation for Environmental and Materials Engineering conference issue.

Author contributions
R.M.S. conceptualized and wrote the article.

[X] Parts added to this chapter, which were not included in the published article, are shown in italic font.

3.1. INTRODUCTION

To overcome the many inefficiencies that current technologies face and the feasibility barriers that hinder the applicability of new technologies, the intensification of processes is an important objective to improve efficiency, cost, and delivery. While the exact definition of process intensification varies, Stankiewicz and Moulijn[1] have put it simply as "any chemical engineering development that leads to a substantially smaller, cleaner, and more energy efficient technology". Process intensification also seeks to bring together fundamental aspects of process engineering technology and to find the most optimum balance between them. In the last decade process intensification has grown and matured; numerous research streams have emerged on solving the most challenging and important technological needs of our time, including the mitigation of greenhouse gases. Herein, intensification routes for mineral carbonation are explored.

Mineral carbonation, as the name suggests, involves the transformation or capture of carbon dioxide in a mineral form. The principal aim and advantage of this approach is the chemical stability and storage safety of mineral carbonates, the opportunities for process integration presented by the technology, and the potential for valorisation of otherwise low-value resources (virgin or waste) into useful products. The main barriers to its deployment in industry, apart from the lack of legislative mandates in place, are one or more of: high energy intensity, low reaction conversion, slow reaction kinetics, complexities of the production chain, process adaptability, and competition for attention with alternative carbon storage technologies. The principal example of the latter is geological sequestration, by means of underground storage in geological formations such as depleted oil and gas fields, saline and basalt formations, and coal seams. It should be noted, however, that mineral carbonation by no means intends to replace the need for geo-sequestration, given the lack of sufficient mineral resources, especially suitable waste by-products, to capture the quantities of CO_2 emitted from industrial sources. It is rather a complementary option, ideal for locations lacking easy access to suitable geological storage sites, or where process integration renders mineral carbonation more economically viable, or where mineral carbonation can contribute to industrial waste stabilization and valorisation.

A number of process challenges limit the successful translation of the theoretical process to industrial scale applications. At the particle level, the three rate limiting steps are: (i) leaching of cations; (ii) solvation and hydration of CO_2; and (iii) diffusion to reaction zone (carbonated shell / depleted matrix). At the reactor level, three more limiting barriers are identified: (a) slow kinetics; (b) energy cost (heating/milling); and (c) mass of material (transport/handling). Numerous parameters are investigated to improve the various routes of mineral carbonation. These include: time, temperature, pressure, CO_2 concentration, pH, liquid-to-solid ratio, leaching agents, particle size, particle crystallinity, particle surface area and agitation. Still, published results over the last 20 years continue to lack the paradigm-shift needed to take mineral carbonation from the laboratory to the field[2]. An engineering catalyst (process intensification) is needed.

The drive to develop carbon capture technologies is centered on the perceived contribution of carbon dioxide emission to global warming due to the enhancement of the greenhouse effect. Kaya[3] has developed an expression that summarizes the factors that lead to anthropogenic CO_2 emissions, called the Kaya Identity and expressed as:

$$CO_2^{\Uparrow} = POP \times \frac{GDP}{POP} \times \frac{BTU}{GDP} \times \frac{CO_2^{\Uparrow}}{BTU} - CO_2^{\Downarrow}$$

In order to reduce CO_2 emissions, one or more of the multipliers on the right-hand-side must be reduced, or the last term must increase. Reducing the population (*POP*) or the standard of living (*GDP/POP*) is unlikely to be considered; on the contrary, these continue to increase as a result of the growth of developing nations. Hence it is necessary to address[4]: (i) energy intensity (*BTU/GDP*; by efficient use of energy); (ii) carbon intensity ($CO_2^{\Uparrow}/BTU$; by switching to non-fossil fuels such as hydrogen and renewable energy); and (iii) carbon capture ($CO_2^{\Downarrow}$; by development of technologies to capture and sequester more CO_2). Process intensification can aid in all three approaches, and in particular (iii) is explored in this work.

3.2. BASICS OF PROCESS INTENSIFICATION AND PROCESS INTEGRATION

Van Gerven and Stankiewicz[5] have categorized Process Intensification (π_1) strategies in four fundamental domains (Figure 3.1: structure, energy, synergy and time), which may take shape of novel equipments and/or processes, and are applied to realize one or more of four objectives (Figure 3.1: i, ii, iii, iv). Each of these objectives can be readily related to the challenges of mineral carbonation. For example, municipal solid waste incinerator bottom ashes are commonly aged (i.e. slowly carbonated) in open-air heaps for months to reduce pH and heavy metal leaching, typically with low success, before being landfilled. In a large heap, not all material is equally exposed to the atmosphere, in fact only the top-most layer does. By moving the heaps occasionally, or by not immediately placing another layer of fresh bottom ash on top of aging ash, it is possible to homogenize the treatment and give the particles more equal experience (point ii).

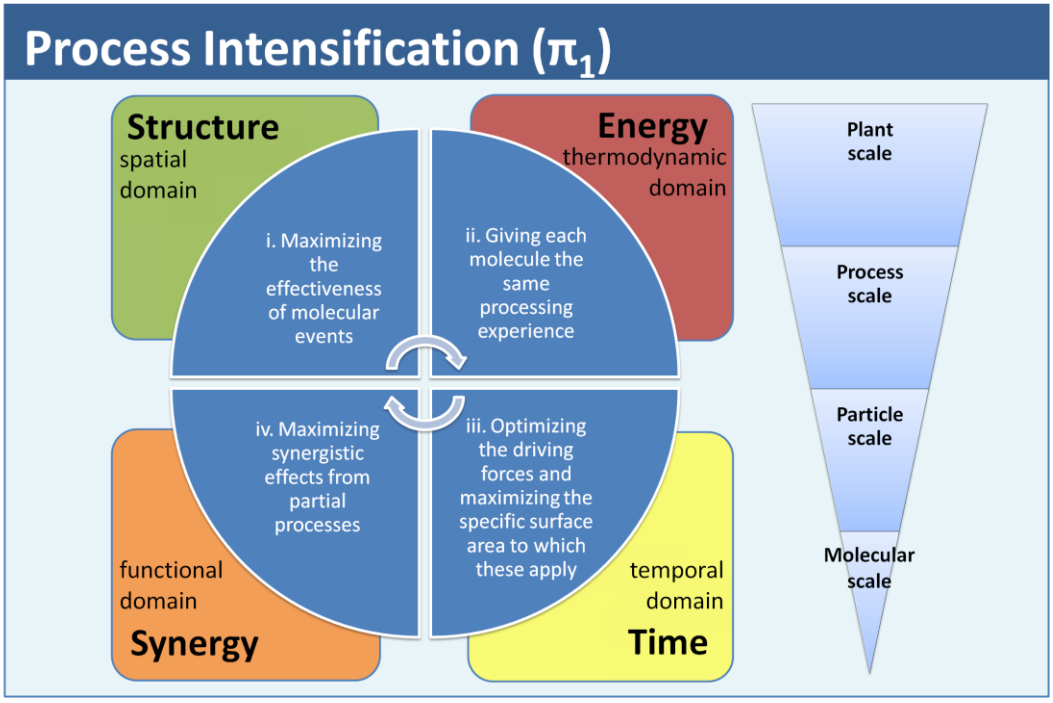

Figure 3.1. Principles of process intensification.

Sustainable use of solid residues and carbon dioxide, the two largest and most important waste products from thermal processes, is an urgent issue both for the industry involved and society as a whole, considering the financial and environmental repercussions of their production. By applying a Process Integration (π_2) approach to mineral carbonation (Figure 3.2), successful routes of waste-to-product valorisation can be developed, including the production of carbon sinks and valorised materials. In combination with intensified processes, the challenging aim of valorising solid materials and carbon dioxide with clear prospects on the economic and legislative feasibility, ecological benefits and societal relevance can be achieved. The combined application of process intensification (π_1) and process integration (π_2) is envisioned to provide the technological leap (π^2) needed to make mineral carbonation industrially feasible, and moreover desirable.

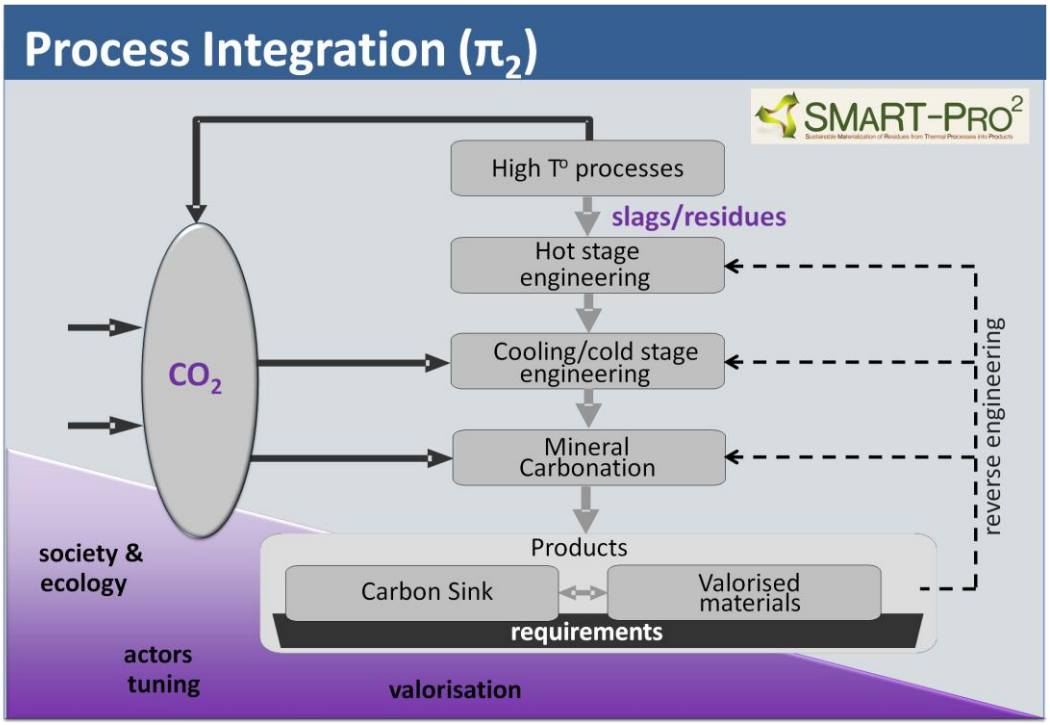

Figure 3.2. Integrated mineral carbonation of thermal residues; a framework of SMaRT-Pro^2.

Next, we present ongoing research routes of the K.U. Leuven's Knowledge Platform on Sustainable Materialisation of Residues from Thermal Processes into Products (SMaRT-Pro^2)[6] on intensified and integrated mineral carbonation (Table 3.1). We investigate the questions of how much and how fast carbon dioxide can be sequestered by alkaline materials (e.g. slag or fly ash), and what are the limiting conditions for process rate and yield. We develop strategies to overcome current process barriers by comparison and optimization of different carbonation strategies, including hot-stage (during material production) and cold-stage (post-production) processes. Localized energy is also used for enhanced diffusion or for abrasion of the particles to obtain new reaction surfaces. For carbonated products, attention is given to the requirements of construction materials with a view to produce building materials in a sustainable way. Possible applications of these new raw materials are: 1) materials replacing natural aggregates in mortar and concrete, in ground stabilization and foundations of roads, in production of building blocks; 2) components that can be integrated in blended cements or binders in general; 3) possible non-structural materials such as thermal insulation material and materials for water barriers, both contributing to the reduction of energy consumption.

Table 3.1. Summary of recent advances made at SMaRT-Pro[2] to overcome mineral carbonation challenges using process intensification strategies.[†]

Work	Challenge	Cause	π^2 Approach	Outcome
François[13]	Carbonation rate and conversion.	Shrinking core, passivating layer.	Sonication.	Particle size reduction, reaction rate improvement.
Ceulemans[14]	Tuned $CaCO_3$ polymorph crystallization.	Calcite thermodynamic stability.	Sonochemistry.	Pure aragonite powder, new crystal morphology.
Vandevelde[18] Santos *et al.*[19]	Stabilization of AOD/CC slags; CO_2 capture.	Mineral disintegration, heavy metal content.	Disintegration = surface area; integrated on-site process.	High carbonation extent, reduced heavy metal leaching.
Ling[21]	Stabilization of BOF slag.	Free lime.	Hot-stage integrated carbonation.	pH and heavy metal leaching reduction.

[†]For more general review of mineral carbonation research status see Zevenhoven *et al.*[2].

3.3. CASE STUDIES

3.3.1. Ultrasound assisted mineral carbonation

Process intensification encompasses a broad range of engineering technologies. Some of the leading areas of development make use of the following technological domains: photocatalysis, magnetic fields, ultrasound, microwaves, and microfluidics. The use of ultrasound in chemical processes, also termed sonochemistry, applies sound waves in the range of 16 to 100 kHz, based on the premise that as frequency is lowered, the power delivered increases. Power is delivered to a solution by inducing cavitation, that is, the formation of small cavities or microbubbles that grow and collapse rapidly. Cavitation generates turbulence/circulation, which enhances mass and heat transfer, both by improving convection mechanisms and by thinning diffusion-limiting boundary layers. The collapsing microbubbles produce high local temperature and pressure and high shear forces. These effects cause solid surface erosion, leading to the removal of passivating layers or to the eventual breakage of particles.

Several works are reported on the use of ultrasound for particle size reduction such as in Lu *et al.*[7] (silica particles), and Isopescu *et al.*[8] (calcium carbonate). Rao *et al.*[9] reported enhancement of carbonation of fluidized bed combustion ash by use of an ultrasound horn, where conversion extent was increased by threefold due to enhanced access of CO_2 to the unreacted lime particle core, originally surrounded by a calcium sulphate shell. López-Periago *et al.*[10] used a sonic bath to increase carbonation conversion of calcium hydroxide (from 65 to 89% over 1 hour) using supercritical CO_2 (13 MPa at 40 ^oC). Different polymorphs of calcium carbonate have been synthesized in the presence of ultrasound. During precipitation of calcium carbonate from supersaturated aqueous solution, Kojima *et al.*[11] observed the promotion of vaterite over calcite under horn sonication (20 and 40 kHz, at room temperature) and the formation of smaller (2 μm compared to 20 μm) particles of calcium carbonate. Zhou *et al.*[12] found pure aragonite to form from $Ca(HCO_3)_2$ solution at 70 ^oC with an ultrasound intensity of 58-99 W at 20 kHz. The high

temperatures and pressures, suitable for aragonite formation, caused by the ultrasound-induced cavitations were attributed to the result.

Ultrasound has been investigated by François[13] (SMaRT-Pro[2]) as a way to promote particle breakage during slurry carbonation, and to remove the carbonated shell or depleted matrix layers that surround the unreacted particle core, thus reducing diffusion limitations and exposing unreacted material to the aqueous phase. Sonication (Hielscher UP200S, 24 kHz, 200 W) was shown to increase the conversion (94% vs. 86% over 25 minutes) and the process kinetics (0.65 vs. 0.59 g-$CaCO_3$/min) of calcium hydroxide carbonation, compared to mechanical stirring. Furthermore, particle size reduction of calcium hydroxide and carbonate powders is significantly greater than of steel slag particles over 30 minutes sonication (Table 3.2). This is likely a result of lower hardness, confirming the premise that sonication can clear the surface of unreacted slag from the rate-limiting coverage of a carbonated shell.

Table 3.2. Particle size reduction by sonication, expressed as Sauter Mean Diameter.

Powder	Original D[3,2] (μm)	Sonicated D[3,2] (μm)	Reduction (%)
$CaCO_3$ <200 μm	5.6	4.8	-14%
$CaCO_3$ 200-500 μm	25.7	6.4	-75%
$Ca(OH)_2$	1.8	0.9	-51%
CC slag <200 μm	2.6	2.5	-5%

Ceulemans[14] (SMaRT-Pro[2]) used ultrasound together with magnesium chloride (as a pseudo-catalyst) to induce the sonochemical formation of aragonite by carbonation of calcium hydroxide. The combined use of these two intensifying approaches permitted pure aragonite formation at 24 °C, substantially lower temperature and higher purity than published in literature.[12,15] The aragonite crystals formed under sonication also exhibited unique crystal morphology (*hubbard squash-like* shape) and reduced particle size. This novel material may have interesting applicability in industry as filler or pigment, as aragonite presents some improved physical and mechanical properties: improved tensile strength, impact strength, glass temperature and decomposition temperature in polymer application; improved brightness, opacity, strength and printability in paper coating application.[16]

A new concept introduced by Ceulemans[14] that can be incorporated into process intensification strategies is called the "surplus of severity"[XI]*. This idea is illustrated in Figure 3.3 for a hypothetical example. Take a process that requires a certain amount of severity (defined as a combination of process conditions like temperature, pressure, reaction time, mixing power, acidity... required to achieve a certain reaction yield or selectivity, for example), valued at 100% (target). A traditional process (e.g. aragonite synthesis) can achieve this by a combination of chemical species used (e.g. $CaCl_2$ and Na_2CO_3, highly soluble compounds), thermal energy applied (e.g. 80°C) and additives ($MgCl_2$ at Mg-to-Ca ratio (MCR) of 3). By applying a new energy source (ultrasound), in combination with a less severe chemical (e.g. $Ca(OH)_2$, cheaper and more readily available than the previous example), an intensified process is achieved. However, in this case, the overall severity is too high (>100%), meaning there is an opportunity for attenuation of process parameters to still achieve the same result (i.e. pure aragonite). Through further process optimization, it is found that at a reduced temperature (30°C), with reduced MCR = 2, and*

[XI] This paragraph and Figure 3.3 were omitted in the published article due to space limitations.

alleviated ultrasound power (60% amplitude), it is still possible to synthesize >99% purity aragonite[14]. The concept of "surplus of severity" is very important to ensure development of intensified technologies remains attractive to industry by not over-intensifying them, which can result, for instance, in less attractive economics.

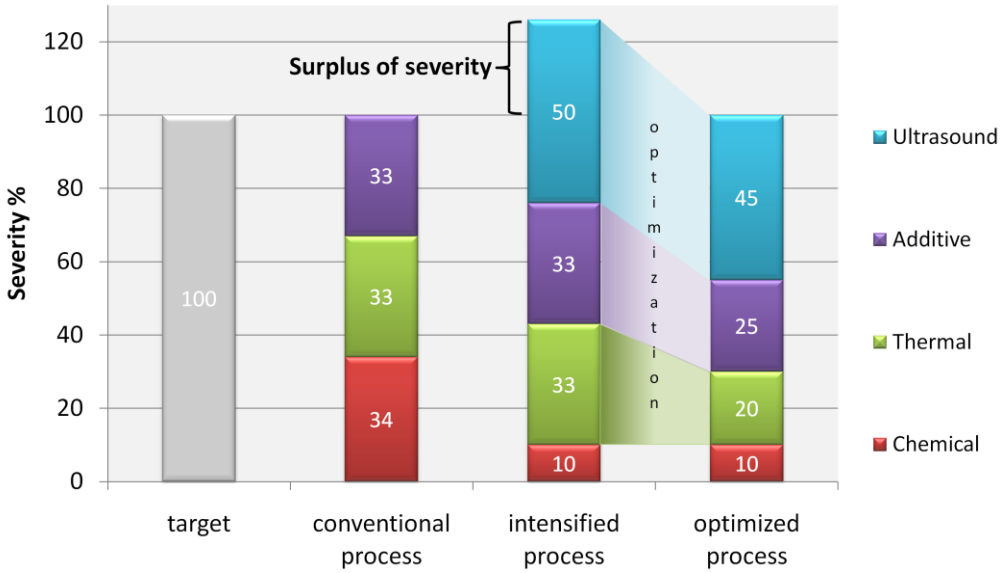

Figure 3.3. *"Surplus of severity" hypothetical sonochemical example (adapted from Ceulemans[14]).*

3.3.2. Intensified carbonation of stainless steel slag

A sustainable solution for the reuse of Argon Oxygen Decarbonisation (AOD) slag, generated in the stainless steel refining step, and Continuous Casting (CC) slag, produced during stainless steel casting, is still to be found. AOD slag exhibits a peculiar disintegration upon cooling due to the phase transformation of β-dicalcium silicate to the more stable, but less dense, γ-dicalcium silicate causing detrimental expansion forces in the material. The slag turns into a fine powder that causes severe dust issues during handling and storage in the steelworks; furthermore the slag in this form cannot be readily re-utilized or valorised, and often must be landfilled. One commonly used solution to avoid this problem is the incorporation of a small amount of doping agent (e.g. B^{3+}) in the crystal structure, which stabilizes the β-phase, and produces a monolith product that has limited industrial application without further processing (e.g. crushing and milling). The boron addition also results in added processing cost and introduces environmental concerns regarding boron leaching. Furthermore, this methodology is not applied to CC slag due to process complexities, and the slag is disposed of in powder form by landfilling. More sustainable solutions leading to more useful products are desired.

One option, applying the principles of process intensification and integration, is to take advantage of the disintegration of AOD slag into a fine powder and apply it in an on-site mineral carbonation process using CO_2-containing flue gases. The increased surface area should lead to increase carbonation reaction rates and conversion, resulting in considerable CO_2 capture capacity (in the order of 0.5 tonne CO_2 per tonne slag) and improved chemical properties (pH and leaching). Baciocchi *et al.*[17] studied the wet carbonation route of boron-free AOD slag (powder), and found maximum CO_2 uptake after 8 hours at 50 ^{o}C, 10 bar CO_2 and 0.4 liquid-to-solid (L/S) ratio. The

differential CO_2 uptake of the aged slag, determined by calcimetry, was about 15 wt%, resulting in 30 wt% overall uptake.

Vandevelde[18] (SMaRT-Pro[2]) studied both boron-free AOD and CC slags (fresh powders) in wet carbonation at very mild conditions. Comparison of carbonation at 30 ^oC and 50 ^oC, 0.1 and 0.2 bar CO_2, and L/S varying from 0 to 0.5, allowed for determination of the optimum process conditions: 30 ^oC, 0.2 bar CO_2, L/S = 0.3. At these conditions, over 6 days, the CO_2 uptake of AOD and CC slags were 11 wt% and 15 wt% respectively, equivalent to 32% and 45% Ca-conversion respectively. Santos *et al.*[19] (SMaRT-Pro[2]) accelerated the process by performing slurry carbonation in a stirred autoclave (Buchi Ecoclave). Over 6 hours, at 60 ^oC and 3 bar CO_2, fresh AOD slag reaches 12 wt% CO_2 uptake (37 % Ca-conversion) and fresh CC slag attains 17 wt% CO_2 (52% Ca-conversion). After 24 hours, CC slag carbonation continues, reaching 21 wt% CO_2 (65% Ca-conversion), likely aided by particle-particle abrasion in the stirred system (1000 rpm), which aids in removing the carbonate passivating layer. This slag as such has been confirmed to be good CO_2 sink and to be susceptible to accelerated carbonation through application of π^2 strategies. Further efforts can still better optimize the process, but a market for the valorised products is yet to be identified.

3.3.3. Intensified carbonation of carbon steel slag

The traditional use of Basic Oxygen Furnace (BOF) steel slag as an aggregate in road construction has been restricted due to the slag's undesirable expansive nature, attributed to the short and long term hydration of free lime (CaO) and magnesium oxide (MgO) content, resulting in rapid deterioration of the roads. To date, four forms of treatment have been widely used to stabilize BOF slag: (i) weathering in slag pits to convert free lime into hydrated lime, which is slow and inefficient; (ii) steam hydration of the slag and (iii) additions of SiO_2 and O_2 (to keep the slag molten) to the slag pot, which are expensive; or (iv) control of slag cooling path to stabilize tri-calcium silicate phase, which is unreliable. A more attractive valorisation option is to take advantage of the waste heat released during BOF slag cooling, which can be used to fuel carbonation at higher temperatures, where the reaction kinetics are more favourable and can stabilize the free lime quickly and with low cost. Mikhail and Turcotte[20] have shown this to be feasible.

Ling[21] (SMaRT-Pro[2]) systematically studied hot-stage carbonation of BOF slag, crushed to particle size between 0.1 and 1.6 mm. Thermodynamic description (FactSage) of the BOF slag shows that of the major mineral phases, both free lime (CaO) and srebrodolskite ($Ca_2Fe_2O_5$) are susceptible to carbonation at up to 880 ^oC and 670 ^oC respectively, at 1 bar CO_2. Optimum carbonation conditions were found to be around 600-700 ^oC, with up to 7 wt% CO_2 uptake achieved in 6 hours for the finest fraction (< 0.5 mm), compared to already 4 wt% CO_2 uptake in only 10 minutes carbonation. Larger particle sizes achieved less carbonation extent, but similar pH reduction (about 1 unit) and heavy metal leaching attenuation (especially Ba, Co and Ni). Vanadium leaching, known to be a problematic element of BOF slag, though presently not regulated in Belgium or Netherlands, increased after carbonation; a solution to this issue is yet to be found. Nonetheless, this hot-stage carbonation routes appears attractive for industrial implementation given the process simplicity (e.g. molten slag granulation combined with fluidized bed reactor), energy efficiency (no external energy supply needed) and in-situ produced waste materials reuse (CO_2 from flue gas and slag).

3.4. CONCLUSIONS

Matching the right alkaline materials with the right mineral carbonation processes is key to overcoming the barriers that prevent this technology from reaching the market; this is the essence of process intensification and integration (π^2). Work at SMaRT-Pro^2 has contributed to the field of mineral carbonation by identifying disintegrated AOD slag as being ideal for slurry carbonation, and BOF slag as being a prime candidate for hot-stage carbonation. In addition, ultrasound has been proven to be a useful tool for intensification of mineral carbonation processes, both as a means of accelerating reaction kinetics and enhancing conversion, and as a promoter of the aragonite polymorph of calcium carbonate for production of unique precipitated crystals. Further optimization of these processes is still required, however with the proof-of-concept now elucidated, it is hoped that soon these technologies will be scaled up, either by academia or industry, or ideally by joint collaboration.

3.5. REFERENCES

1. Stankiewicz AI and Moulijn JA, Process Intensification: Transforming Chemical Engineering. *Chem Eng Prog* **96**(1):22–34 (2000).
2. Zevenhoven R, Fagerlund J and Songok JK, CO_2 mineral sequestration: developments toward large-scale application. *Greenhouse Gas Sci Technol* **1**(1):48–57 (2011).
3. Kaya Y, Impact of Carbon Dioxide Emissions on GNP Growth: Interpretation of Proposed Scenarios. Intergovernmental Panel on Climate Change, Response Strategies Working Group, Geneva (2009).
4. Olajire AA, CO_2 capture and separation technologies for end-of-pipe applications - A review. *Energy* **35**(6):2610–2628 (2010).
5. Van Gerven T and Stankiewicz A, Structure, Energy, Synergy, Time – The Fundamentals of Process Intensification. *Ind Eng Chem Res* **48**(5):2465–2474 (2009).
6. K.U. Leuven Industrial Knowledge Platform on Sustainable Materialization of Residues from Thermal Processes into Products [Online]. Available at: www.smartpro2.eu [August 1, 2011].
7. Lu Y, Riyanto N and Weavers LK, Sonolysis of synthetic sediment particles: particle characteristics affecting particle dissolution and size reduction. *Ultrason Sonochem* **9**(4):181–188 (2002).
8. Isopescu R, Mocioi M, Mihai M, Mateescu C and Dabija G, Modification of precipitated calcium carbonate particle size distribution using ultrasound field. *Rev Chim* **58**(2):246–250 (2007).
9. Rao A, Anthony EJ, Jia L and Macchi A, Carbonation of FBC ash by sonochemical treatment. *Fuel* **86**(16):2603–2615 (2007)
10. López-Periago AM, Pacciani R, García-González C, Vega LF and Domingo C, A breakthrough technique for the preparation of high-yield precipitated calcium carbonate. *J Supercrit Fluids* **52**(3):298–305 (2010).
11. Kojima Y, Yamaguchi K and Nishimiya N, Effect of amplitude and frequency of ultrasonic irradiation on morphological characteristics control of calcium carbonate. *Ultrason Sonochem* **17**(3):617–620 (2010).

12. Zhou GT, Yu JC, Wang XC and Zhang LZ, Sonochemical synthesis of aragonite-type calcium carbonate with different morphologies. *New J Chem* **28**(8):1027–1031 (2004).
13. François D. Ultrasound assisted mineral carbonation [Master's thesis]. Leuven, Belgium: Katholieke Universiteit Leuven; 2010.
14. Ceulemans P. Improved synthesis of aragonite [Master's thesis]. Leuven, Belgium: Katholieke Universiteit Leuven; 2011.
15. Park WK, Ko S-J., Lee SW, Cho K-H, Ahn J-W and Han C, Effects of magnesium chloride and organic additives on the synthesis of aragonite precipitated calcium carbonate. *J Cryst Growth* **310**(10):2593–2601 (2008).
16. Hua Z, Shao M, Cai Q, Ding S, Zhong C, Wei X and Deng Y, Synthesis of needle-like aragonite from limestone in the presence of magnesium chloride. *J Mater Process Technol* **209**(3):1607–1611 (2009).
17. Baciocchi R, Costa G, Di Bartolomeo E, Polettini A and Pomi R, Comparison of different process routes for stainless steel slag carbonation, *Proceedings of the Third International Conference on Accelerated Carbonation for Environmental and Materials Engineering, (ACEME10)*, November 29–December 1, 2010. Turku, pp. 193–202 (2010).
18. Vandevelde E. Mineral Carbonation of Stainless Steel Slag [Master's thesis]. Leuven, Belgium: Katholieke Universiteit Leuven; 2010.
19. Santos R, François D, Vandevelde E, Mertens G, Elsen J and Van Gerven T, Process intensification routes for mineral carbonation, *Proceedings of the Third International Conference on Accelerated Carbonation for Environmental and Materials Engineering, (ACEME10)*, November 29–December 1, 2010. Turku, pp. 13–22 (2010).
20. Mikhail SA and Turcotte AM, Thermal behaviour of basic oxygen furnace waste slag, *Thermochim Acta* **263**:87–94 (1995).
21. Ling D. Thermal stabilization of steelmaking slag through high temperature carbonation treatment [Master's thesis]. Leuven, Belgium: Katholieke Universiteit Leuven; 2011.

4. Ultrasound-intensified mineral carbonation

ABSTRACT – Several aspects of ultrasound-assisted mineral carbonation were investigated in this work. The objectives were to intensify the CO_2 sequestration process to improve reaction kinetics and maximal conversion. Stainless steel slags, derived from the Argon Oxygen Decarburization (AOD) and Continuous Casting / Ladle Metallurgy (CC/LM) refining steps, were used for assessing the technical feasibility of this concept, as they are potential carbon sinks and can benefit from reduction in alkalinity (pH) by mineral carbonation. Ultrasound was applied by use of an ultrasound horn into the reaction slurry, where mineral carbonation reaction took place at 50 ^{o}C for up to four hours; comparison was made to solely mechanically mixed process. It was found that sonication increases the reaction rate after the initial stage, and permits achieving higher carbonate conversion and lower pH. AOD slag conversion increased from 30% to 49%, and pH decreased from 10.6 to 10.1; CC slag conversion increased from 61% to 73% and pH decreased from 10.8 to 9.9. The enhancement effect of ultrasound was attributed to the removal of passivating layers (precipitated calcium carbonate and depleted silica) that surround the unreacted particle core and inhibit mass transfer. Significant particle size reduction was observed for sonicated powders, compared to particle size growth in the case of stirring-only; D[4,3] values increased without sonication by 74% and 50%, and decreased with sonication by 64% and 52%, respectively for AOD and CC slags. Considerations on scale-up of this technology, particularly with regards to energy efficiency, are also discussed.

GRAPHICAL ABSTRACT

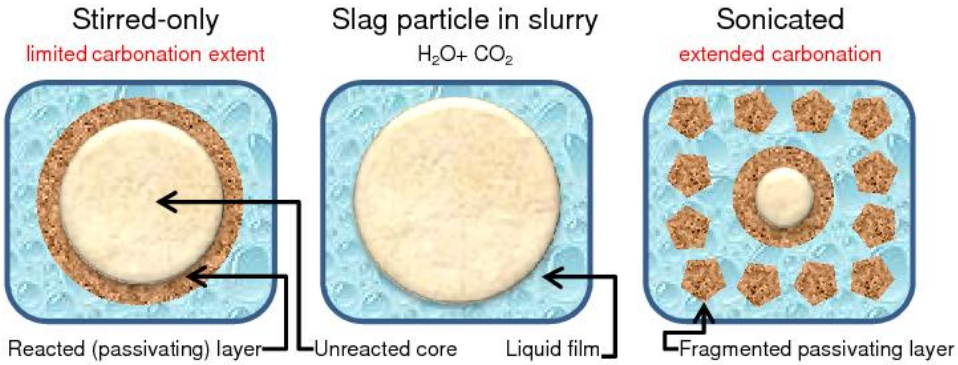

Published as
R.M. Santos, D. François, G. Mertens, J. Elsen, and T. Van Gerven.
"Ultrasound-intensified mineral carbonation".
Applied Thermal Engineering 57(1-2)*, 2013, 154-163.
*Special Issue: Third European Process Intensification Conference.

Author contributions
R.M.S. co-supervised Master's student D. François, performed part of the experimental and analytical work, and wrote the article.

4.1. INTRODUCTION

To overcome inefficiencies faced by current technologies and feasibility barriers that hinder the applicability of new technologies, process intensification (PI) promises to be a key facet of engineering development for years to come. Stankiewicz and Moulijn [1] defined PI as "any chemical engineering development that leads to a substantially smaller, cleaner, and more energy efficient technology". Consequently, process intensification seeks to bring together fundamental aspects of process engineering technology (spatial, thermodynamic, functional, and temporal) and find the most optimum balance between them [2]. In particular, Reay [3] has identified that process intensification offers significant opportunities for reduction of greenhouse gas emissions. With this framework in place, an intensification route for mineral carbonation is explored herein.

Mineral carbonation involves the transformation or capture of carbon dioxide in a mineral form. The principal aims and advantages of this approach are the chemical stability and storage safety of mineral carbonates, the opportunities for process integration offered, and the potential for valorisation of otherwise low-value resources (virgin or waste) into useful products. The main barriers to its deployment in industry are: high energy intensity, slow reaction kinetics, low reaction conversion, complexities of the production chain and process adaptability, and competition for attention with alternative carbon capture technologies [4].

A potential intensification route for mineral carbonation involves the application of ultrasound as a source of focused energy capable of enhancing convective mass transfer, reducing diffusion barriers, activating precipitation sites and controlling crystal growth and morphology [4]. These aspects were studied in the present work in view of enhancing the carbonation of raw materials (calcium oxide) and alkaline waste materials (stainless steel slags), both with respect to conversion extent and pH stabilization.

4.2. BACKGROUND

4.2.1. Mineral carbonation

Mineral carbonation is the reaction of carbon dioxide with alkaline solids. It is a natural process in the global carbon cycle, producing carbonate minerals that are stable over geologic timescales, consequently having potential to sequester carbon dioxide in the effort to reduce greenhouse gas emissions and slow down climate change [5]. The reaction is also important for the production of solid particles in the paper, polymer, environmental protection and fertilizing industries [6,7]. Mineral carbonation can be performed with pure oxides (e.g. CaO, MgO), as well as virgin minerals (e.g. olivine $(Mg,Fe)_2SiO_4$, serpentine $Mg_3Si_2O_5(OH)_4$, wollastonite $CaSiO_3$) and alkaline waste materials (e.g. steel slags [7,8], incinerator and power plant fly ashes [9,10], paper mill waste [11], cement kiln dust [12], air pollution control residue [13], municipal waste incinerator bottom ash [14]). These waste materials can be used for carbonation due to the presence of alkaline oxides, hydroxides and silicates in their composition.

The carbonation process is an example of a gas-solid-liquid system and consists of several steps that can be illustrated in a simple system as follows:[XII]

1. Solvation: $CO_{2(g)} \Leftrightarrow CO_{2(l)}$

[XII] Remark: Steps 1 and 2 can be rate limiting in the carbonation of Ca^{2+} rich solutions, while steps 3 and 4 can be rate limiting during mineral carbonation (i.e. Ca in solid matrix).

2. Reaction: $CO_{2(l)} + H_2O_{(l)} \Leftrightarrow H_2CO_{3(l)} \Leftrightarrow H^+ + HCO_3^- \Leftrightarrow 2H^+ + CO_3^{2-}$
3. Hydration: $CaO_{(s)} + H_2O_{(l)} \Leftrightarrow Ca(OH)_{2(s)}$
4. Ionization: $Ca(OH)_{2(s)} \Leftrightarrow Ca^{2+} + 2OH^-$
5. Precipitation: $Ca^{2+} + 2OH^- + 2H^+ + CO_3^{2-} \Rightarrow CaCO_{3(s)} + 2H_2O_{(l)}$

Kinetics of calcium carbonate precipitation in slurry can be approximated by a pseudo-second-order rate law of the form of Eq. (4.1) [15], where $Conv_{Ca}$ is the percent conversion of calcium from calcium-bearing minerals to calcium carbonate, t is reaction time, and k_p is the rate constant.

$$Conv_{Ca,t} = \frac{Conv_{Ca,\max} \times t}{\left(1/(k_p \times Conv_{Ca,\max})\right) + t} \tag{4.1}$$

A challenge of mineral carbonation reactions is the formation of an increasingly thick and dense carbonate layer surrounding the shrinking unreacted core of the solid particle [8]. This phenomenon, illustrated in Fig. 4.1, creates three rate limiting steps: (i) hydration of oxides/silicates; (ii) leaching of cations; and (iii) diffusion to reaction zone. The result is a limiting of the maximum calcium conversion to calcium carbonate ($Conv_{Ca,max}$, Eq. (4.1)), below 100%.

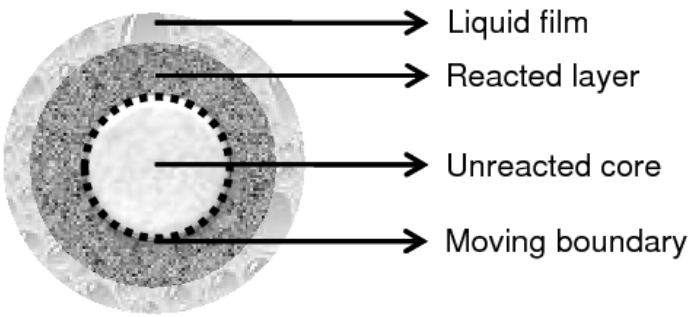

Fig. 4.1. Shrinking core model of wet particle carbonation.

4.2.2. Ultrasound

To intensify the mineral carbonation process, in view of removing diffusion limiting layers and breaking particles, ultrasound was applied in this work. The use of ultrasound in chemical processes, also termed sonochemistry, applies sound waves in the range of 16 to 100 kHz, based on the premise that as frequency is lowered, the power delivered increases. Power is delivered to a solution by inducing cavitation, that is, the formation of small cavities or microbubbles that grow and collapse rapidly. Cavitation generates turbulence/circulation by acoustic streaming, producing fluid flow pattern similar to a jet loop reactor with higher axial velocities than radial velocities; these effects result in enhanced mixing and mass transfer, including dissolution of gases such as CO_2 [16]. The collapsing microbubbles produce high local temperatures, pressures and shear forces, including the formation of microjets. These effects cause solid surface erosion and interparticle collisions, leading to the removal of passivating layers or to the eventual breakage of particles [17].

Several methods exist to induce cavitation, the most common of which use: ultrasound horn, ultrasound bath, or hydrodynamic cavitation. The hydrodynamic method has been found more energy efficient and easier to scale up compared to horns and baths, of which the latter is reportedly more energy efficient due to greater irradiating surface area [18]. Conversely, acoustic equipment

have been found to generate more intense/rigorous cavitation as indicated by greater collapse pressures ($O(10^7\text{-}10^8$ atm)) [18]. Gogate et al. [19] found, by use of a hydrophone to measure collapse pressure as a function of distance from an ultrasound horn tip, that the cavitational field is nonuniform, having spatial variation both in the axial and radial directions. Improvement of acoustic equipment efficiency has been suggested to be possible by geometric reactor configuration optimization, including use of multiple ultrasound transducers and combination of sonication and mechanical mixing [16]. Moreover, several process parameters are known to influence cavitation, both positively and negatively: for example, solids concentrations and gas sparging can contribute to generation of additional nuclei for cavitation, but also cause, respectively, cushioning effect resulting in decreased collapse pressure, and scattering of sound waves decreasing net energy delivery [20].

Ultrasound-mediated particle size reduction has been reported for powders of calcium carbonate [21], silica [22], clay [23], kaolinite [24], and aluminium oxide [25], and on activated sludge [26]. Experimental work is also reported on the use of an ultrasound horn to speed up carbonation and increase conversion. Nishida [27] tested the effect of sonication on the precipitation rate from a supersaturated solution of calcium and carbonate salts ($[Ca^{2+}] + [HCO_3^-]$), Ultrasonic irradiation, proportionally to ultrasound intensity and horn tip diameter, was observed to accelerate the precipitation rate of calcium carbonate, which was optimized as a function of horn immersion depth. The physical mixing effect, macrostreaming, was suggested to cause the enhancement, more so than cavitation induced microstreaming. Morphology and size of calcium carbonate crystals were unaffected. Rao et al. [28] compared stirring versus horn ultrasonic slurry carbonation of fluidized bed combustion ashes. Conversions of CaO were reported to have increased from 23% to 62% at 15 minutes, and from 27% to 83% at 40 minutes. Particle size reduction achieved by sonication was attributed to cause the enhancement, allowing access to unreacted calcium oxide in the ash core. Sonawane et al. [29] passed CO_2 gas through a hole drilled along an ultrasound horn probe into a calcium hydroxide slurry, and found improved mixing and greater reduction of calcium carbonate particle size (from 104 nm to 35 nm), resulting from reduction in induction time (from 110 min to 20 min). López-Periago et al. [30] immersed an autoclave in a sonic bath to improve the carbonation of calcium hydroxide using supercritical carbon dioxide (13 MPa). The conversion to $CaCO_3$ after 60 minutes increased from 50 wt% without agitation, to 65 wt% with mechanical stirring, and 89 wt% with sonication.

4.2.3. Stainless steel slag

A class of waste materials that has good potential for implementation as a feed material for mineral carbonation is steel slags. Treatment and disposal of these slags can be a costly burden on steel plants. Sustainable solutions for the reuse of Argon Oxygen Decarburization (AOD) slag, generated in the stainless steel refining step, and Ladle Metallurgy / Continuous Casting (LM/CC) slag, produced during stainless steel casting, are still to be found. AOD slag exhibits a peculiar disintegration upon cooling due to the phase transformation of β-dicalcium silicate to the more stable, but less dense, γ-dicalcium silicate causing detrimental expansion forces in the material. The slag turns into a fine powder that causes severe dust issues during handling and storage in the steelworks; furthermore the slag in this form cannot be readily re-utilized or valorised, and often must be landfilled. One commonly used solution to avoid this problem is the incorporation of a small amount of doping agent (e.g. B^{3+}) in the crystal structure [31], which stabilizes the β-phase,

producing a monolith product that has limited industrial application without further processing (e.g. crushing and milling). The boron addition also results in added processing cost and introduces environmental concerns regarding boron leaching. Furthermore, this methodology is not applied to CC slag due to process complexities, and the slag is disposed of in powder form by landfilling. More sustainable solutions leading to more useful products are desired. An integrated on-site mineral carbonation approach is envisaged as a possibly economically favorable solution. Boron-free AOD and CC stainless steel slags (in powder form) were used for ultrasound-intensified mineral carbonation in this work.

Baciocchi et al. [32] studied the wet carbonation route of boron-free AOD slag (powder), and found maximum CO_2 uptake after 8 hours at 50 ^oC, 10 bar CO_2 and 0.4 liquid-to-solid (*L/S*) ratio. The CO_2 uptake of the aged slag, determined by calcimetry, was about 30 wt%, equivalent to 70% Ca conversion yield. Vandevelde [33] studied both boron-free AOD and CC slags (fresh powders) in wet carbonation at very mild conditions. Comparison of carbonation at 30 ^oC and 50 ^oC, 0.1 and 0.2 bar CO_2, and *L/S* varying from 0 to 0.5, allowed for determination of the optimum process conditions: 30 ^oC, 0.2 bar CO_2, *L/S* = 0.3. At these conditions, over 6 days, the CO_2 uptake of AOD and CC slags were 11 wt% and 15 wt% respectively, equivalent to 32% and 45% Ca-conversion respectively. Santos et al. [34] accelerated the process by performing slurry carbonation in a stirred autoclave (Buchi Ecoclave). Over 6 hours, at 60 ^oC and 3 bar CO_2, fresh AOD slag reaches 12 wt% CO_2 uptake (37% Ca-conversion) and fresh CC slag attains 17 wt% CO_2 (52% Ca-conversion).

4.3. OBJECTIVES

In view of the available literature on ultrasound-assisted mineral carbonation, the present study identified two main objectives for the intensification of mineral carbonation process:

1-) The effect of ultrasound in reduction of particle size of several powders ($Ca(OH)_2$, $CaCO_3$ and stainless steel slags) was investigated, to confirm the premise that ultrasound is capable of breaking particles and removing passivating layers, in view of permitting faster reaction and greater conversion during aqueous mineral carbonation.

2-) The effect of ultrasound on enhancing the carbonation kinetics and conversion of CaO, AOD and CC stainless steel slags was investigated by comparison of combined sonicated-stirred slurry process to stirred-only process. CO_2 uptake and pH reduction of carbonated materials were assessed.

4.4. MATERIALS AND METHODS

For sonication an ultrasonic processor Hielscher UP200S was used, which operates at 24 kHz frequency. The probe used was an S14 sonotrode, which has a tip diameter of 14 mm, maximal amplitude of 125 µm, and an acoustic power density of 105 W/cm². A PT100 temperature sensor is also connected to the device. Experiments in slurry were conducted using a common glass beaker with a volume of two liters and diameter of approximately 14 cm; the beaker was filled with one liter of distilled water, which reached a height of 7.5 cm. Typical experiments were performed with 10 g of solids (this concentration was chosen to ensure that CO_2 solubility would not become a rate limiting factor under atmospheric conditions, as with higher solids loading the global rate of CO_2 uptake ($mmol_{CO2} \cdot L^{-1}$) would be higher, at least initially). The suspension was mixed solely with a mechanical stirrer (Heidolph type RZ-R1) and straight blade impeller at 340 rpm for stirred

experiments, and in combination with the ultrasound horn during sonication experiments. Carbon dioxide gas was delivered to the solution from a compressed gas cylinder with flow controlled by a Brooks Sho-rate rotameter (R-2-15-AAA) and introduced into the slurry at 0.24 L/min using an aeration stone, which delivered finely dispersed gas bubbles. Temperature was controlled by use of a hot plate (IKAMAG RCT) for heating (in the case of stirred experiments) and water bath for cooling (in the case of sonicated experiments, since ultrasound produces heat, which must be dissipated to maintain a constant temperature). A temperature of 50 ^{o}C was maintained for carbonation experiments.

The following analytical grade materials were used in this study: CaO, $Ca(OH)_2$, $CaCO_3$ (Acros Organics), industrial grade CO_2 ≥99.5% (Praxair). Boron-free AOD and CC stainless steel slag powders were sieved to obtain the 63-200 μm fraction, which corresponded to 56% and 75% of the total slag masses, respectively. This fraction was chosen as the fines (<63 μm) are less susceptible to the shrinking core barrier that hinders carbonation conversion, and the coarse fraction represents a small mass proportion (<6%) that is less susceptible to extensive carbonation. The chemical composition of the slags was determined by X-ray Fluorescence (XRF, Panalytical PW2400) and is presented in Table 4.1. It can be inferred from the calcium content of the slags that the maximum theoretical CO_2 uptake (mass fraction of calcium carbonate) of a fully carbonated specimen would be 30.9 wt% CO_2 for AOD slag, 29.0 wt% CO_2 for CC slag; in comparison pure CaO has a maximum uptake capacity of 44.0 wt% CO_2.

Table 4.1. Elemental composition of AOD and CC slags determined by XRF.

Elements (wt%)	Ca	Si	Mg	Cr	Al	Mn	Ti	Fe	S	V
AOD slag	40.6	15.2	4.2	0.53	0.53	0.33	0.21	0.17	0.16	0.02
CC slag	37.2	12.9	6.0	3.7	0.56	0.43	0.55	0.93	0.32	0.06

The mineral composition of the slags was determined by X-ray Diffraction (XRD, Philips PW1830) with peak analysis done in EVA (Bruker) software and mineral quantification performed using the Rietveld refinement method. Table 4.2 shows the interpreted mineral composition. The main mineral phase of both AOD and CC slags is gamma-dicalcium-silicate (γ-C_2S, Ca_2SiO_4), of which the latter contains significantly greater amount. AOD slag notably contains greater quantities of bredigite ($Ca_{14}Mg_2(SiO_4)_8$), cuspidine ($Ca_4Si_2O_7(F,OH)_2$), β-C_2S (Ca_2SiO_4), and åkermanite ($Ca_2MgSi_2O_7$), while CC slag possesses more periclase (MgO) and portlandite ($Ca(OH)_2$).

Table 4.2. Mineral composition of AOD and CC slags determined by XRD.

Mineral	Chemical formula	AOD slag	CC slag
γ-C_2S	Ca_2SiO_4	28.9	47.4
Bredigite	$Ca_{14}Mg_2(SiO_4)_8$	24.5	5.2
Cuspidine	$Ca_4Si_2O_7(F,OH)_2$	13.9	9.3
β-C_2S	Ca_2SiO_4	8.2	4.0
Merwinite	$Ca_3Mg(SiO_4)_2$	7.3	6.6
Periclase	MgO	6.2	15.5
Åkermanite	$Ca_2MgSi_2O_7$	2.8	0.5
Gehlenite	$Ca_2Al_2SiO_7$	2.7	1.1
Hibonite	$CaAl_{12}O_{19}$	2.5	2.8
Quartz	SiO_2	1.1	0.2
Portlandite	$Ca(OH)_2$	1.1	2.3
Magnetite	Fe_3O_4	0.5	3.4
Lime	CaO	0.3	-
Fayalite magnesian	$(Fe,Mg)_2SiO_4$	-	1.7

Particle size analysis of powder samples was determined by laser diffraction (Malvern Mastersizer). Morphological assessment was performed by imaging with a scanning electron microscope (SEM, Philips XL30 FEG). Carbonation efficiency was quantified by Thermal Gravimetrical Analysis (TGA, Thermo Scientific). An amount of 20-100 mg carbonated slag was weighed in a sample pan heated from 25 to 900 ^oC under a nitrogen atmosphere at a heating rate of 15 ^oC/min. The weight loss was recorded by the TGA microbalance and the amount of CO_2 uptake (wt%) was quantified by the ratio of weight loss between 500-800 ^oC (attributable to $CaCO_3$ decomposition to $CaO_{(s)}$ + $CO_{2(g)}$), over the carbonated sample mass at 500 ^oC (to eliminate any mass gain due to hydration/hydroxylation). Carbonation efficiency was defined as the ratio of actual CO_2 uptake over theoretical CO_2 uptake by the calcium content of the sample. Carbonation of the magnesium content of the slags was disregarded in the present study as the decomposition of magnesium carbonate at temperatures lower than 500 ^oC from TGA measurement is not clearly discernable, due to small conversions of MgO and Mg-silicates at the utilized process conditions, in agreement with results reported by Back et al. [35], and overlap with hydrates and meta-stable carbonates that may form during aqueous carbonation.

4.5. RESULTS AND DISCUSSION

4.5.1. Optimization of horn sonication by calorimetry

In order to optimally position the ultrasound horn in the present system (beaker with liquid slurry), in view of delivering constant, stable and maximal power sonication, experiments were performed to investigate the effect of probe depth and radial position. The ultrasound probe was immersed at several depths (defined as the distance from the probe tip to the air-water interface, ranging from 1 to 7 cm) into 1 liter water at the radial center position of the 2 liter volume beaker, and sonication was performed for 25 minutes. Similarly, to assess the effect of radial position, the probe was placed 2.5 cm from the beaker wall (compared to 7 cm in the case of centrally positioned probe), maintaining a depth of 2 cm for comparison. Sonication effect was measured by

calorimetry, that is, the solution temperature increase over time. In this case the beaker was not immersed in the water bath, so that the temperature could rise freely (except for heat loss due to natural convection to the environment and conduction to the laboratory counter).

Fig. 4.2 presents calorimetry results as a function of probe tip position. A progressive increase in temperature change over time is seen as the depth increases from 1 cm to 5 cm. At 6 cm, a retardation effect is seen, where the temperature takes longer to reach similar values as those for 4-5 cm. At 7 cm depth the temperature change is significantly hampered, indicating that the small distance of the tip to the beaker bottom (0.5 cm) is detrimental to sonication performance. The effect of radial position, on the other hand, is negligible: outer placement of the probe results only in a minor drop in temperature change. It is concluded from these results that a depth of 4.5 cm is optimal for the present system. The small effect of radial position signifies that co-placement of the ultrasound horn and mechanical mixer in the beaker, as done for the remaining experiments, has no detrimental effect on sonication performance.

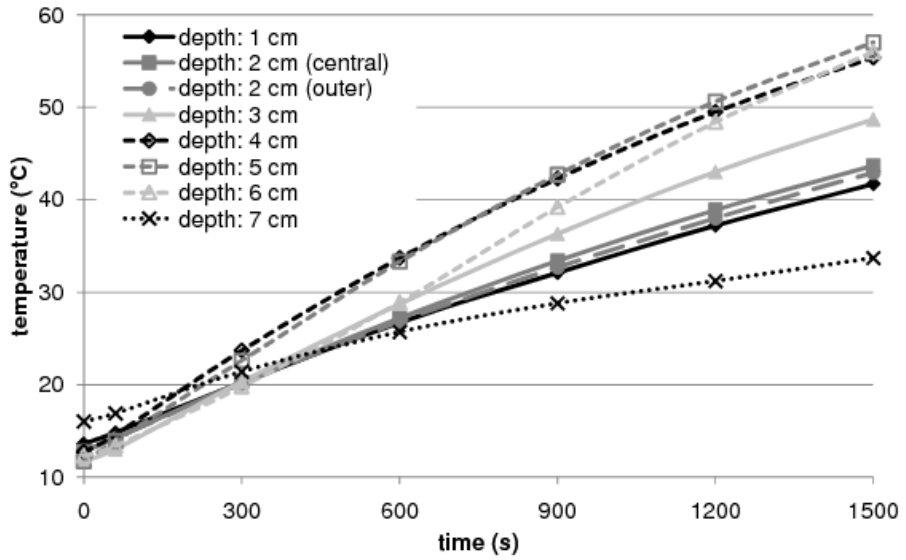

Fig. 4.2. Effect of ultrasound probe axial and radial placement on sonication calorimetry.

Calorimetry results can also be used to estimate ultrasound efficiency, assuming temperature change is solely due to the implosion of cavitations generated by the probe (Table 4.3 shows that stirred unheated system does not yield significant temperature change). Using Eqs. (4.2) and (4.3), the thermal power delivered to the solution (P) and the ultrasound efficiency (η) can be determined. The temperature gradient is taken near the beginning of sonication to eliminate attenuation caused by heat loss to the environment. Using a temperature gradient of 11.5 ^{o}C during the first 400 s (Fig. 4.2, depth = 4 cm), or 0.02875 ^{o}C/s, the power delivered equals 120.2 W. Taking the net power of the ultrasound horn (Φ, calculated by Hielscher software based on gross electrical power consumed and resistance the probe experiences from the medium it is immersed in; i.e. in air equals zero) equal to 204.4 W (in the case of 0 g/l solids), the sonication efficiency equals 59%. In the presence of solids, the net power decreases, yet the temperature change and initial slope (not shown) remain the same. As a result, ultrasound efficiency increases to 72%. The decreased net power is evidence of the cushioning effect and scattering of sound waves described by Gogate et al. [19], while the increased efficiency agrees with their supposition that solids act as nuclei for cavitation formation, but could also be due to heat generation by interparticle attrition.

$$P = m \cdot c_p \cdot dT/dt \qquad (4.2)^{XIII}$$

$$\eta = \frac{P}{\Phi} \qquad (4.3)^{XIV}$$

Table 4.3. Effect of solids content of sonicated (60 min) slurry on ultrasound net power delivered and calorimetry.

Mixing method	stirred	sonicated	sonicated	sonicated	sonicated
Solids content (g/l)	0	0	10	20	50
Avg. net power Φ (W)	-	204.4	173.1	166.9	166.8
ΔT (^{o}C)	0.6	39.9	40.6	40.1	40.1

4.5.2. Effect of sonication on particle size

The carbonation reaction can be enhanced by the use of small particles which have a large surface to volume ratio. This large surface area enhances the hydration and dissolution rate of the calcium oxides and silicates and allows carbonate ions to react immediately without having to diffuse into the solid particle. Sonication was tested as a means of reducing the particle size of four powder materials: AOD and CC slags, calcium hydroxide and ground calcium carbonate (sieved to <200 μm). Experiments were performed with 10 g of solids in 1 liter water, and ultrasound application for 30 minutes. The evolution of the volume-based particle size distributions by the use of ultrasound is shown in Fig. 4.3. The y-axis is plotted in unconventional logarithmic scale for easier visualization of the distribution shifts to smaller particle sizes.

[XIII] c_p = specific heat capacity.

[XIV] Remark: Given that η is the ultrasound efficiency, and P is the sonication power, $(1 - \eta) \cdot P$ is component of the net horn power Φ that ends up as heat loss to the environment and that acts as mixing power. This non-sonication component equals to about 52.9 W (173.1 minus 120.2). The mechanical mixer used delivered less than 1 W of mixing power (assuming a turbulent power number (N_p) of 2.5, typical for Rushton turbines). Seeing that ultrasound alone was found insufficient to suspend the heavier slag particles (that is, its flow-induced macromixing effect is poor), it can be concluded that much of the ultrasound power that is neither used to produce sonication cavitities nor is lost to the environment, likely drives micromixing effects, such as enhanced molecular diffusion. This is therefore a further benefit of sonication over conventional mixing, which delivers primarily macromixing.

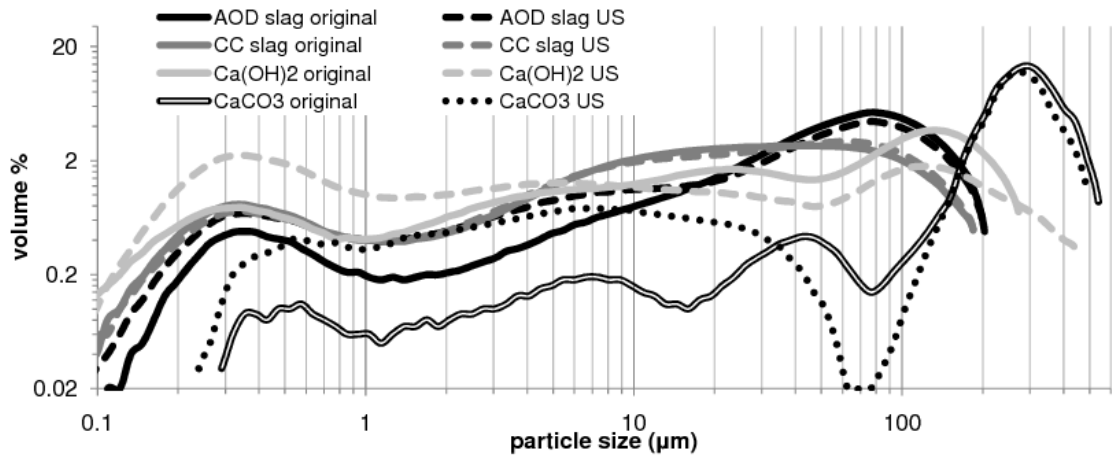

Fig. 4.3. Particle size distributions of original and sonicated (30 min) powders of AOD and CC slags, $Ca(OH)_2$ and $CaCO_3$.

Comparison of the AOD slag particle size distributions before (original) and after (US) sonication shows that ultrasound produces a significant amount of particles of a broad range below 15 µm; these small particles are likely a result of erosion of the original large particles in the size range 20-200 µm. In the case of CC slag, the particle size distribution appears to be unaffected by sonication. Different material mechanical properties such as hardness, toughness, brittleness and ductility, due to somewhat different chemical and mineralogical compositions may be responsible for this. Calcium hydroxide particle size distribution shifts significantly towards smaller values; as $Ca(OH)_2$ is a hydrated mineral, it can be subject to disordered crystal growth and agglomeration during fabrication, and thus it may be easily deagglomerated/fragmented by sonication, compared to dense slag particles.[XV] Ground calcium carbonate powder experiences substantial reduction in quantity of particles ranging from 40 to 150 µm, and a substantial increase in particles smaller than 40 µm; the perfect rhombohedral cleavage planes of calcite make it a favorable material for fragmentation by sonication/attrition. This result suggests that sonication can remove calcium carbonate layers that precipitate on the surface of slag particles during aqueous carbonation.

Table 4.4 presents the corresponding average particle sizes to the distributions in Fig. 4.3. Given are the volume mean diameter (D_{50}), the volume moment mean diameter (D[4,3]), and the surface area moment mean diameter (D[3,2]). The latter is particularly interesting for mineral carbonation as it relates to the active surface area of the material, which is primarily important for susceptibility towards carbonation. With the exception of $Ca(OH)_2$, the reduction in D[3,2] value surpasses those of the other two averages, indicating that particle surface erosion is the predominant consequence of sonication, as opposed to whole particle breakage. This furthermore emphasizes how sonication can be an ideal tool for reducing the rate/conversion limiting layers (carbonate and depleted silica) that form during mineral carbonation.

[XV] Remark: The greater solubility of portlandite over calcite in water ($1.98 \cdot 10^{-2}$ versus $1.19 \cdot 10^{-4}$ molal at 20 °C (Visual MINTEQ)) may also influence the change in particle size distribution observed.

Table 4.4. Average particle sizes of original and sonicated (30 min) powders of AOD and CC slags, $Ca(OH)_2$ and $CaCO_3$.

AOD slag (μm)				$Ca(OH)_2$ (μm)			
	Original	Sonicated	Reduction		Original	Sonicated	Reduction
D_{50}	52.5	41.1	-22%	D_{50}	29.7	5.2	-83%
D[4,3]	58.4	49.8	-15%	D[4,3]	60.7	43.2	-29%
D[3,2]	4.4	2.7	-39%	D[3,2]	1.8	0.9	-51%
CC slag (μm)				$CaCO_3$ (μm)			
	Original	Sonicated	Reduction		Original	Sonicated	Reduction
D_{50}	19.2	21.2	-	D_{50}	266.0	233.8	-12%
D[4,3]	33.0	35.4	-	D[4,3]	236.9	204.0	-14%
D[3,2]	2.6	2.5	-5%	D[3,2]	25.7	6.4	-75%

4.5.3. Effect of sonication on carbonation

Carbonation tests were conducted in slurries of CaO, AOD slag and CC slag using mechanical stirring alone and mechanical stirring combined with ultrasound (US). Process conditions were 10g solids in 1 liter solution at 50 ^{o}C. Carbonation tests were conducted for varying times, from 15 minutes to four hours to obtain information on carbonation kinetics and maximal achievable carbonation conversions. The comparison of sonication with mechanical stirring is made by quantifying the CO_2 uptake of the carbonated solids by thermogravimetric analysis (TGA), and expressing the results as percent calcium conversion to carbonate.

Fig. 4.4 presents carbonation data for the three materials tested. Data points are fitted to the pseudo-second order model equation (Eq. (4.1)), and corresponding coefficients are given in Table 4.5. For all three materials, sonicated carbonation achieves greater carbonation conversions as a function of time, particularly after 30 minutes of reaction, when the formation of rate-reducing carbonate and depleted-silica shells becomes more extensive. Maximal carbonation conversions with ultrasound are also higher for the three materials, an indication that sonication removes the conversion-limiting layers, permitting easier leaching of calcium ions from the unreacted particle core for reaction with carbonate ions. AOD carbonation conversion after four hours with sonication increased by 59%, from 30.5% to 48.5%; CC carbonation conversion, which were comparatively higher than AOD, likely as a result of more favorable mineralogy (e.g. greater γ-C_2S content), increased by a more modest 19%, from 61.6% to 73.2%. Maximal estimated conversions, described by the $Conv_{Ca,max}$ coefficients in Table 4.5, also follow similar trends.

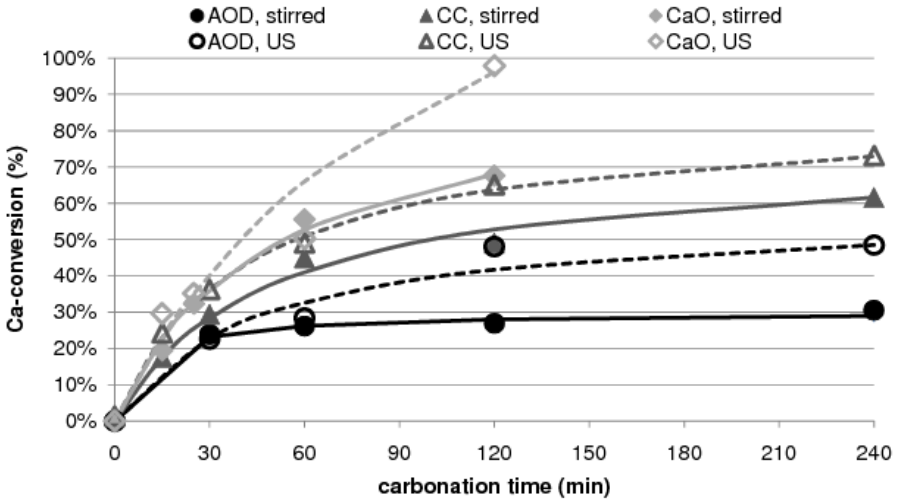

Fig. 4.4. Comparison of calcium carbonation conversion of AOD and CC slags and CaO for stirred and sonicated processes as a function of time; lines denote fitted pseudo-second order models (Eq. (4.1), coefficients given in Table 4.5).

Table 4.5. Fitted pseudo-second order model (Eq. (4.1)) coefficients for stirred and sonicated carbonation of AOD and CC slags and CaO.

	AOD Stirred	AOD US	CC Stirred	CC US	CaO Stirred	CaO US
$Conv_{Ca,max}$	30.1%	58.0%	74.0%	85.3%	96.2%	*
k_p (min^{-1})	0.3715	0.0368	0.0279	0.0290	0.0211	*

* does not follow pseudo-second order model.

In the case of CaO, carbonation was faster, with the ultrasound-intensified process reaching near completion (97.9%) after two hours, compared to 67.6% conversion with mechanical mixing alone. In the case of sonicated CaO carbonation, the kinetics trend no longer follows a pseudo second order model after one hour of carbonation, hence model coefficients were not calculated. For confirmation of suitability of the present process conditions (temperature, CO_2 flow rate, vessel geometry, and stirring speed) for studying carbonation kinetics and conversion, the carbonation rate of CaO during the first 30 minutes of reaction (when the reaction can be assumed to be driven solely by chemical kinetics and not impeded by mass transfer effects) was compared to values reported by Back et al. [35]. In the present work the initial carbonation rate, both with and without sonication, is calculated to be approximately 0.020 $mmol_{CO2} \cdot s^{-1} \cdot L^{-1}$, which matches the average carbonation rate over the initial 30 minutes reported by Back et al. [35] under similar process conditions.

The large content of alkaline minerals in stainless steel slags contributes to its high pH when in solution. High pH is an environmental hazard for slag disposal or reutilization, as it leads to leaching of several heavy metals from the untreated slags (e.g. Cr, Cu, Mo, Ni, Pb, Zn). Carbonation has been shown to lead to reduction of pH and lowering of heavy metal leaching [34,36]. Fig. 4.5 (top) shows the effect of carbonation time on slurry pH of AOD and CC slags for the cases of sonication and mechanical mixing. Carbonated solids were filtered (589/3 filter paper) and oven dried at 105 ^oC for four hours; subsequently two grams of dried powder was added to 100 ml of ultra-pure water in a sealed bottle, agitated for two hours, and pH of the solution was measured. Original pH values of AOD and CC slags, prior to carbonation, were 11.4 and 12.3

respectively. For reactions executed for up to 60 minutes no difference in pH behavior is observed when comparing the cases with and without sonication; pH reduction of 0.3 and 0.9 units is obtained with carbonation of AOD and CC slags, respectively. At two hours of reaction time, no further pH reduction is observed in the case of stirring, but significant pH drops are obtained with sonication: 0.5 and 1.5 pH units further reductions for AOD and CC slags respectively. At four hours, pH values drop for both stirring and sonication, but sonicated samples continue to exhibit significantly lower pH: a difference of 0.5 and 0.9 pH units for AOD and CC slags respectively. In fact, the pH of CC slag is identical to the theoretical pH value of pure $CaCO_3$ (9.91, unsaturated with respect to CO_2, Visual MINTEQ), and AOD slag is only slightly higher.

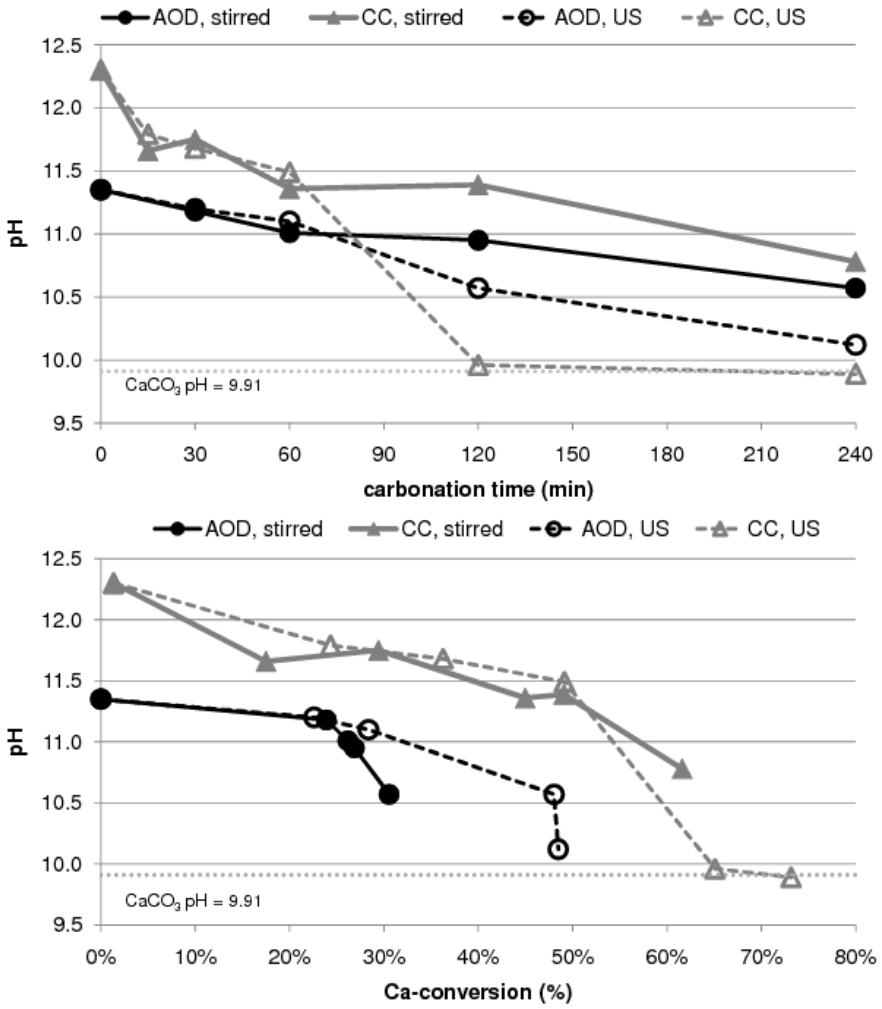

Fig. 4.5. Comparison of effect of carbonation time (top) and calcium carbonation conversion (bottom) of AOD and CC slags for stirred and sonicated processes on carbonated powder slurry pH.

Plotting carbonation conversion versus pH (Fig. 4.5 bottom), it is possible to indirectly assess the effect of sonication on the removal of passivating layers. The removal of passivating layers would be expected, in theory and according to the shrinking core model, to expose the highly alkaline unreacted particle core to the solution, thereby maintaining the pH higher despite carbonation conversion. The results indicate that in the case of CC slag the calcium carbonate layer that forms on carbonated slag under mechanical mixing alone is not sufficient to completely shell the unreacted particle core, since the stirred and sonicated trends overlap. Furthermore, it demonstrates that the removal of the rate/conversion limiting layers (calcium carbonate and

depleted silica) upon sonication is not necessarily detrimental to pH. At similar conversions (e.g. 50%) the pH of both stirred and sonicated samples are identical. In the case of AOD slag, it appears that the stirred carbonated slag reaches lower values of pH at lower carbonation conversion (30%), suggesting that its passivating layers are more effective in shielding the unreacted core. Nonetheless, the greater carbonation conversion achieved with sonication for the same carbonation times (2-4 hours) still demonstrate the benefit of utilizing sonication.

With a view of reducing ultrasound use, for energy conservation, it was tested whether reducing the ultrasound application time by one third could still produce as high levels of carbonation conversion, and as low pH values, as constant (100%) ultrasound application. Fig. 4.6 presents both sets of data for four cases: (i) mechanical stirring alone, (ii) mechanical stirring combined with 100% ultrasound application, (iii) mechanical stirring combined with ultrasound application for 5 minutes every 15 minutes of reaction time (equivalent to 33% US application), and (iv) mechanical stirring combined with constant ultrasound application at 0.33 cycling (c) time (equivalent to 33% US application). Cycling refers to the fraction of experimental time during which sonication is applied, with sonication being pulsed on and off in short time intervals by an internal ultrasound horn setting. Carbonation experiments were conducted for two hours with CC slag. It can be seen from the figure that reducing ultrasound application leads to lower carbonation conversions than the constant US application case, but still better than mechanical stirring alone. Similarly, the pH values are higher when US application is decreased. In both instances, cycling US application over longer time periods (5/15 min) produced better results than the pulsed cycling (c = 0.33). It may be that the passivating layers are better removed by sonication when they acquire a certain minimum thickness, thereby being flaked off by cavitation implosions, microjects and interparticle collisions in near-micron-sized pieces. This would signify that prolonged, more thorough cleansing of the carbonated particle surface is more beneficial than more frequent but less efficient refreshment of the surface.

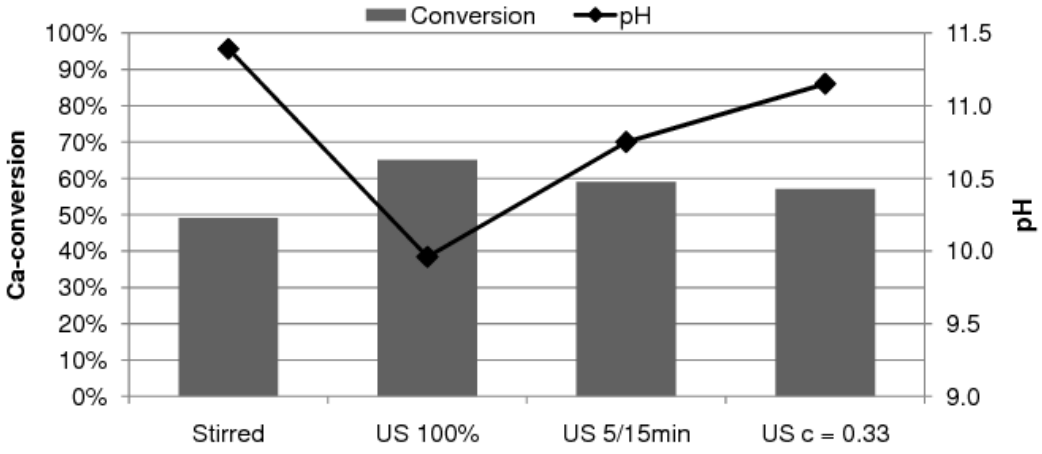

Fig. 4.6. Effect of sonication conditions (US 100% – constant US application; US 5/15min – five minutes US application every 15 minutes experiment time; US c = 0.33 – US application at 0.33 cycling time) on calcium carbonation conversion and carbonated powder slurry pH of CC slag; carbonation time = 120 min.

The effect of sonication on passivating layer removal from the surface of carbonated slag particles was further elucidated by measurement of particle size distributions and imaging of particle morphology. Fig. 4.7 shows volume-based particle size distributions of AOD and CC slag

before carbonation (original) and after four hours of carbonation with (US) and without (stirred) sonication. For both slags similar shifts in particle size distributions take place. With stirring, the particle size distributions shift to larger particles; in fact not only does it appear that large (10-100 μm) particles grow, it also appears that the amount of particles smaller than 10 μm decreases significantly, signifying that agglomeration/joining of carbonated particles takes place. In the case of sonication, the effect is opposite: particle size distributions shift to smaller sizes, with clearly distinguishable creation of particles in the 0.2-1 μm and 2-10 μm ranges, and reduction in the fraction greater than 10 μm. It can be theorized that the smallest particles (0.2-1 μm) are formed by flaking of passivating layers, and the second mode (2-10 μm) is formed by fragmentation of slag particles and/or are the eroded remains of once larger slag particles.

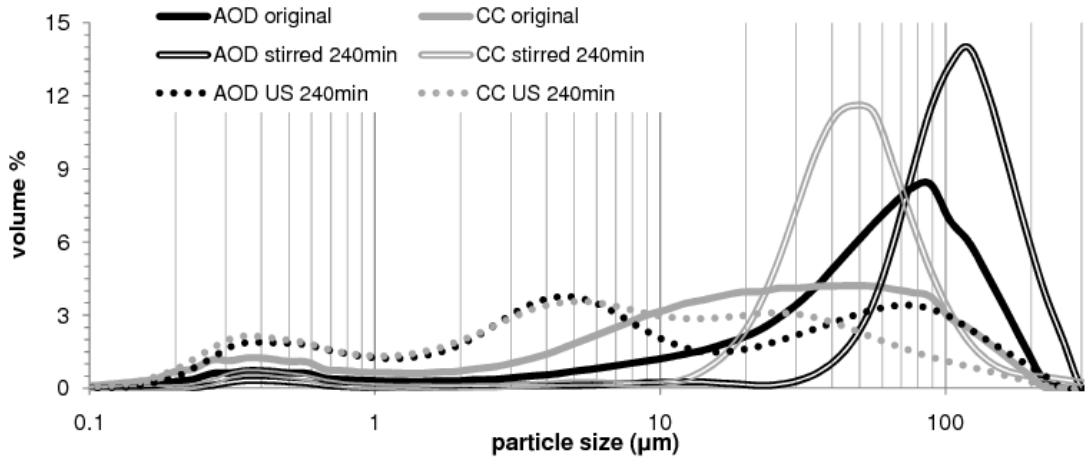

Fig. 4.7. Particle size distributions of original and carbonated (240 min) powders of AOD and CC slags.

Fig. 4.8 presents the average particles sizes of slag samples before and after carbonation as a function of reaction time. In the case of AOD slag under stirred carbonation, average particle sizes significantly increase after already 30 minutes of carbonation; only D[3,2] increases further with reaction time. This is in line with the fact that AOD carbonation with stirring reaches nearly maximum conversion in the first 30 minutes (Fig. 4.4); afterwards increase in D[3,2] likely signifies aggregation of smaller particles with the larger ones. With sonication, however, average particle sizes progressively decrease as a function of time, indicating the continuing effect of ultrasound abrasion/milling. In the case of CC slag carbonation, average particle sizes progressively decrease and increase with and without sonication, respectively. It is interesting to note that CC particle size already clearly reduces after only 30 minutes of sonicated carbonation, when in the case of non-reacting sonication the particle size did not change (Table 4.4). This is suggestive that sonication not only removes the precipitated calcium carbonate layer, but also the depleted silica layer that once constituted the original slag particle material, and that this depleted silica layer is weaker than the original silicate material.

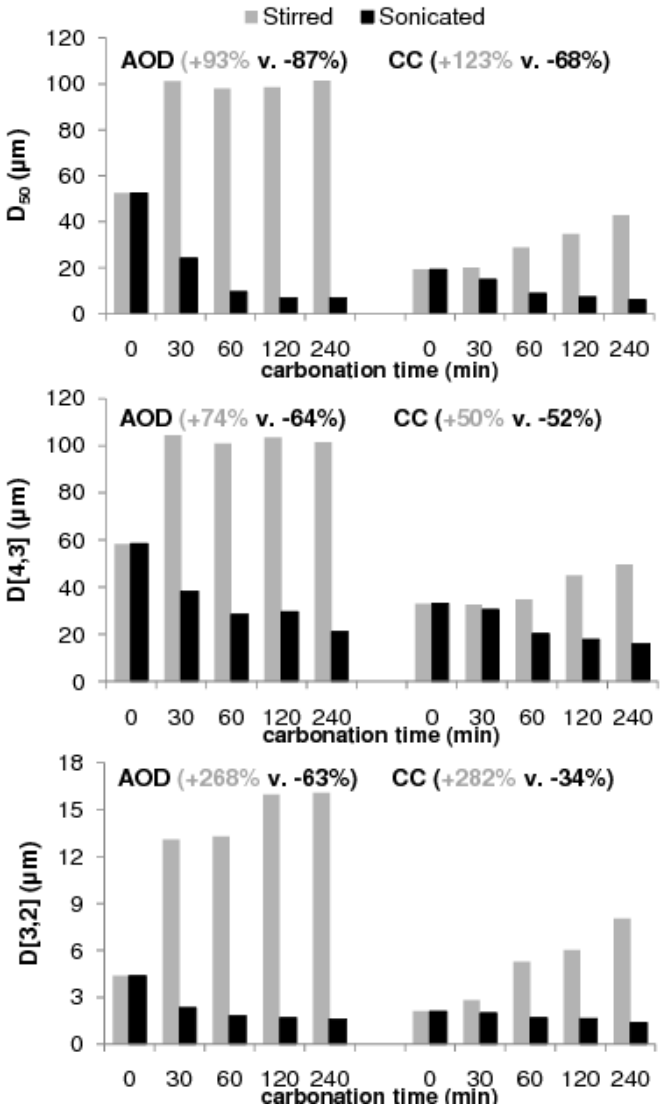

Fig. 4.8. Average particle sizes of AOD and CC slags as a function of carbonation time with stirred and sonicated carbonation; percentage values indicate increase or decrease figures over four hours carbonation.

The morphology of CC slag particles prior and subsequent to carbonation is illustrated in Fig. 4.9. As already indicated by particle size distributions, a clear distinction is seen between stirred and sonicated carbonation, and in relation to the original uncarbonated sample. In the case of stirred carbonation, the absence of particles smaller than 20 µm is confirmed, and the envelopment of slag particles in thick calcium carbonate layers, composed of rhombohedral calcite crystals, is validated. On the other hand, the sample subjected to sonicated carbonation exhibits distinguishably different morphology, being composed mainly of much smaller particles. Two modes are visible, in agreement with laser diffraction results: flaky sub-micron particles, and rounded particles roughly 2-10 µm in size. It would appear that these rounded particles are remnants of larger particles that have been significantly eroded over time and/or particles whose rugged corners have been polished by sonication. These results substantiate the supposition that ultrasound is capable of removal of passivating layers and exposure of unreacted particle core to the reacting solution, overcoming the rate/conversion limiting shrinking core phenomenon and contributing to the intensification of the mineral carbonation reaction.

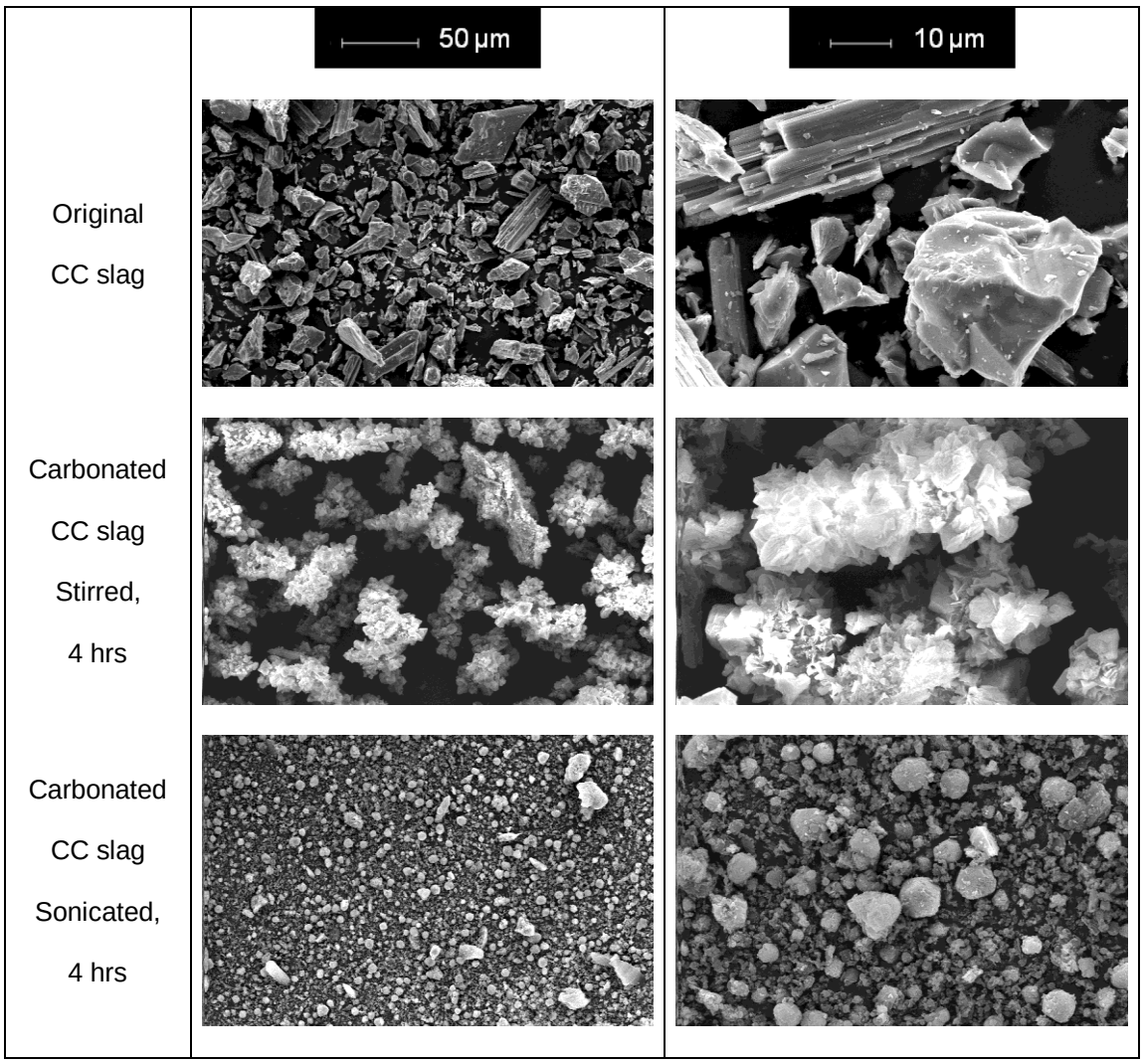

Fig. 4.9. Comparison of particle morphology of original, stirred carbonated, and sonicated carbonated CC slag powders.

4.5.4. Energy efficiency and scale-up considerations

In the present work, the process conditions utilized are not optimized for scaled-up application; they are meant to provide proof-of-concept. In particular, the power consumption of the ultrasound horn is unfeasibly high compared to the CO_2 capture obtained. For instance, taking the gross power consumption figure of 200 W, and two hours reaction time, the energy consumption of the process is 0.4 kWh. Using the average CO_2 emissions intensity for electricity generation in Belgium in 2009 of 198 gCO_2/kWh [37], CO_2 emissions of the ultrasound-intensified mineral carbonation process would be 79.2 grams. In comparison, the CO_2 uptake of CC slag under the present process conditions is only 2.3 grams per 10 g slag. It should be noted, however, that mineral carbonation of stainless steel slags is not meant only as a method for carbon capture, it is also a waste treatment solution, and potentially even a waste-to-product valorisation route. Taking the electricity price for industrial consumers in Belgium of 10 Euro cents per kilowatt-hour [38], the treatment cost per tonne of slag would be 4000 Euros; also as unfeasibly high as the CO_2 emissions. Essentially these calculations suggest two orders of magnitude reduction are needed; i.e. if the CO_2 emissions were 0.8 grams per 10 g slag (giving 65% CO_2 capture efficiency) and treatment cost 40 Euros per tonne, the process would be industrially interesting.

There are several approaches to improve the feasibility of the process. First, the use of renewable electricity could make the CO_2 balance much more favorable. The Belgian electricity production sector is composed of a mix of nuclear (55%), gas (30%) and coal (10%), with minor contributions from wind and renewables [37]. These energy sources are notorious high CO_2 emitters (nuclear = 65 gCO_2/kWh, fossil fuels = 600-1200 gCO_2/kWh), compared to wind energy for example (15-25 gCO_2/kWh) [39]. This approach is only valid, however, if the captured CO_2 emissions originate from processes that cannot avoid CO_2 production (such as solid waste incineration, cement and steel production), rather than to curb CO_2 derived from fossil fuel power plants (in which case replacing fossil fuel based processes with renewable ones would be more efficient). Second, electricity prices are market dependant, with certain countries and jurisdictions charging less than half the price in Belgium. Third, the solids concentration in solution could be increased from 10 g/l to more typical values used in industrial slurry processes around 100-300 g/l. However, increasing solids concentration may cause the soluble concentration of CO_2 to be a rate limiting factor, thus increasing reaction time. As a response, it may be necessary to operate the process at higher CO_2 partial pressure, and utilize a combination of temperature and pH buffering that maximize dissociation of carbonic acid to carbonate ions, while still being favorable for calcium carbonate precipitation. A fourth approach, and perhaps most important, is optimization of ultrasound use, or utilization of other cavitation generating technologies. As Gogate et al. [18] suggested, hydrodynamic cavitation generation can be significantly more energy efficient than ultrasound horn (60% vs. <10% respectively); one note is that this study was conducted with the model reaction of decomposition of potassium iodide; efficiency results may differ when it comes to using ultrasound as an abrasion/milling mechanism. Moreover, Gogate et al. [16] have identified numerous parameters that should be considered for scale-up of ultrasound-assisted processes. These include ultrasound frequency (value and whether mono/multi/variable application), ultrasound probe dimensions (diameter and surface area, which affect US amplitude), liquid medium (e.g. additives that influence viscosity, vapor pressure and surface tension can be beneficial), and reactor configuration (flow geometry and ultrasound transducer placement). In summary they state that the "development of continuous reactors with tubular or hexagonal geometry is key to effective large scale operation, and use of multiple transducers with a possibility of multiple frequency operation is recommended to get required cavitational effects while also minimizing the required energy consumption."

The combination of all these factors may allow ultrasound-intensified mineral carbonation to become an industrially feasible technology. Further work to meet these goals is intended by this research group. Moreover, with proof-of-concept confirmation on the application of ultrasound for overcoming the shrinking core barrier of liquid-solid processes, the approach utilized here can be extended to other chemical reactions that require intensification. In those cases, more favorable process conditions (e.g. material properties, reaction kinetics, required intensification extent) and economical incentives (e.g. product value, high cost competing technology) may permit more immediate application of this technology.

4.6. CONCLUSIONS

Ultrasound has been proven to be a potentially useful tool for intensification of mineral carbonation processes. Due to enhanced mixing, particle breakage and removal of passivating layers it was possible to accelerate the reaction kinetics, and achieve greater carbonation extent in shorter

times and greater maximal conversion. The ultrasound enhancement mechanism has been attributed to the removal of the precipitated calcium carbonate and depleted silica layers that surround the carbonated particle and contribute to rate/conversion limiting effect due to mass transfer inhibition, thereby exposing the unreacted particle core to the reacting solution. These effects were evidenced in the present work by analysis of particle size distributions (via laser diffraction) and particle morphology (via scanning electron microscopy). When applied to argon oxygen decarburization (AOD) and continuous casting / ladle metallurgy (CC/LM) stainless steel slags, which are problematic waste materials posing environmental threat due to high alkalinity and heavy metal leaching potential, resulting in expensive disposal costs, ultrasound-intensified mineral carbonation has the potential to stabilize the materials and turn them into carbon sinks. It was found in the present work that sonicated carbonation resulted in significantly lower pH values of the carbonated materials, approaching the theoretical pH value of pure calcium carbonate, which should reduce their heavy metal leaching potential.

4.7. REFERENCES

1 A.I. Stankiewicz, J.A. Moulijn, Process Intensification: Transforming Chemical Engineering. Chemical Engineering Progress 96 (2000) 22–34.

2 T. Van Gerven, A. Stankiewicz, Structure, Energy, Synergy, Time - The Fundamentals of Process Intensification. Industrial & Engineering Chemistry Research 48 (2009) 2465–2474.

3 D. Reay, The role of process intensification in cutting greenhouse gas emissions. Applied Thermal Engineering 28 (2008) 2011–2019.

4 R.M. Santos, T. Van Gerven, Process Intensification Routes for Mineral Carbonation. Greenhouse Gases: Science and Technology 1 (2011) 287–293.

5 K.S. Lackner, D.P. Butt, C.H. Wendt, Progress on binding CO_2 in mineral substrates. Energy Conversion and Management 38 (1997) S259–S264.

6 F.W. Tegethoff, J. Rohleder, E. Kroker, Calcium carbonate: from the Cretaceous period into the 21st century. Birkhauser Verlag, Basel, 2001.

7 S. Eloneva, A. Said, C.-J. Fogelholm, R. Zevenhoven, Preliminary assessment of a method utilizing carbon dioxide and steelmaking slags to produce precipitated calcium carbonate, Applied Energy 90 (2011) 329–334.

8 W.J.J. Huijgen, G.-J. Witkamp, R.N.J. Comans, Mineral CO_2 Sequestration by Steel Slag Carbonation. Environmental Science & Technology 39 (2005) 9676–9682.

9 X. Li, M.F. Bertos, C.D. Hills, P.J. Carey, S. Simon, Accelerated carbonation of municipal solid waste incineration fly ashes. Waste Management 27 (2007) 1200–1206.

10 G. Montes-Hernandez, R. Pérez-López, F. Renard, J.M. Nieto, L. Charlet, Mineral sequestration of CO_2 by aqueous carbonation of coal combustion fly-ash. Journal of Hazardous Materials 161 (2009) 1347–1354.

11 R. Pérez-López, G. Montes-Hernandez, J.M. Nieto, F. Renard, L. Charlet, Carbonation of alkaline paper mill waste to reduce CO_2 greenhouse gas emissions into the atmosphere. Applied Geochemistry 23 (2008) 2292–2300.

12 D.N. Huntzinger, J.S. Gierke, L.L. Sutter, S.K. Kawatra, T.C. Eisele, Mineral carbonation for carbon sequestration in cement kiln dust from waste piles. Journal of Hazardous Materials 168 (2009) 31–37.

13 V. Prigiobbe, A. Polettini, R. Baciocchi, Gas–solid carbonation kinetics of Air Pollution Control residues for CO_2 storage. Chemical Engineering Journal 148 (2009) 270–278.

14 T. Van Gerven, E. Van Keer, S. Arickx, M. Jaspers, G. Wauters, C. Vandecasteele, Carbonation of MSWI-bottom ash to decrease heavy metal leaching, in view of recycling. Waste Management 25 (2005) 291–300.

15 G. Montes-Hernandez, F. Renard, N. Geoffroy, L. Charlet, J. Pironon, Calcite precipitation from CO_2–H_2O–$Ca(OH)_2$ slurry under high pressure of CO_2. Journal of Crystal Growth 308 (2007) 228–236.

16 P.R. Gogate, V.S. Sutkar, A.B. Pandit, Sonochemical reactors: Important design and scale up considerations with a special emphasis on heterogeneous systems. Chemical Engineering Journal 166 (2011) 1066–1082.

17 R.M. Wagterveld, L. Boels, M.J. Mayer, G.J. Witkamp, Visualization of acoustic cavitation effects on suspended calcite crystals. Ultrasonics Sonochemistry 18 (2011) 216–225.

18 P.R. Gogate, I.Z. Shirgaonkar, M. Sivakumar, P. Senthilkumar, N.P. Vichare, A.B. Pandit, Cavitation Reactors: Efficiency Assessment Using a Model Reaction. AIChE Journal 47 (2001) 2526–2538.

19 P.R. Gogate, P.A. Tatake, P.M. Kanthale, A.B. Pandit, Mapping of Sonochemical Reactors: Review, Analysis, and Experimental Verification. AIChE Journal 48 (2002) 1542–1560.

20 P.R. Gogate, A.B. Pandit, Sonochemical reactors: scale up aspects. Ultrasonics Sonochemistry 11 (2004) 105–117.

21 R. Isopescu, M. Mocioi, M. Mihai, C. Mateescu, G. Dabija, Modification of precipitated calcium carbonate particle size distribution using ultrasound field. Revista de Chimie 58 (2007) 246–250.

22 Y. Lu, N. Riyanto, L.K. Weavers, Sonolysis of synthetic sediment particles: particle characteristics affecting particle dissolution and size reduction. Ultrasonics Sonochemistry 9 (2002) 181–188.

23 A.L. Poli, T. Batista, C.C. Schmitt, F. Gessner, M.G. Neumann, Effect of sonication on the particle size of montmorillonite clays. Journal of Colloid and Interface Science 325 (2008) 386–390.

24 F. Franco, L.A. Pérez-Maqueda, J.L. Pérez-Rodríguez, The effect of ultrasound on the particle size and structural disorder of a well-ordered kaolinite. Journal of Colloid and Interface Science 274 (2004) 107–117.

25 V. Raman, A. Abbas, Experimental investigations on ultrasound mediated particle breakage. Ultrasonics Sonochemistry 15 (2008) 55–64.

26 R.O. King, C.F. Forstert, Effects of sonication on activated sludge. Enzyme and Microbial Technology 12 (1990) 109–115.

27 I. Nishida, Precipitation of calcium carbonate by ultrasonic irradiation. Ultrasonics Sonochemistry 11 (2004) 423–428.

28 A. Rao, E.J. Anthony, L. Jia, A. Macchi, Carbonation of FBC ash by sonochemical treatment. Fuel 86 (2007) 2603–2615.

29 S.H. Sonawane, S.R. Shirsath, P.K. Khanna, S. Pawar, C.M. Mahajan, V. Paithankar, V. Shinde, C.V. Kapadnis, An innovative method for effective micro-mixing of CO_2 gas during synthesis of nano-calcite crystal using sonochemical carbonization. Chemical Engineering Journal 143 (2008) 308–313.

30 A.M. López-Periago, R. Pacciani, C. García-González, L.F. Vega, C. Domingo, A breakthrough technique for the preparation of high-yield precipitated calcium carbonate. The Journal of Supercritical Fluids 52 (2010) 298–305.

31 Y. Pontikes, P.T. Jones, D. Geysen, B. Blanpain, Options to prevent dicalcium silicate-driven disintegration of stainless steel slags. Archives of Metallurgy and Materials 55 (2010) 1167–1172.

32 R. Baciocchi, G. Costa, E. Di Bartolomeo, A. Polettini, R. Pomi, Carbonation of Stainless Steel Slag as a Process for CO_2 Storage and Slag Valorization. Waste and Biomass Valorization 1 (2010) 467–477.

33 E. Vandevelde, Mineral Carbonation of Stainless Steel Slag, Master's thesis, Katholieke Universiteit Leuven, Leuven, Belgium, 2010.

34 R.M. Santos, D. Ling, M. Guo, B. Blanpain, T. Van Gerven, Valorisation of thermal residues by intensified mineral carbonation, in: Proceedings of the 50th Conference of Metallurgists and the 6th International Symposium on Waste Recycling in Mineral and Metallurgical Industries (COM2011), Montreal, 2011, art.nr. 47189.

35 M. Back, M. Bauer, H. Stanjek, S. Peiffer, Sequestration of CO_2 after reaction with alkaline earth metal oxides CaO and MgO. Applied Geochemistry 26 (2011) 1097–1107.

36 R. Baciocchi, G. Costa, A. Polettini, R. Pomi, The influence of carbonation on major and trace elements leaching from various types of stainless steel slag, in: Proceedings of the Third International Conference on Accelerated Carbonation for Environmental and Materials Engineering (ACEME10), Turku, 2010, pp. 215–226.

37 Belgium Energy Efficiency Report, ABB. < http://www.abb.com > [accessed 04.09.11].

38 Europe's Energy Portal. <http://www.energy.eu> [accessed 04.09.11].

39 M. Lenzen, Life cycle energy and greenhouse gas emissions of nuclear energy: A review. Energy Conversion and Management 49 (2008) 2178–2199.

5. Synthesis of pure aragonite by sonochemical mineral carbonation

ABSTRACT – The objective of this work was to promote the formation of the aragonite polymorph of calcium carbonate, which has some valuable applications in industry, via the mineral carbonation route. The combination of ultrasound with magnesium ions promoted the formation of pure aragonite crystals at optimum conditions. It was possible to synthesize high purity aragonite precipitates at temperatures ranging from 24 ^{o}C to 70 ^{o}C, with the resulting powders possessing varying particle size distributions (from sub-micron up to 20 μm) and crystal morphologies (from acicular needles to novel *hubbard squash-like* particles). Several process parameters were found to influence the produced calcium carbonate polymorph ratios (aragonite over calcite). Higher values of magnesium-to-calcium ratio, intermediate ultrasound amplitude (60%), continuous ultrasound application (100% cycle), introduction of ultrasound pre-breakage, lowering of the CO_2 flow rate, and increase in the relative concentration (g/L $Ca(OH)_2$), all promoted aragonite formation. A potential route for industrial production of this material has been identified via a fed-batch process, which effectively reutilizes magnesium chloride while maintaining high aragonite yield. The results presented herein are significantly superior to aragonite formation using only single promoting techniques, typically found in literature, and go beyond by focusing on pure (>99%) aragonite formation.

GRAPHICAL ABSTRACT

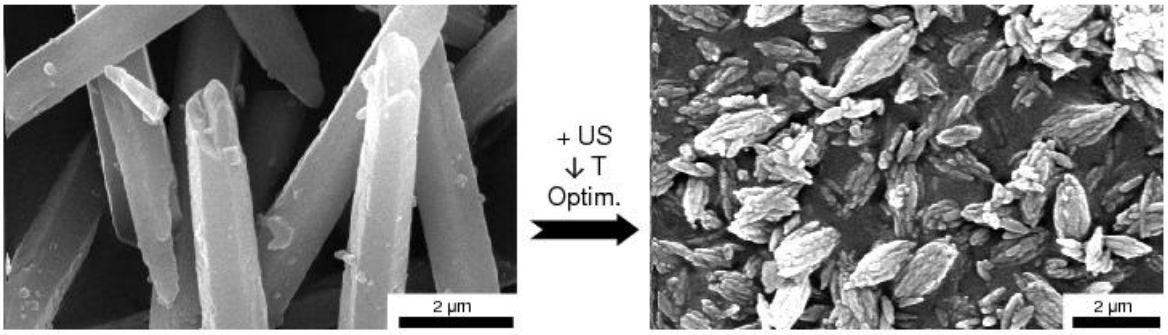

Published as
R.M. Santos, P. Ceulemans, and T. Van Gerven.
"Synthesis of pure aragonite by sonochemical mineral carbonation".
Chemical Engineering Research and Design 90(6)*, 2012, 715–725.
*Special Issue on the 3rd European Process Intensification Conference.

Author contributions
R.M.S. conceived the research, supervised Master's student P. Ceulemans, performed part of the analytical work, and wrote the article.

5.1. INTRODUCTION

Calcium carbonate ($CaCO_3$) is an abundant mineral in nature; approximately 5 % of the Earth's crust consists of it, in the form of limestone (Stearn and Carroll, 1989). It is an important building material in living organisms as bones, teeth and shells; moreover it can be found in several industrial applications. Calcium carbonate is used as filler or coating pigment in paper, plastics, rubbers and adhesives; as filler, extender and pH buffer in paints; as filler and color stabilizer in concrete; for environmental pollution control and remediation in flue gas and water treatment; in fertilizers and animal feed as calcium supply; among other uses in glass, ceramics, cosmetics and hygienic products (CCA Europe, 2011).

Calcium carbonate appears in nature in three polymorphs. The most common is calcite, as it is the most stable polymorph at ambient temperature and pressure. Its crystal system is trigonal, and appears in a range of morphologies, the most common being rhombohedral and scalenohedral forms (Vecht and Ireland, 2000). Aragonite is a metastable polymorph, commonly occurring in aquatic environments, formed by biological or physical precipitation mediated by suitable pressure, ionic concentration and pH; it can be found in shell structures of shellfish (e.g. oysters and abalones)[XVI], pearls and sediments in hot springs (Ryu et al., 2010). At standard temperature and pressure, it converts into calcite over several million years. Its crystal system is orthorhombic, and crystals are most commonly needle-like (acicular) or spindle-like, although flower-like (flos-ferri), cauliflower- and flake-like crystals are also reported (Zhou et al., 2004). Lastly, vaterite, which has a hexagonal crystal system and spherical morphology (Wang et al., 1999), is the rarest polymorph, being unstable and rapidly reverting to one of the more stable forms.

Calcium carbonate that is industrially used as a filler or pigment is most commonly calcite due to easy production routes. Aragonite, however, presents some improved physical and mechanical properties. Polyvinyl alcohol or polypropylene composites with aragonite filler show improved tensile strength, impact strength, glass temperature and decomposition temperature (Hu et al., 2009), while aragonite-containing paper coating benefits from improved brightness, opacity, strength and printability (Katayama et al., 1992). Given the differences in material physical properties (Table 5.1) between the polymorphs are small, the improved aragonite performance is attributable to morphological differences (e.g. particle aspect ratio and packing density).

[XVI] Remark: According to Lee et al. (Int. J. Miner. Process. 92 (2009) 190–195), the occurence of aragonite in nature, forming at ambient temperatures and low pressures, can be explained as follows: "certain living organisms...are capable of synthesizing higher-order architectures composed of aragonite under ambient atmospheric conditions. To delineate the role of organic species on the biomineralization of aragonite, many researchers have developed the stereochemical recognition model, in which it is envisaged that these shapes are stabilized through the binding of peptides and proteins to otherwise unstable faces, presumably because the stereochemical match to the crystal lattice lowers their surface energies".

Table 5.1. Physical properties of calcite and aragonite (Dimmick, 2003; Haynes, 2011; Roberts et al., 1990).

Property	Calcite	Aragonite
Solubility product (K_{sp})	3.36×10^{-9}	6×10^{-9}
Density (g/cm^3)	2.71	2.93
Hardness (Mohs scale)	3	3.5–4
Refractive index	1.58	1.63
Coordination number	6	9

Aragonite synthesis by mineral carbonation is favored at 60 to 70 °C (Hu and Deng, 2003). At higher temperatures (and ambient pressure), aragonite is unstable and polymorph change towards calcite takes place (Passe-Coutrin et al., 1995). At lower temperatures, such as ambient, vaterite formation is possible; however its conversion to calcite is rapid (Wang et al., 1999). On the other hand, aragonite is calcium carbonate's high-pressure polymorph: increasing the pressure advances the stability of the crystals (Zhou et al., 2004).

Aragonite synthesis can also be promoted by controlling the aqueous chemistry of the precipitation solution, an example being the control of the saturation degree (SS). A low degree of supersaturation (SS << 1) has been found to favor aragonite formation (Hu and Deng, 2003). Matsumoto et al. (2010) used the minute gas–liquid interface around CO_2/NH_3 microbubbles as a reaction field to promote aragonite nucleation. It was possible to adjust the concentration of Ca^{2+} and CO_3^{2-} ion concentrations at the interface by varying solution pH and gas composition, which affected the electric charge on the bubble surface and the difference between local and bulk pH. At a solution pH of 9.7-10.5 the crystallization of aragonite was accelerated remarkably with a decrease in the CO_2/NH_3 ratio and gas bubble size (<100 μm).

Additionally, additives have been found to enhance aragonite formation in several studies. Ota et al. (1995) was able to obtain aragonite whiskers from the carbonation of a mixture of calcium hydroxide and magnesium chloride, at a molar Mg-to-Ca ratio (MCR) of 1.52, at 80 ^oC. Similarly, Katayama et al. (1992) used phosphoric acid as an additive instead of magnesium, at 2 wt% to $Ca(OH)_2$, and obtained 20 μm long aragonite needles at 50 ^oC. The most relevant study to date on aragonite synthesis for the carbonation system of interest in the present study is that of Park et al. (2008). They investigated the influence of the concentration of magnesium ions ($MgCl_2$) on the carbonation of $Ca(OH)_2$ slurry in a reactor at 80 °C. It was found that when the magnesium concentration is higher than 71 mol%, corresponding to a magnesium-to-calcium ratio (MCR) greater than 2, pure aragonite can be synthesized. Moreover, increasing the MCR resulted in smaller particles, with a maximal aspect ratio occurring in the interval of 71–75 mol%. They postulated that the magnesium ions bind to the calcite microcrystal surface, inhibiting the nucleation and growth of calcite crystals. In an earlier study, Ahn et al. (2004) had found that aragonite formation had no permanent relation to the pH value, the MCR, or the Mg^{2+}/Ca^{2+} concentrations in solution. It was suggested that synthesis of aragonite requires a concentration of magnesium ions in the appropriate range (0.10–0.26 M) and a concentration of calcium ions below a certain range (< 0.16–0.25 M); otherwise an excess of calcium ions or magnesium ions would favor calcite formation.

Finally, ultrasound (US) has also been seen to promote precipitation of the different polymorphs of calcium carbonate. The use of ultrasound in chemical processes, also termed sonochemistry, applies sound waves in the range of 16 to 100 kHz. Power is delivered to a solution by inducing cavitation, that is, the formation of small cavities or microbubbles that grow and

collapse rapidly. The collapsing microbubbles produce high local temperatures and pressures and high shear forces. Experimental work is reported on the use of ultrasound to speed up carbonation of an aqueous calcium carbonate salt solution (Nishida, 2004) and the seeded sonocrystallization of calcite at constant composition conditions (Boels et al., 2010). Rao et al. (2007) found that ultrasound increased the carbonation conversion of fluidized bed combustion ash, and López-Periago et al. (2010) used a sonic bath to enhance carbonation of calcium hydroxide using supercritical CO_2. The formation of vaterite with ultrasound has been reported from aqueous salt solutions (Kojima et al., 2010; Price et al., 2011). Zhou et al. (2004) found pure aragonite to form from $Ca(HCO_3)_2$ solution at 70 ^oC with an ultrasound intensity of 58–99 W (in 250 mL) at 20 kHz. The high temperatures and pressures, suitable for aragonite formation, caused by the ultrasound-induced cavitations were attributed to the result. Mateescu et al. (2007) mixed $Ca(NO_3)_2$ drop-wise into a solution of K_2CO_3 in a sonic bath at 40 ^oC and obtained preferential formation of aragonite and vaterite when maintaining the pH constant at 10.

Process Intensification (PI) seeks to bring together fundamental aspects of process engineering technology and to find the most optimum balance between them (Santos and Van Gerven, 2011). With a view of finding a PI route to aragonite synthesis by mineral carbonation, the main objectives of this work were:

i. To improve aragonite synthesis by the combined use of ultrasound and chemical additives to promote pure aragonite formation at economical process conditions; emphasis was given to the synthesis of pure aragonite at low temperatures ($\leq$ 30 ^oC).
ii. To explore the influencing parameters that induce aragonite formation based on directions given in literature, but herein performed systematically and dedicated to the mineral carbonation process; the aims were to confirm and extend the state of knowledge, and to find the optimum aragonite-promoting process conditions.

5.2. EXPERIMENTAL SECTION

For sonication an ultrasonic processor Hielscher UP200S was used, which operates at 24 kHz frequency and delivers 200 W gross power. The probe used was an S14 sonotrode, which has a tip diameter of 14 mm, maximal amplitude of 125 μm, and an acoustic power density of 105 W/cm². A PT100 temperature sensor connected to the device monitored solution temperature. Experiments in slurry were conducted using a laboratory glass beaker with a volume of two liters and diameter of approximately 14 cm; the beaker was filled with one liter of distilled water, reaching a height of 7.5 cm. The probe tip was immersed up to 3.5 cm from the bottom. Typical experiments were performed with 3.7 g/L of $Ca(OH)_2$ solids. The suspension was mixed solely by the ultrasound horn during sonication experiments, or with a mechanical stirrer (Heidolph type RZ-R1) and straight blade impeller at 340 rpm for stirred experiments. CO_2 was delivered to the solution from a compressed gas cylinder with flow controlled by a rotameter (Brooks Sho-rate). Temperature was controlled by use of a hot plate (IKAMAG RCT) for heating and water bath for cooling; because ultrasound produces heat, it must be dissipated to operate at lower temperatures or simply to maintain a constant temperature. The experimental set-up used is illustrated in Fig. 5.1. The following analytical grade materials were used in this study: $Ca(OH)_2$ (Acros Organics), $MgCl_2 \cdot 6H_2O$ (Chem-Lab), industrial grade CO_2 ≥99.5% (Praxair).

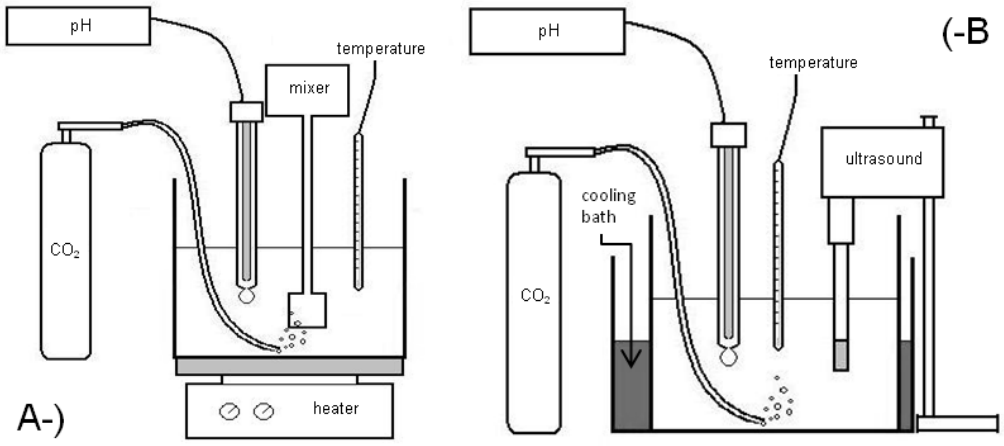

Fig. 5.1. Schematic overview of mechanically mixed (A) and ultrasound mixed (B) slurry carbonation experimental set-ups.

The typical experimental procedure commenced by dissolving the desired amount of magnesium chloride hexahydrate (e.g. 30.5 g/L for MCR = 3) in one liter ultrapure water (18.2 MΩ·cm). Then, the desired amount of calcium hydroxide powder (typically 3.7 g/L, referred to herein as relative concentration (RC) of 1) was poured into the beaker. While mixing (by ultrasound or mechanical agitation), the mixture is heated to the desired temperature, either solely by the ultrasonic device or the hot plate. When the desired temperature is reached, the carbonation reaction is started by bubbling CO_2 gas (typical flow rate 0.24-0.72 NL/min) through the slurry. Carbonation continues until the solution pH reaches a constant value, indicating reaction completion, typically within 30 to 120 minutes. The slurry then is filtered (589/3 filter paper), rinsed, and dried at 105 °C for four hours to recover the calcium carbonate crystals.

Particle size analysis of precipitate samples was determined by laser diffraction (LD) (Malvern Mastersizer S). Morphological assessment was performed by imaging with a scanning electron microscope (SEM) (Philips XL30 FEG). Mineralogical analysis was conducted by X-ray diffraction (XRD) (Philips PW1830), equipped with a graphite monochromator and a gas proportional detector, using Cu Kα radiation at 30 mA and 45 kV, step size of 0.03° 2θ and counting time 2 s per step, over 5 to 70° 2θ range; mineral identification was done in DiffracPlus EVA (Bruker) software.

Quantification of calcite and aragonite in completely carbonated samples was performed using Eq. (5.1), where F_a is the fraction (wt%) of aragonite and I is the intensity of an associated peak: I_{111} and I_{221} refer to the aragonite peaks at 26.3° and 45.9° 2θ, I_{104} is the intensity of the calcite peak at 29.5°. This equation is derived from the equation used by Park et al. (2008), but fitting the coefficients to calibration performed using pure standards at three aragonite (A):calcite (C) mixture ratios: 25% A:75% C, 55% A:45% C, and 75% A:25% C. The quantification uncertainty is estimated at approximately ±0.5%.

$$F_a = \frac{I_{111} + 0.215 \cdot I_{221}}{I_{111} + 0.215 \cdot I_{221} + 0.472 \cdot I_{104}} \tag{5.1}$$

5.3. RESULTS AND DISCUSSION

5.3.1. Influence of stirring mode and temperature

A combination of the approaches of Park et al. (2008) and Zhou et al. (2004) was used to promote the formation of aragonite from the carbonation of calcium hydroxide powder; that is, both magnesium ions and ultrasound were used in slurry carbonation. The first series of experiments involved testing the hypothesis that ultrasound promotes aragonite synthesis. This was accomplished by comparing the mineralogy of samples carbonated with ultrasound mixing and with mechanical mixing. Furthermore, the temperature of the reaction was varied to find out if aragonite formation is possible at temperatures lower than those reported in literature (70 ^{o}C (Zhou et al., 2004), 80 ^{o}C (Ota et al., 1995; Park et al., 2008)). A magnesium-to-calcium ratio (MCR) of 3 was chosen for these experiments (according to the MCR > 2 criteria of Park et al. (2008)).

Fig. 5.2 shows XRD diffractograms of the synthesized precipitates at the four temperatures using mechanical mixing (left) and ultrasound mixing (right). At 70 °C, essentially pure aragonite (>99%) is formed with both mixing methods. Lowering the reaction temperature elevates the calcite content. At 55 °C with mechanical mixing the amount of calcite is still small, but at lower temperatures (40 °C and 30 °C) the calcite phase becomes dominant. Based on the peak heights at 55 ^{o}C and the data presented in Table 5.2, it appears >99% aragonite can be obtained at temperatures just slightly higher. These results suggest a slight improvement with regards to synthesis temperature in comparison with results of Ota et al. (1995) and Park et al. (2008), and confirm the effect of temperature on promoting aragonite formation in the presence of magnesium ions.

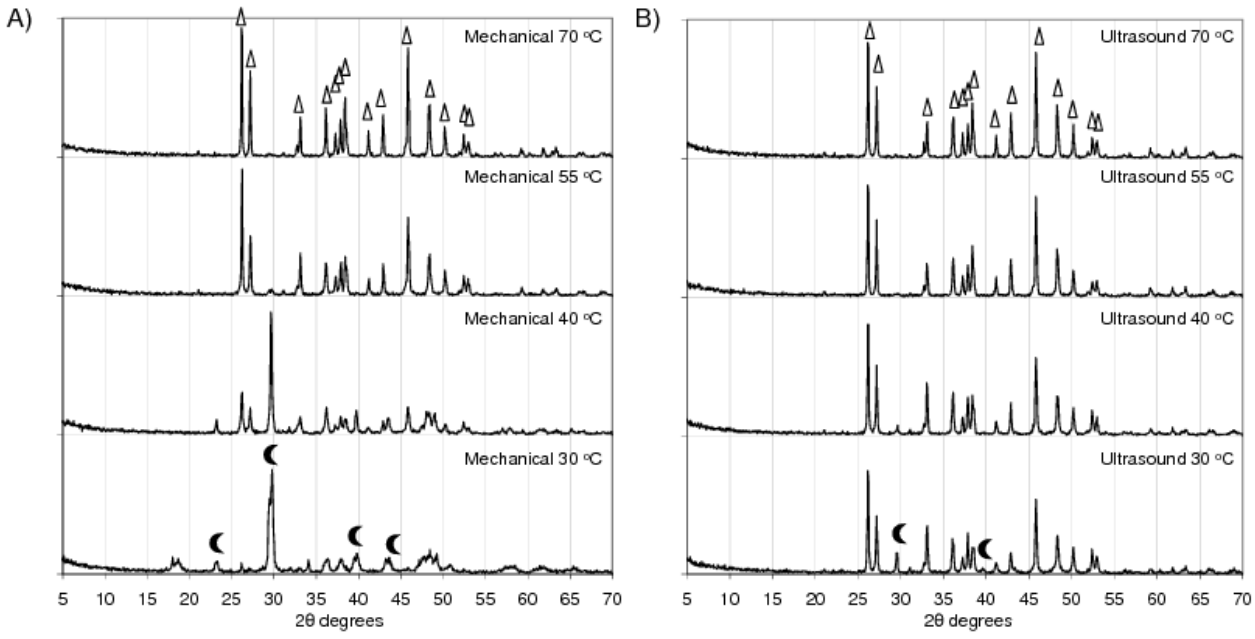

Fig. 5.2. Calcium carbonate polymorphism, determined by XRD, as a function of agitation method (mechanical, A; ultrasound, B) and temperature. MCR = 3, US amplitude/cycle = 1, RC = 1, CO_2 = 0.72 NL/min; Δ = aragonite, ☾ = calcite.

Table 5.2. Aragonite fractions as function of agitation method and temperature. MCR = 3, US amplitude/cycle = 1, RC = 1, CO_2 = 0.72 NL/min; letter-indexes (a–f) refer to images in Fig. 5.3.

Temperature	Ultrasound mixing	Mechanical mixing
70 °C	99.6% (a)	99.5% (e)
55 °C	99.6% (b)	98.7% (f)
40 °C	96.9% (c)	44.6% (g)
30 °C	92.7% (d)	20.4% (h)

The effect of ultrasound on aragonite formation is confirmed by comparison with the mechanical agitation results in Fig. 5.2. It is evident that at every temperature lower than 70 ^{o}C the amount of aragonite is greater with use of ultrasound. Moreover, at 30 ^{o}C and 40 ^{o}C aragonite remains as the dominant polymorph when using ultrasound, compared to nearly complete reversal to calcite (and magnesian-calcite at 30 ^{o}C inferred from the double peak at 29.5–30^{o}) with mechanical mixing. These results are reaffirmed by the quantitative analysis reported in Table 5.2. At 55 ^{o}C essentially pure aragonite (99.6%) is formed with ultrasound. It is clear that the use of ultrasound in the presence of magnesium ions allows for pure aragonite formation at lower temperatures than reported by Zhou et al. (2004).

It is believed that the cavitations formed by the use of ultrasound introduce two effects that promote the formation of aragonite. First, the imploding cavities generate localized, micron-sized or smaller, regions of high temperature, even though the bulk solution temperature may be fixed at a low value (e.g. 30 ^{o}C). Since aragonite formation is promoted at higher temperatures, it can be expected that these high temperature regions, even if in existence for fractions of a second, lead to the nucleation of aragonite seeds, which then can grow into larger aragonite crystals at bulk solution temperatures. Second, the generation of nucleation sites is likely greatly enhanced by sonication, therefore even if crystal growth of aragonite at lower bulk temperature is comparatively slow, the constant generation of aragonite seeds enables aragonite crystal growth to remain statistically preferable over calcite. These mechanisms can also explain the morphological differences seen in the precipitates, discussed next.

The morphology of the crystals produced is illustrated in Fig. 5.3 for eight cases: ultrasound at four different temperatures: 70 ^{o}C (a), 55 ^{o}C (b), 40 ^{o}C (c), 30 ^{o}C (d); and mechanical mixing at four different temperatures: 70 ^{o}C (e), 55 ^{o}C (f), 40 ^{o}C (g), 30 ^{o}C (h). The aragonite contents of these samples correspond to the letter-indexed values listed in Table 5.2. It can be clearly seen that at 70 ^{o}C the particle morphology resembles needle-like aragonite reported in literature, regardless of mixing method. Also with both mixing methods, lowering temperature results in reduction of particle size.[XVII] However with ultrasound mixing, the particles remain aragonite, achieving newly observed particle morphology at 30 ^{o}C (*hubbard squash-like*), shown in more detail on Fig. 5.4. As aforementioned, these smaller aragonite crystals may be a product of slower aragonite crystal growth at lower temperatures, combined with increased aragonite nucleation in the presence of ultrasound. The *hubbard squash-like* morphology can also be seen in selected particles in Fig. 5.3h, achieved with mechanical mixing; however in this case scalenohedral calcite crystals are dominant.

[XVII] Remark: While the mineral content of the mechanical mixing sample prepared at 55 ^{o}C and the ultrasound sample prepared at 40 ^{o}C are similar (>95% aragonite), the particle morphologies differ, with ultrasound resulting in smaller particles and different particle shape.

This further reaffirms that the unique morphology is due to synthesis at low temperature rather than solely due to sonication-induced breakage of the forming crystals.

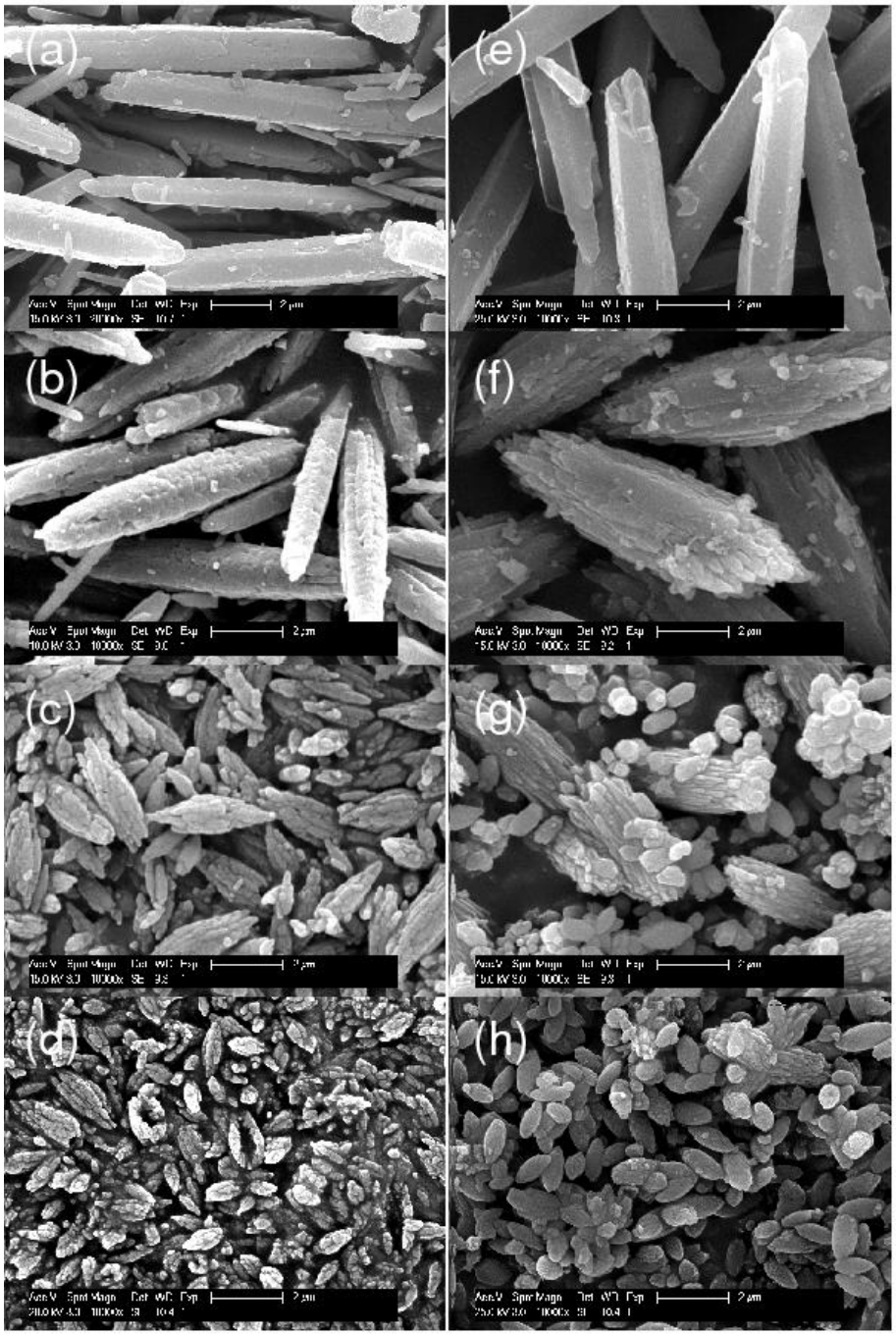

Fig. 5.3. Comparison of $CaCO_3$ crystal morphology as a function of carbonation process conditions: (a) US 70 °C, >99% aragonite; (b) US 55 °C, >99% aragonite; (c) US 40 °C, 97% aragonite; (d) US 30 °C, 93% aragonite; (e) mechanical 70 °C, >99% aragonite; (f) mechanical 55 °C, 99% aragonite; (g) mechanical 40 °C, 45% aragonite; and (h) mechanical 30 °C, 20% aragonite.

The images in Fig. 5.3b, c, f and g show transitionary crystal morphologies. With ultrasound, the crystals at 55 ^{o}C still resemble needles but become scaly, while with mechanical mixing the needle-like particles appear more degraded and have lower aspect ratio. At 40 ^{o}C, ultrasound mixing yields particles that begin to resemble the low temperature morphology, but having larger size. In comparison, the 40 ^{o}C mechanical mixing sample is composed of a mixture of aragonite

particles similar to those at 55 ^{o}C but smaller, and nano-sized calcite crystals both of rhombohedral and scalenohedral morphologies.

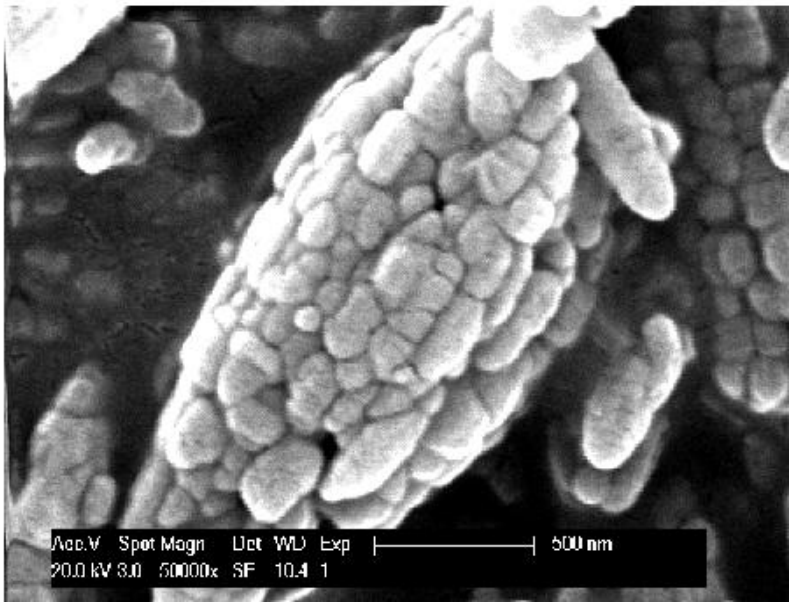

Fig. 5.4. Close-up image of *hubbard squash-like* aragonite crystal formed at low temperature (30 ^{o}C).

5.3.2. Influence of MCR

In an ultrasonic environment with an MCR of 3, pure aragonite can be synthesized at 55 °C, as shown previously. It was of interest to know if a higher MCR allows for production of pure aragonite at lower temperatures (30 ^{o}C). Also, it was of interest to know if an optimal MCR exists at different temperatures (i.e. can the MCR be lowered at 55 ^{o}C while still obtaining >99% aragonite). Carbonation experiments were conducted by varying the MCR between 0 and 6, at 30 ^{o}C and 55 ^{o}C, with use of ultrasound mixing in $Ca(OH)_2$ slurry as described previously. Fig. 5.5 presents the aragonite content of the calcium carbonate precipitates produced. Aragonite was more easily formed at higher temperature; at 55 °C, pure aragonite can be synthesized with MCR = 2.5, whereas at 30 °C an MCR = 6 is necessary. Already with MCR = 1 it is possible to synthesize over 50% aragonite at 55 ^{o}C, and over 90% at MCR = 1.5; similar results are only achieved at 30 ^{o}C with a half unit greater MCR. It is concluded that there is in fact an optimal MCR for each temperature. Moreover it is proven possible to synthesize pure aragonite close to room temperature at optimized conditions.

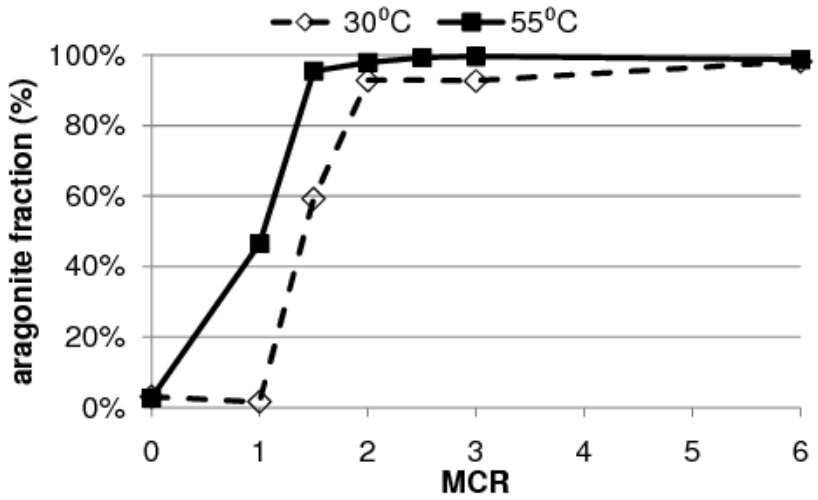

Fig. 5.5. Aragonite fractions as function of MCR and temperature using ultrasound. US amplitude/cycle = 1, RC = 1, CO_2 = 0.72 NL/min.

Additionally, a possible explanation of the mechanism of magnesium ions in participating in the carbonation reaction to promote aragonite was observed. Upon addition of magnesium chloride to solution, magnesium ions reacted with water and precipitated as brucite ($Mg(OH)_2$). Brucite formation was found to be quite fast, as evidence by large brucite peaks in XRD analysis for samples filtered minutes after mixing. Furthermore, unreacted portlandite peaks were found to nearly disappear, indicating that calcium ions had been leached into solution, forming dissolved calcium chloride (Eq. (5.2)). Over time, it is believed that as calcium ions react with carbonate ions, brucite solubilizes back into magnesium chloride, and calcium carbonate is precipitated (Eq. (5.3)). This is also confirmed by reduction in brucite peak heights by XRD, and complete disappearance once the carbonation reaction is completed. These reaction steps were confirmed by Visual MINTEQ chemical equilibrium modeling and are presented in more detail in Ceulemans (2011). The promotion of aragonite in the presence of magnesium chloride thus may be linked with the carbonation reaction taking place in solution rather than by direct mineral carbonation (Eq. (5.4)).

$$Ca(OH)_2 + MgCl_{2(aq)} \rightarrow Mg(OH)_2 + CaCl_{2(aq)} \quad (5.2)$$

$$CaCl_{2(aq)} + CO_{2(aq)} + Mg(OH)_2 \rightarrow CaCO_3 + H_2O + MgCl_{2(aq)} \quad (5.3)$$

$$Ca(OH)_2 + CO_{2(aq)} \rightarrow CaCO_3 + H_2O \quad (5.4)$$

5.3.3. Influence of ultrasound parameters

The ultrasound probe used allows the setting of two process parameters: amplitude and cycle. The amplitude is the distance the sonotrode surface travels within an oscillation stroke. Larger amplitude leads to higher rate at which the cavity pressure increases and decreases at each stroke, and increased displacement volume, resulting in a larger cavitation volume (bubble size and/or number). When applied to slurries, higher amplitudes provide greater potential for solid particle breakage (Hielscher, 2006). Amplitude is expressed as a percentage of the maximum amplitude (125 µm). Cycle refers to the fraction of experimental time during which sonication is applied. The ultrasound can be used in such way that the sonication is pulsed on and off in short time intervals. Cycle is expressed as a percentage of total experimental time. Previous experiments were performed with 100% amplitude and cycle. In this section, experiments are executed at an intermediate MCR

value (1.5 at 30 °C) so that the effect of varying amplitude and cycle on aragonite fraction can be investigated. The objective is the optimum ultrasound setting that maximizes aragonite content.

Fig. 5.6 shows the effect of amplitude and cycle on aragonite synthesis. Using either cycles of 20% and 100%, there is a maximum aragonite fraction at an intermediate amplitude (60%). Higher cycle (100%), meaning more ultrasound use, also leads to greater aragonite synthesis. Therefore the optimal configuration is found to be 60% amplitude and 100% cycle. Zhou et al. (2004) also found intermediate amplitudes to favor aragonite. However in their case the competing polymorph at higher amplitudes was vaterite; vaterite was not detected in this work.

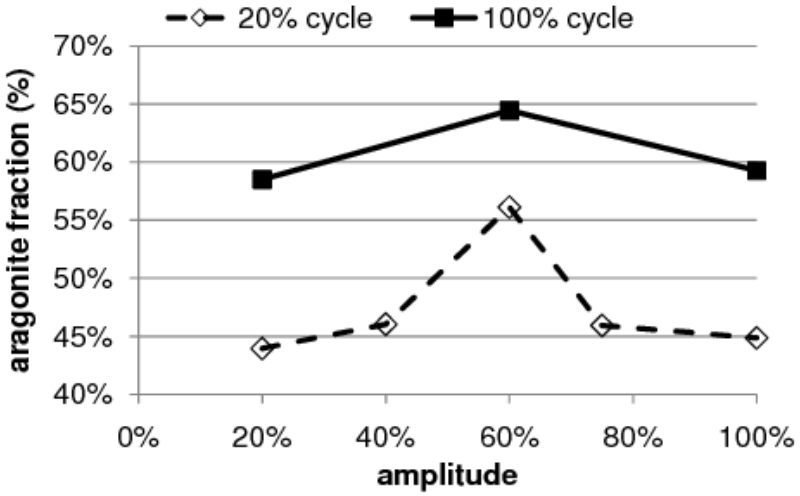

Fig. 5.6. Aragonite fractions as function of ultrasound parameters (amplitude and cycle). MCR = 1.5, T = 30 °C, RC = 1, CO_2 = 0.72 NL/min.

The reason for intermediate amplitudes being optimal may lie in the effect of ultrasound intensity on the generation rate of cavities and their resulting collapse pressure (Gogate et al., 2003). Gogate et al. (2003) have found by computational modeling that although an increase in ultrasound intensity leads to bubble growth, it also leads to a reduction of the bubble wall pressure at the collapse point of the cavity, due to dissipation of energy from the longer-living bubble to the liquid medium. They postulate that upon increasing intensity, there is an optimal point where the overall pressure pulse, defined as the product of the number of cavities in the system and the collapse pressure due to the single cavity, is greatest, beyond which it decreases due to leveling off of cavity generation. For the present system (i.e. ultrasonic processor, sonotrode probe, 1 liter water medium volume, and 2 liter glass beaker receptacle) it may well be that the optimal overall pressure pulse occurs near 60% amplitude.

5.3.4. Influence of other process parameters

Three additional process parameters were investigated for their effect on aragonite formation: ultrasound pre-breakage, CO_2 flow rate, and relative concentration. Results are shown in Table 5.3 for varying sets of process conditions.

Table 5.3. Effect of US pre-breakage, CO_2 flow rate and relative concentration on aragonite fractions for various process conditions.

Pre-breakage time (min)	MCR	Temperature (°C)	Mixing	Relative conc. (w/w)	CO_2 flow (NL/min)	Aragonite fraction
Effect of US pre-breakage						
0	1.5	30	60% US	1/3	0.24	**40.4%**
20	1.5	30	60% US	1/3	0.24	**55.6%**
0	1.5	30	60% US	1	0.72	**25.4%**
45	1.5	30	60% US	1	0.72	**41.5%**
0	3	30	Mech	1	0.24	**91.0%**
45	3	30	Mech	1	0.24	**93.0%**
0	6	30	60% US	1	0.24	**99.3%**
20	6	30	60% US	1	0.24	**99.0%**
Effect of CO_2 flow rate						
0	1.5	30	60% US	1	**0.72**	**64.5%**
0	1.5	30	60% US	1	**0.24**	**68.9%**
0	1.5	30	60% US	1	**0.12**	**74.7%**
0	3	30	Mech	1	**0.72**	**20.4%**
0	3	30	Mech	1	**0.24**	**91.0%**
Effect of relative concentration						
0	3	30	100% US	**2**	0.72	**98.8%**
0	3	30	100% US	**1**	0.72	**92.7%**
0	3	30	100% US	**1/2**	0.72	**75.0%**
0	1.5	30	60% US	**1**	0.24	**68.9%**
0	1.5	30	60% US	**1/3**	0.24	**40.4%**

Pre-breakage is defined as sonication time applied to the calcium hydroxide slurry prior to CO_2 gas introduction into the solution. The objective is to reduce the particle size induced by the imploding cavitations, thereby increasing uncarbonated material surface area, which should have an effect both on the dissolution and the carbonation reaction kinetics and equilibria. Table 5.3 presents four sets of data, comparing samples subjected or not to pre-breakage (from 0 to 45 minutes). These sets utilize varying process conditions (pre-breakage times, MCR, mixing, relative concentration and CO_2 flow). It can be seen that under all process condition combinations, save the last, pre-breakage promotes greater aragonite synthesis, expressed as the aragonite fraction of the resulting calcium carbonate precipitates. In the first two cases the benefit is greater since the process conditions lead to intermediate aragonite purity, while for the later two cases the benefit is smaller to nil, given aragonite purity is greater than 90% already. It is theorized that pre-breakage promotes aragonite synthesis by improving the reaction between calcium hydroxide and magnesium chloride prior to carbonation, whereas without pre-breakage there is greater likelihood that calcium ions dissolved directly from unreacted calcium hydroxide will form calcite.

The next process parameter discussed is CO_2 flow rate. Table 5.3 presents results from two series of experiments conducted with varying CO_2 flow rates, and identical remaining parameters. It is found that increasing the CO_2 flow rate leads to greater calcite formation, whereas lowering the CO_2 flow rate promotes aragonite; this result is particularly noticeable with mechanical mixing,

where the aragonite content increases from 20.4% to 91% at MCR = 3 and 30 ^{o}C. This effect can be directly linked to reaction time. As shown in Fig. 5.7, with a flow rate of 0.72 NL/min the reaction is completed (pH drop levels off) in approximately 50min, while at 0.24 NL/min and 0.12 NL/min the reaction is completed only after 2h15min and 4h30min, respectively. It is thought that the lower CO_2 flow rate leads to a lower level of solubilized CO_2 (i.e. under saturation), decreasing the probability of carbonate ions reacting with calcium ions leached directly from $Ca(OH)_2$, rather than the dissociated calcium chloride species. These results are in agreement with those of Hu and Deng (2003), who found a low degree of supersaturation to promote aragonite synthesis. However in comparison, aragonite fractions in the present study are much higher than those reported therein (~20% at 36 ^{o}C), which were synthesized from sparingly soluble calcium salts.

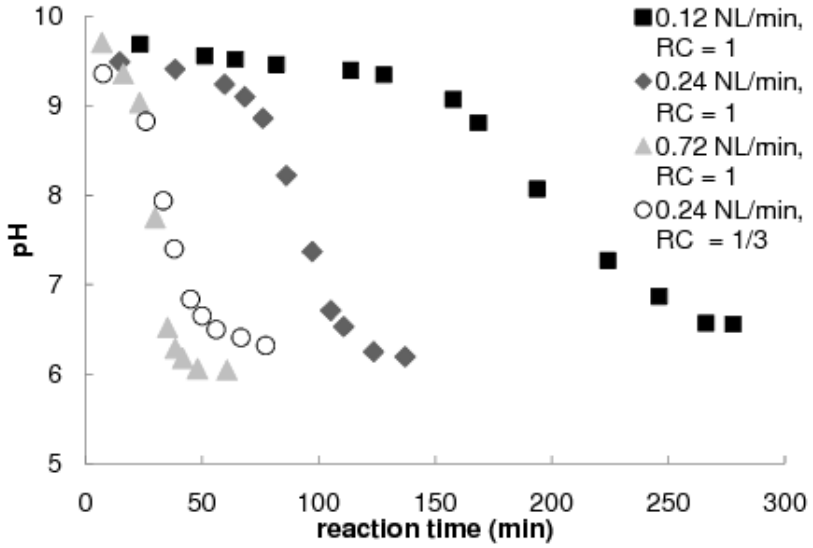

Fig. 5.7. Carbonation kinetics, expressed in pH, as a function of CO_2 flow rate; MCR = 1.5, 30 ^{o}C. 60% US, 0' PB.

Lastly, the effect of relative concentration (RC) on aragonite formation was tested. Relative concentration is defined as the initial calcium hydroxide concentration in slurry relative to the typical value of 3.7 g/L used in most experiments (e.g. RC = 2 means $Ca(OH)_2$ = 7.2 g/L). It should be noted that the magnesium chloride concentration is adjusted accordingly to maintain the same MCR for comparison purpose. Table 5.3 presents two sets of experiments where RC was varied; process parameters such as MCR, US amplitude and CO_2 flow rate differ between these two sets. It is found that lower RC is detrimental to aragonite formation in both cases. In fact, by doubling the relative concentration for the first series, the aragonite content at 30 ^{o}C nearly reaches 99%, compared to just under 93% at typical concentrations and MCR = 3. In this case, the aragonite promoting effect may be linked to the increased magnesium chloride concentration when RC is larger. Increasing the concentration of $Ca(OH)_2$ should not significantly change the rate or extent of calcium dissolution, given all slurries are over-saturated with respect to $Ca(OH)_2$. As a result, by maintaining the MCR constant, the concentration of soluble chloride species, both Mg and Ca, significantly increases, thereby increasing the effective influence of magnesium chloride (i.e. at RC = 2 and MCR = 3, it is as if the MCR was 6). These results are in agreement with observations of Ahn et al. (2004), who postulated that magnesium concentration rather than MCR controls aragonite formation, with a minimum Mg concentration being required to suppress calcite formation. Along these lines, in Table 5.3 it can be seen that when RC = 1/2 or 1/3 the aragonite

fractions drops significantly. A last note to be made about relative concentration is that the carbonation reaction time decreases at lower RC, as can be seen in Fig. 5.7 for RC = 1/3. This finding will be used later on in the section about a fed-batch process.

5.3.5. Synthesis at optimized conditions and lowest temperature

Up to this point, investigating and optimizing influencing parameters has resulted in a list of optimal values, which can be combined to improve the low-temperature synthesis of aragonite. Of particular note, rather than using RC = 2 with MCR = 3, it was decided to maintain RC = 1 with MCR = 6, to reduce the reaction time. Also the CO_2 flow rate chosen was 0.24 NL/min, again to reduce the reaction time compared to using the 0.12 NL/min found to be optimal for aragonite selectivity. The final combination conditions utilized for the optimized synthesis, which resulted in 99.0% aragonite precipitate with the morphology shown in Fig. 5.8a, were:

- T = 30 °C
- RC = 1
- MCR = 6 (3.7 g $Ca(OH)_2$ + 61 g $MgCl_2 \cdot 6H_2O$ in 1 liter DI water)
- US amplitude = 60%; US Cycle = 100%
- CO_2 flow = 0.24 NL/min
- PB = 20 minutes

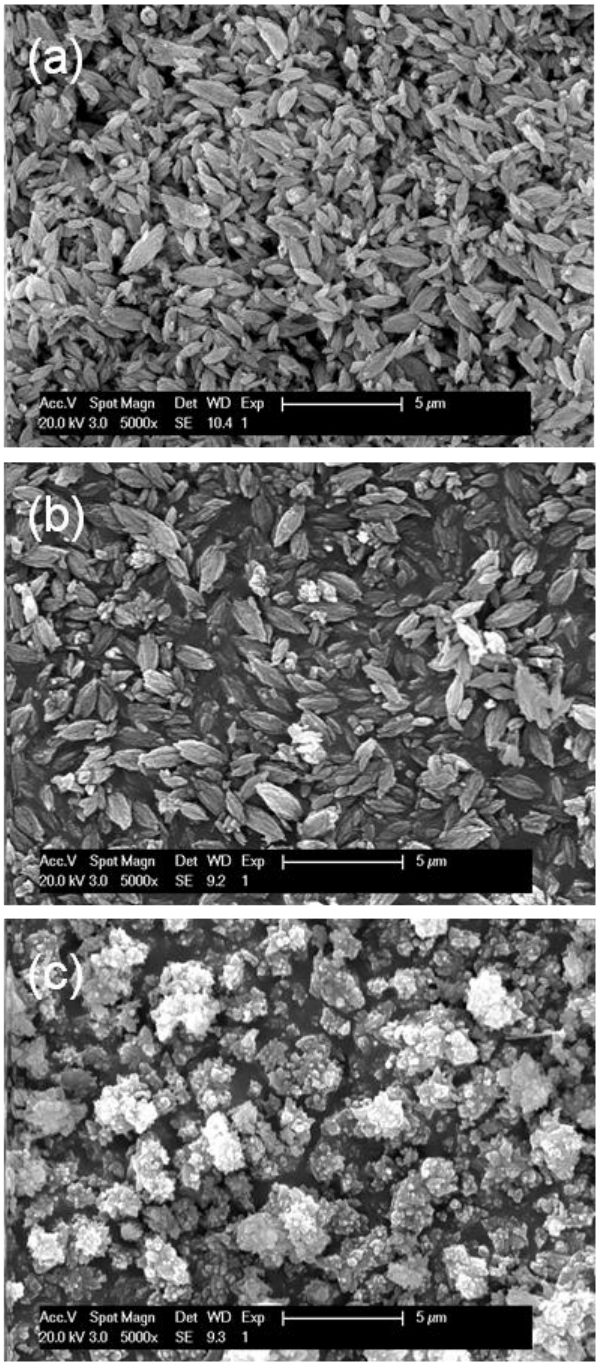

Fig. 5.8. Particle morphology at optimized synthesis conditions: (a) 30 ^{o}C; (b) 24 ^{o}C; (c) fed-batch.

A final attempt was made to reduce the synthesis temperature even further. The reaction temperature was lowered to 24 °C, and more severe aragonite-favoring conditions were chosen: MCR = 8 and CO_2 flow = 0.12 NL/min. While the reaction time was rather long (4.5 hours), the aragonite purity obtained was very satisfactory: 98.6%. The crystal morphology is shown in Fig. 5.8b, possessing the unique *hubbard squash-like* shape. The XRD pattern of this sample is compared to that at 30 ^{o}C in Fig. 5.9, both being essentially identical except for slightly higher I_{111}:I_{021}, I_{112}:I_{022} and I_{141}:I_{113} ratios at 24 ^{o}C.

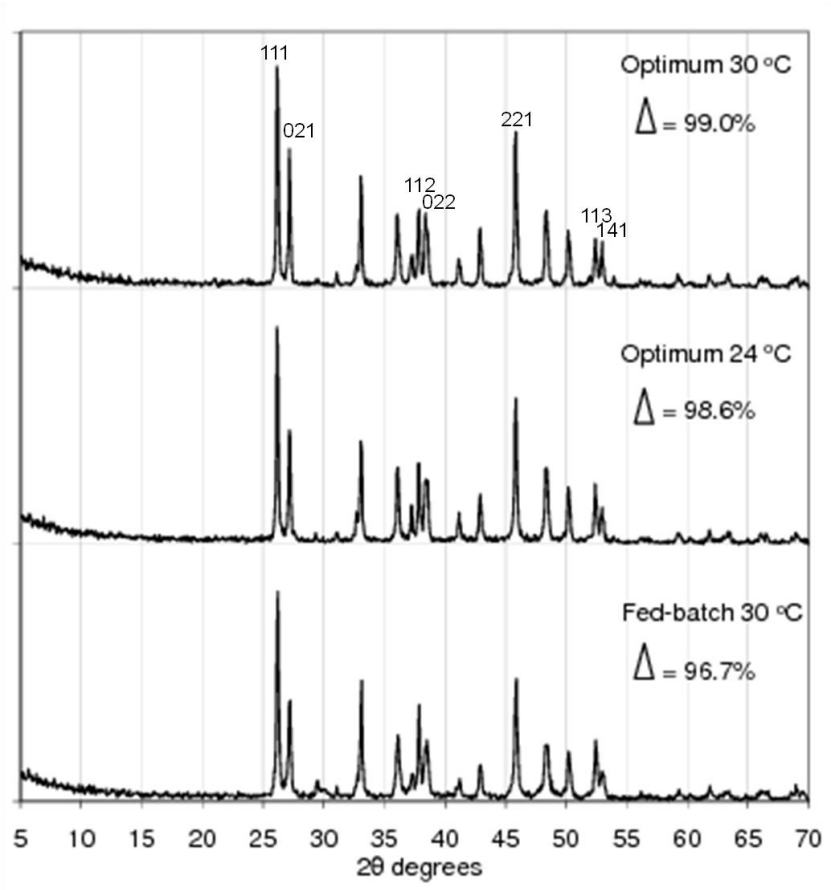

Fig. 5.9. Mineral analysis by XRD of precipitates produced at optimized aragonite synthesis conditions; Δ = aragonite fraction.[XVIII]

5.3.6. Fed-batch process

To make this synthesis process interesting from an industrial production perspective the efficiency of this process must be higher. Indeed, in 1 liter water at RC = 1 there will be only five grams of aragonite produced according to this process. Furthermore, for synthesizing those five grams, 61 g of magnesium chloride hexahydrate are needed. This ratio appears wasteful, unless the magnesium chloride can be proven to be reusable. Two ideas were considered: (i) filtering the carbonated slurry and reutilizing the solution for further synthesis cycles with addition of new $Ca(OH)_2$, or (ii) adding new $Ca(OH)_2$ to the synthesis slurry on a continuous basis for an extended period of time (i.e. a fed-batch process (e.g. Ahn et al., 2007)). The second solution was found to be the preferred route, as in the first case the filtration proved difficult to perform in a timely manner and the synthesis product suffered from contamination with brucite ($Mg(OH)_2$) when the reaction had not been fully completed prior to filtration (Ceulemans, 2011). The following process conditions were chosen for the fed-batch process:

- T = 30 °C
- $Ca(OH)_2$ = 1.2 g every 12 minutes
- Mg = 61 g $MgCl_2 \cdot 6H_2O$, one time addition, in 1 liter DI water
- Time = 144 minutes (12 additions)
- US amplitude = 60 %; US Cycle = 100 %

[XVIII] Peak indices not shown in publication.

The resulting fed-batch-produced calcium carbonate precipitate contained 96.7% aragonite, as shown in Fig. 5.9. The cause of the small calcite formation is possibly due to addition of fresh $Ca(OH)_2$ directly to the slurry during carbonation, while in previous single batch experiments the calcium hydroxide was pre-mixed with magnesium chloride prior to CO_2 introduction. A small portion of the newly added $Ca(OH)_2$ may react directly with carbonate ions forming calcite, prior to magnesium chloride taking its full effect in equilibrating with the unreacted material. The aragonite purity may improve further if $Ca(OH)_2$ addition is done in a truly continuous basis with a feeding pump. The particle morphology also changed from the *hubbard squash-like* shape to what appear to be clustered crystal particles of 1-3 μm in size. By inspection of Fig. 5.8c, it appears additional crystal growth occurs due to prolonged exposure of early synthesized aragonite crystals to the reacting slurry. Maintenance of the *hubbard squash-like* likely requires immediate separation of the formed crystals prior to solution re-utilization.

5.3.7. Precipitate powder characterization by laser diffraction

Pure aragonite precipitates were synthesized in this study at a range of temperatures spanning from 24 ^{o}C to 70 ^{o}C. As has been shown by SEM analysis (Fig. 5.3), particle morphology changes as a function of temperature and so does particle size. Particle size and particle size distribution are important parameters of powder materials for certain industrial applications such as paper coating or polymer filler; these data are not typically reported in literature for novel calcium carbonate morphologies, making it impractical to assess their suitability for industrial use. As such, the effect of synthesis temperature on aragonite particle size was studied in more detail by laser diffraction.

Table 5.4 lists average particle sizes by volume, expressed as D50 (mean volume diameter), D[3,2] (surface area moment mean diameter) and D[4,3] (volume moment mean diameter), and Fig. 5.10 shows the volume-based size distributions. All samples were synthesized with ultrasound and contain greater than 98% aragonite as indicated. In general, lowering the synthesis temperature results in shifting of the distribution to the left (smaller sized). This is confirmed in Table 5.4 for the three listed size averages. The distributions of precipitates synthesized at higher temperatures have bimodal/trimodal characteristics, having a primary peak between 1 μm and 20 μm (and an intermediate peak at 2 μm for the 70 ^{o}C case) and a secondary peak below 1 μm. The larger mode likely represents the needle-shaped particles, while the smaller modes may be fragmented particles, due to sonication, and/or particles that formed near the end of the experiments when crystal growth could be hindered by diminishing calcium concentration in solution. Samples from low temperature synthesis (24 ^{o}C and 30 ^{o}C) have unimodal distributions below 3 μm. The low temperatures, which may hinder crystal growth throughout the experiment, could be attributed to the smaller particle sizes. The fed-batch sample was found to have a bimodal distribution, likely comprised, as suggested by SEM images, of larger clustered crystals and smaller ultrasound-cleavaged particles.

Table 5.4. Average particle sizes of pure aragonite synthesized with ultrasound at different temperatures.

Temperature °C	D50 µm	D[3,2] µm	D[4,3] µm	Aragonite %
70 °C	4.15	1.31	6.48	99.5%
55 °C	1.33	0.78	1.87	98.7%
40 °C	0.98	0.65	1.27	98.6%
30 °C	0.85	0.69	1.23	99.3%
24 °C	0.84	0.79	1.09	98.6%
Fed-batch (30 °C)	1.74	0.87	2.22	96.7%

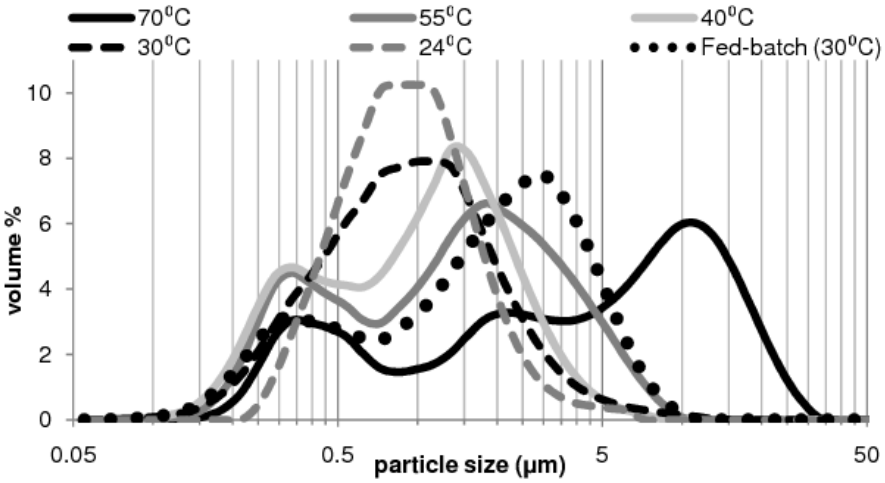

Fig. 5.10. Particle size distributions of pure aragonite precipitates at varying temperatures.

5.4. CONCLUSIONS

Ultrasound has been proven, in combination with magnesium chloride in solution, to enhance the synthesis of aragonite crystals by mineral carbonation, both by reducing the required concentration of magnesium and reducing the required reaction temperature to near ambient conditions. While in literature the synthesis temperature of aragonite normally is situated in the 60 °C to 90 °C range, in the present work high purity aragonite precipitates were produced even at 24 °C using a combination of optimized process parameters found by application of the principles of Process Intensification.

The effect of several process parameters on aragonite synthesis was systematically studied beyond temperature, including the magnesium-to-calcium ratio (MCR), ultrasound (US) settings (amplitude and cycle), US pre-breakage (PB), CO_2 flow rate, and relative concentration (RC). It was found that higher values of MCR promoted aragonite, but in the presence of ultrasound the MCR corresponding to a similar level of aragonite fraction of the carbonate precipitates decreased in comparison with standard mechanical mixing. An intermediate ultrasound amplitude (60%) was most beneficial to aragonite promotion at intermediate MCR levels, similar to reported observations by Zhou et al. (2004), while aragonite purity was proportional to ultrasound application, with 100% cycle (continuous US) being best. Ultrasound pre-breakage is theorized to promote aragonite synthesis by improving the reaction between calcium hydroxide and magnesium chloride prior to

carbonation, reducing the likelihood that calcium ions dissolved directly from unreacted calcium hydroxide will form calcite. Lowering the CO_2 flow rate was also found to promote aragonite synthesis, leading to lower level of supersaturation that has been reported to favor aragonite (Hu and Deng, 2003). Finally the aragonite promoting effect of relative concentration was linked to the increased magnesium chloride concentration when RC is larger, though the MCR remains the same; this response has also been previously suggested by Ahn et al. (2004).

While other authors have reported similar strategies to promote aragonite, none have combined them to find an optimal process that produces pure aragonite; in fact most studies only report aragonite production at low purity levels or even in near trace amounts, unless the reaction temperature is kept relatively high. In this work not only low temperature aragonite synthesis was proven, but also crystals with new particle morphology (*hubbard squash-like*) were produced.[XIX] This material may have interesting industrial applications, which are yet to be identified. A potential route for industrial production of nearly pure aragonite at low temperature has been identified via a fed-batch process, which effectively reutilizes magnesium chloride while maintaining high aragonite yield, though the crystal morphology changes due to prolonged ultrasound exposure and clustered crystal growth.

5.5. REFERENCES

Ahn, J.-W., Choi, K.-S., Yoon, S.-H., Kim, H., 2004. Synthesis of Aragonite by the Carbonation Process. J. Am. Ceram. Soc. 87, 286–288.

Ahn, J.-W., Kim, J.-H., Ko, S.-J., 2007. Novel Manufacturing Method of Aragonite Calcium Carbonate. WIPO Patent 2007/078017, July 12, 2007.

Boels, L., Wagterveld, R.M., Mayer, M.J., Witkamp, G.J., 2010. Seeded calcite sonocrystallization. J. Cryst. Growth 312, 961–966.

CCA Europe, 2011. Mineral applications. http://www.cca-europe.eu/mineral-applications.html (accessed 07/13/2011).

Ceulemans, P., 2011. Improved synthesis of aragonite. M.Sc. Thesis, Katholieke Universiteit Leuven, July, 2011.

Dimmick, A., 2003. Influence of the average particle size of aragonitic precipitated calcium carbonate on coated paper properties. In Proceedings of TAPPI 2003 Spring Technical Conference and Exhibit and 8th Advanced Coating Fundamentals Symposium, Chicago, USA, 11–15 May 2003.

Gogate, P.R., Wilhelm, A.M., Pandit, A.B., 2003. Some aspects of the design of sonochemical reactors. Ultrason. Sonochem. 10, 325–330.

Haynes, W.M., 2011. CRC Handbook of Chemistry and Physics, 91st Edition, CRC Press/Taylor and Francis, Boca Raton.

Hielscher, T., 2006. Ultrasound as a processing technology for the production of nanomaterials. In Proceedings of Micro & Nano Encapsulation, London, UK, 16–17 February 2006.

[XIX] Remark: Sonication results in different products compared to mechanical mixing, not only promoting high aragonite content but also different particle morphologies (shape and size distribution) not obtainable in the absence of ultrasound. Therefore energetic comparison between the two methods is not so important, since unique products may fetch added economic value that 'pays' for the cost of sonication. Processing cost of sonochemical carbonation deserves future attention, taking into account optimization strategies described in Section 4.5.4.

Hu, Z., Deng, Y., 2003. Supersaturation control in aragonite synthesis using sparingly soluble calcium sulfate as reactants. J. Colloid Interface Sci. 266, 359–365.

Hu, Z., Shao, M., Cai, Q., Ding, S., Zhong, C., Wei, X., Deng, Y., 2009. Synthesis of needle-like aragonite from limestone in the presence of magnesium chloride. J. Mater. Process. Technol. 209, 1607–1611.

Katayama, H., Shibata, H., Fujiwara, T., 1992. Process for producing aragonite crystal form calcium carbonate with acicular shape. US Patent 5,164,172, November 17, 1992.

Kojima, Y., Yamaguchi, K., Nishimiya, N., 2010. Effect of amplitude and frequency of ultrasonic irradiation on morphological characteristics control of calcium carbonate. Ultrason. Sonochem. 17, 617–620.

López-Periago, A.M., Pacciani, R., García-González, C., Vega, L.F., Domingo, C.J., 2010. A breakthrough technique for the preparation of high-yield precipitated calcium carbonate. Supercrit. Fluids 52, 298–305.

Mateescu, C.D., Mocioi, M., Sarbu, C., Branzoi, F., Chilibon, I., 2007. Morphology of $CaCO_3$ Precipitated in Ultrasonic Field. AIP Conf. Proc. 899, 626.

Matsumoto, M., Fukunaga, T., Onoe, K., 2010. Polymorph control of calcium carbonate by reactive crystallization using microbubble technique. Chem. Eng. Res. Des. 88, 1624–1630.

Nishida, I., 2004. Precipitation of calcium carbonate by ultrasonic irradiation. Ultrason. Sonochem. 11, 423–428.

Ota, Y., Inui, S., Iwashita, T., Kasuga, T., Abe, Y., 1995. Preparation of Aragonite Whiskers. J. Am. Ceram. Soc. 7, 1983–1984.

Park, W.K., Ko, S.-J., Lee, S.W., Cho, K.-H., Ahn, J.-W., Han, C., 2008. Effects of magnesium chloride and organic additives on the synthesis of aragonite precipitated calcium carbonate. J. Cryst. Growth 310, 2593–2601.

Passe-Coutrin, N., N'Guyena, Ph., Pelmard, R., Ouensanga, A., Bouchon, C., 1995. Water desorption and aragonite-calcite phase transition in scleractinian corals skeletons. Thermochim. Acta 265, 135–140.

Price, G. J., Mahon, M.F., Shannon, J., Cooper, C., 2011. Composition of Calcium Carbonate Polymorphs Precipitated Using Ultrasound. Cryst. Growth Des. 11, 39–44.

Rao, A., Anthony, E.J., Jia, L., Macchi, A., 2007. Carbonation of FBC ash by sonochemical treatment. Fuel 86, 2603–2615.

Roberts, W.L., Campbell, T.J., Rapp, G.R., 1990. Encyclopedia of Minerals, 2nd ed. Van Nostrand Reinhold, New York.

Ryu, M., Kim, H., Lim, M., You, K., Ahn, J., 2010. Comparison of Dissolution and Surface Reactions Between Calcite and Aragonite in L-Glutamic and L-Aspartic Acid Solutions. Molecules 15, 258–269.

Santos, R.M., Van Gerven, T., 2011. Process Intensification Routes for Mineral Carbonation. Greenhouse Gas Sci. Technol. 1, 287–293.

Stearn, C.W., Carroll, R.L., 1989. Paleontology - The Record of Life, John Wiley & Sons, New York.

Vecht, A., Ireland, T.G., 2000. The role of vaterite and aragonite in the formation of pseudo-biogenic carbonate structures: Implications for Martian exobiology. Geochim. Cosmochim. Acta 64, 2719–2725.

Wang, L., Sondi, I., Matijevic, E., 1999. Preparation of Uniform Needle-Like Aragonite Particles by Homogeneous Precipitation. J. Colloid Interface Sci. 218, 545–553.

Zhou, G.-T., Yu, J.C., Wang, X.-C., Zhang, L.-Z., 2004. Sonochemical synthesis of aragonite-type calcium carbonate with different morphologies. New J. Chem. 28, 1027–1031.

6. Magnesium chloride as a leaching and aragonite-promoting self-regenerative additive for the mineral carbonation of calcium-rich materials

ABSTRACT – Two approaches for the intensification of the mineral carbonation reaction are combined and studied in this work, namely: (i) the calcium leaching and aragonite promoting effects of magnesium chloride ($MgCl_2$), and (ii) the passivating layer abrasion effect of sonication. The alkaline materials subjected to leaching and carbonation tests included lime, wollastonite, steel slags, and air pollution control (APC) residue. Batch leaching tests were conducted with varying concentrations of additives to determine extraction efficiency, and with varying solids-to-liquid ratios to determine solubility limitations. Aqueous mineral carbonation tests, with and without the use of ultrasound, were conducted applying varying concentrations of magnesium chloride and varying durations to assess CO_2 uptake improvement and characterize the formed carbonate phases. The leaching of calcium from lime with the use of $MgCl_2$ was found to be atom-efficient (1 mol Ca extracted for every mole Mg added), but the extraction efficiency from slags and APC residue was limited to 26–35 % due to mineralogical and microstructural constraints. The addition of $MgCl_2$ notably improved argon oxygen decarburization (AOD) slag carbonation extent under sonication, where higher additive dosage resulted in higher CO_2 uptake. Without ultrasound, however, carbonation extent was reduced with $MgCl_2$ addition. The benefit of $MgCl_2$ under sonication can be linked to the preferential formation of aragonite (85 wt% of formed carbonates), which precipitates on the slag particles in the form of acicular crystals with low packing density, thus becoming more susceptible to the surface erosion effect of sonication, as evidenced by the significantly reduced carbonated slag particle size.

Published as
R.M. Santos, M. Bodor, P.N. Dragomir, A.G. Vraciu, M. Vlad, and T. Van Gerven.
"Magnesium chloride as a leaching and aragonite-promoting self-regenerative additive for the mineral carbonation of calcium-rich materials".
Minerals Engineering*, 2013, doi:10.1016/j.mineng.2013.07.020.
*Special Issue on the 4th International Conference on Accelerated Carbonation for Environmental and Materials Engineering.

Author contributions
R.M.S. conceived the research, co-supervised student P.N. Dragomir and A.G. Vraciu, performed part of the analytical work, and wrote the article.

6.1. INTRODUCTION

Mineral carbonation is an attractive route for the storage of CO_2 due to the geochemical stability of the formed carbonates, and is also a potentially viable route for the valorisation of alkaline waste or low-value materials, such as industrial slags, ashes and tailings, due to the reduction of basicity, the predominant stabilization of leaching, and the formation of more marketable mineral products (Bobicki et al., 2012; Pan et al., 2012; Sanna et al., 2012; Bodor et al., 2013; Kirchofer et al., 2013). Much work has been done in recent years to identify suitable materials for mineral carbonation, to understand the fundamental mechanisms that control kinetics and conversion, and to develop processing routes that intensify the reaction whilst reducing energy demand (Zevenhoven et al., 2011; Santos and Van Gerven, 2011). Two main mineral carbonation routes have been established: (i) indirect carbonation, wherein the alkaline-earth components (mainly Ca and/or Mg) are first extracted from the solids into an aqueous solution, which is then contacted with CO_2 for precipitation of the carbonates, and (ii) direct carbonation, wherein the solids (dry, wet or in aqueous slurry) are directly reacted with CO_2, and thus the carbonate products are formed together with the inert and residual minerals. In either case, the mobility of the alkaline-earth elements from the solids is a major limitation for achieving high conversion rates and CO_2 uptake.

To overcome this problem, researchers have turned to finding suitable leaching agents, which ideally should have high extraction efficiency, but at the same time should have less affinity for the alkaline-earth elements than the carbonate ion (CO_3^{2-}), to allow the precipitation of carbonates upon pH-swing. Acetic acid (CH_3COOH) has been successfully applied for the production of precipitated calcium carbonate (PCC) from steel slag (Eloneva et al., 2008), but after extraction it is necessary to add a strong base (e.g. NaOH) to neutralize the acid and promote carbonate precipitation; the neutralized acetate can potentially be regenerated into acetic acid, but at a large processing cost. To avoid regeneration, Eloneva et al. (2009) also tested the efficacy of ammonium salts (NH_4Cl, CH_3COONH_4, NH_4NO_3) and found positive results with steel converter slag, but the efficiency was poorer for blast furnace and ladle slags; this was attributed to calcium being predominantly bound as silicates in these materials (as opposed to free lime (CaO) in converter slag). The loss of ammonia (NH_3) in the off-gas also becomes an added concern when using these additives (Eloneva et al., 2011).

In the present work, a novel approach to enhancing calcium mobility is investigated, namely the use of magnesium chloride ($MgCl_2$) as a leaching agent. This concept has its roots in a recent study conducted by our group (Santos et al., 2012) on the sonochemical synthesis at low temperatures of pure aragonite precipitates possessing novel crystal morphology (*hubbard squash-like*). Aragonite is a polymorph of calcium carbonate typically formed at higher temperatures (90–450 °C) and in marine environments (Kitano and Hood, 1962; Passe-Coutrin et al., 1995; Santos et al., 2013b). The strategy of using $MgCl_2$ to promote aragonite during mineral carbonation had been described in earlier studies (Ahn et al., 2007; Hu et al., 2008), with the mechanism being tentatively attributed to the binding of Mg^{2+} to the calcite polymorph crystal surface, thus inhibiting its growth, and to the reduction in supersaturation with respect to [CO_3^{2-}] as a result of pH reduction. Santos et al. (2012) found that by combining $MgCl_2$ with ultrasound, it is possible to obtain high purity aragonite at temperatures as low as 24 °C. It was also observed, in agreement with reported findings of Xiang et al. (2006), that $MgCl_2$ also acts as a calcium leaching agent, as upon its addition to a slurry of $Ca(OH)_2$, the calcium becomes solubilised, while the magnesium precipitates as $Mg(OH)_2$

(Eq. 6.1). Subsequently, upon carbonation, the calcium precipitates as $CaCO_3$, while the magnesium returns into solution with the chloride (Eq. 6.2). Both steps are exothermic, but most of the reaction heat is released in the carbonation step.

$$Ca(OH)_{2(s)} + MgCl_{2(aq)} + H_2O_{(l)} \rightarrow Mg(OH)_{2(s)} + CaCl_{2(aq)} \quad (6.1)$$
$$\Delta H^{\circ}_{Eq.\ (6.1)} = -19.4 \text{ kJ/mol}$$

$$CaCl_{2(aq)} + H_2CO_{3(aq)} + Mg(OH)_{2(s)} \rightarrow CaCO_{3(s)} + MgCl_{2(aq)} + 2H_2O_{(l)} \quad (6.2)$$
$$\Delta H^{\circ}_{Eq.\ (6.2)} = -160.8 \text{ kJ/mol}$$

These reaction steps are illustrated in Fig. 6.1 with crystallographic data from Ceulemans (2011). At first, when magnesium chloride is added to a slurry of calcium hydroxide (portlandite), formation of brucite ($Mg(OH)_2$) is seen. Once CO_2 is introduced into the slurry, carbonic acid reacts with dissolved calcium, forming calcite and aragonite polymorphs of calcium carbonate (the ratio of these depends on other reacting conditions, studied by Santos et al. (2012)). As the reaction progresses, carbonate diffraction peaks become predominant while brucite peaks shrink, indicating solubilisation back into magnesium chloride. If the reaction is halted prior to completion, the product will contain brucite; this is undesirable as it signifies loss of additive and low product purity. When the reaction is completed, only the diffraction patterns of calcium carbonates can be seen, meaning that magnesium chloride has been fully regenerated.

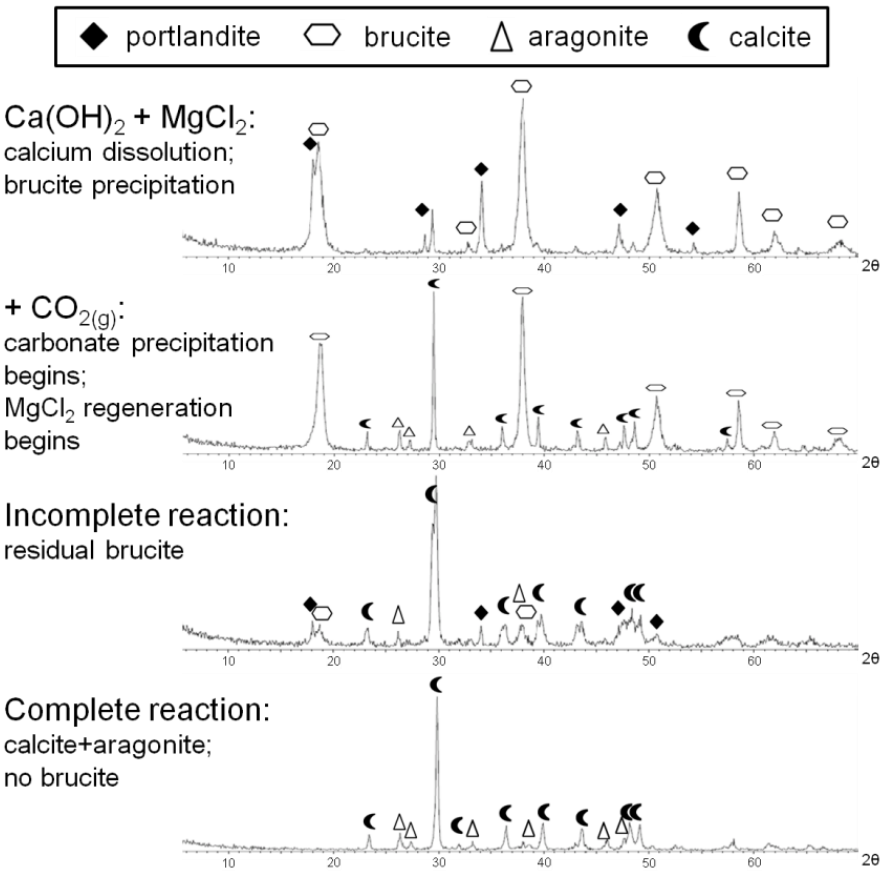

Fig. 6.1. Self-regenerative cycle of $MgCl_2$ as applied during carbonation of $Ca(OH)_2$; adapted from Ceulemans (2011).

Key to these reaction steps are the greater solubility of $CaCl_2$ over $MgCl_2$, and the lower solubility of $CaCO_3$ over Mg-carbonates (Hu et al., 2008). This mechanism prevents the formation of Mg-carbonates in the product, thus ensuring high $CaCO_3$ product purity and additive regeneration. Concurrent precipitation of Ca- and Mg-carbonates is also prevented since it would imply the formation of HCl in solution, unless this was neutralized with, for example, ammonia (NH_3) (Ferrini et al., 2009). As such, this self-regenerative mechanism also enables the re-utilization of the magnesium chloride-rich solution in further carbonation cycles without the need for purification or re-crystallization (Ma et al., 2011; Santos et al., 2012). One constraint of this approach, however, is that it is applicable only to direct carbonation systems, as the leached solids, containing the precipitated $Mg(OH)_2$, cannot be separated from the Ca-rich solution prior to carbonation. Besides leaching of CaO, $MgCl_2$ also has the potential to leach calcium from siliceous materials, as it is a known contributor to cement and concrete corrosion exposed to saline waters (Kurdowski and Duszak, 1995).

Based on these findings, the present work aims to study the calcium leaching efficiency of $MgCl_2$ for a variety of alkaline materials useful for mineral carbonation, with particular emphasis in accessing the ability of $MgCl_2$ to leach calcium from Ca-silicate, Ca-ferrite, Ca-sulphate and Ca-aluminate rich materials. Furthermore, this study also investigates the effect of $MgCl_2$ on the mineral carbonation kinetics and conversion. For this purpose, the methodology utilized in another of our studies, reported in Santos et al. (2013a), wherein both mechanical mixing and sonication were utilized for the carbonation of stainless steel slags, is herein adopted. In that study, the application of ultrasound was successfully shown to intensify the mineral carbonation reaction, via the reduction in particle size and the removal of passivating layers (residual silica and mainly calcitic precipitates), thus increasing the specific surface area and exposing the unreacted particle core to the reactive medium.

Here, it is theorized that by combining $MgCl_2$ with ultrasound during the carbonation of silicate-rich and microstructurally heterogeneous alkaline materials, the precipitated carbonate layer will become enriched in aragonite. This effect can have implications on the morphology and on the packing density of carbonate layer, given the different crystal shapes formed by each polymorph: rhombohedral and scalenohedral for calcite, and acicular (needle-like) for aragonite (Santos et al., 2012). In turn, the porosity/permeability of the passivating layer may improve, and it may become more fragile to abrasion/attrition (caused by inter-particles collisions or by sonication cavitations). The ultimate consequence of these effects may be improved carbonation kinetics and/or more extensive carbonation conversion (i.e. greater CO_2 uptake); these aspects are investigated in the present work.

6.2. METHODOLOGY

6.2.1. Alkaline materials

A total of six calcium-containing alkaline materials were utilized in leaching and carbonation experiments. Analytical grade lime, with CaO content of 98.3 wt%, was obtained from Chem-Lab. Milled wollastonite (D_{50} = 57 μm), with CaO content of 51.2 wt%, was obtained from Sibelco Specialty Minerals Europe. Argon Oxygen Decarburization (AOD) and Continuous Casting (CC) slags, with CaO contents of 56.8 wt% and 52.1 wt%, respectively, were obtained from a stainless steel producer and sieved to < 500 μm. Basic Oxygen Furnace (BOF) slag, with CaO content of

49.0 wt%, was obtained from a steel producer and milled to < 80 μm. Municipal solid waste incineration (MSWI) air pollution control (APC) residue, with CaO content of 49.8 wt%, was obtained from an incinerator operator and used as received. The complete chemical and mineralogical compositions of the alkaline materials are presented in Tables 6.1 and 6.2, respectively.

Table 6.1. Chemical composition (expressed as wt% oxides) of alkaline materials (in order of CaO content) determined by XRF (normalized to 100 wt% total; ≥ 1.0 wt% shown).

	Al_2O_3	CaO	Cl	Fe_2O_3	K_2O	MgO	MnO	Na_2O	SO_3	SiO_2	TiO_2
CaO	<	98.3	<	<	<	1.1	<	<	<	<	<
AOD slag	1.0	56.8	<	<	<	7.5	<	<	<	32.5	<
CC slag	1.1	52.0	<	1.3	<	9.9	<	<	<	27.5	<
Wollastonite	<	51.2	<	<	<	<	<	<	<	46.4	<
APC residue	1.5	49.8	22.2	<	2.7	<	<	10.9	6.4	2.9	1.1
BOF slag	2.5	49.0	<	29.5	<	1.0	3.6	<	<	12.4	<

<: less than 1.0 wt%.

Table 6.2. Mineral composition of alkaline materials determined by QXRD (wt% of crystalline total, normalized to 100%).

Mineral name	Chemical formula	CaO	Wollastonite	AOD slag	CC slag	BOF slag	APC residue
Åkermanite	$Ca_2MgSi_2O_7$	nd	nd	1.2	1.7	nd	nd
Anhydrite	$CaSO_4$	nd	nd	nd	nd	nd	12.5
Bredigite	$Ca_7Mg(SiO_4)_4$	nd	nd	24.1	6.7	nd	nd
Brucite	$Mg(OH)_2$	nd	nd	0.2	0.0	1.0	1.1
Calcium chloride hydroxide	Ca(OH)Cl	nd	nd	nd	nd	nd	12.3
Chlorapatite	$Ca_5(PO_4)_3Cl$	nd	nd	nd	nd	nd	15.7
Clinoenstatite	$Mg_2Si_2O_6$	nd	nd	1.9	10.7	4.9	nd
Cuspidine	$Ca_4Si_2O_7F_2$	nd	nd	13.5	6.4	nd	nd
β-Dicalcium silicate	Ca_2SiO_4	nd	nd	7.7	7.1	19.4	nd
γ-Dicalcium silicate	Ca_2SiO_4	nd	nd	28.9	43.8	3.5	nd
Fayalite	Fe_2SiO_4	nd	nd	0.2	0.7	0.7	nd
Ferrosilite	$(Fe^{(II)},Mg)_2Si_2O_6$	nd	nd	nd	nd	1.0	nd
Gehlenite	$Ca_2Al_2SiO_7$	nd	nd	1.0	0.1	nd	nd
Halite	NaCl	nd	nd	nd	nd	nd	23.4
Hematite	Fe_2O_3	nd	nd	nd	nd	8.8	nd
Hydromolysite	$FeCl_3{\cdot}6(H_2O)$	nd	nd	nd	nd	nd	2.4
Iron	Fe	nd	nd	nd	nd	0.4	nd
Lime	CaO	86.4	nd	0.4	0.4	12.3	2.2
Magnetite	Fe_3O_4	nd	nd	0.7	1.0	1.0	nd
Merwinite	$Ca_3Mg(SiO_4)_2$	nd	nd	11.1	6.1	nd	nd
Periclase	MgO	nd	nd	5.6	12.4	0.8	0.2
Portlandite	$Ca(OH)_2$	13.6	nd	0.4	1.0	5.6	20.5
Quartz	SiO_2	nd	9.3	0.9	0.4	1.2	0.0
Srebrodolskite	$Ca_2Fe_2O_5$	nd	nd	nd	nd	37.8	nd
Sylvine	KCl	nd	nd	nd	nd	nd	6.4
Tachyhydrite	$CaMg_2Cl_6{\cdot}12H_2O$	nd	nd	nd	nd	nd	3.4
Wollastonite	$CaSiO_3$	nd	90.7	2.4	1.6	nd	nd
Wüstite	FeO	nd	nd	nd	nd	1.6	nd
Total crystalline		100	100	100	100	100	100

nd: not detected.

6.2.2. Leaching tests

Leaching tests were performed in sealed polyethylene bottles by mixing one gram of alkaline solids, ultrapure water, and the desired amount of leaching agent, to a total aqueous volume of 100 ml, and shaking on a vibration table (Gerhardt Laboshake) at 160 rpm and 25 °C for 24 hours. Selected experiments were also conducted with varying solids loading (up to 25 g/100ml) and leaching duration (30 min to 48 hrs) to study the effect of these parameters. At leaching completion, the slurries were filtered with 0.45 μm membrane filter, and the solutions were analyzed for dissolved calcium and magnesium contents.

The following reagents were used as leaching agents in this study: magnesium chloride hexahydrate ($MgCl_2{\cdot}6H_2O$, 99 wt%, Chem-Lab), hereafter referred to as MCH, sodium chloride (NaCl, 99.8 wt%, Chem-Lab), and hydrochloric acid (HCl, 37 wt%, Chem-Lab; diluted to 1 N prior

to use). The different additives were added on the basis of equivalent moles of chloride (namely 2.0, 3.9, 7.9, 15.7 and 31.5 mmol/100ml) to facilitate comparison of the results.

6.2.3. Carbonation tests

Slurry carbonation experiments were conducted using a laboratory glass beaker with a volume of two litres and diameter of approximately 14 cm. The slurry suspension was mixed solely by a mechanical stirrer (Heidolph type RZ-R1) with straight blade impeller at 340 rpm for stirred experiments, or in combination with an ultrasound horn during sonication experiments. The ultrasound horn consisted of a Hielscher UP200S processor, which operates at 24 kHz frequency and delivers 200 W gross power, coupled to an S14 sonotrode, which has a tip diameter of 14 mm, maximal amplitude of 125 μm, and an acoustic power density of 105 W/cm². The horn was operated at maximum power (net delivery ~170 W) and 60 % amplitude (according to optimal conditions found by Santos et al. (2012)). A PT100 temperature sensor was used to monitor solution temperature.

Carbonation experiments were performed with 10 g AOD slag in one litre of ultrapure water, which reached a height of 7.5 cm; for sonication experiments the probe tip was immersed 3.5 cm from the beaker bottom, placed parallel to the stirrer shaft but slightly off-centred due to space constraint. For experiments with MCH addition, the desired amount (2.05, 4.1, 8.3 or 16.6 g)[XX] was added prior to slag addition to allow for complete dissolution. Temperature was controlled by use of a hot plate (IKAMAG RCT) for heating (in the case of stirred experiments) and water bath for cooling (in the case of sonicated experiments, since ultrasound produces heat, which must be dissipated to maintain a constant temperature). A temperature of 50 °C was maintained during carbonation experiments. Carbon dioxide addition commenced once the target temperature was reached, delivered to the solution by bubbling from a compressed gas cylinder ($\geq$ 99.5 % CO_2 purity), with flow controlled at 0.72 NL/min by a Brooks Sho-rate rotameter. Carbonation duration varied from 30 to 240 min, after which the slurry was filtered (Whatman No. 2), and the recovered solids were dried at 105 °C overnight.

6.2.4. Analytical methods

Chemical composition of solid samples was determined by X-ray Fluorescence (XRF, Panalytical PW2400). Mineralogical composition was determined by X-Ray Diffraction (XRD), performed on a Philips PW1830 equipped with a graphite monochromator and a gas proportional detector, using Cu Kα radiation at 30 mA and 45 kV, step size of 0.03° 2θ and counting time of 2 s per step, over 10–65° 2θ range. Mineral identification was done in Diffrac-Plus EVA (Bruker) and mineral quantification (QXRD) was performed by Rietveld refinement technique using Topas Academic v4.1 (Coelho Software). The volume-based particle size distributions and mean particle diameters were determined by wet Laser Diffraction (LD, Malvern Mastersizer). The powder morphology was observed by Scanning Electron Microscopy (SEM, Philips XL30). The CO_2 uptake of carbonated materials was quantified by Thermal Gravimetric Analysis (TGA, Netzsch STA 409), operated from 25 to 900 °C under nitrogen flow at a heating rate of 15 °C/min. The amount of CO_2 released was quantified by the weight loss between 500–800 °C, which is attributable to $CaCO_3$ decomposition. Determination of aqueous elemental concentrations was

[XX] 2–16 mmol,Cl/100 ml.

performed by Inductively Coupled Plasma Mass Spectroscopy (ICP-MS, Thermo Electron X Series) on samples diluted in 0.3 M nitric acid solution.

6.3. RESULTS AND DISCUSSION

6.3.1 Leaching results

6.3.1.1. Aqueous phase analyses

The results of batch leaching tests, utilizing six different alkaline materials and three different leaching agents, are presented in Fig. 6.2. Leaching results are expressed as percentage fraction of calcium extracted from the alkaline materials, based on the XRF determined CaO composition of the solids. To facilitate comparison of the results, the amounts of leaching agents are normalized on the basis of moles of added chloride, the chemical species that combines with calcium to form soluble $CaCl_2$.

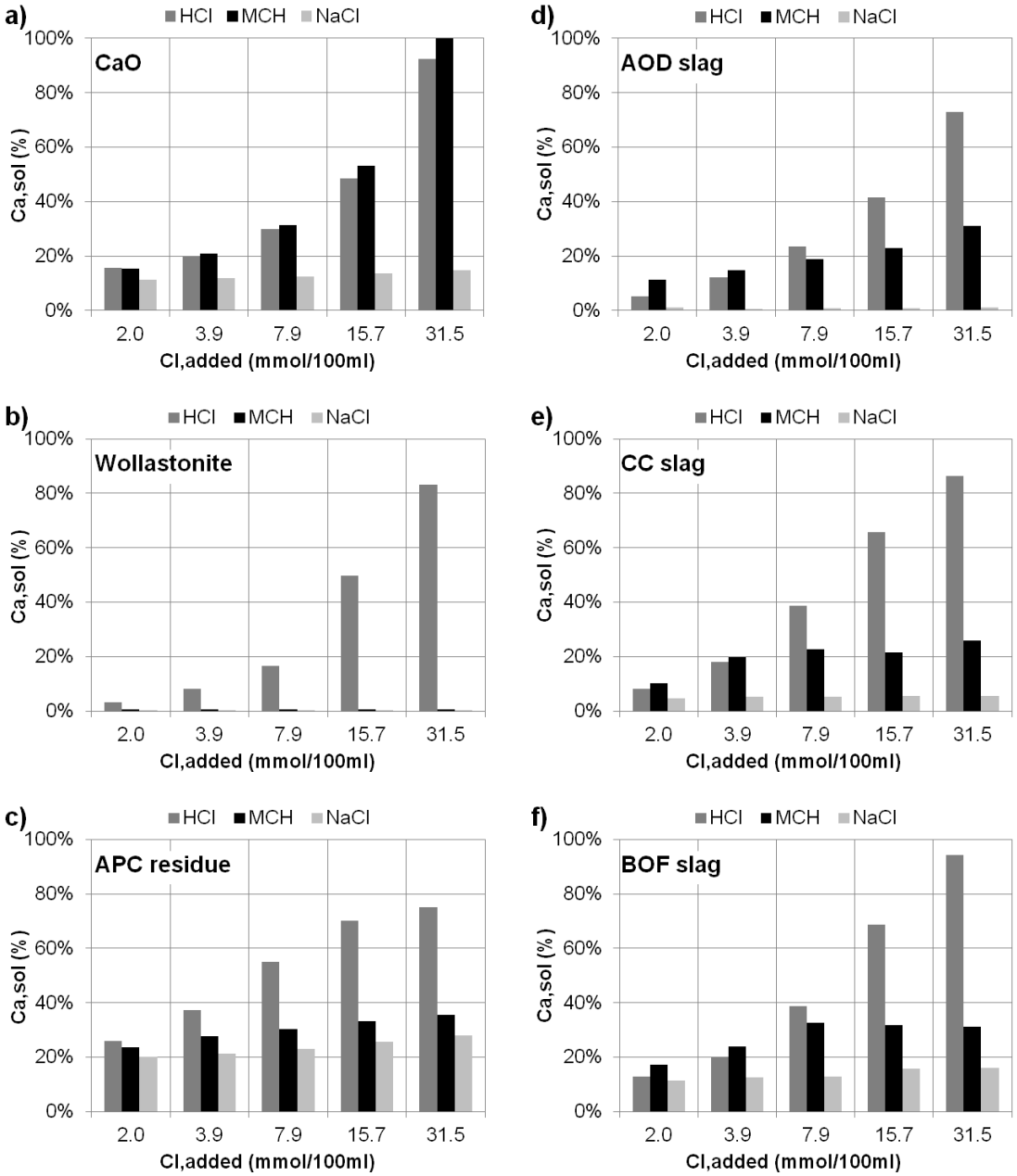

Fig. 6.2. Extent of calcium leaching from CaO (a), wollastonite (b) APC residue (c), AOD slag (d), CC slag (e) and BOF slag (f) as a function of HCl, $MgCl_2 \cdot 6H_2O$ (MCH) and NaCl additions, expressed on the basis of moles of added chloride; 1 g/100ml solids used.

The results indicate that sodium chloride is a generally ineffective calcium leaching agent, as its addition results in only incremental improvement beyond the innate solubility of calcium from the differing materials. Jo et al. (2012) similarly obtained only 1 % improvement in calcium leaching extent (from 4.6 to 5.6 %) from Ordinary Portland Cement (OPC) in 0.5 M NaCl. This confirms that calcium leaching is driven by the greater solubility of calcium hydroxide over the hydroxide of the additive; that is, as NaOH is more soluble than $Ca(OH)_2$, the addition of NaCl does not result in significant calcium leaching.

The most effective leaching agent is HCl, unsurprisingly as this is the most acidic additive, enabling 73–94 % Ca extraction efficiency from the different solids at the highest tested dosage. The strong affinity of hydronium ions (H_3O^+) for hydroxyl ions (OH^-), leading to the neutralization reaction, results in the formation of highly soluble chlorides of the alkali components of the solid

substrates. This effect, however, means that HCl is not selective for calcium, being able to solubilise other major components of the alkaline materials, especially Mg (74–100 % extraction from three slags and APC residue at highest dosage).

Magnesium chloride hexahydrate (MCH) proves to be even more efficient than HCl for calcium leaching from CaO at every dosage tested, up to a maximum leaching of 100 %. For the three slags and the APC residue, MCH performed moderately well, achieving 26–35 % calcium leaching. For wollastonite, however, the extraction efficiency of MCH was essentially nil. This suggests that mineralogy is the most likely reason for the lower calcium extraction efficiency of MCH versus HCl, given that the slags and APC residue are predominantly composed of silicates, ferrites, sulphates and aluminates, most of which likely require lower pH to hydrolyze compared to lime. In particular, the monocalcium silicate ($CaSiO_3$) that makes up wollastonite (Table 6.2) appears to be substantially less reactive with respect to MCH than the complex silicates that make up the slags (e.g. β- and γ-dicalcium silicates, bredigite, merwinite...). Analogously, it is known that wollastonite requires much more aggressive conditions (i.e. higher T and P) to be susceptible to aqueous mineral carbonation than steel slags (Huijgen et al., 2006).

Fig. 6.3a presents the dissolution of calcium from CaO on a molar basis, as a function of moles MCH added. This plot enables the determination of how atom-efficiently MCH extracts calcium. It can be seen that the amount of solubilised calcium (denoted Ca(sol) in the graph) is linearly proportional to the amount of MCH added, and is constantly greater than the 1:1 relationship. Upon further inspection, it is found that the difference between the experimental and 1:1 lines is equal to the solubility of CaO in pure water (first data point). Hence, by deducting this value from the experimental data points, the new line (denoted Ca(+sol), to refer to the added Ca solubilisation obtained by additive use) lies precisely on the 1:1 line. This means that MCH atom-efficiently leaches calcium from CaO (i.e. 1 mmol Ca leached for every millimole Mg added) and that the innate solubility of $Ca(OH)_2$ (from CaO hydration) is unaffected by the addition of MCH.

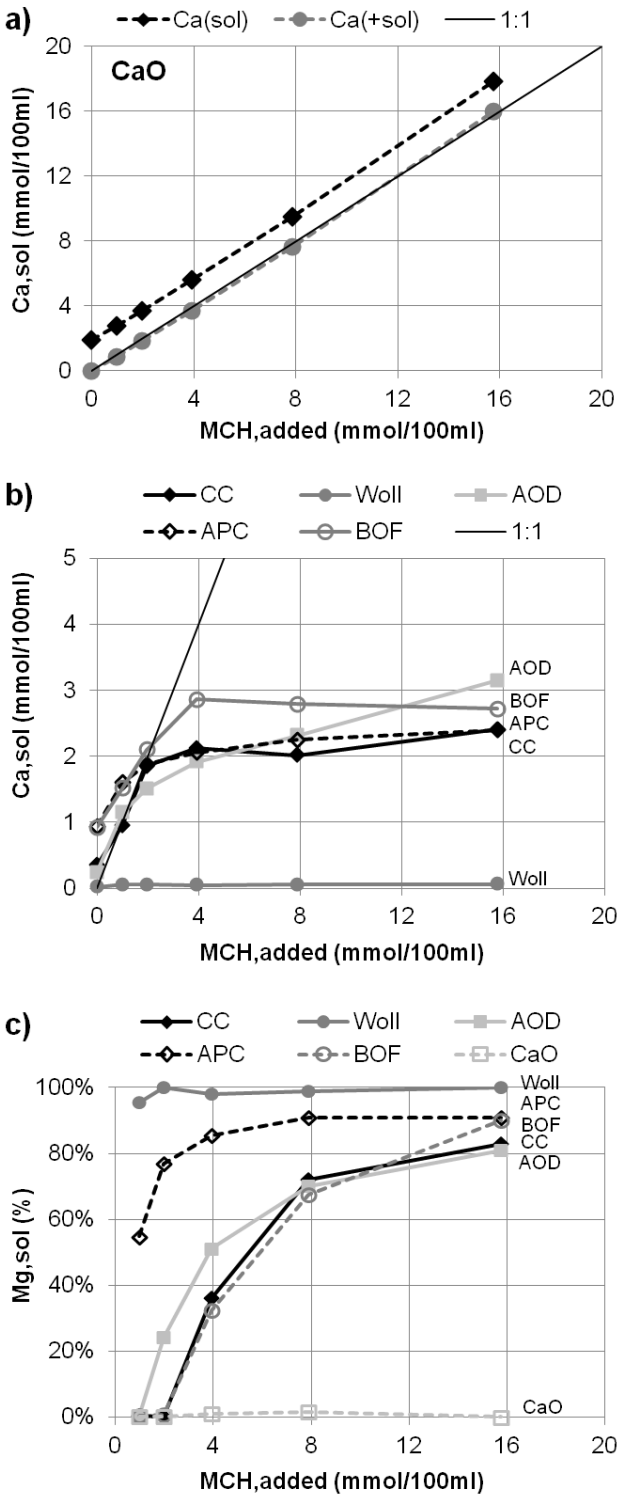

Fig. 6.3. Calcium solubility from CaO (a) and other alkaline materials (b) as a function of amount of MCH added; and fraction of added Mg remaining in solution as a function of amount of MCH added to each alkaline material solution (c).

On Fig. 6.3b the molar solubilisation of calcium from the other five alkaline materials as a function of MCH addition is presented. It is noted that, with the exception of the unresponsive wollastonite, calcium leaching at first increases proportionally to MCH addition, but eventually deviates from the slope of the 1:1 line, finally stabilizing at comparable levels (2.4–3.2 mmol/100ml). Incomplete leaching can occur due to the exhaustion of minerals susceptible to leaching by MCH, but can also be caused by the formation of a Ca-depleted silica-rich layer (Daval

et al., 2009) or a layer of deposited precipitates (namely brucite ($Mg(OH)_2$)) that surrounds the unreacted material present in the particle core (Kurdowski et al., 2004), possibly reducing permeability and/or increasing diffusion length, and thus limiting the extraction extent. However, brucite deposition might not be the cause, as it crystallizes into loosely packed fibrous structures (Ceulemans, 2011), and in an analogous study (Sinadinović et al., 1997), where $CaCl_2$ was used for leaching Pb from $PbSO_4$, resulting in the precipitation of a layer of insoluble $CaSO_4$, this layer was found to be porous and to not appreciably impede leaching. It is also apparent from Fig. 6.3b that leaching from BOF slag and APC residue at zero MCH addition (i.e. in water only) is greater than from the stainless steel slags, which is attributable to greater contents of lime (for BOF slag), portlandite ($Ca(OH)_2$) and calcium chloride hydroxide (Ca(OH)Cl) (for APC residue) in their mineral composition (Table 6.2).

The atom-efficiency of MCH used as a calcium leaching agent is further elucidated in Fig. 6.3c, where the percentage of added Mg remaining in solution after leaching (Mg,sol) is plotted versus the amount of added MCH. It should be restated that the calcium leaching mechanism involves the precipitation of brucite ($Mg(OH)_2$), and thus effective use of MCH should result in disappearance of Mg from solution. This is indeed the case for CaO; Fig. 6.3c shows that dissolved Mg remains essentially nil up to 16 mmol/100ml (sufficient to leach 0.9 g CaO). The opposite occurs for wollastonite, with essentially all added Mg remaining in solution due to the low reactivity of the material. In the case of the steel slags, the amount of solubilised Mg is nil for low MCH additions, indicating high leaching efficiency ($\geq$ 99 %), but eventually increases as the amount of extractable calcium (i.e. calcium amiable to MCH leaching) in the slags decreases. In contrast, in the case of APC residue, the leaching efficiency (100 % – % Mg,sol) of MCH is consistently lower, even for the smallest amount of MCH addition (45 %). This can be explained by the fact that much of the calcium leaching at this level is due to the inherent solubility of the residue, and so only part of the magnesium added participates in the leaching/precipitation extraction mechanism.

To test if solubility limitation may also limit calcium extractability, besides the other possible aforementioned mineralogical mechanisms, and to assess the scalability of MCH-enhanced leaching in view of mineral carbonation processes, experiments were performed using CC slag with increasing solids concentrations (from 1.0 to 25.0 g/100ml), at fixed MCH to slag ratio of 0.8:1, and 24 hours duration. These results are presented in the first set of data of Fig. 6.4, where the amount of soluble calcium is normalized on the basis of millimoles leached per gram solids. As can be seen, the normalized concentration of calcium remains essentially constant (within an experimental variability of ± 3 %) up to 10 g/100ml, and slightly decreases at 25 g/100ml, possibly as a result of poor mixing at this high solids loading.

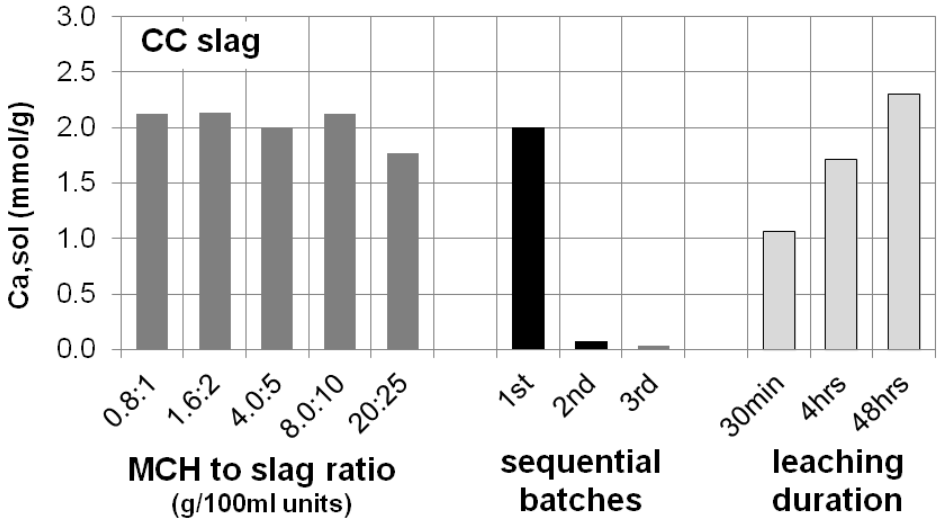

Fig. 6.4. Calcium solubilisation from CC slag as a function of: increasing solids concentration at fixed MCH to slag ratio (g/100ml units) and 24 hours duration; sequential leaching for 24 hours each batch with MCH to slag ratio of 4.0:5, and; leaching duration with MCH to slag ratio of 0.8:1.

Another experimental variation presented in the second set of data of Fig. 6.4, also aiming to test extraction limitations, consisted in sequentially leaching CC slag with MCH three times, for 24 hours each batch, at a fixed MCH to slag loading ratio of 4.0:5 (g/100ml units). Calcium leaching from the second and third extractions was found to be negligible. Based on these two sets of experiments, it can be said that MCH-enhanced calcium leaching does not reach a limiting capacity in the operating range tested. Thus mineralogical mechanisms are most likely responsible for limiting MCH-enhanced calcium extraction to lower levels than those achieved with HCl (26 % versus 86 % in the case of CC slag (Fig. 6.2)).

Lastly, the effect of leaching duration was also assessed using a fixed MCH to slag loading ratio of 0.8:1; results are presented in the third set of data of Fig. 6.4. It is found that MCH leaching is time-dependent, but that in the first 30 minutes approximately half of the leaching that occurs after 48 hours takes place. This is satisfactory, since carbonation reactions of Ca-bearing materials usually last for tens of minutes to a few hours, and thus the leaching and carbonation reactions can potentially occur simultaneously.

6.3.1.2. Solid phase analyses

More insight on the mineralogical mechanisms of MCH-assisted Ca-leaching was gained by analyzing leached solids by QXRD and comparing the mineralogical changes to the pre-leaching materials. Results are presented in Fig. 6.5, which includes superimposed pre- and post-leaching diffractograms and quantitative comparative data. These experiments were conducted with MCH to solids loading ratio of 4.0:5 to produce sufficient leached materials for analysis.

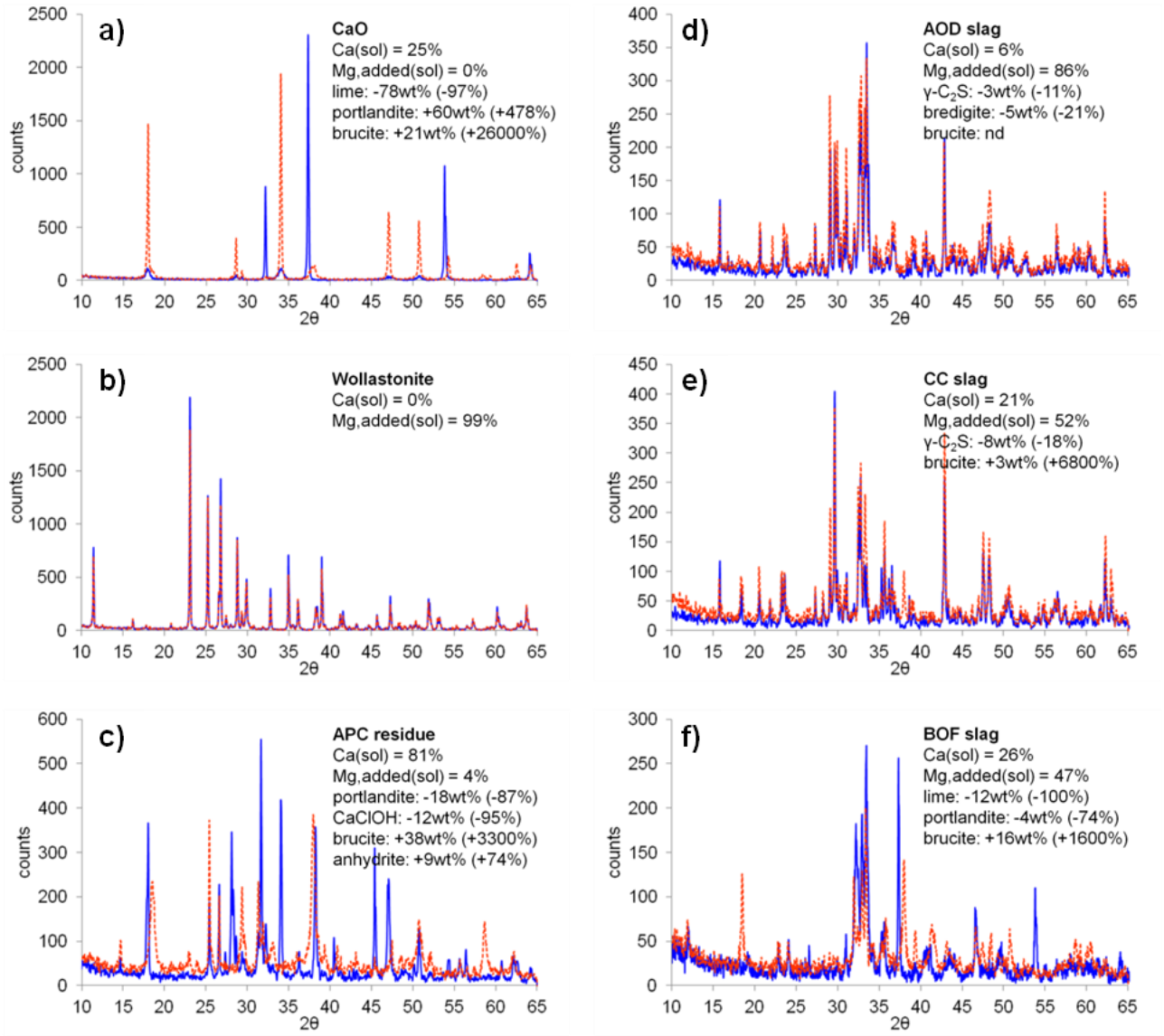

Fig. 6.5. Change of mineralogical composition of alkaline materials after leaching with MCH for 24 hours using MCH to solids ratio of 4.0:5, determined by QXRD; blue solid lines represent original materials, and red dashed lines are leached materials (colour in electronic version); Ca(sol) is percentage fraction of calcium dissolved from solids; Mg,added(sol) is percentage fraction of added magnesium that remained in solution; changes in mineral composition of main dissolved, precipitated or enriched phases is shown (in wt% change and % change compared to original composition).

In the case of CaO, Fig. 6.5a shows that, predictably, lime is at first transformed to portlandite ($Ca(OH)_2$). The calcium leaching from this material is reflected by the significant amount of brucite ($Mg(OH)_2$) formation (21 wt% in the leached solids). Evidently, since the amount of MCH in this experiment was not sufficient to fully leach all the calcium (~18 g MCH would have been required for complete leaching of 5 g CaO), the leached solids still contain a substantial amount of portlandite.

In the case of wollastonite (Fig. 6.5b), the diffractograms of the pre- and post-leaching materials are virtually identical, in agreement with its negligible response to MCH leaching. The APC residue underwent significant mineralogical changes (Fig. 6.5c). In particular, portlandite and calcium chloride hydroxide were almost completely dissolved (87–95 %), while significant

formation of brucite was detected (38 wt%). The increase of anhydrite ($CaSO_4$) concentration is most likely a result of mass enrichment, since a substantial proportion of the material dissolved into the MCH solution (due to MCH-induced leaching as well as innate dissolution of soluble salts inherently present, including halite, sylvite and tachyhydrite (Table 6.2)).

The stainless steel slags underwent less significant changes in mineralogy (Figs. 6.5d and 6.5e), with some reduction (11–21 %) in the amounts of γ-dicalcium silicate and bredigite (the latter only for AOD slag). It is possible that other alkali phases partially solubilise, but if they do so in similar proportions (i.e. congruently), it becomes difficult to gauge such changes by XRD analysis. Also, only modest deposition of brucite was detected in CC slag (3 wt%), possibly as the complex diffraction patterns of the slags can mask small changes in composition. Finally, the simple calcium minerals from BOF slag (lime and portlandite) were, as could be expected, significantly solubilised in the presence of MCH (Fig. 6.5f). This resulted in appreciable precipitation of brucite (16 wt%).

6.3.2. Carbonation results

In view of the positive effect of magnesium chloride in enhancing the leaching of calcium from alkaline materials, experiments were conducted to test if the use of MCH as an additive to aqueous mineral carbonation improves carbonation kinetics or extends carbonation conversion, and for that matter CO_2 uptake. An additional hypothesis to be tested was if the promotion of the aragonite polymorph of calcium carbonate, known to occur at moderate reaction temperatures in the presence of dissolved Mg coupled to sonication (Santos et al., 2012), could also affect the kinetics, conversion and uptake. As such, a series of experiments was conducted emulating the carbonation conditions utilized in Santos et al. (2013a), wherein the effect of ultrasound for the intensification of the carbonation of AOD and CC slags was tested and confirmed.

In the current study, AOD slag was selected as the carbonating material. This slag was chosen as, compared to CC slag and based on our prior works (Santos et al., 2013a and b), it stands to benefit most from improved conversion. Four experimental variations were performed: (i) mixer-only without MCH; (ii) mixer-only with MCH; (iii) combined mixer/ultrasound without MCH; and (iv) combined mixer/ultrasound with MCH. The other experimental parameters varied were reaction time (30, 120 and 240 minutes) and, for experiments with MCH addition, amount of MCH added (2.05, 4.1, 8.3 and 16.6 g/L).

6.3.2.1. CO_2 uptake analysis

The results of carbonation tests, expressed in the form of CO_2 uptake determined by TGA, are presented in Figs. 6.6a (mixer-only) and 6.6b (combined mixer/ultrasound). The maximal theoretical CO_2 uptake capacity of AOD slag, based on its CaO composition, is 0.446 g,CO_2/g,slag. The CO_2 uptake was significantly enhanced with the use of ultrasound, for both the cases with and without MCH (increasing from a range of 0.10–0.14 to the range of 0.19–0.27 g,CO_2/g,slag after 240 minutes). This finding agrees with our previous work (Santos et al. 2013a), and can be attributed to the reduction in particle size and removal of passivating layers (Ca-depleted silica-rich layer, and deposited carbonates) caused by sonication (see Fig. 6.7b; further discussion follows in Section 6.3.2.2).

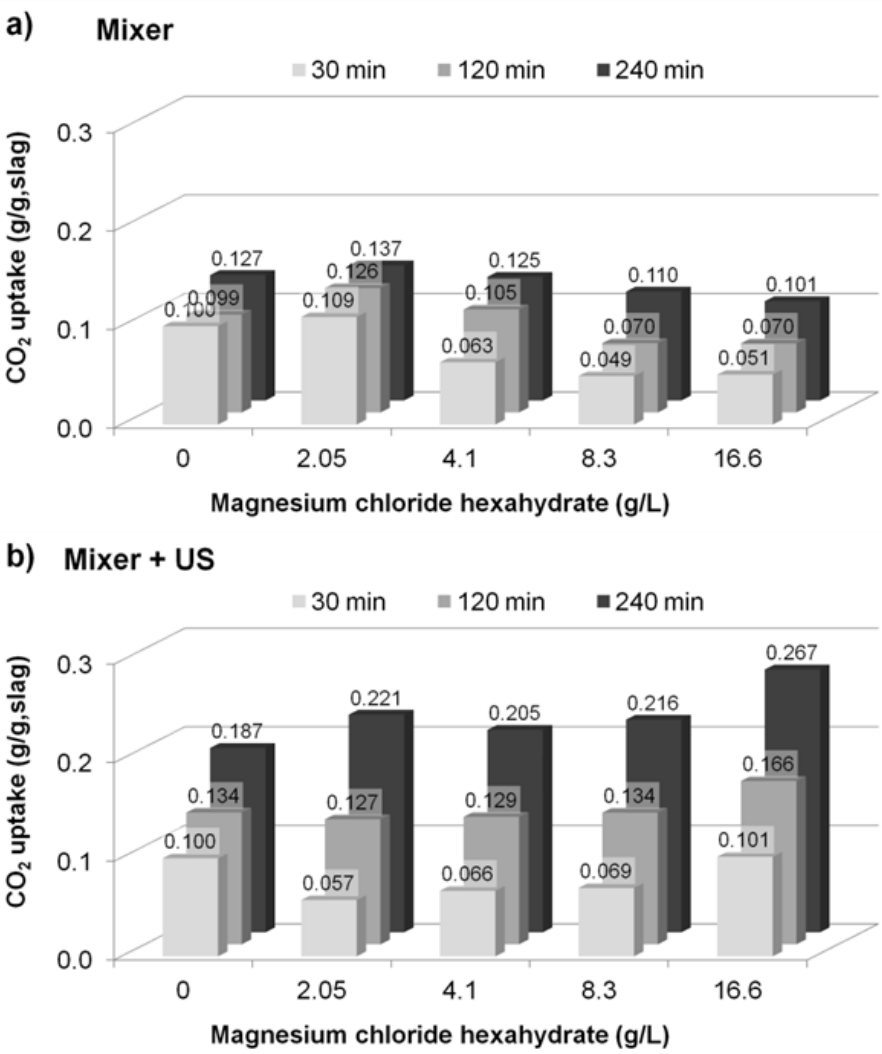

Fig. 6.6. CO_2 uptake of carbonated AOD slag using mixer-only (a) and combination mixer/ultrasound (b) as a function of amount of MCH added and reaction time.

The addition of MCH notably improved carbonation extent when using ultrasound (Fig. 6.6b), where higher MCH dosage resulted in higher CO_2 uptake for each reaction duration used. For the case of mixer-only, however, it is seen that only for the lowest MCH dosage the CO_2 uptake is slightly enhanced (Fig. 6.6a); at higher MCH dosages the carbonation extent is reduced, for each of the reaction durations used. It is also found that the CO_2 uptake of mixer/ultrasound + MCH experiments significantly surpasses those of mixer-only + MCH at longer reaction times only (120 and 240 min), while at 30 min the CO_2 uptakes are comparable.

These observations suggest that the carbonation enhancement effect of MCH is not due to calcium leaching enhancement; in fact, it appears that MCH leaching delays the carbonation kinetics (this was also experienced with $Ca(OH)_2$ carbonation experiments conducted by Santos et al. (2012)). Mignardi et al. (2011) suggest that $MgCl_2$ lowers the degree of CO_2 degassing, thus regulating the availability of carbonic ions in solutions. Verification by geochemical modelling (Table 6.3) confirms that MCH additions to calcite-saturated solution enhances the dissociation of carbonic acid ($H_2CO_{3(aq)}$). These same simulations also show that the salting-out effect, where the solubility of CO_2 decreases as a function of electrolyte concentration (Yasunishi and Yoshida, 1979), is prevented in a calcite-saturated system. Kinetic effects, however, are not captured in these equilibrium simulations, and could play a role in the slowing of MCH-mediated carbonation. It thus

appears that mineralogical and microstructural effects are most likely responsible for the carbonation improvement achieved in the sonicated experiments, as discussed next.

Table 6.3. Geochemical modeling (Visual MINTEQ) results of the effect of MCH addition (81.65 mM) and calcite saturation on the CO_2 solubility and H_2CO_3 dissociation; $P(CO_2)$ = 1 atm, T = 50 °C.

Log activity (M)	0 mM MCH + pure water	81.65 mM MCH + pure water	0 mM MCH + calcite-saturated	81.65 mM MCH + calcite-saturated
Ca^{+2}	-	-	-2.496	-2.619
$CaCl^{+}$	-	-	-	-3.127
$CaCO_{3(aq)}$	-	-	-5.166	-5.166
$CaHCO_3^{+}$	-	-	-3.288	-3.349
$CaOH^{+}$	-	-	-8.322	-8.383
Cl^{-}	-	-0.959	-	-0.962
CO_3^{-2}	-10.175	-10.268	-6.167	-6.044
H^{+}	-3.998	-3.952	-6.002	-6.064
$H_2CO_{3(aq)}$	-1.711	-1.711	-1.711	-1.711
HCO_3^{-}	-3.998	-4.045	-1.995	-1.933
Mg^{+2}	-	-1.706	-	-1.733
$Mg_2CO_3^{+2}$	-	-10.091	-	-5.919
$MgCl^{+}$	-	-2.011	-	-2.04
$MgCO_{3(aq)}$	-	-8.888	-	-4.69
$MgHCO_3^{+}$	-	-4.664	-	-2.578
$MgOH^{+}$	-	-8.287	-	-6.201
OH^{-}	-9.242	-9.289	-7.238	-7.177
Total $CO_{2(aq)}$	-1.709	-1.708	-1.521	-1.465
Concentration (M)				
Total $CO_{2(aq)}$	0.0196	0.0187	0.0316	0.0387

6.3.2.2. Mineralogical and morphological analyses

The mineralogical composition of the three main carbonate products formed in the carbonated slags, determined by QXRD, is presented in Fig. 6.7a. The values for experiments performed with different MCH dosages have been averaged for ease of comparison, as the quantification variability was relatively low (± 10 wt%). It is apparent that in experiments without MCH addition, calcite was the predominant carbonate phase formed. The addition of MCH to mixer-only experiments led to the formation of significant quantities of magnesian calcite (nominal chemical formula $Ca_{1-x}Mg_xCO_3$, where x is typically 0–0.15 (Kitano et al., 1979)), although aragonite was predominant at 120 min. It is possible that small quantities of Mg from MCH additions became incorporated in the forming carbonates in these experiments, as was observed by Kim et al. (2006). The morphologies of the precipitated layers of these two carbonate products around the slag particles are very distinct: magnesian calcite crystals form into compact agglomerates (Figs. 6.8b and 6.8e) while aragonitic acicular (needle-like) crystals effloresce into less microstructurally packed formations (Figs. 6.8a and 6.8d).

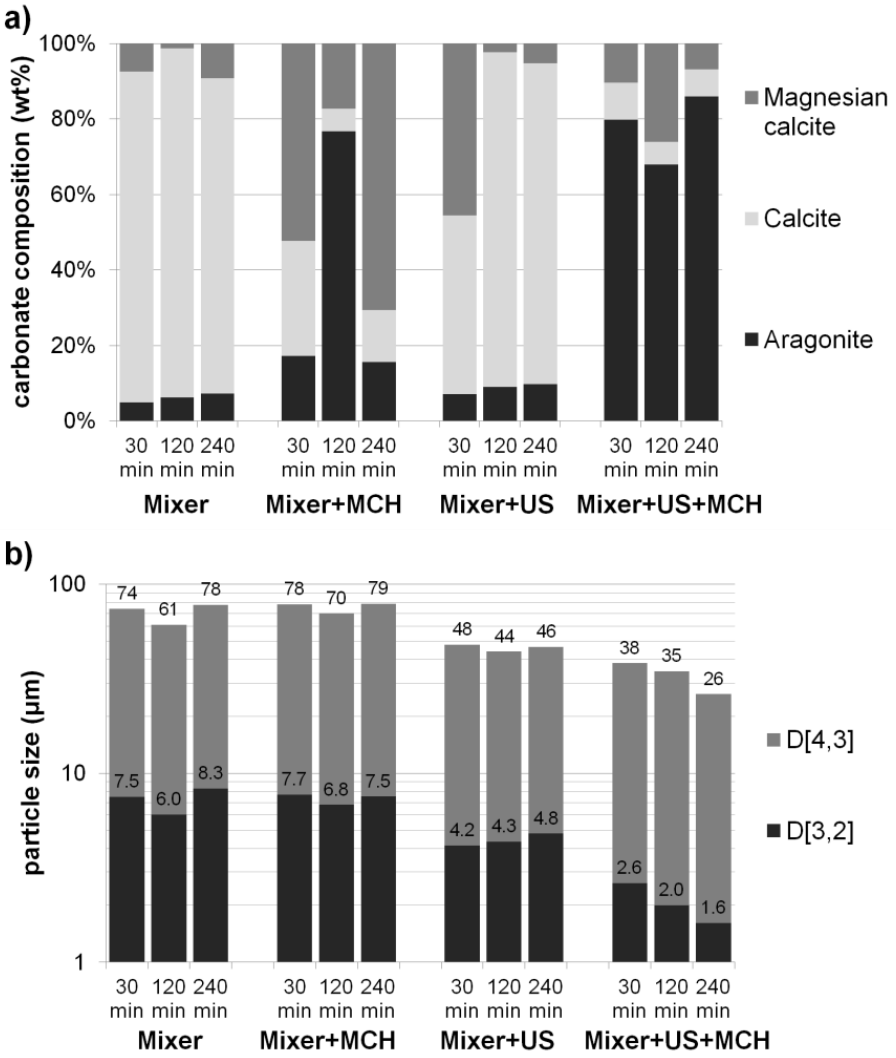

Fig. 6.7. Carbonate composition (a) and mean particle diameters (b) of carbonated AOD slag using mixer-only, combination mixer/ultrasound, with and without MCH addition, as a function of reaction time; results with varying MCH dosages were averaged to facilitate plotting.

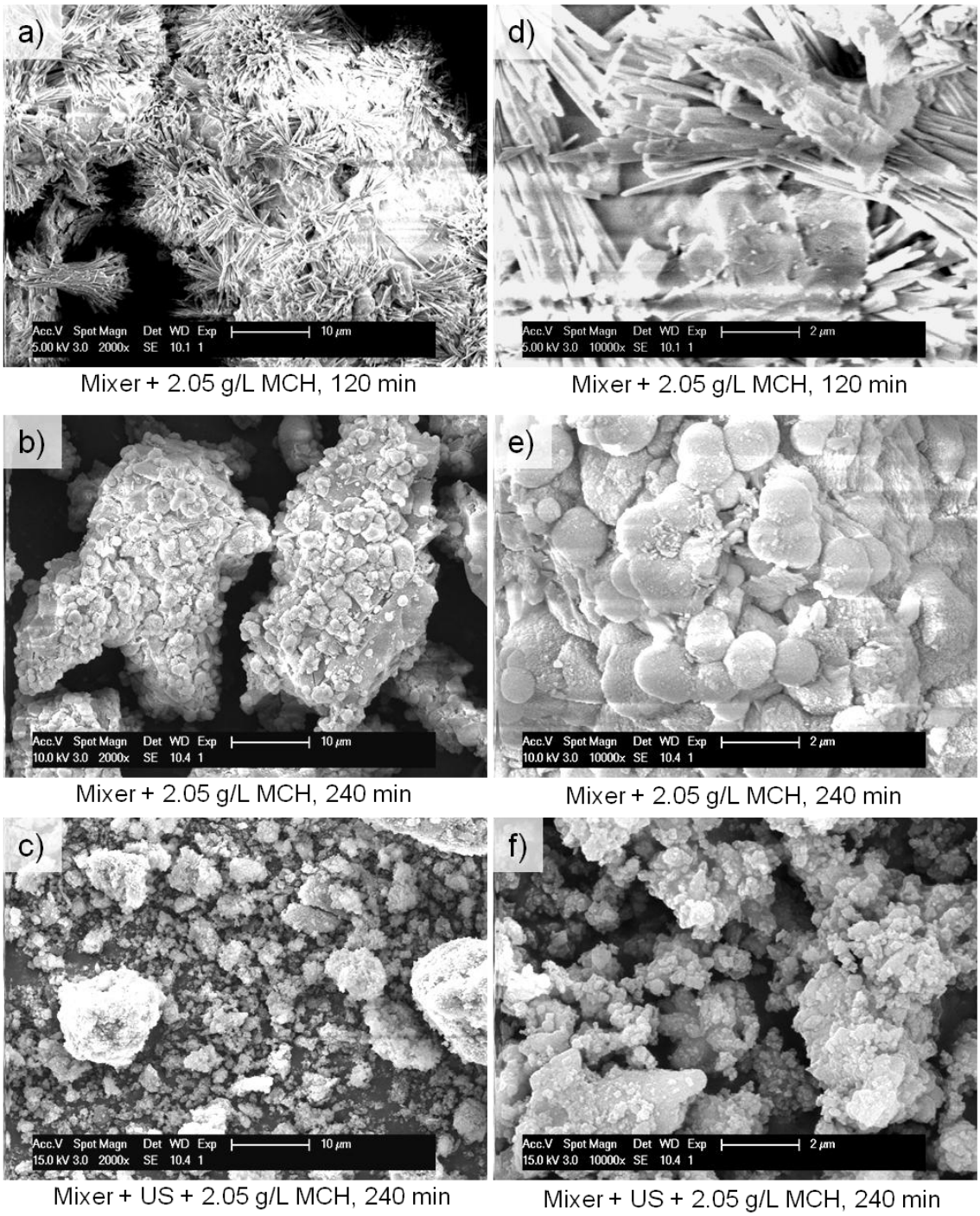

Fig. 6.8. Morphology of carbonated AOD slag particles using mixer-only with MCH after 120 (a,d) and 240 (b,e) minutes reaction time, and using combination mixer/ultrasound with MCH after 240 minutes reaction time (c,f).

In the case of sonicated experiments with MCH, the preferential formation of aragonite is clearly evidenced in Fig. 6.7a; however, due to extensive attrition of the particles caused by sonication, the crystal morphology is not clearly discernible in Figs. 6.8c and 6.8f. Santos et al. (2012) attributed the formation of aragonite under sonication to two mechanisms: (i) imploding cavities generate localized regions of high temperature that can lead to the nucleation of aragonite seeds, given aragonite formation is promoted at higher temperatures; and (ii) the nucleation rate may be enhanced by sonication, thus maintaining stochastically preferable aragonite formation over calcite even at low crystal growth bulk temperatures. It should also be noted that insignificant

amounts of brucite were detected in the carbonated slags (< 0.5 wt%), suggesting that the passivation of the particles by brucite deposition was not the cause of the detrimental effect of MCH on the CO_2 uptake of mixer-only experiments.

The formation of aragonite can be tied to the further reduction in particle size for experiments combining ultrasound with MCH (Fig. 6.7b). The use of ultrasound, without MCH, reduces the volume moment mean diameter (D[4,3]) of the carbonated slag from the range of 61–78 μm to a range of 44–48 μm, and the surface area moment mean diameter (D[3,2]) from 6.0–8.3 μm to 4.2–4.8 μm. The addition of MCH to sonicated tests further reduces the D[4,3] and D[3,2] to as low as 26 and 1.6 μm, respectively, after 240 min reaction time (particle morphology shown in Figs. 6.8c and 6.8f).

These reductions are significant, and can be explained by two mechanisms (Santos et al., 2013a): (i) the erosion of large particles is indicated primarily by the D[4,3] value (as it is sensitive to particle volume changes), and (ii) the formation of micron- to sub-micron sized fragments is reflected on the D[3,2] value (which is sensitive to the formation of surface area). It thus appears that aragonitic crystals, due to their acicular morphology and arrangement, are more easily cleaved off the surface of the carbonated particles due to sonication, either through the induction of cavitation shock waves and micro-jetting on the particle surface (as observed by Shu et al. (2012)), or through enhanced inter-particle collisions (as recorded by Prozorov et al. (2004)).

6.4. CONCLUSIONS

This work studied the utilization of magnesium chloride ($MgCl_2$) as an additive for the improvement of the mineral carbonation of alkaline materials. The objective was to leverage two aspects of $MgCl_2$ to improve the carbonation reaction kinetics and extent: (i) its ability to enhance the leaching of calcium, via a reversible precipitation/solubilisation reaction mechanism, and (ii) its ability to promote (at suitable temperatures or in the presence of sonication) the preferential crystallization of the acicular (needle-like) aragonite polymorph of calcium carbonate ($CaCO_3$).

Leaching of lime (CaO) by $MgCl_2$ was found to be atom-efficient; that is, one mole of Ca is extracted for every mole of Mg added. For the waste-derived materials (slags and APC residue), however, the efficiency at the highest tested dosage (0.316 M chloride basis) reduced to levels around 26–35 %, significantly lower than that with HCl (73–94 %), but much superior to that of NaCl (1–28 %). This leaching limitation of $MgCl_2$ can be linked to the mineralogy of the waste materials, which are predominantly made up to silicates, ferrites, sulphates and aluminates. This effect was particularly evident from the very poor calcium leaching performance from wollastonite ($CaSiO_3$). Conversely, the greater proportion of simple calcium minerals (e.g. lime, portlandite and calcium chloride hydroxide) in BOF slag and APC residue aided in the dissolution of calcium from these materials, as verified by X-ray diffraction. In addition, the formation of a Ca-depleted silica-rich layer surrounding the Ca-rich particle core can increase the diffusion length and contribute to the leaching limitation. Solubility limits, on the other hand, were not reached in the concentration range tested, and leaching kinetics were found to be sufficiently fast, thereby conforming to typical conditions of aqueous mineral carbonation. These results suggest that $MgCl_2$ has the potential to contribute to the intensification of the mineral carbonation reaction.

The effect of $MgCl_2$ on the mineral carbonation of AOD stainless steel slag was tested in both mechanically mixed and sonicated reaction systems. The addition of $MgCl_2$ to mixer-only experiments resulted in reduced carbonation conversion at every reaction duration tested, indicating

that it slows the reaction kinetics, proportionally to the additive concentration. In sonicated experiments, however, there was significant improvement in CO_2 uptake with the addition of $MgCl_2$, increasing from 0.19 to 0.27 g,CO_2/g,slag (60 % of the theoretical capacity) after 240 min with 82 mM $MgCl_2$. At the same time, the preferential formation of aragonite was detected (86 wt% of the total formed carbonates). Given the acicular crystal morphology of aragonite, and its resulting low packing density when formed as a precipitated carbonate layer that surrounds the unreacted particle core, it appears that the surface erosion effect of sonication, caused by cavitation, shock waves and inter-particle collisions, becomes enhanced under these conditions. This is evidenced in the noticeable reduction in the volume moment (D[4,3]) and surface area moment (D[3,2]) mean particle diameters after the carbonation reaction. These observations suggest that, in the conditions tested, the carbonation enhancement effect of $MgCl_2$ is in fact not due to calcium leaching enhancement, but rather caused by its influence on mineralogical and microstructural properties. Under other processing conditions,[XXI] however, the calcium leaching enhancement of $MgCl_2$ may be better exploited and this can be the subject of future research.

6.5. REFERENCES

Ahn, J.-W., Park, W.K., You, K.-S., Cho, H.-C., Ko, S.-J., Han, C., 2007. Roles of additives on crystal growth rate of precipitated calcium carbonate. Solid State Phenomena 124-126, 707-710.

Bobicki, E.R., Liu, Q., Xu, Z., Zeng, H., 2012. Carbon capture and storage using alkaline industrial wastes. Progress in Energy and Combustion Science 38, 302-320.

Bodor, M., Santos, R.M., Van Gerven, T., Vlad, M., 2013. Recent developments and perspectives on the treatment of industrial wastes by mineral carbonation - A review. Central European Journal of Engineering, DOI:10.2478/s13531-013-0115-8.

Ceulemans, P., 2011. Improved synthesis of aragonite. M.Sc. Thesis, Katholieke Universiteit Leuven, Leuven.

Daval, D., Martinez, I., Guigner, J.-M., Hellmann, R., Corvisier, J., Findling, N., Dominici, C., Goffé, B., Guyot, F., 2009. Mechanism of wollastonite carbonation deduced from micro- to nanometer length scale observations. American Mineralogist 94, 1707-1726.

Eloneva, S., Mannisto, P., Said, A., Fogelholm, C.-J., Zevenhoven, R., 2011. Ammonium salt-based steelmaking slag carbonation: Precipitation of $CaCO_3$ and ammonia losses assessment. Greenhouse Gases: Science and Technology 1 (4), 305-311.

Eloneva, S., Teir, S., Revitzer, H., Salminen, J., Said, A., Fogelholm, C.-J., Zevenhoven, R., 2009. Reduction of CO_2 emissions from steel plants by using steelmaking slags for production of marketable calcium carbonate. Steel Research International 80 (6), 415-421.

Eloneva, S., Teir, S., Salminen, J., Fogelholm, C.-J., Zevenhoven, R., 2008. Steel converter slag as a raw material for precipitation of pure calcium carbonate. Industrial & Engineering Chemistry Research 47, 7104-7111.

Ferrini, V., De Vito, C., Mignardi, S., 2009. Synthesis of nesquehonite by reaction of gaseous CO_2 with Mg chloride solution: Its potential role in the sequestration of carbon dioxide. Journal of Hazardous Materials 168, 832-837.

[XXI] Remark: E.g. at higher temperatures and CO_2 partial pressures, in a pre-treatment step prior to carbonation, or using other calcium-rich materials that are not silicate based, such as ashes and sludges.

Hu, Z.S., Shao, M.H., Li, H.Y., Cai, Q., Ding, S.G., Wei, X.P., Deng, Y.L., 2008. Mg2+ content control of aragonite whisker synthesised from calcium hydroxide and carbon dioxide in presence of magnesium chloride. Materials Science and Technology 24 (12), 1438-1443.

Huijgen, W.J.J., Witkamp, G.-J., Comans, R.N.J., 2006. Mechanisms of aqueous wollastonite carbonation as a possible CO_2 sequestration process. Chemical Engineering Science 61, 4242-4251.

Jo, H., Jang, Y.-N., Jo, H.Y., 2012. Influence of NaCl on mineral carbonation of CO_2 using cement material in aqueous solutions. Chemical Engineering Science 80, 232-241.

Kim, J.-H., Ahn, J.-W., Ko, S.-J., Park, W.-K., Han, C., 2006. Inhibition mechanism of magnesium ion on carbonation reaction with $Ca(OH)_2$ and CO_2. Materials Science Forum 510-511, 990-993.

Kirchofer, A., Becker, A., Brandt, A., Wilcox, J., 2013. CO_2 mitigation potential of mineral carbonation with industrial alkalinity sources in the United States. Environmental Science & Technology, 47, 7548−7554.

Kitano, Y., Hood, D.W., 1962. Calcium carbonate crystal forms formed from sea water by inorganic processes. The Journal of the Oceanographic Society of Japan 18 (3), 141-145.

Kitano, Y., Tokuyama, A., Arakaki, T., 1979. Magnesian calcite synthesis from calcium 726 bicarbonate solution containing magnesium and barium ions. Geochemical Journal 13, 181-185.

Kurdowski, W., 2004. The protective layer and decalcification of C-S-H in the mechanism of chloride corrosion of cement paste. Cement and Concrete Research 34, 1555-1559.

Kurdowski, W., Duszak, S., 1995. Changes of C-S-H gel in strong chloride solution. Advances in Cement Research 7 (28), 143-149.

Ma, J., Liu, H.-Y., Chen, Y.-F., 2011. Reuse of $MgCl_2$ as crystal controlling agent in the synthesis process of needle-like calcium carbonate. Journal of Inorganic Materials 26 (11), 1199-1204.

Mignardi, S., De Vito, C., Ferrini, V., Martin, R.F., 2011. The efficiency of CO_2 sequestration via carbonate mineralization with simulated wastewaters of high salinity. Journal of Hazardous Materials 191, 49-55.

Pan, S.-Y., Chang, E.E., Chiang, P.-C., 2012. CO_2 capture by accelerated carbonation of alkaline wastes: a review on its principles and applications. Aerosol and Air Quality Research 12, 770-791.

Passe-Coutrin, N., N'Guyen, Ph., Pelmard, R., Ouensanga, A., Bouchon, C., 1995. Water desorption and aragonite–calcite phase transition in scleractinian corals skeletons. Thermochimica Acta 265, 135-140.

Prozorov, T., Prozorov, R., Suslick, K.S., 2004. High velocity interparticle collisions driven by ultrasound. Journal of the American Chemical Society 126 (43), 13890-13891.

Sanna, A., Hall, M.R., Maroto-Valer, M, 2012. Post-processing pathways in carbon capture and storage by mineral carbonation (CCSM) towards the introduction of carbon neutral materials. Energy & Environmental Science 5, 7781–7796.

Santos, R.M., Ceulemans, P., Van Gerven, T., 2012. Synthesis of pure aragonite by sonochemical mineral carbonation. Chemical Engineering Research and Design 90 (6), 715-725.

Santos, R.M., François, D., Mertens, G., Elsen, J., Van Gerven, T., 2013a. Ultrasound-intensified mineral carbonation. Applied Thermal Engineering 57(1-2), 154-163.

Santos, R.M., Van Bouwel, J., Vandevelde, E., Mertens, G., Elsen, J., Van Gerven, T. 2013b. Accelerated mineral carbonation of stainless steel slags for CO_2 storage and waste valorization: effect of process parameters on geochemical properties. International Journal of Greenhouse Gas Control 17, 32-45.

Santos, R.M., Van Gerven, T., 2011. Process intensification routes for mineral carbonation. Greenhouse Gases: Science and Technology, 1(4), 287-293.

Shu, D., Sun, B., Mi, J., Grant, P.S., 2012. A high-speed imaging and modeling study of dendrite fragmentation caused by ultrasonic cavitation. Metallurgical and Materials Transactions A 43(10), 3755-3766.

Sinadinović, D., Kamberović, Ž., Šutić, A., 1997. Leaching kinetics of lead from lead (II) sulphate in aqueous calcium chloride and magnesium chloride solutions. Hydrometallurgy 47, 137-147.

Xiang, L., Wen, Y., Wang, Q., Jin, Y., 2006. Synthesis of dispersive $CaCO_3$ in the presence of MgCl2. Materials Chemistry and Physics 98, 236-240.

Yasunishi, A., Yoshida, F., 1979. Solubility of carbon dioxide in aqueous electrolyte solutions. Journal of Chemical and Engineering Data 24 (1), 11-14.

Zevenhoven, R., Fagerlund, J., Songok, J.K., 2011. CO_2 mineral sequestration: developments toward large-scale application. Greenhouse Gases: Science and Technology 1 (1) 48-57.

7. Stabilization of basic oxygen furnace slag by hot-stage carbonation treatment

ABSTRACT – Treatment and disposal of Basic Oxygen Furnace (BOF) slag, a residue of the steel production process characterized by high basicity and propensity for heavy metal leaching, is a costly burden on metallurgical plants; a sustainable valorization route is desired. The stabilization of BOF slag utilizing hot-stage carbonation treatment was investigated; this approach envisions carbonation during the hot-to-cold pathway followed by the material after the molten slag is poured and solidified. Three experimental methodologies were employed: (i) in-situ thermogravimetric analyzer (TGA) carbonation was used to assess carbonation reaction kinetics and thermodynamic equilibrium at high temperatures; (ii) pressurized basket reactor carbonation was used to assess the effects of pressurization, steam addition and slag particle size; and (iii) atmospheric furnace carbonation was used to assess the effect of carbonation on the mineralogy, basicity and heavy metal leaching properties of the slag. Free lime was found to be the primary mineral participating in direct carbonation of BOF slag. Initial carbonation kinetics were comparable at temperatures ranging from 500 to 800 ^{o}C, but higher temperatures aided in solid state diffusion of CO_2 into the unreacted particle core, thus increasing overall CO_2 uptake. The optimum carbonation temperature of both BOF slag and pure lime lies just below the transition temperature between carbonation stability and carbonate decomposition: 830-850 ^{o}C and 750-770 ^{o}C at 1 atm and 0.2 atm CO_2 partial pressures, respectively. Pressurization and steam addition contribute marginally to CO_2 uptake. CO_2 uptake progressively decreases with increasing particle size, but basicity reduction is similar independent of particle size. The solubility of some heavy metals reduced after carbonation (barium, cobalt and nickel), but vanadium and chromium leaching increased.

GRAPHICAL ABSTRACT

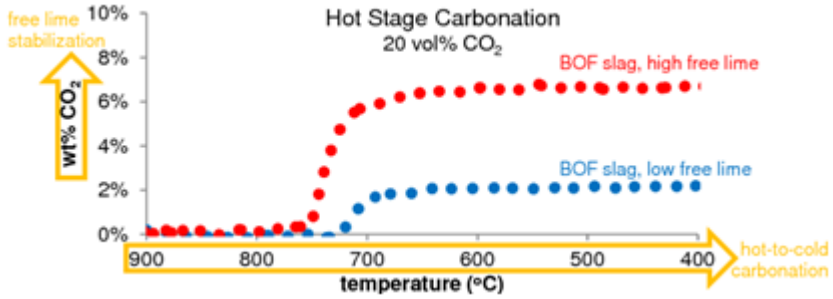

Published as
R.M. Santos, D. Ling, A. Sarvaramini, M. Guo, J. Elsen, F. Larachi, G. Beaudoin, B. Blanpain, and T. Van Gerven.
"Stabilization of basic oxygen furnace slag by hot-stage carbonation treatment".
Chemical Engineering Journal 203, 2012, 239-250.

Author contributions
R.M.S. conceived the research, established collaboration with Laval University, supervised Master's student D. Ling, performed part of the experimental and analytical work, and wrote the article.

7.1. INTRODUCTION

Integrated carbon steel production consists of ironmaking in the Blast Furnace (BF), steelmaking in the Basic Oxygen Furnace (BOF), and continuous casting of steel billets, slabs and blooms. For over a century, with iron and steel industry booming worldwide, a vast amount of slag has been produced as an inevitable by-product of the steelmaking process. While valuable applications have been found for BF slag, mostly in the construction sector such as in cement manufacturing and as a cement replacement in concrete, much of BOF slag production, estimated at 60-120 kg/t steel presently, still ends up in landfill sites [1-3]. The traditional use of BOF slag in road construction, as an aggregate, base or sub-base coarse, has been restricted due to the slag's undesirable expansive nature, resulting in rapid deterioration of the roads [4]. The volume expansion (up to 10% [5]) is attributed to the short term hydration and the long term carbonation of free lime (CaO) and magnesium oxide (MgO) content [6].

To date, four forms of treatment have been commercially used to stabilize BOF slag: (i) weathering in slag pits to convert free lime into hydrated lime, which has been found slow and inefficient [7]; (ii) steam hydration of the slag, utilized by Nippon Steel [8]; (iii) additions of SiO_2 and O_2 (to keep the slag molten) to the slag pot, which act to dissolve the free lime and chemically bond it as silicate, utilized by Thyssen Krupp [7]; and (iv) control of the slag cooling path to stabilize the C_3S (tri-calcium silicate) phase (which otherwise is transformed into C_2S, di-calcium silicate, plus free lime), utilized by Baosteel [9,10].

An alternative and possibly more attractive and low-cost route is the reaction of the alkaline oxides with CO_2, leading to the formation of geochemically stable carbonates (e.g. $CaCO_3$) [11]. Besides capture of CO_2, desirable for emissions reduction, mineral carbonation has also been reported to yield positive effects in terms of the leaching behavior of alkaline earth metals, heavy metals and metalloids from steel slag [12], which can lead to further valorization of the waste material. Numerous studies in recent years have assessed the potential of steel slag carbonation for storage of CO_2 utilizing a variety of aqueous carbonation routes, including slurry carbonation [13,14], wet carbonation [15], block carbonation [16], and two-step carbonation (i.e. leaching of Ca and Mg followed by carbonation of the extracted solution) [17]. However, the major drawbacks of these approaches include the required energy intensive steps (e.g. crushing/milling of the iron-rich monolith slag, prolonged mixing, pressurization, separation, and regeneration of extractants) and the generation of products having low market demand (e.g. carbonated powdery materials) or that are still troublesome (e.g. destabilized heavy-metal containing residual solids, and salt and heavy metal laden wastewater).

To overcome the aforementioned disadvantages of conventional mineral carbonation a novel approach is herein explored, hot-stage carbonation. This approach utilizes two domains of process intensification, namely functional (thus maximizing synergistic effects from partial processes) and temporal (thus optimizing the driving forces and maximizing the specific area to which these apply) [18]. The principal concept is to take advantage of the high temperature source of the slag, and perform mineral carbonation during slag cooling at still high (optimized) temperatures, where the kinetics are more favorable and the (thermal) energy is freely available. In particular, it is envisaged that in order to carbonate the slag while (a) it is still hot, (b) it is solidified, and (c) the material surface area is compatible with requirement for carbonation (i.e. not a monolith), a practical approach to hot-stage carbonation would be to apply it concurrently with hot-stage granulation (see Fig. SC-7.1 in the Supplementary Content for a conceptual scheme).

High temperature carbonation is already applied in CO_2 capture and separation systems that utilize lime-based sorbents subject to looping carbonation/calcination cycles, which typically conduct carbonation in the flue gas temperature range of 600 to 700 ^oC at atmospheric pressure [19-21]. Prigiobbe et al. [22] tested high temperature carbonation of air pollution control residues in the temperature range of 350-500 ^oC, obtaining fast carbonation kinetics (50% conversion in less than one minute) and high conversions (nearly 80%). Mikhail and Turcotte [6] were the first investigators to report carbonation of BOF slag at high temperature; while limited, their findings provided proof-of-concept for this approach. BOF slag was carbonated at 550 ^oC in moist CO_2 in a thermogravimetric analyzer (TGA), and 8% mass gain was attributed to $CaCO_3$ formation. More recently, Kao [23] studied the high temperature carbonation of BOF slag for the purpose of using the slag as a CO_2 sorbent. Breakthrough curves of the CO_2 content of the outlet gas from a tubular reactor, analyzed by infra-red (IR) detection, were reported, with optimum conditions identified as being 500 ^oC, 40% CO_2 inlet concentration and 10% inlet gas relative humidity. Characteristics of the carbonated solids were not extensively assessed. Yu and Wang [24] found BOF slag to carbonate well (up to 20% calcium utilization after 20 minutes reaction time) at temperatures between 500 and 550 ^oC, using CO_2 concentrations between 10-100%; however data and analyses were insufficient to provide clear insight on mineralogical effects or carbonation mechanisms and kinetics.

The present work presents a detailed and systematic study of high temperature BOF slag carbonation, with particular emphasis on carbonation kinetics and conversion. The effect of several process parameters (particle size, temperature, pressure, time and steam addition) on CO_2 uptake and free lime conversion are tested. In addition, the chemical behavior of the treated materials, namely basicity and heavy metal leaching, is assessed. The investigation is centered on the concept of hot-stage carbonation of the slag, that is, experimental methods are designed to simulate the hot-to-cold stage path of the just-produced slag and to elucidate the susceptibility of the slag to carbonation along this route. To achieve these objectives, three hot-carbonation methodologies are applied, which provide varying levels of insight into the technology.

7.2. MATERIALS AND METHODS

7.2.1. BOF slag

7.2.1.1. Slag feedstock

Two freshly produced BOF slag batches were used, containing differing amounts of free lime; they will be referred to as BOF_I (lower free lime) and BOF_{II} (higher free lime). The slags, having been solidified under production conditions, were crushed (jaw crusher) and sieved to four particle size fractions for carbonation studies: < 0.08 mm, 0.08-0.5 mm, 0.5-1.0 mm and 1.0-1.6 mm. These particle sizes were chosen as they are analogous to values reportedly produced during BOF slag dry granulation ([10,25]). The three coarser fractions were wet-sieved to remove fines; calcium saturated water was used to limit dissolution. Finely milled samples were also produced using a McCrone Micronizing Mill. Pure oxide minerals (CaO, 99% purity; Fe_2O_3, >99% purity; MgO, 98% purity; Sigma Aldrich) were also utilized for carbonation for comparison purposes.

7.2.1.2. Slag characterization methodology

Particle size analysis was performed by laser diffraction (LD, Malvern Mastersizer). Specific surface area (S_{BET}) was measured by nitrogen adsorption (Micromeritics TRISTAR 3000) using the BET (Brunauer–Emmett–Teller) model. Material specific density was measured using a pycnometer (Micromeritics AccuPyc 1330). The chemical composition of each BOF slag batch was determined by X-ray Fluorescence (XRF, Panalytical PW2400), and the mineral composition was determined by X-ray Diffraction (XRD, Philips PW1830) with Rietveld refinement technique (Topas Academic v4.1). The distribution of the mineral phases in BOF slag was observed by analysis of the polished cross-sections of millimetre-sized particles of BOF_I slag by Scanning Electron Microscopy (SEM) coupled with Backscattered Electrons (BSE) and Energy Dispersive X-ray Spectroscopy (EDX) (Philips XL30 FEG).

7.2.2. High temperature carbonation methodology

To study the carbonation reaction of BOF slag at high temperature, three experimental approaches were used to provide different insights into the effects of material properties and process conditions on the CO_2 uptake, carbonation conversion of the mineral phases, basicity and heavy metal leaching stabilization. The thermodynamics of the relevant carbonation reactions were assessed by FactSage 6.2 modeling.

7.2.2.1. In-situ TGA carbonation

The first experimental methodology made use of a thermogravimetric analyzer (Perkin Elmer Lab System Diamond TGA-DTA) to conduct in-situ studies of BOF slag carbonation; this method and the equipment used were adapted from the methodology applied in Larachi et al. [26] for the carbonation of chrysotile mining residues. Three variations of this experimental method were used (depicted in Fig. SC-7.2). All experiments used approximately 50 mg of sample (finely-milled BOF slags, or reference pure materials CaO, MgO and Fe_2O_3), which was placed in a tared alumina crucible. All experimental variations commenced with a calcination step to produce 'fresh slag' as is produced industrially from the hot-stage process. This step consisted in heating the sample to 900 ^oC in nitrogen atmosphere (100 ml/min gas flow rate) at 20 ^oC/min heating rate to decompose pre-existing hydrates/hydroxides/carbonates from the material. It should be noted that as all samples underwent this initial calcination step, they experienced equal thermal histories (an important distinction as reported by Bhatia and Perlmutter [27]). Following calcination, experiments denominated as "hot-to-cold TGA carbonation" consisted in cooling the samples from 900 ^oC to 200 ^oC in 20% or 100% carbon dioxide atmosphere (100 ml/min gas flow rate) at 5 ^oC/min cooling rate to carbonate the material. Several flue gas streams in steel plants contain roughly 20% CO_2 [28-29], therefore this value was used for comparison with pure CO_2, which could also be produced from flue gas using one of several established CO_2 separation processes. Experiments denominated as "cold-to-hot TGA carbonation" consisted in cooling the samples from 900 ^oC to 80 ^oC in inert nitrogen atmosphere at 20 ^oC/min cooling rate, followed by heating from 80 ^oC to 1000 ^oC in carbon dioxide atmosphere at 5 ^oC/min heating rate to carbonate the material. Finally, experiments denominated as "fixed temperature TGA carbonation" consisted in cooling the samples from 900 ^oC to a desired temperature (between 500 ^oC and 800 ^oC) in inert nitrogen atmosphere at 20 ^oC/min

cooling rate, followed by holding at the desired temperature in carbon dioxide atmosphere for 60 minutes to carbonate the material. For all experiments the sample weight (loss during calcination step and gain during carbonation step) was continuously monitored to determine CO_2 uptake. A mass spectrometer with quadrupole analyzer (Thermostar Prisma QMS200, Pfeiffer Vacuum) was used to monitor the outlet gas composition and to confirm that the gas composition transition (from N_2 to CO_2) occurred quickly enough; for all practical purposes it was found that the gas composition reached nearly complete transition (> 90% CO_2) in less than one minute.

7.2.2.2. Pressurized basket reactor carbonation

The second experimental methodology (depicted in Fig. SC-7.3) made use of a pressurized basket reactor to study carbonation at high pressure conditions, as well as the effect of steam addition and slag particle size. This method and the equipment used were adapted from the methodology applied in Larachi et al. [30] for the carbonation of chrysotile mining residues. The equipment is shown in Fig. SC-7.4 in the Supplementary Content. Approximately two grams of material was placed in a small stainless-steel mesh basket that allowed the process gas to creep into the sample material bed. The basket was slid coaxially and positioned midway in a steel cylindrical enclosure (1.65 cm internal diameter, 30 cm long) using a hollow metallic stem hosting a thermocouple driven in the middle of the bed. The cylindrical reactor was fit in an electrically-heated temperature-controlled ceramic furnace that could be operated up to 900 ^oC. Prior to carbonation, samples were first heated to 900 ^oC for calcination in argon atmosphere. Upon purging the reactor with argon flow and cooling to the desired reaction temperature (350-650 ^oC), carbon dioxide and steam were introduced up to the desired total pressure (up to 20 bar), consisting of 4 to 20 bar CO_2 and 0 to 8 bar steam partial pressures. Carbonation reaction was conducted for 30 minutes. Following carbonation, the reactor was immediately purged with nitrogen gas flow (300 ml/min) to preclude further carbonation. Once purged, the reactor was heated up to 900 ^oC for calcination. During calcination the reactor outlet gas was directed to an infra-red (IR) detector (ABB AO2000 Uras14) for in-situ quantification of the released CO_2 amounts (i.e. integration of CO_2 gas content over time) and determination of the material CO_2 uptake. Several tests were performed in duplicate to ascertain the accuracy of the measured effects.

7.2.2.3. Atmospheric furnace carbonation

In order to produce larger amounts of high-temperature carbonated materials for XRD, basicity and leaching testing, a horizontal furnace was used. The carbonation methodology (depicted in Fig. SC-7.5) was analogous to the basket reactor methodology, except that up to 10 grams of material could be carbonated at a time in the furnace (it was possible to carbonate 3 grams of material in each of three alumina crucibles that could be placed simultaneously in the furnace to test different materials or particle sizes at identical process conditions, or 10 grams of a single material in a larger crucible). Carbonation experiments were conducted with 100% CO_2 gas flow at near atmospheric pressure (slight positive pressure to prevent infiltration) for varying reaction times (10 minutes to 6 hours) at fixed temperatures (200-800 ^oC). Following carbonation, samples were immediately withdrawn from the furnace to cease carbonation, and allowed to cool in air. The CO_2 uptake was quantified by ex-situ TGA; an amount of 30-50 mg carbonated sample was weighed in a sample pan heated from 25 to 900 ^oC under a nitrogen atmosphere at a heating rate of 15 ^oC/min.

The weight loss was recorded by the microbalance and the amount of CO_2 uptake was quantified by the weight loss between 500-800 ^oC, which can be related to calcium carbonate decomposition [13]. Validation of the accuracy of CO_2 uptake determination via TGA and via calcination coupled to IR detection was performed by comparison of analysis results of identical samples examined with both methodologies; the average discrepancy between the two methods was 4% of the measured values (see Figs. SC-7.6 and SC-7.7 in the Supplementary Content).

7.2.3. Basicity and leaching tests

Batch leaching tests were performed on both carbonated and fresh slag samples to determine the effect of carbonation on the solubility of heavy metals and on the solution pH value. Determination of aqueous elemental concentration was performed in triplicate by Inductively Coupled Plasma Mass Spectroscopy (ICP-MS, Thermo Electron X Series). An amount of two grams of solids was mixed with 100 ml MilliQ water (L/S = 50) in a sealed polyethylene bottle, and shaken on a vibration table for 24 hours. Solution pH was measured and the solution was filtered using 0.45 μm membrane filter prior to dilution for ICP-MS measurement. Solution matrix for ICP-MS measurement was 2% nitric acid. The following elements (in atomic weight order) were analyzed: V, Cr, Co, Ni, Cu, Zn, As, Se, Mo, Cd, Sn, Sb, Ba, and Pb. Table 7.1 presents leaching limits (in milligrams metal leached per kilogram dry solid) of the most pertinent heavy metals for the present work (i.e. those with notable measurable concentrations and that are affected by carbonation, as reported in Section 7.3). It was verified using fresh slags that the liquid-to-solid ratio (L/S) of 50 (utilized for testing of carbonated slags due to limitation of material available) provides leaching values that are similar to, and in most cases exceeding, tests using lower L/S values (10 and 20; see Fig. SC-7.8 in the Supplementary Content); this is due to the solubility controlled (rather than availability controlled) equilibrium established. Therefore it is possible to compare results of tests using L/S = 50 to the leaching limits established for tests using L/S = 10 for assessment of material compliance.

Table 7.1. Heavy metal leaching limits for waste material re-use in Belgium [31,32].

	V	Cr	Co	Ni	Mo	Ba
Limit [c] (mg/kg)	0.80 [a]	1.00 [b]	1.00 [b]	2.00 [b]	1.50 [b]	1.60 [a]

[a] Flemish/Dutch: NEN7343; [b] Walloon: DIN 38414/EN 12457-4/CEN TC 292.
[c] Walloon testing procedure uses batch extraction test at L/S = 10; Flemish testing procedure uses column leaching test at L/S = 10.

7.3. RESULTS AND DISCUSSION

7.3.1. Characterization of BOF slags

Average particle sizes by volume and specific surface areas of the two finest sieved fractions and the micronized samples are presented in Table 7.2. Specific densities of the slags were found to be 3.69 and 3.78 g/cm^3 for BOF_I and BOF_{II}, respectively.

Table 7.2. Average particle sizes of prepared BOF slag fractions determined by laser diffraction and specific surface areas determined by nitrogen adsorption (BET).

Slag batch	BOF_I	BOF_{II}	BOF_I	BOF_{II}	BOF_I	BOF_{II}
Particle size range	micronized	micronized	< 0.08 mm	< 0.08 mm	0.08-0.5 mm	0.08-0.5 mm
D[4,3] (μm)	13.6	13.5	38.0	31.0	252.5	203.9
D[3,2] (μm)	1.7	1.3	2.9	2.5	68.4	49.7
D_{50} (μm)	10.7	7.3	30.5	23.5	224.7	179.5
S_{BET} (m^2/g)	8.2	10.5	5.4	7.8	1.6	1.7

Table 7.3 presents the elemental composition of the slags determined by XRF. It can be inferred from the calcium content that the maximum theoretical CO_2 content (in the form of calcium carbonate) of a fully carbonated specimen would be 28.0 wt% CO_2 (equivalent to 0.39 g,CO_2/g,slag) for BOF_I and 31.2 wt% CO_2 (or 0.45 g,CO_2/g,slag) for BOF_{II}.

Table 7.3. Elemental composition of BOF slag batches determined by XRF (measured as oxides, presented as elemental).

Elements (wt%)	Ca	Fe	Si	Mn	Al	Mg	Ti	Cr	V	Balance (H, C, O, trace)
BOF_I slag	35.3	21.1	5.5	2.7	1.1	0.52	0.40	0.32	0.17	32.9
BOF_{II} slag	41.3	15.8	5.9	2.9	0.62	0.33	0.30	0.12	0.15	32.6

Table 7.4 shows the interpreted mineral composition determined by XRD. Samples were heated to 900°C in an argon atmosphere prior to analysis to decompose pre-existing hydroxides and carbonates formed due to exposure of the samples to ambient air (i.e. natural aging). The main mineral phases of the BOF slags were identified as srebrodolskite (C_2F), the beta polymorph of di-calcium silicate (β-C_2S), and free lime (CaO). The theoretical CO_2 uptake capacity of these materials based solely on their free lime content would be 7.7 wt% CO_2 (equivalent to 0.083 g,CO_2/g,slag) for BOF_I and 13.9 wt% CO_2 (or 0.162 g,CO_2/g,slag) for BOF_{II}.

Table 7.4. Mineral composition (wt%) of BOF slag batches determined by XRD with Rietveld refinement (normalized to 100% of the identified crystalline phases).

Mineral	Chemical formula	BOF_I	BOF_{II}
Srebrodolskite (C_2F)	$Ca_2Fe_2O_5$	37.2	31.0
β-C_2S	Ca_2SiO_4	21.5	22.0
Lime	CaO	10.6	20.6
γ-C_2S	Ca_2SiO_4	7.3	7.9
Fayalite	Fe_2SiO_4	5.5	4.2
Hematite	Fe_2O_3	4.1	2.0
Enstatite	$MgSiO_3$	3.8	1.9
Ferrosilite	$FeSiO_3$	2.8	3.6
Quartz	SiO_2	2.8	1.4
Wollastonite	$CaSiO_3$	1.1	0.7
Wüstite	FeO	1.1	2.2
Magnetite	Fe_3O_4	0.8	0.4
Periclase	MgO	0.7	1.6
Iron	Fe	0.4	0.3

Analysis of the polished cross-section of a millimetre-sized particle of BOF_I slag by SEM-BSE-EDX is shown in Fig. 7.1. The morphology and distribution of the major mineral phases quantified by XRD can be visualized in the image. Two types of free lime are observed: precipitated free lime and residual free lime. Precipitated free lime originates from the decomposition of tri-calcium silicate to di-calcium silicate during slag cooling [33]. Residual free lime is lime that was added during the steelmaking process as a flux, and either was added in excess or not allowed enough time to dissolve [34], as a means to increase steel productivity. The type of free lime is suspected to influence the slag reactivity and propensity for instability through volume expansion [35]. Wachsmuth et al. [34] pointed out that for BOF slag containing high amounts of free lime, residual free lime is the dominant form; this was confirmed for the present samples by inspection of several slag particles by SEM-BSE-EDX. In terms of the other minor elements detected by XRF analysis (Table 7.3), Mn and Mg were detected in the BOF slag in solid solution with iron oxides, while Al, Ti, V and Cr were found at the grain boundaries of C_2S and residual free lime phases. These interpretations are in accordance with reported observations of Waligora et al. [35] and van Zomeren et al. [15].

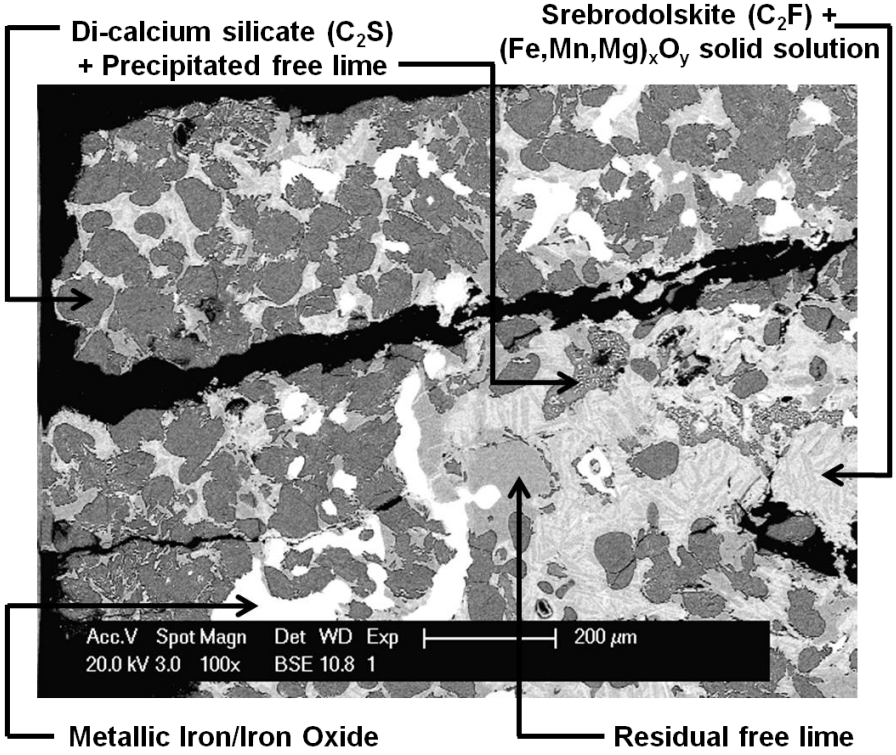

Fig. 7.1. Major mineral phases of BOF_I slag identified via SEM-BSE-EDX.

7.3.2. High temperature carbonation

The desire to attempt BOF slag carbonation at high temperature stems from the fact that the carbonation thermodynamics of the alkaline components of the slag are favorable (negative Gibbs free energy of reaction change) up to high temperatures (Table 7.5). Lime (CaO) carbonation (Eq. (7.1)) is theoretically possible up to 861 ^oC at 1 atm CO_2 pressure, while other common slag minerals such as C_2S (Eq. (7.2)), C_2F (Eq. (7.3)), and periclase (Eq. (7.4)) reach carbonation/calcination equilibrium at lower temperatures of 400, 664 and 400 ^oC, respectively. Beyond these temperatures the reactions reverse and CO_2 is released into the gas phase, a process commonly called calcination. Carbonation susceptibility is also affected by the partial pressure of carbon dioxide. In the case of lime, reducing the CO_2 partial pressure to levels present in the atmosphere (0.0003 atm), reduces the equilibrium temperature to 511 ^oC. However, at levels of CO_2 typically found in flue gases of thermal processes (e.g. 0.1 atm [22]) the equilibrium temperature is significantly higher at 732 ^oC. Thermodynamics also suggest that pressurization can be useful, as the equilibrium temperature at 5 atm CO_2 partial pressure rises to 971 ^oC (this condition could be achieved, for example, using a purified CO_2 stream from flue gas via capture and concentration processes).

Table 7.5. Carbonation/calcination equilibrium temperatures (Gibbs free energy of reaction equal to zero) for alkaline mineral components of BOF slag (FactSage 6.2 modeling).

Mineral	Reaction Eq.	$P(CO_2)$ (atm)	T ($\Delta G = 0$) (^oC)
CaO	(7.1)	0.0003	511
CaO	(7.1)	0.01	627
CaO	(7.1)	0.1	732
CaO	(7.1)	1	861
CaO	(7.1)	5	971
Ca_2SiO_4	(7.2)	1	400
$Ca_2Fe_2O_5$	(7.3)	1	664
MgO	(7.4)	1	400

$$CaO + CO_2 = CaCO_3 \quad (7.1)$$
$$Ca_2SiO_4 + 2CO_2 = 2CaCO_3 + SiO_2 \quad (7.2)$$
$$Ca_2Fe_2O_5 + 2CO_2 = 2CaCO_3 + Fe_2O_3 \quad (7.3)$$
$$MgO + CO_2 = MgCO_3 \quad (7.4)$$

However, favorable thermodynamics do not guarantee that these carbonation reactions will occur fast enough, as reaction kinetics also play an important role. Therefore it was the objective of this work to confirm the susceptibility of BOF slag carbonation at high temperature, both with regards to carbonation kinetics and CO_2 uptake, using three carbonation methodologies as will be detailed next.

7.3.2.1. In-situ TGA carbonation

To gain insight on the interaction of BOF slag with CO_2 at high temperatures comparable to the conditions in the cooling path of the slag during metallurgical processing, in-situ TGA carbonation tests were performed. Fig. 7.2 presents experimental results applying the in-situ TGA carbonation methodologies for both hot-to-cold (subfigures a and b) and cold-to-hot (subfigure c) carbonation directions. For comparison, pure CaO, MgO and Fe_2O_3 as well as micronized BOF_I and BOF_{II} slag samples were tested. The hot-to-cold carbonation direction is meant to simulate the carbonation path BOF slag would undertake in the industrial setting when being reacted immediately after slag solidification from the molten stage. Carbonation was conducted from 900 to 400 ^oC, with 5 ^oC/min cooling rate. The cold-to-hot direction, though not representative of the envisioned hot-stage carbonation technique, was also utilized for comparison and to aid gaining insight on carbonation kinetics and mechanisms. In this case the heating rate was 5 ^oC/min, and carbonation took place from 80 to 1000 ^oC. Two CO_2 partial pressures were applied: 20 vol% (balanced with N_2) and 100 vol% CO_2 at atmospheric total pressure.

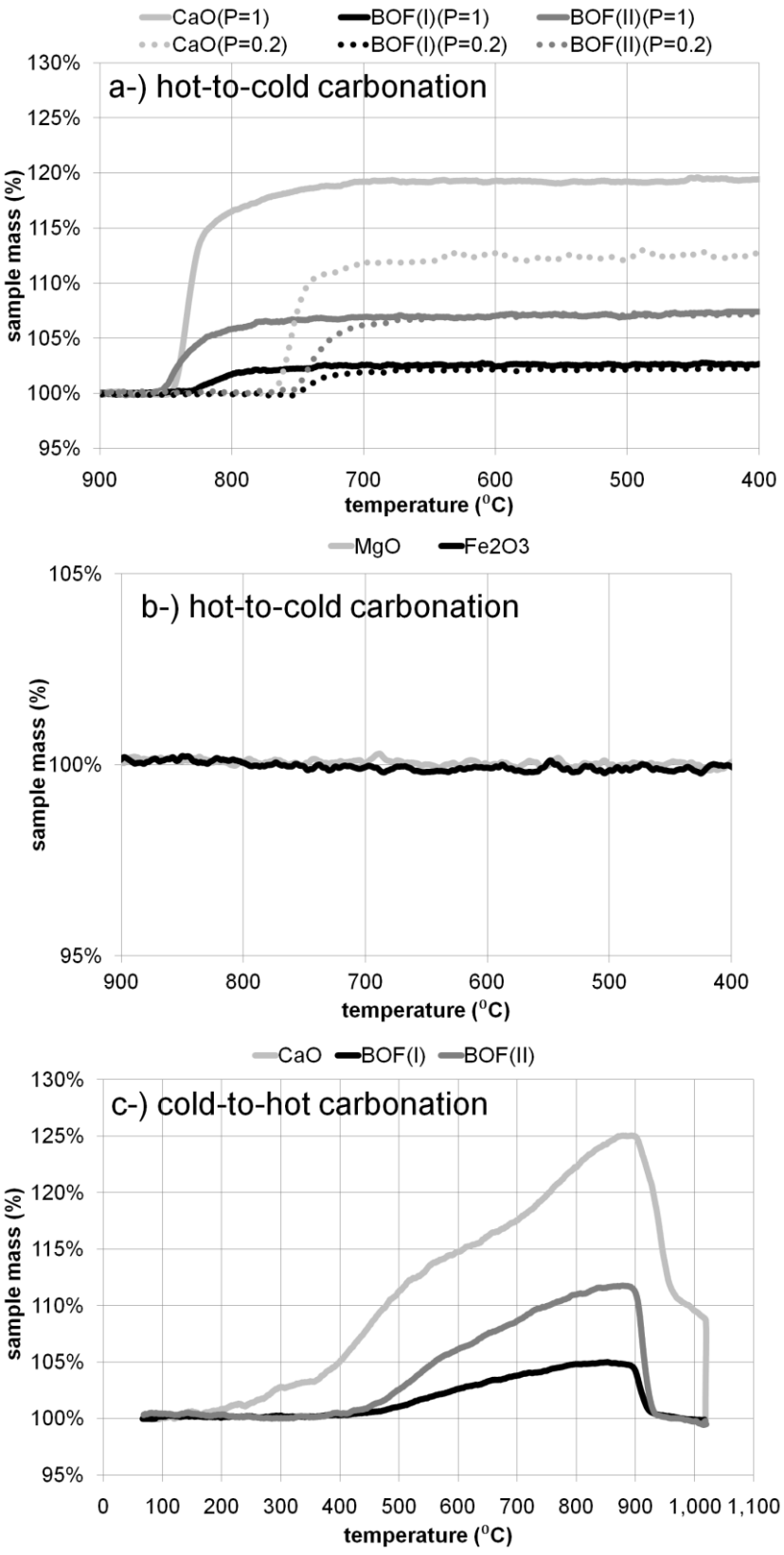

Fig. 7.2. In-situ TGA carbonation of pure oxides (CaO, MgO and Fe_2O_3) and micronized slags (BOF_I and BOF_{II}): hot-to-cold (subfigures a and b) and cold-to-hot (subfigure c) methodologies; P_{CO2} = 1 atm, except where indicated.

It is immediately possible to conclude from Fig. 7.2a that carbonation extent (sample mass gain due to CO_2 incorporation as carbonates) is directly proportional to the free lime content: pure CaO achieved significantly higher uptake than the slags, of which BOF_{II}, having greater free lime content

(Table 7.4), and slightly higher specific surface area (Table 7.2), carbonated more than BOF_I. In contrast the other two oxides tested (MgO and Fe_2O_3) did not carbonate in the temperature range tested (Fig. 7.2b). Stainless steel slag samples containing mainly calcium silicates (including C_2S) and no free lime also did not exhibit reactivity to direct carbonation at these temperatures (see Fig. SC-7.9 in the Supplementary Content); in contrast these materials react well in aqueous carbonation [36]. Given the large content of calcium in BOF slags (Table 7.3), a major part being present as C_2F (Table 7.4), and the comparatively low CO_2 uptakes compared to pure CaO, it can be concluded that C_2F reactivity to direct carbonation is also low, despite favorable thermodynamics (Table 7.5). Available literature lacks extensive data on C_2F carbonation, but Schmidt [37] found it possible to carbonate a similar mineral, $Sr_2Fe_2O_5$, at 800 ^oC, though kinetics were slow (order of hours). C_2F likely suffers from too slow kinetics to influence CO_2 uptake in the time frame of the present experiments. Therefore it is concluded that free lime is the principal mineral in BOF slag responsible for CO_2 uptake during direct high temperature carbonation. Under this premise, the carbonation conversions of CaO to $CaCO_3$ for BOF_I and BOF_{II} are 32.4% and 45.7%, respectively. These conversions on the basis of the total Ca content of the slags are equivalent to 7.0% and 16.3%, respectively.

Furthermore, while for CaO there are two distinct carbonation regimes (one kinetically controlled and a second diffusion-controlled), for the slag samples a single regime dominates. From the CaO trends, it is observable that upon commencement of carbonation, the uptake rate is sharp and linear. After this linear region, carbonation of CaO continues at a reduced rate, which levels off over time (temperature decrease) until carbonation ceases. These trends are similar at both partial pressures of CO_2, except that at lower partial pressure CaO carbonation reaches lower final uptake level. In the case of slag samples, carbonation from the start behaves similar to the second stage of CaO carbonation, that is, it is gradual and declining in rate over time. These effects can be explained by the necessity of CO_2 to diffuse across a native inert layer into slag particles from the start of carbonation to achieve further uptake, and a second regime does not occur since emerging carbonates form a dispersed patchwork within the particle, rather than a dense shell. In the case of pure CaO, significant carbonation at the exposed outer surface occurs immediately, only later to be followed by diffusion through the reacted carbonate layer into the particle core.

It is also inferred that carbonation commences at approximately the same temperature for the three reacting materials at each partial pressure: 830-850 ^oC at 100% CO_2, and 750-770 ^oC at 20% CO_2. These carbonation temperatures as a function of CO_2 partial pressure correspond to predicted values from reaction thermodynamics presented earlier (Table 7.5). Distinctly from CaO, however, the slag samples reached the same final carbonation extent values at both CO_2 partial pressures. This signifies that CO_2 diffusion is hindered equally by the dense unreactive mineral phases of the slags regardless of diffusion driving force (partial pressure and temperature). In the case of CaO, higher driving forces (temperature and partial pressure) and higher CO_2 concentration aid further carbonation extent, possibly by better displacement of inert gas contained in the particle pores. The indifference of slag carbonation to CO_2 partial pressure is positive for industrial implementation as it means costly and energy intensive enrichment of flue gases may not be required. Further discussion on the benefit of CO_2 pressurization is given in Section 7.3.2.2.

Fig. 7.2c demonstrates that carbonation in the cold-to-hot direction differs from the hot-to-cold trends. Most striking are the higher carbonation extents achieved with all three materials (CaO and micronized BOF_I and BOF_{II}). Also, CaO begins carbonating at a lower temperature (approx. 200 ^oC) than the slags (> 400 ^oC). Maximum carbonation extent is reached slightly prior to reaching 900 ^oC for the three samples. After this point, in spite of the presence of CO_2, the carbonation

reaction reverses, and $CaCO_3$ decomposition proceeds until the sample masses return to their initial values upon holding them at 1000 ^oC for several minutes. The higher carbonation extents may be explained by the ever increasing CO_2 solid-state diffusivity over time, opposite to the case of hot-to-cold carbonation. In addition, it can be expected that in the hot-to-cold case, due to the higher carbonation rates at higher temperatures (more data and discussion to follow), the carbonate layer formed at the outer particle surface quickly becomes denser and less permeable than when it is formed at lower temperatures, thus deterring carbonation continuance already at an early stage. Nevertheless, as mentioned earlier, this type of carbonation methodology has a major disadvantage, as it does not take advantage of the slag cooling path but rather would require external (thermal) energy input; therefore these results are meant to aid discussion only and are not deemed industrially feasible.

As the previously performed tests applied carbonation at varying temperatures, it was not possible to infer precisely the kinetics of the reaction. Therefore fixed temperature in-situ TGA carbonation experiments were performed with both micronized slag samples (BOF_I and BOF_{II}) and pure CaO as a reference material. Results are presented in Fig. 7.3 for five temperatures: 500, 575, 650, 725 and 800 ^oC. For all experimental runs, CO_2 was introduced at the two minute mark in these plots, hence all carbonation reactions can be deemed to have started at the same time. As can be observed, carbonation of all materials at all tested temperatures commences promptly after CO_2 introduction. It can also be noted from the vertical axes that BOF_I carbonation once again achieves lower extents compared to BOF_{II}, which itself achieves lower extents than CaO at comparable temperatures. For all materials, carbonation extent is greatest at the highest temperature, 800 ^oC.

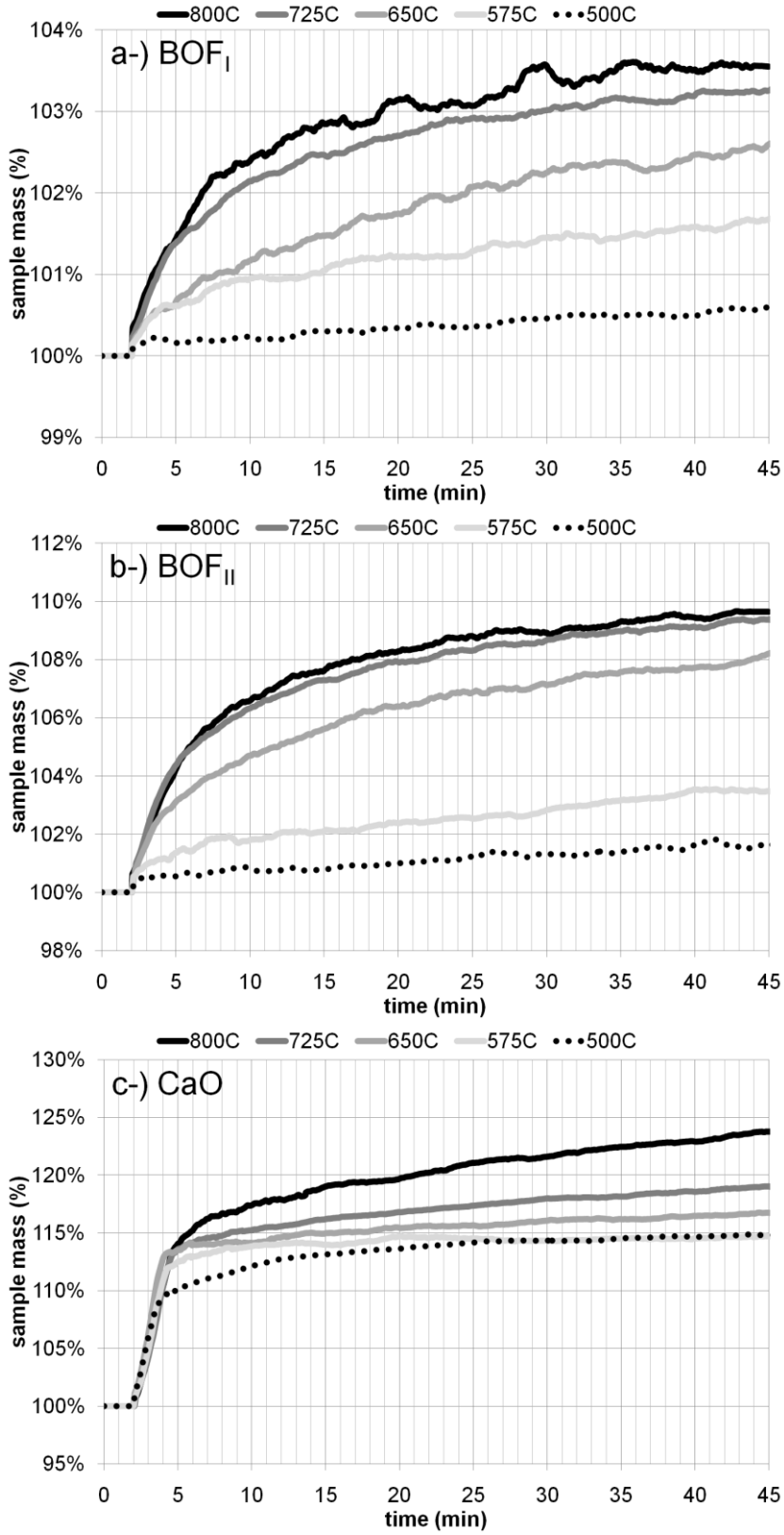

Fig. 7.3. In-situ TGA carbonation of micronized slags (BOF_I (a) and BOF_{II} (b)) and pure CaO (c): fixed temperature (500, 575, 650, 725 and 800 ^oC) methodology; P_{CO2} = 1 atm.

Similar to trends observed in the hot-to-cold carbonation experiments, CaO demonstrates dual regimes of carbonation, a rapid linear stage followed by another of diminishing reactivity. The CaO carbonation rate during the first stage is independent of temperature, and is measured to be on average 58 ± 5 mg,CO_2/g,CaO/min. In contrast, BOF slags have a very short initial steep uptake as

a result of surface/outer pore carbonation (< 1 min), thereafter transitioning into the decaying-rate-type trend during which CO_2 slowly penetrates deeper into the particles for the reaction, and thus mass gain, to continue. Because of this, temperature-controlled CO_2 diffusivity is a greater limiting factor for slag carbonation than reaction kinetics. This is evidenced by the greater effect of temperature on BOF slag carbonation extent than for CaO. In the case of the latter, after 45 minutes the carbonation extent at 800 ^oC is 60% higher (expressed as percent mass gain) than at 500 ^oC. In comparison, for the slags, BOF_I achieves nearly five times greater mass gain and BOF_{II} more than four times greater mass gain at the highest temperature over the lowest temperature.

In comparison with literature reported carbonation values for CaO in direct high temperature carbonation, the carbonation conversions achieved in the experiments so far presented in this study were lower than some studies (for example, at 800 ^oC, CaO carbonation conversion was 27% of the theoretical maximum carbonation extent, compared to 60-80% reported values [27,38]). Other studies, however, have also found conversion in the 20-30% range [19,39,40]. For the other two experimental methods reported herein, pressurized basket reactor carbonation and atmospheric furnace carbonation, it was verified that CaO carbonation achieved conversions over 60% at optimized process conditions. The cause of these discrepancies was identified for the present experimental system as being due to the CO_2 flow rate utilized (100 ml/min). When the flow rate was increased to 300 ml/min, the carbonation conversion at 800 ^oC increased to 64% (Fig. SC-7.10a in the Supplementary Content), though the initial carbonation rates, within the first 2.5 minutes of CO_2 introduction, were identical. This suggests that in both cases, sufficient CO_2 initially contacts the free lime surface, which carbonates equally rapidly. As the reaction progress, nitrogen gas contained within the sample crucible and inside the particle pores must be displaced by CO_2 gas for the reaction to continue. However, when using a lower gas flow rate, sweeping of the displaced nitrogen is reduced, thereby CO_2 diffusion into the particles is slowed. Slower CO_2 diffusion leads to earlier occurrence of pore blockage due to carbonate formation close to the particle surface, and a limited final conversion compared to the high flow case. In the case of BOF slag, the effect of CO_2 flow rate was smaller and opposite (Fig. SC-7.10b in the Supplementary Content); 100 ml/min resulted in slightly higher carbonation extent. The micronized slag's relatively high surface area and presence of macropores compared to commercial CaO [40], and its dispersed free lime concentration likely attenuate the effect of nitrogen displacement, and pore narrowing/blockage is less dependent on CO_2 flow rate. Seeing the high variability of results in the literature, it is advisable future researchers consider the effect of flow rate on their in-situ TGA carbonation experiments.

7.3.2.2. Pressurized basket reactor carbonation

Pressurized basket reactor carbonation experiments were conducted to investigate process effects that could not be assessed with the previously presented TGA methodology. These include the effect of CO_2 pressurization, up to 20 bar, the effect of steam addition (8 bar partial pressure), and the effect of particle size (up to 1.6 mm) on BOF slag carbonation extent. Fig. 7.4 presents results on the effect of three CO_2 pressures (4, 12 and 20 bar) on the carbonation of the 0.08-0.5 mm sieved fraction of BOF_{II} slag, performed at three temperatures (350, 500 and 650 ^oC) for 30 minutes reaction duration. These sets of conditions were chosen to ensure the effects of the process parameters could be observed (i.e. carbonation for longer duration or at higher temperature would mask the effect of pressure). It was found that the effect of CO_2 pressure on CO_2 uptake (reported as

wt% CO_2 in the carbonated sample, determined by in-situ calcination and IR CO_2 detection) is more important at lower temperatures, having a significant effect at 350 ^oC (176% improvement at 20 bar over 4 bar), a much reduced effect at 500 ^oC (7% improvement), and no effect at 650 ^oC. The effect of temperature, at fixed CO_2 pressures, was more striking, as had been presented with the in-situ TGA carbonation methodology. At 4 bar CO_2 pressure there was a 400% improvement in CO_2 uptake at 650 ^oC over 350 ^oC; significant improvements were also measured at 12 bar (+130%) and 20 bar (+80%).

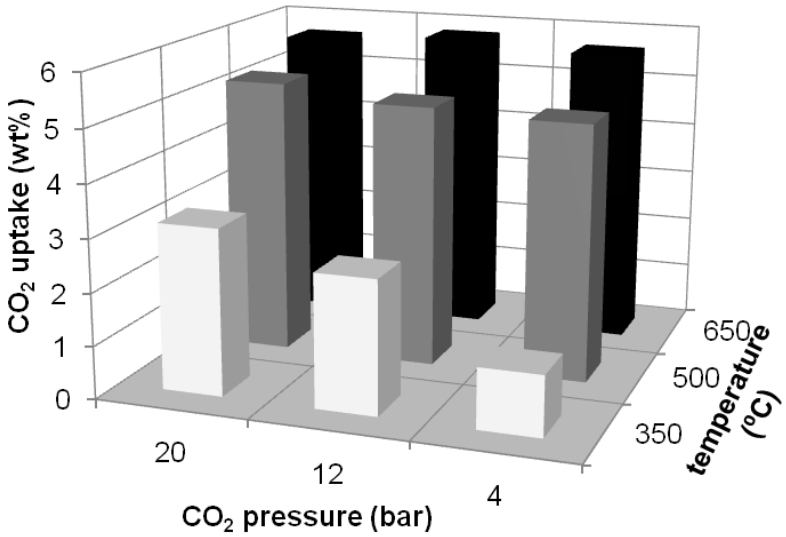

Fig. 7.4. Pressurized basket reactor carbonation of 0.08-0.5 mm particle size fraction of BOF_{II} slag at multiple temperatures (350, 500 and 650 ^oC) and CO_2 pressures (4, 12 and 20 bar) for 30 minutes reaction time.

Fig. 7.5 presents pressurized basket reactor carbonation results on the effect of slag particle size for both types of BOF slag (BOF_I and BOF_{II}). Furthermore, these experiments tested the effect of steam addition (8 bar partial pressure) on CO_2 uptake. The experimental temperature was fixed at 650 ^oC, the best value from the previous set of experiments presented, reaction time was 30 minutes, and total pressure was maintained at 20 bar (CO_2 + H_2O where applicable). Steam had a positive effect on CO_2 uptake for all particle size fractions, though the effect was reduced for the largest particles. Furthermore, on a percent improvement basis, BOF_I benefited more from steam addition than the more reactive (due to greater free lime content) BOF_{II}. For reference, pure CaO was also carbonated in the pressurized basket reactor at 650 ^oC and 20 bar total pressure with and without steam. Steam addition allowed carbonation conversion to reach 100% of the theoretical value, compared to 64% in dry CO_2.

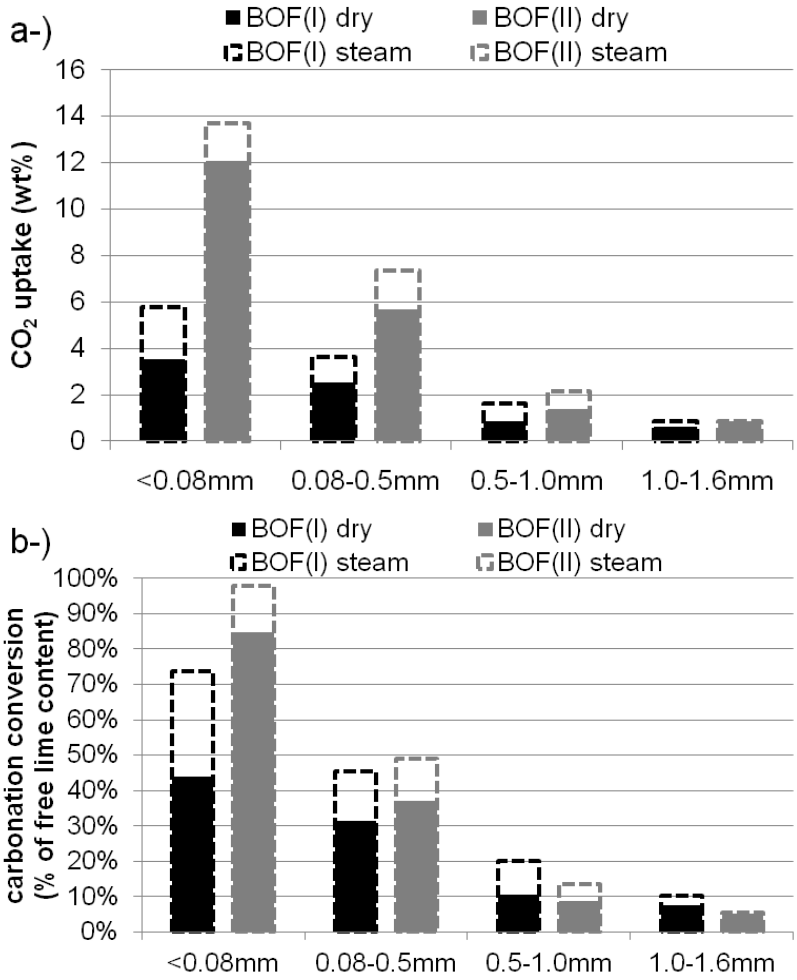

Fig. 7.5. Pressurized basket reactor carbonation of BOF_I and BOF_{II} slag samples of varying particle size fractions (< 0.08, 0.08-0.5, 0.5-1.0 and 1.0-1.6 mm) at 650 ^oC with dry or wet CO_2 at 20 bar total pressure and 30 minutes reaction time: results expressed as (a) wt% CO_2 uptake, and (b) carbonation conversion of free lime content.

The effect of steam on lime carbonation has previously been reported in literature by Yang and Xiao [39] and Manovic and Anthony [38]; however the mechanism of action has not yet been fully characterized. Yang and Xiao [39] suggest steam introduces a 'catalytic effect', related to the adsorption of hydroxyl groups and the formation of bicarbonate intermediates, though no experimental data is provided to confirm this hypothesis. They claim $Ca(OH)_2$ is not likely formed since carbonation temperatures in their tests were above the decomposition temperature of $Ca(OH)_2$ at the utilized vapor pressures of water. Indeed, it would appear difficult to base the effect of steam on the hydration of free lime, given experimental conditions for hot-stage carbonation normally use temperatures beyond the decomposition temperature of calcium hydroxide at trace vapor pressure of water (i.e. condition within a TGA using inert carrier gas) of approximately 350-400 ^oC. However, in the present experiment the vapor pressure of water was 8 bar, which applying the model of Hartman and Martinovský [41] yields a decomposition temperature (dehydroxylation reaction $\Delta G = 0$) of 660 ^oC. Therefore it is plausible to assert that the presently observed steam-enhanced CO_2 uptakes may be related to an intermediate hydroxylation step prior to carbonation. This would be in agreement with reported results of Materic and Smedley [42], who found that hydration of lime prior to atmospheric carbonation can result in greater carbonation conversion when applying lime as a sorbent in calcium looping processes for CO_2 capture and concentration.

Manovic and Anthony [38], on the other hand, provide experimental evidence that the steam-enhancement of carbonation may be caused by improvement in solid state diffusion rather than hydroxylation. They show that steam does not improve carbonation kinetics during the initial fast (kinetically controlled) carbonation stage, but rather aids in carbonation extent improvement over prolonged time (i.e. during the diffusion controlled stage). The exact mechanism of how steam improves solid state diffusion, however, is not provided. In any case, regardless of the actual mechanism of steam assistance, the present experiments show that steam improvement of carbonation conversion of the slags is modest (i.e. coarse particles remain distant from theoretical maximum uptake). Therefore industrial application of steaming during hot-stage carbonation of BOF slag could be deemed optional, depending on process complexity and required or desired final product properties.

It is evident from Fig. 7.5 that particle size, and hence surface area, has a significant effect on CO_2 uptake. This is not surprising since direct carbonation is a surface based and diffusion controlled reaction. Moreover, BOF_I CO_2 uptake (Fig. 7.5a) was consistently lower than BOF_{II}, which is attributable to its lower free lime content (10.6 wt% versus 20.6 wt%). Converting CO_2 uptake into carbonation conversion of the free lime content of the slags (i.e. assuming, based on experimental evidence collected in this study, that free lime is the only mineral participating in BOF slag direct high-temperature carbonation), the difference between BOF_I and BOF_{II} diminishes (Fig. 7.5b). In fact, based on the shrinking core model, it would be expected that carbonation conversion of the two slag samples would be identical if: (i) solid state diffusivity of CO_2 in the two slags were equal; (ii) free lime was equally distributed within the particles of both slags (radially and concentrically); and (iii) the proportion of free lime present in each slag as precipitated free lime and residual free lime were equal. Fig. 7.5b indicates that the two finest fractions of BOF_{II} maintain an advantage with regards to carbonation conversion over BOF_I. This can be attributed to the moderately higher specific surface areas and lower average particle sizes of the two finest fractions of BOF_{II} compared to BOF_I (Table 7.2), and may also be due to differences in dispersion and morphology of free lime inclusions (precipitated and residual) in the two slags (for example, residual free lime may carbonate more/better than the precipitated variety). For the two coarser fractions, dry carbonation conversions were more similar, as it can be expected that carbonation of these samples is mainly controlled by solid state diffusion rather than their limited (not measured) surface areas. Still, the average percentage improvement in steam-assisted carbonation conversion for the two coarse fractions was similar to that of the two finest fractions (+46% and +40%, respectively). Therefore improvement of solid state diffusivity as proposed by Manovic and Anthony [38] appears to be a plausible explanation of the mechanism, though hydroxylation or another ‘catalytic’ effect cannot be entirely ruled out.

7.3.2.3. Atmospheric furnace carbonation

Subsequent to the two previously described experimental methods (in-situ TGA carbonation and pressurized basket reactor carbonation), atmospheric furnace carbonation experiments were conducted for two main reasons. Firstly, atmospheric carbonation appears to be a more feasible route for industrial implementation of hot-stage carbonation, as it appears from previous tests that pressure is not a critical parameter for satisfactory direct carbonation extent, and it should reduce technical complexity and thus processing cost. Secondly, with regards to the laboratory scale equipment used in this study, this methodology allowed production of larger quantities (up to 10 g)

of carbonated material at one time (i.e. identical processing conditions), enabling detailed study on the mineralogy, basicity and heavy metal leaching properties of the carbonated products.

Similar to the previous methodologies, the effect of temperature on CO_2 uptake was studied to ensure furnace carbonation delivered equivalent results based on previous findings, and to elucidate unforeseen effects at atmospheric pressure. Furthermore, the effect of reaction time was studied, varied between 10 minutes (in-situ TGA carbonation indicated rapid CO_2 uptake in the first 10 minutes of reaction time) and 6 hours (longest reaction time tested thus far, to ensure cessation of CO_2 uptake). Fig. 7.6a shows that, in what appears to be the optimal temperature range of 650 to 750 ^oC, there is only a small increase in carbonation extent when increasing the reaction time from 10 minutes to 6 hours. At lower temperatures, such as 500 ^oC, the effect of time is more evident, but below this temperature, especially in the range of 200 to 400 ^oC, the carbonation extent is much smaller. Above 750 ^oC the stability of $CaCO_3$ decreases due to the low CO_2 pressure (Table 7.5), and at 800 ^oC the carbonation extent significantly decreases with 10 minutes reaction time (possibly the furnace is not completely purged of inert gas within 10 minutes of CO_2 introduction, hence the CO_2 partial pressure is somewhat lower than 1 atm, compromising $CaCO_3$ stability at this temperature). Results are very similar for both batches of BOF used, the difference being BOF_{II}, which contained more free lime, achieved greater CO_2 uptake amounts.

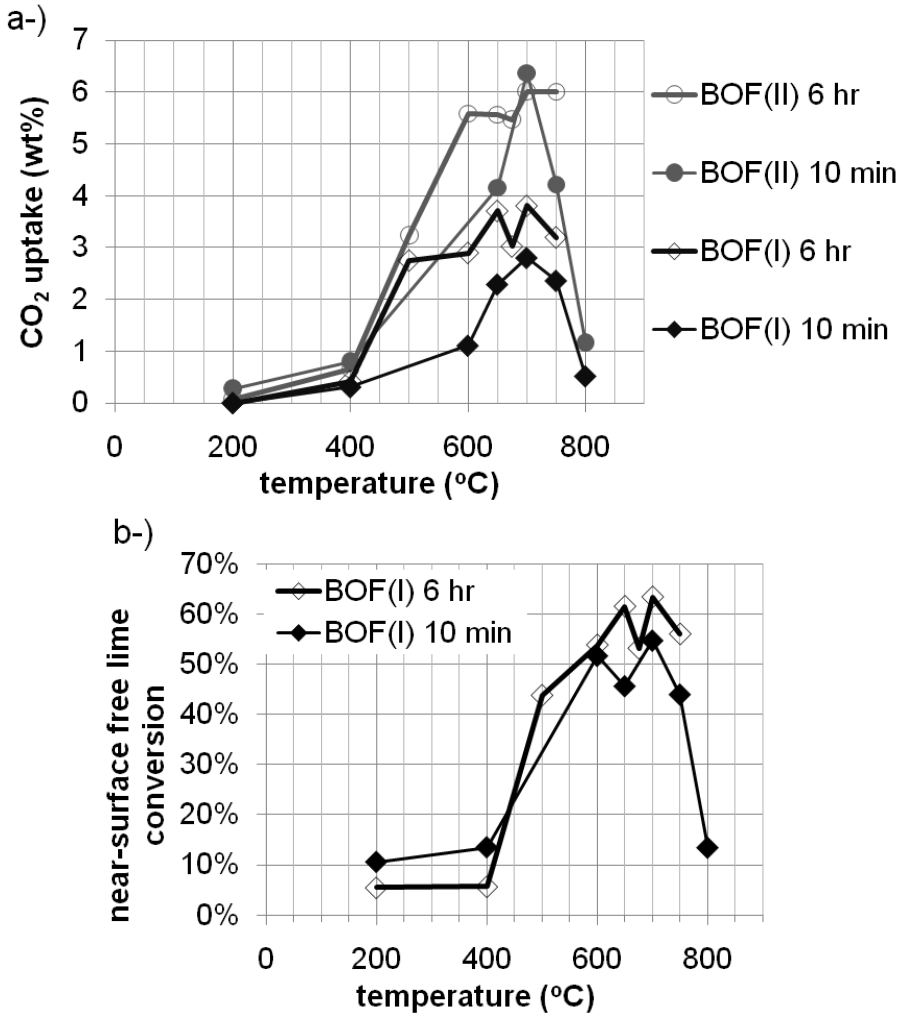

Fig. 7.6. Atmospheric furnace carbonation results: (a) CO_2 uptake (determined by TGA analysis) and (b) peripheral near-surface free lime conversion (determined by unmilled XRD analysis with Rietveld refinement) for carbonation of 0.08-0.5 mm particle size fractions of BOF_I and BOF_{II} slags at varying fixed temperatures (200 to 800 ^oC) for 10 minutes and 6 hours reaction time.

Quantitative XRD was also used to assess the carbonation extent of atmospheric furnace carbonated BOF_I slag samples (Fig. 7.6b). These analyses were conducted on unmilled 0.08-0.5 mm particle size fraction samples (i.e. not micronized to 5-10 μm as normally done for compositional analysis using XRD). The aim was to limit X-ray penetration into the particle to determine the conversion of free lime closer to the particle surface, which is the region that controls material basicity and heavy metal leaching. It is estimated that the X-ray penetration depth is limited to tens of microns up to 100 microns (depending on X-ray source and target material) [43], which is to some extent less than average particle radius based on D_{50} and D[4,3] values (Table 7.2). By comparing the calcite ($CaCO_3$) amounts to the remaining free lime (CaO) and portlandite ($Ca(OH)_2$) amounts, it was possible to determine carbonation conversion of the free lime present in the region penetrated by the X-rays. Values between 50-60% conversions are obtained in the optimal temperature range (600 to 750 ^oC), slightly higher than overall free lime conversions based on total CO_2 uptake (40-50%). Given that the carbonation depth may be smaller than the X-ray penetration depth, and/or that CaO grains are not fully carbonated due to formation of dense carbonated shell surrounding the unreacted core, detection by XRD of free lime present in regions of the particles

that are not accessible to CO_2 is possible, therefore truly geometrical peripheral near-surface carbonation extent is likely to be higher.

The effect of particle size on CO_2 uptake by atmospheric furnace carbonation (Fig. 7.7a) was analogous to results obtained by pressurized basket reactor carbonation (Fig. 7.5a). The 1.0-1.6 mm particle size fraction of BOF_I slag achieved significantly lower CO_2 uptake than the finer 0.08-0.5 mm fraction after one hour carbonation at 700 ^oC. The reduction in basicity of the coarser sample, however, was very similar to the reduction obtained with the finer sample (Fig. 7.7b). This is explained by the fact that carbonation primarily occurs near the particle surface, which contacts the liquid phase and controls pH. Therefore reduction in basicity is not always directly proportional to CO_2 uptake, but rather depends on particle size and most importantly on exposed surface area.

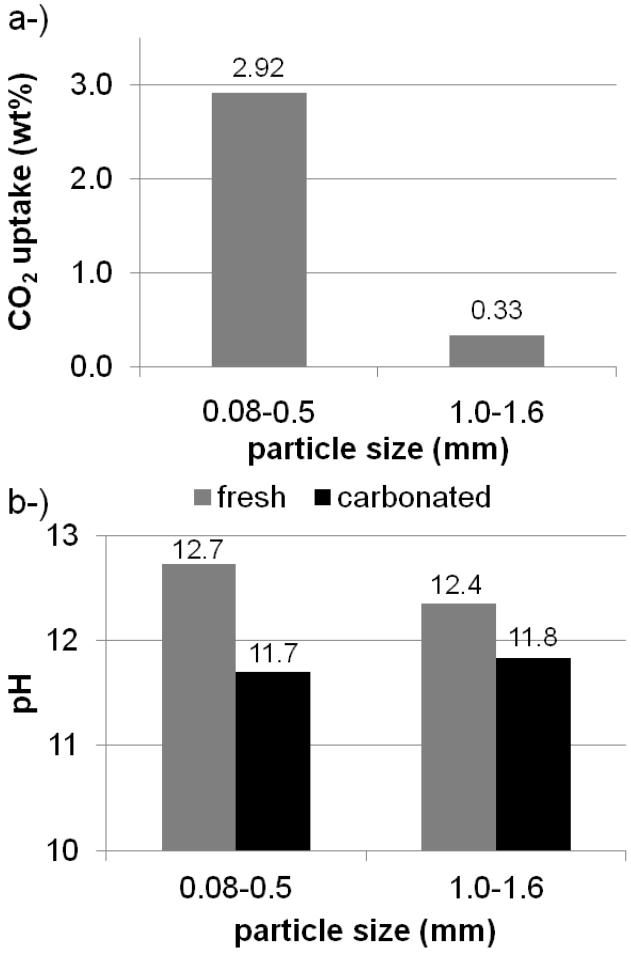

Fig. 7.7. Atmospheric furnace carbonation results: (a) CO_2 uptake and (b) basicity for carbonation of two particle size fractions (0.08-0.5, 1.0-1.6 mm) of BOF_I slag at 700 ^oC for 1 hour reaction time.

7.3.3. Basicity and heavy metal leaching

The native basicity of BOF slag can be directly linked to its free lime content, which is detrimental to its valorization as a construction material. Furthermore, materials with high basicity when in contact with water produce alkaline solutions, which contribute to the leaching of several heavy metal contaminants [32,44,45]. For a specific slag particle size fraction, CO_2 uptake and basicity reduction are proportionally linked. Atmospheric furnace carbonation resulted in improvement of solution pH values of the 0.08-0.5 mm particle size fraction of BOF_I slag; the basicity reduction was proportional to CO_2 uptake, as presented in Fig. 7.8. BOF_I, having less free

lime, achieved just under one pH unit reduction with 10 minutes reaction time (Fig. 7.8a), and reached incrementally better results after 6 hours reaction time (Fig. 7.8b). BOF_{II} benefitted more from increased reaction time, probably due to its significantly greater free lime content and moderately higher specific surface area. Nevertheless, at the optimal conditions (e.g. 700°C) the final pH values for BOF_I and BOF_{II} after 10min/6h carbonation were 11.6/11.6 and 12.1/11.7, respectively. This reduction in pH may be sufficient to increase the marketability of BOF slag into applications in the construction industry; however it remains to be tested whether swelling propensity sufficiently decreases given the incomplete free lime conversions achieved.

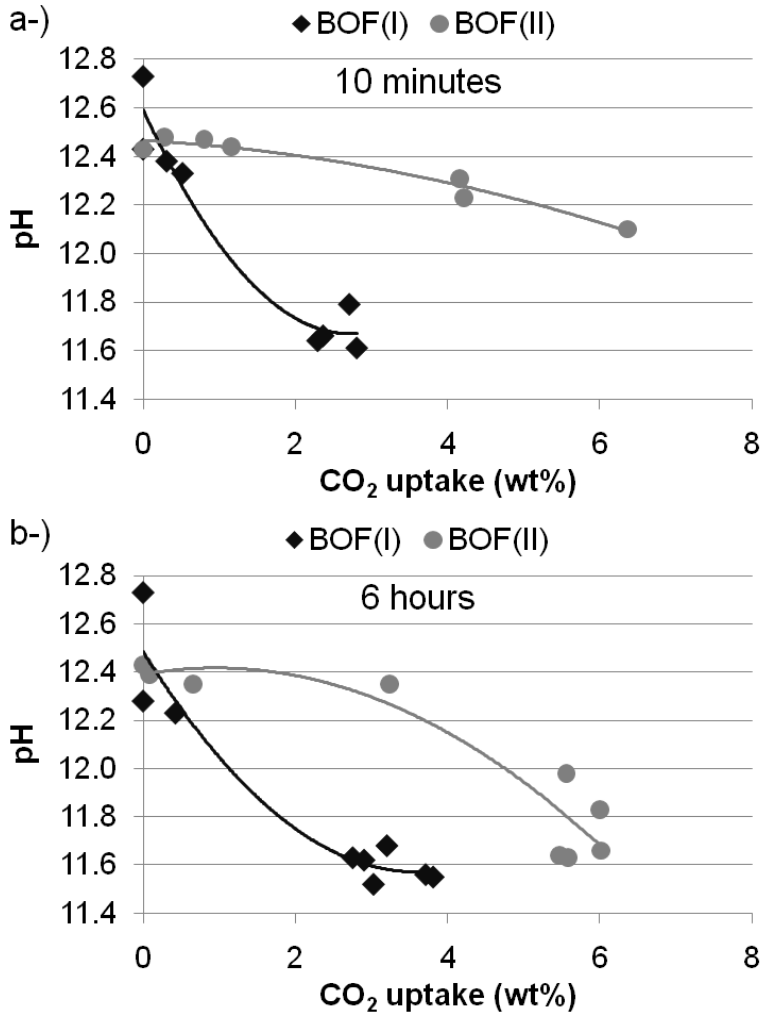

Fig. 7.8. Atmospheric furnace carbonation results: basicity of 0.08-0.5 mm particle size fractions of BOF_I and BOF_{II} slags as a function of CO_2 uptake for 10 minutes (a) and 6 hours (b) carbonation reaction time. Varying CO_2 uptakes resultant from carbonation at multiple temperatures (i.e. same samples presented in Fig. 7.6a).

Positive effects on the leaching of heavy metals also resulted from carbonation of BOF slags. Leaching results as a function of atmospheric-furnace-carbonated sample pH are plotted in Fig. 7.9. For further insight, leaching results as a function of CO_2 uptake and reaction time are illustrated in Figs. SC-7.11 and SC-7.12 in the Supplementary Content, the former for 10 minutes reaction time, and the latter for 6 hours reaction time. The 0.08-0.5 mm particle size fraction carbonated samples were used to generate these data.

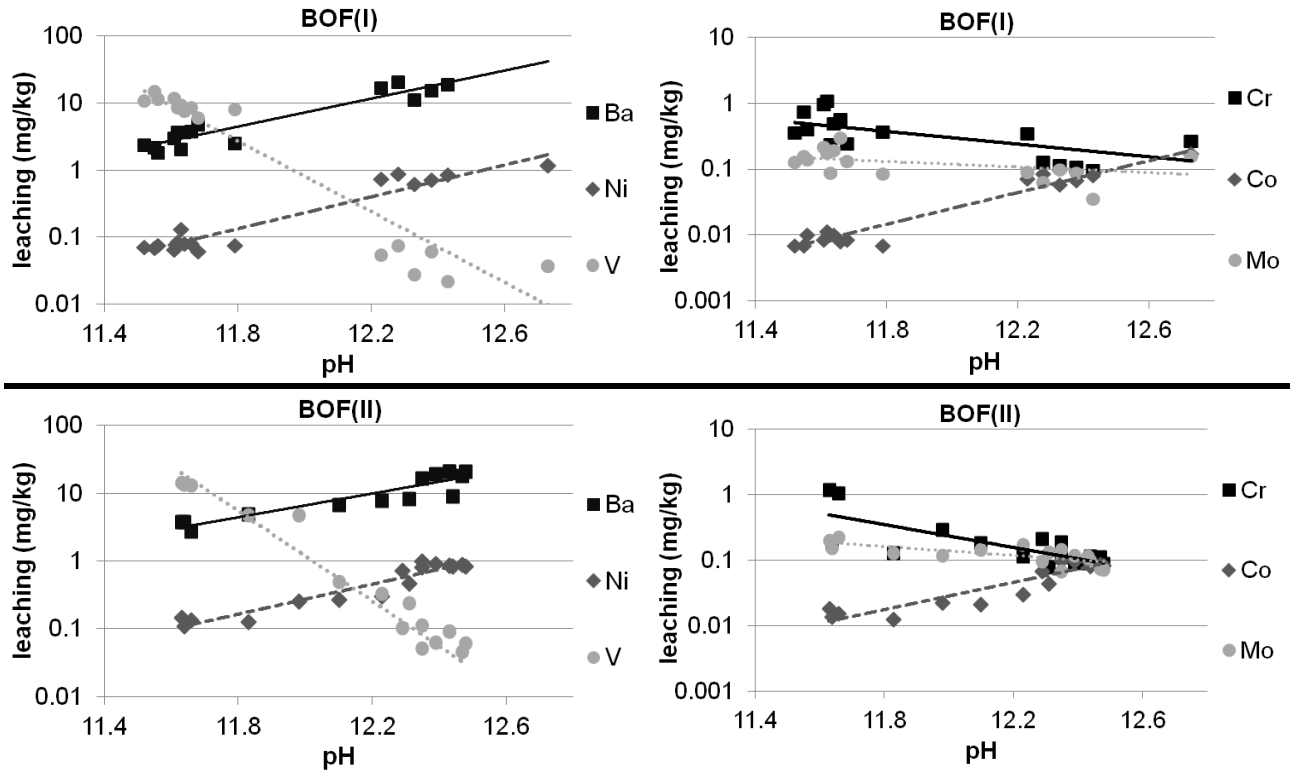

Fig. 7.9. Atmospheric furnace carbonation results: leaching of heavy metals (Ba, Ni, V (left-side); Cr, Co, Mo (right-side)) from 0.08-0.5 mm particle size fractions of BOF_I (top) and BOF_{II} (bottom) slags as a function of pH. Varying pH values resultant from carbonation at multiple temperatures and reaction times (i.e. same samples presented in Fig. 6a).

Carbonation was found to have a noticeable positive effect on reducing leaching of barium, nickel and cobalt. These results can be attributed to pH reduction (Fig. 7.9), which decreases the solubility and/or changes the speciation of some metals, and the formation of less soluble compounds (e.g. $BaCO_3$, $BaSO_4$ [44]). Vanadium leaching, on the other hand, increases after carbonation, reaching 10 mg/kg (well above the regulatory limit of 0.8 mg/kg [32]) for three of the four sample sets. The only exception is 10 minutes carbonated BOF_{II} slag (Fig. SC-7.11), which remains below the limit. This can be explained by the lower reduction in basicity of this material (Fig. 7.8a), as vanadium is known to be more prone to solubilization at lower pH [15,45]. Chromium and molybdenum leaching also increase after carbonation (pH reduction), the former more than the latter; however their values remain below regulatory limits (Table 7.1). Chromium leaching, like vanadium, is also proportional to basicity reduction [45], as inferred from the 10 minutes carbonated BOF_{II} slag presenting marginal leaching increase (Fig. SC-7.11) compared to 6 hours reaction time (Fig. SC-7.12). Competition of carbonate ions with oxyanionic species can also play a role in controlling the solubility of chromate, molybdate and vanadate ions [32].

It can be concluded that the balance of basicity reduction and heavy metal leaching via carbonation is a challenge for the reutilization of BOF slag. While the solubility of some metals reduced after carbonation (barium, cobalt and nickel), vanadium and chromium leaching increased. With more moderate carbonation extent (10 minutes reaction time), the rate of solubility increase of these metals was lower, conforming to regulatory limits. Therefore, in view of industrial implementation of BOF slag carbonation, it should be considered whether a higher or lower carbonation extent is more interesting for commercialization of carbonated BOF slag. The increased solubility of vanadium (and to a smaller extent chromium) after carbonation can be used as a means

to ease their recovery from the residues, in comparison to energy intensive traditional methods for vanadium recovery from waste materials [46], as these metals can be of commercial value. Alternatively, if the carbonated BOF slag is used as a fine aggregate in cement mortar/concrete, there are possibilities to introduce additives to the matrix (such as zeolitic sorbents) to contain leaching from the aggregate material. Moreover, the matrix itself can act as a sink for heavy metals, by incorporation of metalloids including Cr and V in hydration products [47], thereby suppressing leaching.[XXII]

7.4. CONCLUSIONS

This work has investigated the hot-stage carbonation of Basic Oxygen Furnace (BOF) steel slag, with the objective of converting its high free lime content (10-20 wt%) to calcium carbonate and stabilizing its negative properties (high basicity and heavy metal leaching) that prevent material valorization. By performing hot-to-cold carbonation experiments in a TGA, it was observed that the optimum carbonation temperature lies just below the transition temperature between carbonation stability and carbonate decomposition: 830-850 ^{o}C at 1 atm CO_2, and 750-770 ^{o}C at 0.2 atm CO_2. Pressurization and steam addition were found not to contribute significantly to CO_2 uptake enhancement; for instance, diffusion limitations prevent free lime conversion from surpassing 50% for the 0.08-0.5 mm particle size fraction of the BOF_{II} slag batch. Instead, it appears feasible to apply flue gases from steel production plants directly (e.g. 0.2 atm CO_2 partial pressure) without need for additional and costly CO_2 separation/concentration processes. Improvement in basicity was independent of particle size; that is, even the coarser fractions achieved similar reduction in basicity despite significantly lower CO_2 uptake. However, the effect of carbonation on heavy metal leaching was mixed: while the solubility of some metals reduced after carbonation (barium, cobalt and nickel), vanadium and chromium leaching increased. Post-carbonation extraction of leachable components or mixing of carbonated slag with sorbent materials would be required for meeting hazardous materials regulations and enable slag commercialization. Otherwise, heavy metal leaching could be suppressed by applying carbonated BOF slag as a fine aggregate in cement mortar/concrete, where the encasing matrix could act as a sink for mobile metals.[XXII]

Further optimization of hot-stage carbonation is still required prior to industrial implementation of this technology. Despite suitable reaction kinetics and enhanced CO_2 diffusivity at high temperatures, complete conversion of free lime is still limited by the ability of CO_2 to diffuse into the particle core, even for the 0.08-0.5 mm particle size fraction utilized. This size fraction is at the low-end of the expected particle size achieved by hot-stage granulation (as envisaged in Fig. SC-7.1 and reported in [10,25]). Therefore in order to achieve reasonably high levels of free lime conversion, development of granulation/hot-stage-milling technology capable of delivering sub-millimeter sized particles appears to be essential. Furthermore, investigation is warranted on finding the necessary level of free lime conversion needed to satisfactory stabilize BOF swelling in construction material applications. For instance, it should be assessed whether 50% conversion or more is required for complete stabilization, or if near-surface carbonation, which is enough to reduce basicity (as achieved in this work with 1.0-1.6 mm BOF particle size fraction), may be sufficient to improve material properties and enable its valorization.

[XXII] Ongoing work in this area is briefly described in Section 10.3.

7.5. REFERENCES

[1] Y. Topkaya, N. Sevinç, A. Günaydın, Slag treatment at Kardemir integrated iron and steel works, Int. J. Miner. Process. 74 (2004) 31–39.

[2] R. Dippenaar, Industrial uses of slag (the use and re-use of iron and steelmaking slags), Ironmaking Steelmaking 32 (2005) 35–46.

[3] J.-M. Delbecq, Steel Slags as cementitious materials, in: Seminário Internacional - Aplicação de Escória de Aciaria, Belo Horizonte, Brazil, 2010.

[4] G. Wang, Y. Wang, Z. Gao, Use of steel slag as a granular material: Volume expansion prediction and usability criteria, J. Hazard. Mater. 184 (2010) 555–560.

[5] J.J. Emery, Slag Utilization in Pavement Construction, Extending Aggregate Resources, ASTM Spec. Tech. Publ. 774 (1982) 95–118.

[6] S.A. Mikhail, A.M. Turcotte, Thermal behaviour of basic oxygen furnace waste slag, Thermochim. Acta 263 (1995) 87–94.

[7] H. Motz, J. Geiseler, 2001, Products of steel slags an opportunity to save natural resources, Waste Manage. 21 (2001) 285–293.

[8] K. Toshiyuki, K. Akio, Treatment of Cooling Steelmaking Slag, Japan Patent, JP-06-184610, 05 July 1994.

[9] S. Chengxiao, L. Yongqian, W. Jiangang, L. Yin, Technology of slag processing by rotary cylinder at Baosteel, Rev. Metall. 1 (2004) 39–42.

[10] O. Sang-Yoon, Method for Stabilizing Slag and Novel Materials Produced Thereby, US Patent, US2009/0193849, 06 Aug 2009.

[11] K.S. Lackner, D.P. Butt, C.H. Wendt, Progress on binding CO_2 in mineral substrates, Energy Convers. Manage. 38, (1997) S259–S264.

[12] W.J.J. Huijgen, R.N.J. Comans, Carbonation of Steel Slag for CO_2 Sequestration: Leaching of Products and Reaction Mechanisms. Environmental Sci. Technol. 40 (2006) 2790–2796.

[13] W.J.J. Huijgen, G.-J. Witkamp, R.N.J. Comans, Mineral CO_2 Sequestration by Steel Slag Carbonation, Environ. Sci. Technol. 39 (2005) 9676–9682.

[14] E.-E. Chang, C.-H. Chen, Y.-H. Chen, S.-Y. Pan, P.-C. Chiang, Performance evaluation for carbonation of steel-making slags in a slurry reactor, J. Hazard. Mater. 186 (2011) 558–564.

[15] A. van Zomeren, S.R. van der Laan, H.B.A. Kobesen, W.J.J. Huijgen, R.N.J. Comans, Changes in mineralogical and leaching properties of converter steel slag resulting from accelerated carbonation at low CO_2 pressure, Waste Manage. 31 (2011) 2236–2244.

[16] T. Isoo, T. Takahashi, M. Fukuhara, Using Carbonated Steelmaking Slag Blocks to Help Reduce CO_2, Am. Ceram. Soc. Bull. 80 (2001) 73–75.

[17] S. Eloneva, S. Teir, H. Revitzer, J. Salminen, A. Said, C.-J. Fogelholm, R. Zevenhoven, Reduction of CO_2 Emissions from Steel Plants by Using Steelmaking Slags for Production of Marketable Calcium Carbonate, Steel Res. Int. 80 (2009) 415–421.

[18] R.M. Santos, T. Van Gerven, Process Intensification Routes for Mineral Carbonation, Greenhouse Gas Sci. Technol. 1 (2011) 287–293.

[19] E.P. Reddy, P.G. Smirniotis, High-Temperature Sorbents for CO_2 Made of Alkali Metals Doped on CaO Supports, J. Phys. Chem. B 108 (2004) 7794–7800.

[20] J. Blamey, E.J. Anthony, J. Wang, P.S. Fennell, The calcium looping cycle for large-scale CO_2 capture, Prog. Energy Combust. Sci. 36 (2010) 260–279.

[21] V. Manovic, E.J. Anthony, Lime-Based Sorbents for High-Temperature CO_2 Capture—A Review of Sorbent Modification Methods, Int. J. Environ. Res. Public Health 7 (2010) 3129–3140.

[22] V. Prigiobbe, A. Polettini, R. Baciocchi, Gas–solid carbonation kinetics of Air Pollution Control residues for CO_2 storage, Chem. Eng. J. 148 (2009) 270–278.

[23] L.-C. Kao, Sorption of Carbon Dioxide at High Temperatures by Slag, Master's Thesis, National Cheng Kung University, Tainan City, Taiwan, 2009.

[24] J. Yu, K. Wang, Study on Characteristics of Steel Slag for CO_2 Capture, Energy Fuels 25 (2011) 5483–5492.

[25] G. Li, H. Ni, Recent progress of hot stage processing for steelmaking slags in China considering stability and heat recovery, in: Proceedings of the Second International Slag Valorisation Symposium: The transition to sustainable materials management, Leuven, Belgium, 2011.

[26] F. Larachi, I. Daldoul, G. Beaudoin, Fixation of CO_2 by chrysotile in low-pressure dry and moist carbonation: Ex-situ and in-situ characterizations, Geochim. Cosmochim. Acta 74 (2010) 3051–3075.

[27] S.K. Bhatia, D.D. Perlmutter, Effect of the Product Layer on the Kinetics of the CO_2-Lime Reaction, AIChE J. 29 (1983) 79–86.

[28] D. Gielen, CO_2 removal in the iron and steel industry, Energy Convers. Manage. 44 (2003) 1027–1037.

[29] A. Tobiessen, Process Evaluations and Simulations of CO_2 Capture from Steel Plant Flue Gases, in: CCS in the Iron and Steel Industry: Challenges and Opportunities of CO_2 Capture and Storage in the Iron and Steel Industry, Dusseldorf, Germany, 2011.

[30] F. Larachi, J.-P. Gravel, B.P.A. Grandjean, G. Beaudoin, Role of steam, hydrogen and pretreatment in chrysotile gas–solid carbonation: Opportunities for pre-combustion CO_2 capture, Int. J. Greenhouse Gas Control 6 (2012) 69–76.

[31] Ministere de la Region Wallonne, Arrêté du Gouvernement wallon favorisant la valorisation de certains déchets, Moniteur Belge 2 (2001) 23859–23883.

[32] T. Van Gerven, E. Van Keer, S. Arickx, M. Jaspers, G. Wauters, C. Vandecasteele, Carbonation of MSWI-bottom ash to decrease heavy metal leaching, in view of recycling, Waste Manage. 25 (2005) 291–300.

[33] K. Mohan, F.P. Glasser, The thermal decomposition of Ca_3SiO_5 at temperatures below 1250°C I. Pure C_3S and the influence of excess CaO or Ca_2SiO_4, Cem. Concr. Res. 7 (1977) 1–7.

[34] F. Wachsmuth, J. Geiseler, W. Fix, K. Koch, K. Schwerdtfeger, Contribution to the Structure of BOF-Slags and its Influence on Their Volume Stability, Can. Metall. Q. 20 (1981) 279–284.

[35] J. Waligora, D. Bulteel, P. Degrugilliers, D. Damidot, J.L. Potdevin, M. Measson, Chemical and mineralogical characterizations of LD converter steel slags: A multi-analytical techniques approach, Mater. Charact. 61 (2010) 39–48.

[36] R.M. Santos, D. François, G. Mertens, J. Elsen, T. Van Gerven, Ultrasound-Intensified Mineral Carbonation, Appl. Therm. Eng. (2012) doi:10.1016/j.applthermaleng.2012.03.035.

[37] M. Schmidt, Mechanical and thermal carbonation of strontium ferrite $SrFeO_x$, Mater. Res. Bull. 37 (2002) 2093–2105.

[38] V. Manovic, E.J. Anthony, Carbonation of CaO-Based Sorbents Enhanced by Steam Addition, Ind. Eng. Chem. Res. 49 (2010b) 9105–9110.

[39] S. Yang, Y. Xiao, Steam Catalysis in CaO Carbonation under Low Steam Partial Pressure, Ind. Eng. Chem. Res. 47 (2008) 4043–4048.

[40] C. Chen, S.-T. Yang, W.-S. Ahn, Calcium oxide as high temperature CO_2 sorbent: Effect of textural properties, Mater. Lett. 75 (2012) 140–142.

[41] M. Hartman, A. Martinovský, Thermal stability of the magnesian and calcareous compounds for desulfurization processes, Chem. Eng. Commun. 111 (1992) 149–160.

[42] V. Materic, S.I. Smedley, High Temperature Carbonation of $Ca(OH)_2$, Ind. Eng. Chem. Res. 50 (2011) 5927–5932.

[43] J. Liu, R.E. Saw, Y.-H. Kiang, Calculation of Effective Penetration Depth in X-Ray Diffraction for Pharmaceutical Solids, J. Pharm. Sci. 99 (2010) 3807–3814.

[44] A.-M. Fällman, Leaching of chromium and barium from steel slag in laboratory and field tests — a solubility controlled process?, Waste Manage. 20 (2000) 149–154.

[45] G. Cornelis, A. Johnson, T. Van Gerven, C. Vandecasteele, Leaching mechanisms of oxyanionic metalloid and metal species in alkaline solid wastes: A review, Appl. Geochem. 23 (2008) 955–976.

[46] G.Z. Ye, Vanadium Recovery from LD Slag, A State of the art report, Part I - Facts and metallurgy of Vanadium, Internal MEFOS report, MEF06001, Stockholm, Sweden, 2006.

[47] N. Saikia, G. Cornelis, G. Mertens, J. Elsen, K. Van Balen, T. Van Gerven, C. Vandecasteele, Assessment of Pb-slag, MSWI bottom ash and boiler and fly ash for using as a fine aggregate in cement mortar, J. Hazard. Mater. 154 (2008) 766–777.

7.6. SUPPLEMENTARY CONTENT

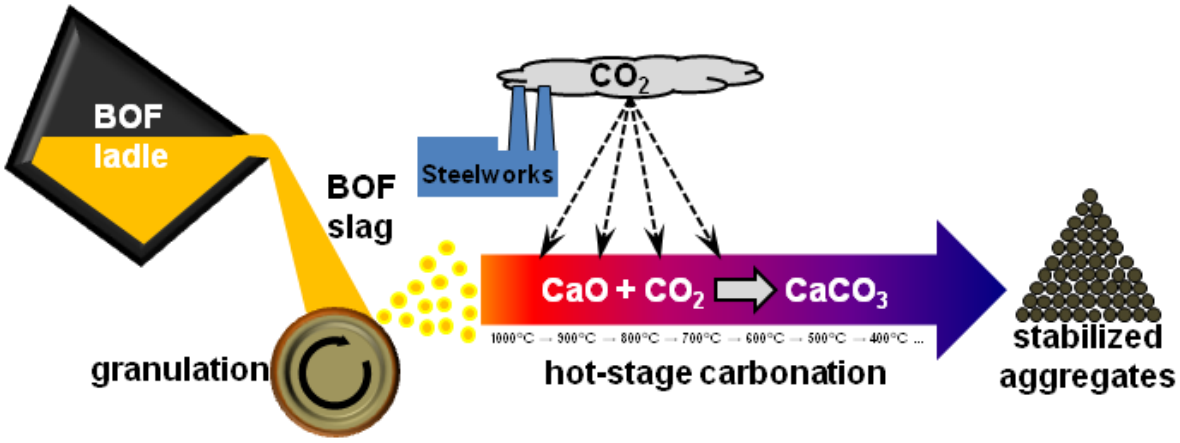

Fig. SC-7.1. Conceptual scheme of the proposed BOF slag hot-stage carbonation treatment process, including: hot slag pouring, hot slag granulation, carbonation of the cooling granulated slag in the hot-to-cold route using flue-gas CO_2, and production of stabilized slag material to be used as aggregates.

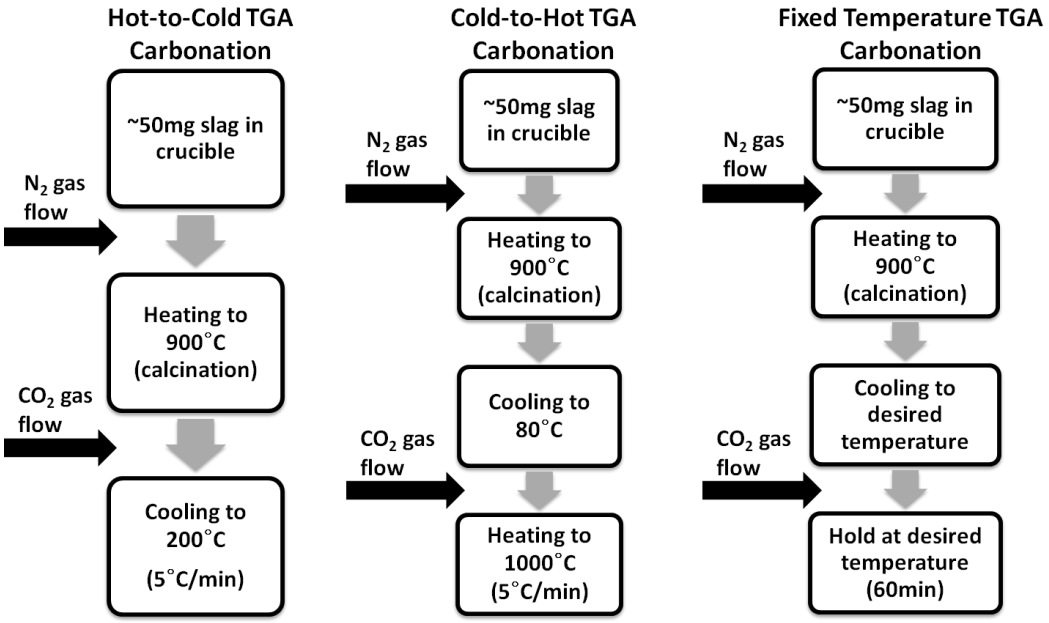

Fig. SC-7.2. Experimental methodologies of in-situ TGA carbonation: hot-to-cold, cold-to-hot, fixed temperature.

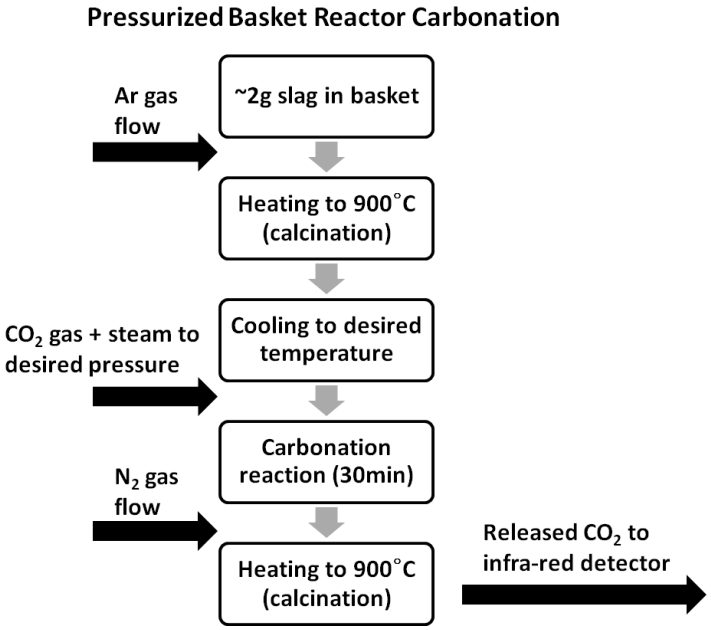

Fig. SC-7.3. Experimental methodology of pressurized basket reactor with in-situ CO_2 uptake determination by IR.

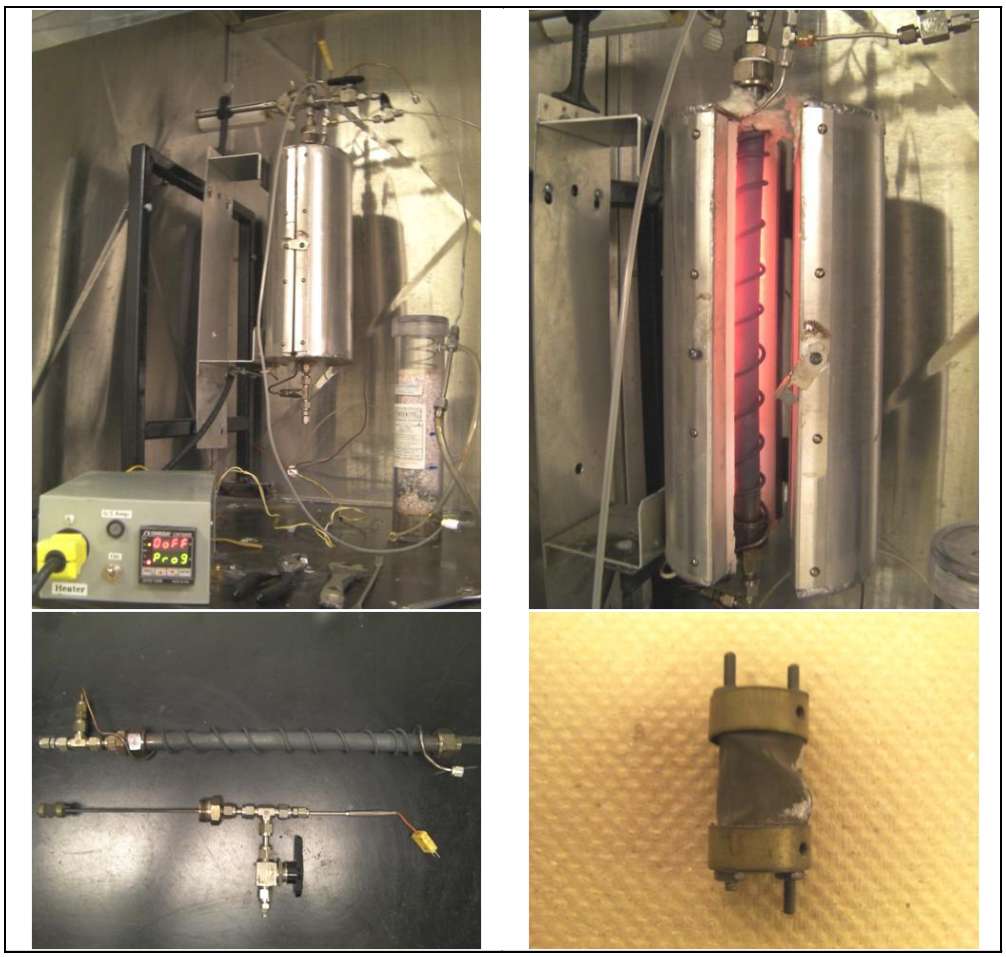

Fig. SC-7.4. Pressurized basket reactor apparatus: (top-left) set-up overview including furnace, outlet gas drier and temperature controller; (top-right) view of opened furnace in operation with tubular reactor inside; (bottom-left) tubular reactor disassembled, showing inner thermocouple with basket at the end (left-hand side); (bottom-right) sample-containing basket assembly.

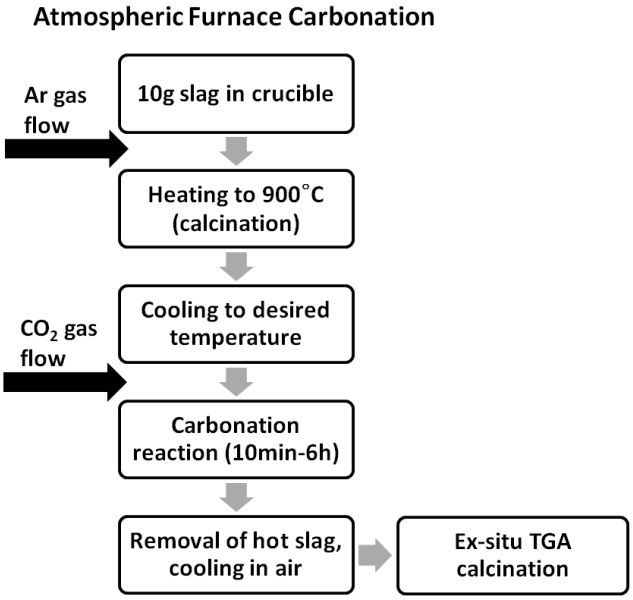

Fig. SC-7.5. Experimental methodology of atmospheric furnace carbonation.

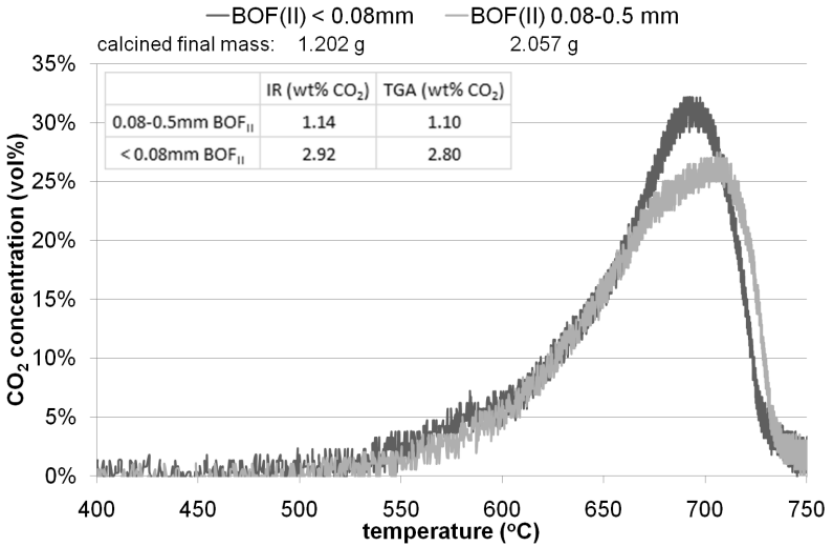

Fig. SC-7.6. Determination of CO_2 uptake by IR analysis; comparison with TGA analysis results for two BOF slag samples.

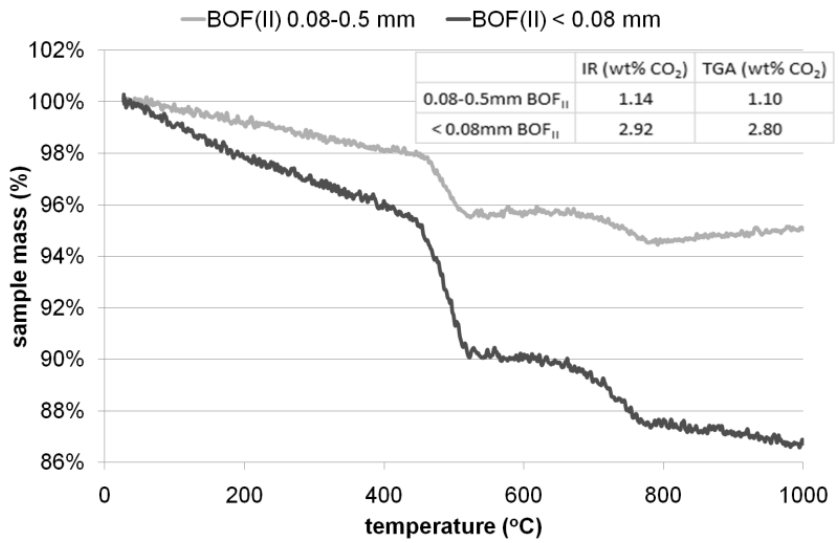

Fig. SC-7.7. Determination of CO_2 uptake by TGA analysis; comparison with IR analysis results for two BOF slag samples.

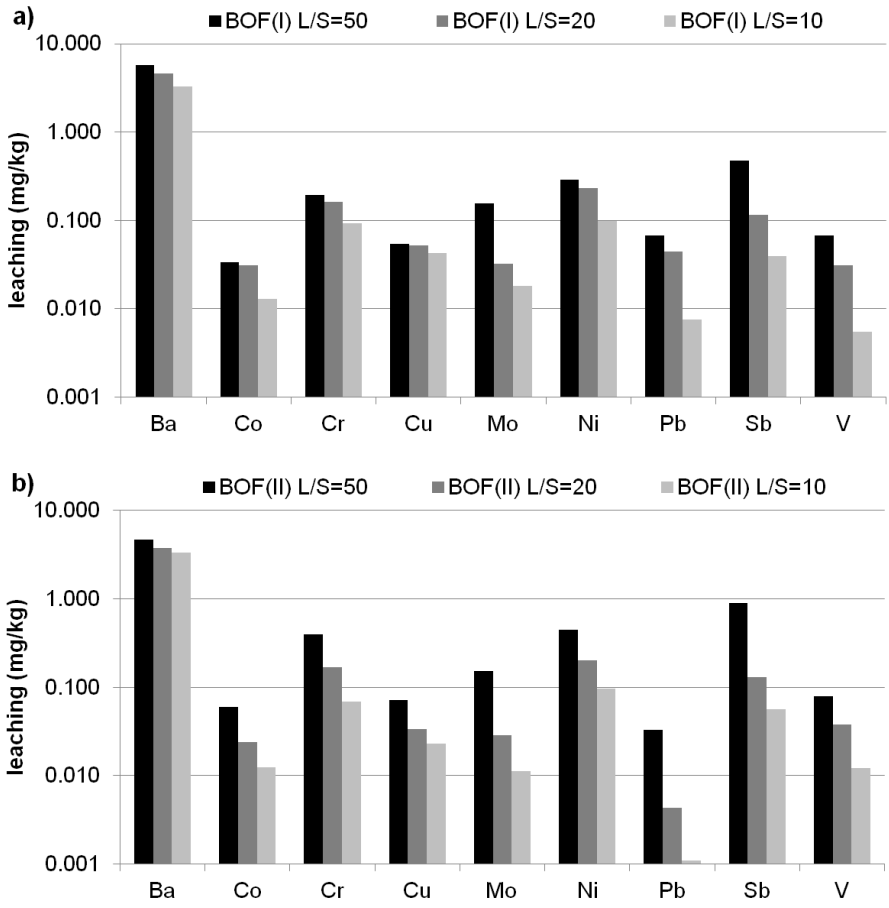

Fig. SC-7.8. Batch leaching tests conducted using three values of liquid-to-solid ratios (L/S = 10, 20 and 50) for fresh BOF_I (a) and BOF_{II} (b) slags; results demonstrate L/S = 50 is a 'worst-case scenario', making it appropriate for comparison with regulatory limits established for L/S = 10.

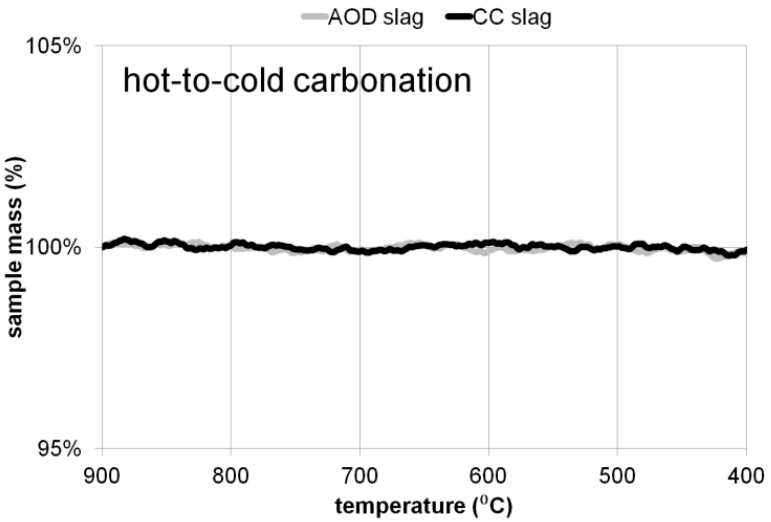

Fig. SC-7.9. In-situ TGA carbonation of argon oxygen decarburization (AOD) and continuous casting (CC) stainless steel slags using hot-to-cold methodology; P_{CO2} = 1 atm. Mineralogy of these materials reported in Santos et al. [36].

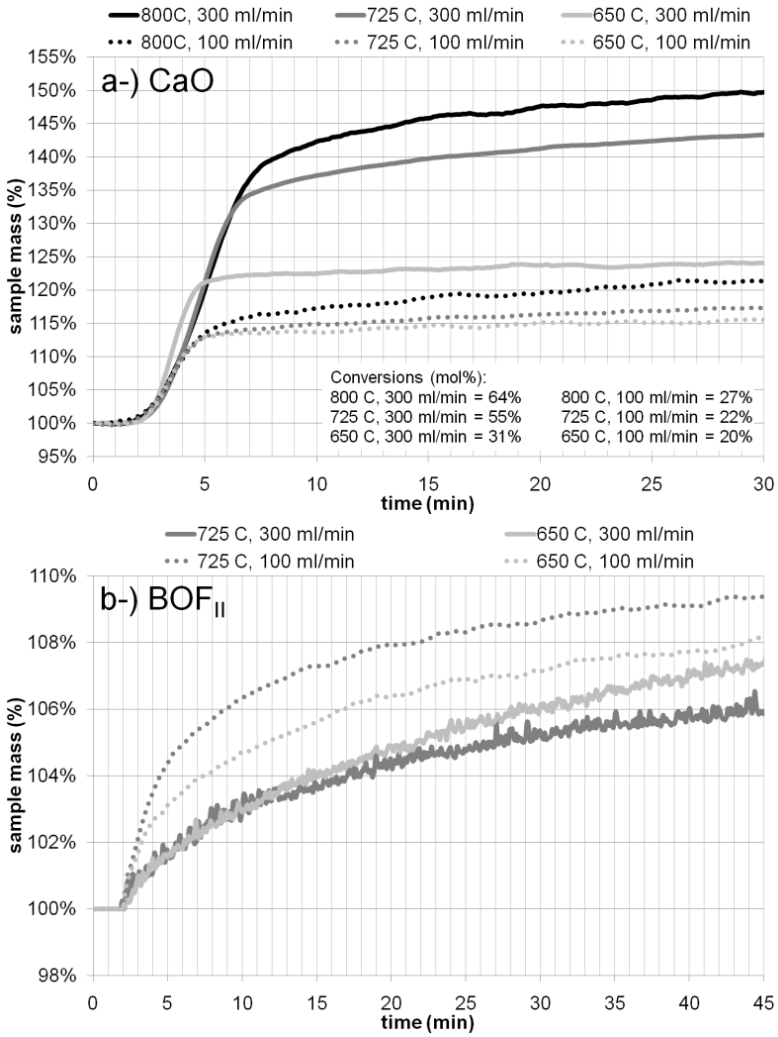

Fig. SC-7.10. In-situ TGA carbonation of pure CaO (a) and BOF_{II} (b) using two CO_2 flow rates (100 and 300 ml/min) and multiple fixed temperatures (650, 725 and 800 ^{o}C); P_{CO2} = 1 atm.

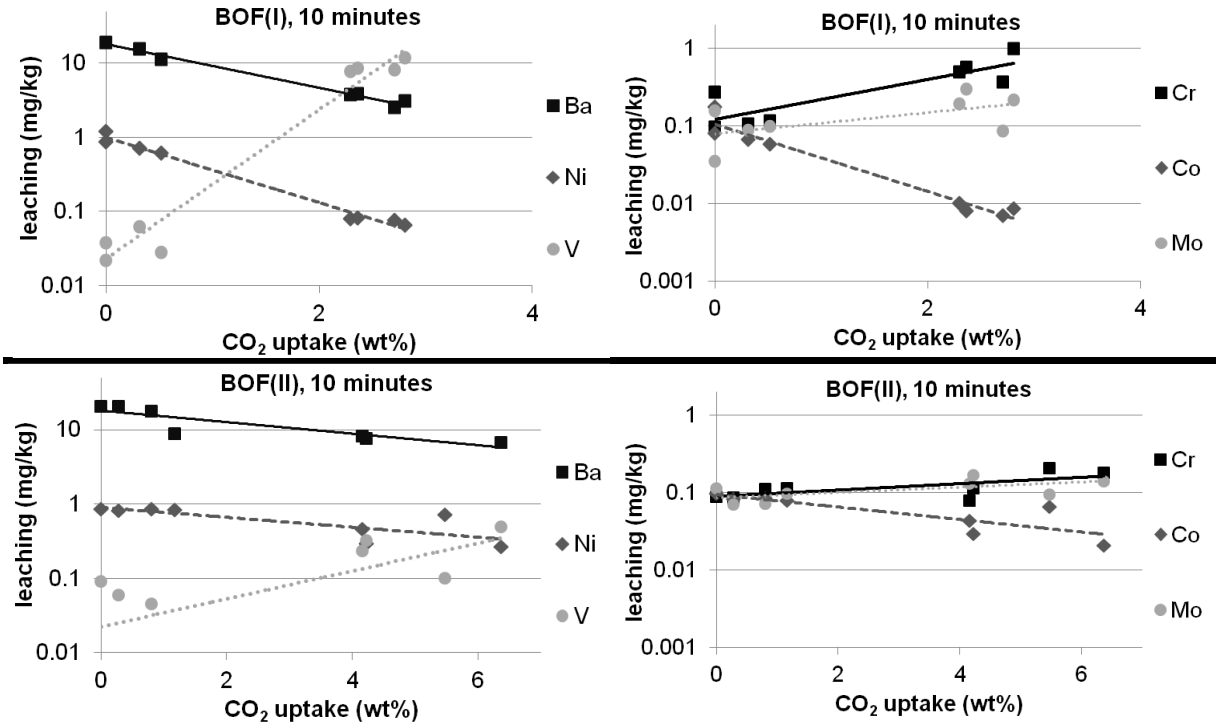

Fig. SC-7.11. Atmospheric furnace carbonation results: leaching of heavy metals (Ba, Ni, V (left-side); Cr, Co, Mo (right-side)) from 0.08-0.5 mm particle size fractions of BOF_I (top) and BOF_{II} (bottom) slags as a function of CO_2 uptake for 10 minutes carbonation reaction time. Varying CO_2 uptakes resultant from carbonation at multiple temperatures (i.e. same samples presented in Fig. 7.6a).

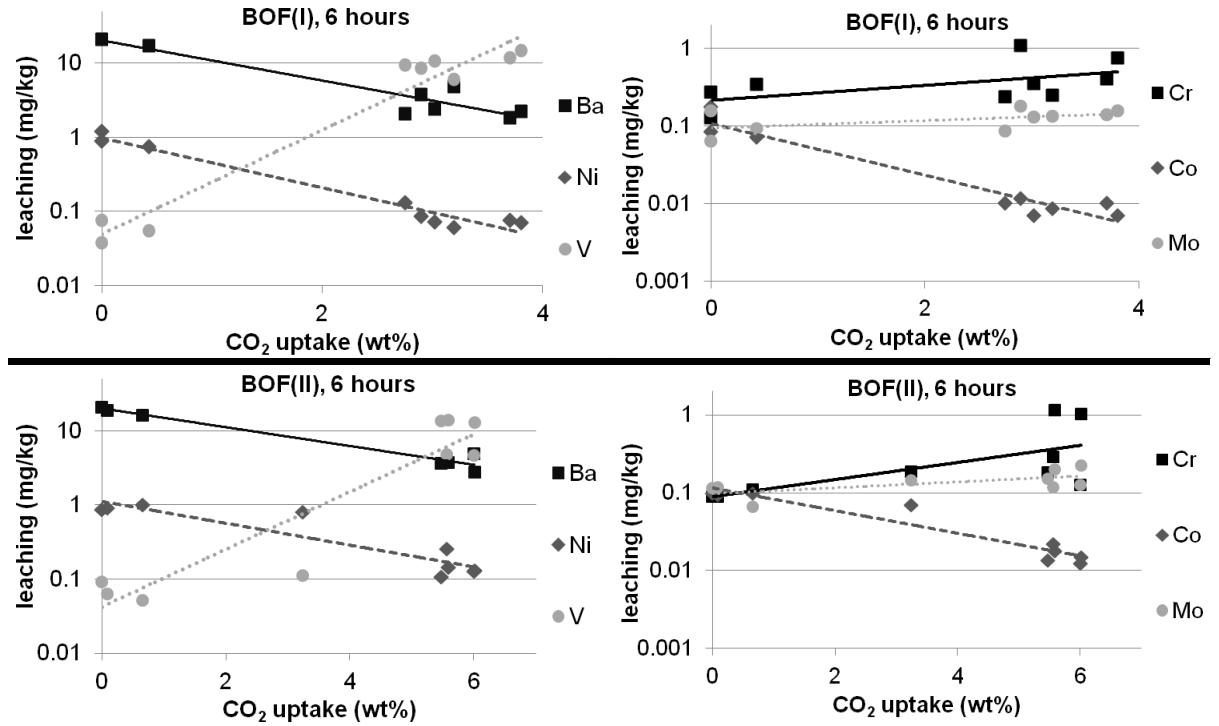

Fig. SC-7.12. Atmospheric furnace carbonation results: leaching of heavy metals (Ba, Ni, V (left-side); Cr, Co, Mo (right-side)) from 0.08-0.5 mm particle size fractions of BOF_I (top) and BOF_{II} (bottom) slags as a function of CO_2 uptake for 6 hours carbonation reaction time. Varying CO_2 uptakes resultant from carbonation at multiple temperatures (i.e. same samples presented in Fig. 7.6a).

8. Susceptibility of mineral phases of steel slags towards mineral carbonation: mineralogical, morphological and chemical assessment

ABSTRACT – Process limitations have thus far prevented mineral carbonation of alkaline wastes from been widely applied. These barriers are caused by inefficient processing, but also by mineralogical aspects inherent to the materials. Better understanding and predictability of the effects of mineral carbonation on alkaline materials could be obtained by studying the carbonation susceptibility of constituent minerals separately, allowing for detailed and accurate analysis of their reaction kinetics and maximal conversions and of the carbonate products formed. For this purpose, this paper presents the synthesis and carbonation of the seven most abundant alkaline minerals found in AOD, CC and BOF slags, namely: åkermanite ($Ca_2MgSi_2O_7$), bredigite ($Ca_7Mg(SiO_4)_4$), cuspidine ($Ca_4Si_2O_7F_2$), β– and γ–C_2S (Ca_2SiO_4), merwinite ($Ca_3Mg(SiO_4)_2$), and srebrodolskite ($Ca_2Fe_2O_5$). Two experimental approaches to mineral carbonation of increasing levels of process severity are utilized: (mild) incubator carbonation, and (accelerated) pressurized slurry carbonation. In addition, the slags and two free oxides (CaO and MgO) are equally carbonated and evaluated. Data regarding CO_2 uptake, mineral conversion and formed carbonate and non-carbonate products in the samples were obtained through TGA, QXRD (Rietveld refinement) and SEM techniques. Reduction in material basicity and evolution of particle morphology were also assessed. The synthesized mineral purities (> 70 wt% target mineral phase) were found sufficient for more accurate assessment of carbonation behaviour of the individual minerals. Bredigite was found to be the most reactive mineral under all processing conditions; C_2S and wollastonite were more reactive under slurry carbonation, while srebrodolskite and calcium monoferrite were found to be more reactive under moist carbonation. Merwinite and diopside had the slowest carbonation conversions. Calcite and aragonite were the dominant carbonate products formed, whereby aragonite formation was promoted in Mg-containing materials. The morphology of aragonite crystals and the packing density of its product layer were found to vary depending on the parent mineral. Characteristic slag carbonation products, not observed as extensively from synthetic mineral samples, were magnesian calcite from slurry carbonation, and monohydrocalcite and vaterite from moist carbonation. Wollastonite was the main crystalline non-carbonate product, occurring predominantly from slag carbonation, while silica-rich amorphous matter formed in all samples proportionally to CO_2 uptake. Free lime, when present, controlled material basicity above pH 12, while silicates were found to typically possess pH in the range of 11.3–11.9, and Ca-carbonates eventually controlled the pH of well carbonated samples to values under 10.

Published as
M. Bodor, **R.M. Santos**, L. Kriskova, J. Elsen, M. Vlad, and T. Van Gerven.
"Susceptibility of mineral phases of steel slags towards mineral carbonation: mineralogical, morphological and chemical assessment".
European Journal of Mineralogy*, 2013, doi:10.1127/0935-1221/2013/0025-2300.
*Special issue of the First European Mineralogical Conference.

Author contributions
R.M.S. conceived the research, performed part of the analytical work, and co-wrote the article.

8.1. INTRODUCTION

Steel slags are a large burden for steel complexes around the world. Covering extensive land areas and containing valuable unrecovered elements, these materials represent an environmental threat and also a financial drawback for the steelmakers. These issues have promoted the pursuit of attractive routes for the stabilization and valorisation of the slags. Due to its suitable chemistry and mineralogy, Blast Furnace Slag (BFS), once extensively stockpiled, has found utilization in the construction domain, as an additive in lightweight mortars, as a component of concrete mixtures**,** as aggregates in road building, or as a raw material for the preparation of ceramic glass, silica gel, ceramic tiles and bricks (Wang & Emery, 2004; Das *et al.*, 2007). Similar aims are intended for other types of steelmaking slags, including Basic Oxygen Furnace (BOF), Argon Oxygen Decarburization (AOD) and Continuous Casting (CC) slags, but various reasons, such as large free lime and iron contents, high basicity, propensity for heavy metal leaching and bulk or particle sizes, have made the reutilization of these materials challenging (Chaurand *et al.*, 2007; Santos *et al.*, 2012c).

In order to improve the negative properties of steel slags and enable greater opportunities for recycling, BOF, AOD and CC slags have been the subject of mineral carbonation research in recent years, with the purpose of CO_2 sequestration, due to the geochemical stability of alkaline earth metal carbonates (IPCC, 2005), and waste valorization (Huijgen *et al.*, 2005; Baciocchi *et al.*, 2010a; Santos *et al.*, 2012b,c). Various applications of the resulting carbonated materials are envisioned, though yet not commercialized, which include marine blocks as artificial reefs used to develop seaweed beds (Oyamada *et al.*, 2008), precipitated calcium carbonate (PCC) for use as paper or polymer fillers (Teir *et al.*, 2007)**,** high strength building materials (Quaghebeur *et al.*, 2010), or reuse in other chemical, environmental or civil engineering applications (Lim *et al.*, 2010).

Process limitations, including high energy intensity, low reaction conversion, and slow reaction kinetics, have thus far prevented mineral carbonation of waste materials from been widely applied. These barriers are caused by inefficient or unoptimized processing and reactor technologies, morphological limitations (shrinking core model), and mineralogical aspects inherent to the materials. While the first two motives have been well reported in literature (e.g. Baciocchi *et al.* (2009), Santos *et al.* (2012c)), little attention has been paid to mineralogical susceptibility of individual minerals. Alkaline waste materials are typically composed of several mineral phases that may or may not be susceptible to mineral carbonation, and which, if reactive to CO_2, may exhibit varying degrees of carbonation kinetics and influence on the material's basicity. The formation and character of passivating layers (e.g. thickness, porosity) can also be affected by the relative solubility of the minerals (Engström, 2010).

Most carbonation studies to date, however, have focussed on the chemical composition of these materials rather than on their mineralogical composition. The commonly used Steinour equation (Steinour, 1959) relies solely on the amounts of alkali oxides to predict CO_2 uptake capacity. Though stoichiometrically accurate, this prediction can be overly optimistic, causing doubts whether carbonation processes are ineffective in reaching complete conversion (due to insufficient process severity or formation of passivating layers), or if the unreacted material is inert to carbonation. Doucet (2010) studied the solubility of the major silicate and ferrite minerals of BOF slag by acidification, and found that, based on the dissolved amounts of Ca and Mg in 0.5 M HNO_3,

the CO_2 uptake of the slag is likely at least 25% lower than its theoretical capacity estimated on the basis of total calcium and magnesium content of the slag.

Assessment of the mineralogical behaviour during mineral carbonation can be attained by applying Rietveld refinement to X-ray diffraction (XRD) data (Rietveld, 1969); however complex diffraction patterns of steel slags add uncertainty to this type of interpretation (mineral phase identification and quantification accuracy) (Mahieux *et al*., 2010). Better understanding and predictability of the CO_2 capture capacity of alkaline materials can be obtained by studying the carbonation susceptibility of constituent minerals separately, allowing for detailed and accurate analysis of their conversion and characterization of the carbonate products formed. To date, Bukowski & Berger (1979) studied the carbonation of γ–dicalcium silicate (C_2S) and monocalcium silicate (CS) powders and mortars, at atmospheric and pressurized conditions, finding greatest conversions for mortars at elevated pressure (up to 56 bar). Goto *et al*. (1995) studied the carbonation of synthesized β– and γ–C_2S powders in a moist 5 vol% CO_2 chamber at room temperature, and observed the formation of solely aragonite, and of a mixture of aragonite, calcite and vaterite, respectively, as carbonation products. More recently, Ibanez *et al*. (2007) and Saito *et al*. (2010) studied the carbonation of synthesized β– and γ–C_2S, respectively, for the purpose of research on cement and concrete curing, though these studies lacked quantitative assessment. The carbonation susceptibility of other major minerals found in steel slags is unavailable in present literature.

To this end, this paper presents the synthesis and carbonation of the seven most abundant alkaline minerals found in BOF, AOD and CC slags, namely: åkermanite ($Ca_2MgSi_2O_7$), bredigite ($Ca_7Mg(SiO_4)_4$), cuspidine ($Ca_4Si_2O_7F_2$), β– and γ–C_2S (Ca_2SiO_4), merwinite ($Ca_3Mg(SiO_4)_2$), and srebrodolskite ($Ca_2Fe_2O_5$). Two experimental approaches to mineral carbonation of increasing levels of process severity are utilized: (mild) incubator carbonation, and (accelerated) pressurized slurry carbonation. In addition, the slags and two free oxides (CaO and MgO) are equally carbonated and evaluated. The carbonation products, which include various forms of calcium and magnesium carbonates (e.g. aragonite, calcite), residual silica (crystalline and amorphous) and intermediate products (e.g. enstatite, wollastonite), are characterized, both with respect to composition and to the process conditions that promote their formation. Reduction in material basicity and evolution of particle morphology are also assessed.

8.2. MATERIALS AND METHODS

8.2.1. Steel slags

Four types of steel slags were used in the experiments. Two BOF slags, BOF-ro and BOF-be, were respectively sourced from steel plants in Romania and Belgium. The AOD and CC stainless steel slags were obtained from a Belgian steelworks. Prior to analyses or experimentation, the materials were prepared by first crushing (for BOF slags) using a jaw-crusher (Retsch BB100) or sieving (for AOD and CC slags) to < 500 µm particle size, followed by milling using a centrifugal mill (Retsch ZM100) operated at 1400 rpm rotating speed with an 80 µm sieve mesh. The obtained particle size for all materials was < 80 µm.

The chemical composition of the slags was obtained by X-ray Fluorescence (XRF, Panalytical PW 2400) analysis; results are presented in Table 8.1. All slag materials contain high concentrations of calcium, which imparts these materials their alkaline properties and reactivity towards mineral

carbonation. In comparison, the magnesium contents of these slags are relatively low, with greater quantities (4.5–6 wt%) found in the stainless steel slags. In contrast, BOF slags contain large quantities of iron, an undesirable loss of product from the steelmaking process. All slags also possess significant quantities of silicon, important for the formation of silicate minerals.

Table 8.1. Chemical composition of Basic Oxygen Furnace (BOF), Argon Oxygen Decarburization (AOD) and Continuous Casting (CC) steel slags, determined by XRF, in wt%.

Element (wt%)	BOF-ro	BOF-be	AOD	CC
Al	0.89	1.3	0.53	0.56
Ca	23.3	35.0	40.6	37.2
Cr	0.43	0.27	0.53	3.7
Fe	23.6	20.6	0.17	0.93
Mg	1.7	0.61	4.5	6.0
Mn	5.6	2.8	0.33	0.43
Ni	0.16	0.08	0.01	0.02
Si	9.2	5.8	15.2	12.9
Ti	0.37	0.40	0.21	0.55

The chemical composition of the slags has a great influence on the material's reactivity towards mineral carbonation and its CO_2 uptake capacity. The mineralogical composition of the slags was determined by Quantitative X-Ray Diffraction (QXRD), adopting the methodology of Snelling *et al*. (2010); corundum (Al_2O_3) was used as an internal standard for amorphous phase determination. Measurements were performed on a Philips PW1830 equipped with a graphite monochromator and a gas proportional detector, using Cu Kα radiation at 30 mA and 45 kV, step size of 0.03° 2θ and counting time 2 s per step, over 5–70° 2θ range. Mineral identification was done in Diffrac-Plus EVA (Bruker) and mineral quantification was performed by Rietveld refinement technique using Topas Academic v4.1 (Coelho Software). The diffractograms of these materials are provided in Fig. 8.1. The quantification results are presented in Table 8.2.

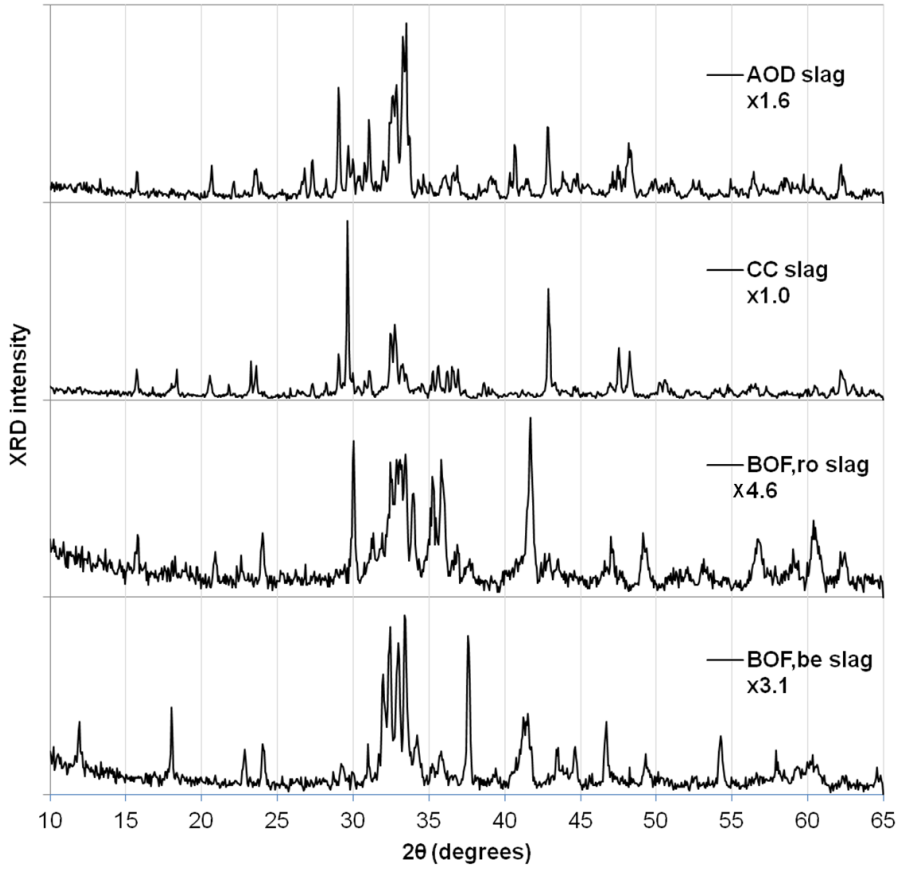

Fig. 8.1. X-ray diffractograms of fresh steel slags. Intensities have been normalized for better viewing; multipliers are indicated on figure below sample labels.

Table 8.2. Mineralogical composition of steel slags, determined by QXRD, in wt%.

Mineral name	Chemical formula	BOF-ro	BOF-be	AOD	CC
Åkermanite	$Ca_2MgSi_2O_7$	**-**	**-**	**3.1**	**2.3**
Bredigite	$Ca_7Mg(SiO_4)_4$	**-**	**-**	**28.0**	**20.9**
Clinoenstatite	$Mg_2Si_2O_6$	6.5	1.9	4.9	9.9
Cuspidine	$Ca_4Si_2O_7F_2$	**-**	**-**	**10.2**	**3.5**
β–C_2S	Ca_2SiO_4	**17.5**	**30.8**	**4.6**	**5.4**
γ–C_2S	Ca_2SiO_4	**3.0**	**0.8**	**19.2**	**25.5**
Merwinite	$Ca_3Mg(SiO_4)_2$	**-**	**-**	**17.3**	**6.3**
Srebrodolskite	$Ca_2Fe_2O_5$	**26.7**	**32.3**	**-**	**-**
Wollastonite	$CaSiO_3$	4.6	2.9	1.2	2.9
Lime	CaO	-	8.8	-	-
Portlandite	$Ca(OH)_2$	3.8	3.1	0.2	2.7
Periclase	MgO	-	1.1	7.0	6.1
Brucite	$Mg(OH)_2$	2.1	2.4	0.2	-
Wuestite	FeO	11.3	6.7	-	-
Magnetite	Fe_3O_4	6.4	-	0.9	6.3
Ferrosilite	$(Fe^{(II)},Mg)_2Si_2O_6$	6.1	2.2	-	-
Fayalite	Fe_2SiO_4	4.7	3.8	1.2	2.7
Other	-	3.3	3.2	2.0	5.5
Amorphous	-	4.0	-	-	-

Predominant minerals in all four slags are Ca– and Mg–silicates; the minerals synthesized in this study, presented in bold, make up the majority of the mineralogical composition of the analyzed slags. Dicalcium silicates (C_2S) are present in all slags, although BOF slags contain greater quantities of the β–polymorph, while the stainless steel slags contain greater amounts of the γ-polymorph. The BOF slags contain large quantities of the dicalcium–ferrite srebrodolskite, a product of their high iron contents. Stainless steel slags are rich in bredigite, cuspidine and merwinite. All slags also contain free oxides and hydroxides, which contribute to their high basicity and structural instability (Santos *et al.*, 2012c). Several Fe-oxides and silicates are also present, especially in the BOF slags. Other phases present in minor quantities include gehlenite ($Ca_2Al_2SiO_7$), hematite (Fe_2O_3), iron (Fe), and quartz (SiO_2), as determined by QXRD.

8.2.2. Synthetic minerals

The desired silicate mineral phases of the steel slags are unavailable commercially and are rare in nature; therefore they were synthesized in laboratory by solid state sintering methodology for study in the present work. Sintering temperatures, duration and cooling trajectories were chosen based on available literature for the synthesis of the desired minerals (see Goto *et al.* (1995), Berliner *et al.* (1997), Laursen & White (2003), De Paula & Francisco (2008), Engström (2010), Mirhadi *et al.* (2012)), with minor adaptations. Table 8.3 presents the synthesis conditions for the seven target minerals. All minerals were synthesized using analytical grade stoichiometric quantities of their constituent oxides (CaO, MgO, SiO_2, Fe_2O_3) and CaF_2 in the case of cuspidine. Calcium oxide was produced prior to mineral synthesis from the thermal decomposition of pure $CaCO_3$ at 900 °C; likewise MgO was refreshed to remove possible pre-existing hydroxides and carbonates. To stabilize the β–polymorph of C_2S, 0.4 wt% B_2O_3 was added to its mixture. Synthesized minerals were produced in batches of 50 g; to obtain sufficient material for the experiments in the present study, two batches of each mineral were produced.

Prior to sintering, the mixtures were mixed in ball mill (Retsch PM 400 MA-type) with ZrO_2 vial and balls (ø 10 mm). A 10:1 ball to powder ratio was used, milling speed was 250 rpm for two hours duration, and 2 ml of ethanol was added to prevent powder adhesion on the milling balls. For bredigite synthesis, five rounds of milling were performed, with vial wall cleaning and ethanol addition before each round. As in Mirhadi *et al.* (2012), it was found that prolonged milling was required to obtain sufficient bredigite purity, possibly due to the high Ca:Mg ratio of this mineral. Milled mixtures were pelletized into 10 mm pellets at 15 kN/cm^2 pressure to promote better solid state sintering interaction between the mixture components. Pellets were placed in a platinum crucible and heat treated in a high temperature bottom loading furnace (AGNI ELT 160-02). Slow cooling was performed within the furnace, while rapid cooling was performed by dropping the hot crucible on a pan and cooling under air flow. After heat treatment, the mineral samples were milled to < 80 μm in the centrifugal mill, and the purity of the samples was assessed by QXRD. It was desired to obtain at least 70 wt% purity of the target mineral and < 10 wt% free oxides content (sum of CaO, MgO, $Ca(OH)_2$ and $Mg(OH)_2$). If these targets were not met, the mineral samples were sintered again until the targets were satisfied.

Table 8.3 presents the final target mineral purity and free oxide content of each 100 g mixed mineral sample; the diffractograms of these materials are presented in Fig. 8.2. All samples meet the desired targets. Fig. S8.1 (in the Supplementary Material) provides a sample Rietveld refinement

plot of fresh and carbonated bredigite. Quantification of additional mineral phases found in the synthesized minerals is provided in Table S8.1 (in the Supplementary Material).

Table 8.3. Mineral synthesis conditions and target mineral purity, determined by QXRD.

Mineral name	Milling time (h)	Temperature (^oC) / Time (h)	Cooling method	Number of runs	Target mineral (wt%)	Free oxides (wt%)
Åkermanite	2	1,300 / 24	5^{o}C/min	4	74.6	0.0
Bredigite	10	1,200 / 1	5^{o}C/min	1	81.7	0.5
Cuspidine	2	1,100 / 20 (Ar atmosphere)	5^{o}C/min	1	83.6	0.2
β–C_2S	2	1,450 / 3	Rapid cooling in air flow	2	73.8	5.5
γ–C_2S	2	1,400 / 48	5^{o}C/min	1	73.0	9.5
Merwinite	2	1,500 / 20	1^{o}C/min	1	74.2	0.2
Srebrodolskite	2	800 / 1 + 1,100 / 36	5^{o}C/min	2	70.5	0.0

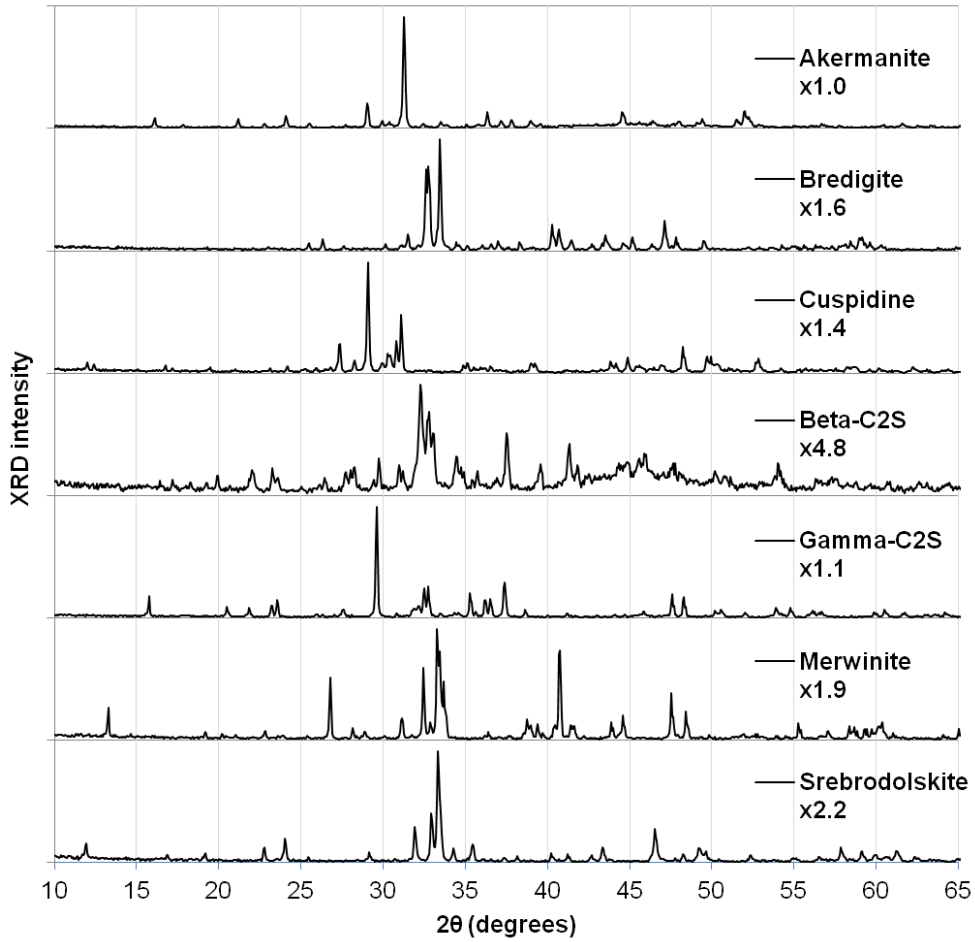

Fig. 8.2. X-ray diffractograms of fresh synthesized minerals. Intensities have been normalized for better viewing; multipliers are indicated on figure below sample labels.[XXIII]

[XXIII] Crystal and morphology systems: tetragonal scalenohedral (Åkermanite); orthorhombic pyramidal (Bredigite); orthorhombic dipyramidal (γ–C_2S and Srebrodolskite); monoclinic prismatic (Cuspidine, β–C_2S (Larnite) and Merwinite).

8.2.3. Pressurized slurry carbonation

Prepared slags, synthesized minerals and pure Ca and Mg oxides were carbonated under pressure and elevated temperature in a 1.1 L stirred batch autoclave reactor (Buchi Ecoclave 300 type 3E). Experimental procedures and conditions were adapted from Van Bouwel (2012), who studied pressurized slurry carbonation of stainless steel slags.[XXIV] For all the experiments, 10 g of material was added to 800 ml ultrapure water (18.2 MΩ·cm); the slurry was stirred by a turbine impeller rotating at 1000 rpm. Carbonation was conducted at 90 °C and 20 bar CO_2 partial pressure, for 15 minutes and 4 hours durations. The carbonated slurry was filtered and the recovered solids were dried for 24 hours at 105 °C prior to analyses. Each experiment was performed in duplicate for data validation; analysis data presented hereafter are averages of well reproducible values.

8.2.4. Incubator carbonation

The second type of carbonation experiments was performed in a CO_2 incubator (Sanyo MCO-17A1). Experimental procedures and conditions were adapted from Vandevelde (2010), who studied the moist carbonation of stainless steel slags.[XXV] The materials were initially wetted with ultrapure water to attain 30 wt% moisture content (4.3 ml + 10 g) and spread on the bottom of 10 cm wide crucibles. CaO and MgO were hydrated separately first to promote formation of their hydroxides; the hydrated materials were subsequently used in incubator experiments. These crucibles were placed in the incubator for seven days at 30 °C, 20 vol% CO_2 at atmospheric pressure, and ~95% relative humidity. After two and five days, extra 2.15 ml water was added to the samples to maintain the moisture content between 15–50 wt% for the duration of the experiment; sample dry-out can occur due to the exothermic heat of reaction during carbonation (Bukowski & Berger, 1979). This moisture interval is required to sustain the thin-film moist carbonation reaction (Baciocchi *et al*., 2010b). At the same time as re-wetting, samples were lightly deagglomerated using a pestle, as carbonation can lead to cementitious behaviour of the stationary material, thus decreasing powder surface area and hindering carbonation progression (Vandevelde, 2010). After one week, the sample crucibles were removed from the incubator and placed for 24 hours at 105°C for drying. The final moisture contents of the samples were determined by gravimetry.

8.2.5. Analytical tests

Carbonated materials were analyzed by QXRD to determine mineralogical composition, allowing for quantification of the carbonation conversion of mineral phases, and quantification of the formation of Ca–, Ca_xMg_y– and Mg–carbonate and non-carbonate (crystalline and amorphous) products. The CO_2 uptake of the samples was determined by Thermogravimetrical Analysis (TGA) by measuring the mass loss between 300–800 °C, corresponding to the temperature interval where carbonates decompose. Dehydroxylation is also possible in this temperature range; however

[XXIV] Work of Van Bouwel (2012) was subsequently expanded into the work presented in Chapter 9; detailed experimental procedures and conditions can be found there.

[XXV] Results of Vandevelde (2010), published in Santos et al. (2010), are presented in Section 9.8.

formation of hydroxylated phases has been deemed negligible compared to carbonates, as assessed by QXRD. Fig. S8.2 (in the Supplementary Material) shows good agreement between CO_2 uptakes determined by TGA and QXRD (overestimation of slag CO_2 uptakes by QXRD is caused by peak overlap due their complex diffraction patterns, inducing underestimation of non-carbonate phases). It was also verified by TGA that all fresh materials (slags and synthetic minerals) contained < 1 wt% CO_2 prior to carbonation experiments. The morphology of fresh and carbonated powders was observed and inspected by Scanning Electron Microscopy (SEM) with Energy-dispersive X-ray Spectroscopy (EDX) (Philips XL30); powder samples were mounted on carbon tape and sputtered with gold (Edwards S150) prior to analysis. Material basicity was determined by measuring sample pH in slurry; 2 g solids were placed in 100 ml ultrapure water and shaken for 24 hr prior to pH reading. Measured basicity values were compared to the values of pure carbonates modelled using Visual MINTEQ (ver. 3.0, KTH).

8.3. RESULTS AND DISCUSSION

8.3.1 CO_2 uptake of carbonated materials

Two carbonation methods were used to carbonate the synthetic minerals produced in this study, as well as the steel slags of interest and the two main alkaline oxides present in these materials (CaO and MgO). The intention was to compare the carbonation susceptibility of the different materials to the comparatively mild CO_2 incubator (IC) carbonation process, versus the more intense pressurized slurry autoclave (AC) carbonation process. Fig. 8.3 presents carbonation results expressed as percentage values of the maximal CO_2 uptake of each material, calculated based on the Ca and Mg contents of the materials according to Eq. (8.1):

$$CO_2 \text{ uptake (\% maximal)} = (Q_{CO2}/MW_{CO2})/(w_{Ca}/MW_{Ca}+w_{Mg}/MW_{Mg}) \quad (8.1)$$

In Eq. (8.1) Q_{CO2} is the CO_2 uptake determined by TGA and expressed as grams CO_2 captured per gram of initial material mass, *MW* are elemental molar masses, and *w* are elemental mass fractions in the original material. Also marked on Fig. 8.3 are maximal theoretical CO_2 uptakes based on Ca content only, useful for assessment of the CO_2 uptake capacity if only Ca, and not Mg, reacts. This is one existing hypothesis as to why the Steinour equation overpredicts CO_2 uptake capacity.

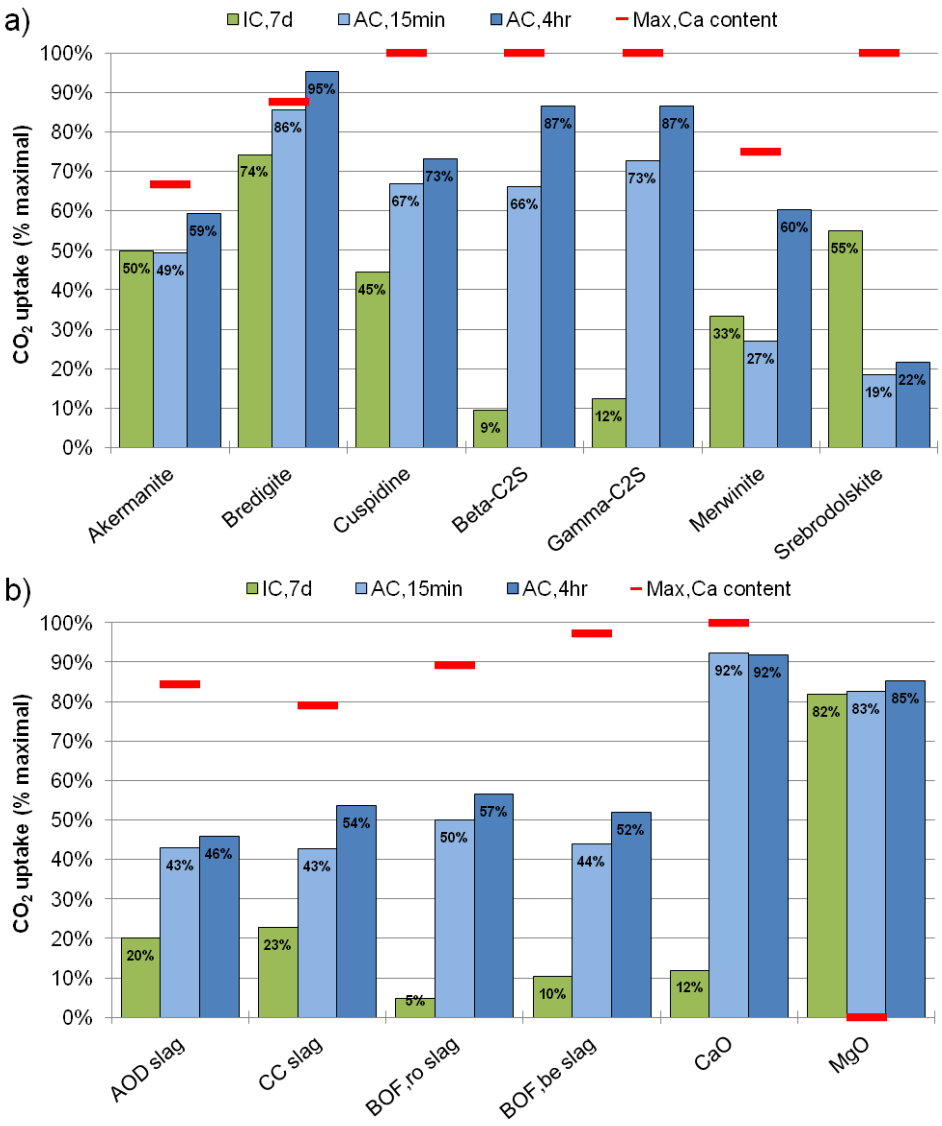

Fig. 8.3. CO_2 uptake of carbonated synthetic minerals (a) and steel slags (b), determined by TGA.

Fig. 8.3a shows that synthetic bredigite achieved the highest CO_2 uptakes for both IC and AC carbonation methodologies. The two synthesized C_2S materials performed poorly in IC experiments, while synthetic srebrodolskite did not carbonate well in AC experiments. Other synthetic mineral samples had intermediate performances, invariably carbonating better in the autoclave than in the incubator. The effect of carbonation time, varied between 15 minutes and 4 hours in the AC experiments, had mixed results. Åkermanite, bredigite, cuspidine and srebrodolskite achieved at most an extra 10% CO_2 uptake improvement, while β–C_2S, γ–C_2S and merwinite benefited more (14–33% increase) from extended carbonation time, suggesting slower carbonation kinetics of these materials. It must be noted, however, that these CO_2 uptakes do not discriminate between the carbonation conversions of the target mineral phase and secondary minerals also present in these materials. As such, detailed Rietveld analysis results are presented in Section 8.3.2 to elucidate carbonation susceptibility and kinetics more accurately.

Also in Fig. 8.3, subfigure b presents the CO_2 uptakes of carbonated steel slags and pure Ca– and Mg–oxides. All slags carbonated substantially better in the autoclave; yet uptakes did not surpass 60% of the theoretical maximal, in contrast with some synthetic minerals which surpassed the 80% mark. The mixed mineralogy of the slags may be attributable to these results; more detailed discussion is provided in Section 8.3.2 based on Rietveld analyses. As for the pure oxides,

CaO carbonation reached near completion in autoclave experiments, but performed poorly in the incubator. This is possibly due to sample hardening that occurs in the incubator, due to formation of cementitious carbonate phase, which blocks access of CO_2 to the powder layer interior, and to the formation of dense calcium carbonate layers around particle surfaces, also inhibiting access of CO_2 to the particle cores. In the autoclave, continuous mixing acts to promote carbonation homogeneity and interparticle interaction, while the slurry phase also promotes bulk solution precipitation of solubilised Ca, rather than solely surface or intraparticle precipitation in the case of moist incubator carbonation. MgO achieved nearly identical CO_2 uptakes in all experiments, 82–85%; more insight on this outcome is presented in Section 8.3.4.

8.3.2. Carbonation conversion of individual mineral phases

Rietveld analysis of XRD diffractograms allows for detailed assessment of the behaviour of the constituent minerals of the carbonated materials tested when exposed to CO_2. Fig. 8.4 presents the carbonation conversion of the target minerals present in the synthesized samples (subfigure a), as well as the carbonation conversion of the most predominant secondary mineral phases found in these same samples (subfigure b). The mineral conversion values, expressed as percentage converted, were calculated by translating mass fractions delivered by Rietveld analysis into molar fractions normalized against the pre-carbonation mass of the materials (to discount the CO_2 uptake mass after carbonation, which artificially lowers the mass fractions of non-carbonate components) and taking into account the formation of amorphous materials during carbonation (which, if ignored, causes overestimation of mineral mass fractions). This data handling procedure, exemplified in Table S8.2 (in the Supplementary Material), enhances the accuracy of conversion values and allows for more precise comparison of the results, as opposed to the simple comparison of pre-carbonation composition to post-carbonation composition.

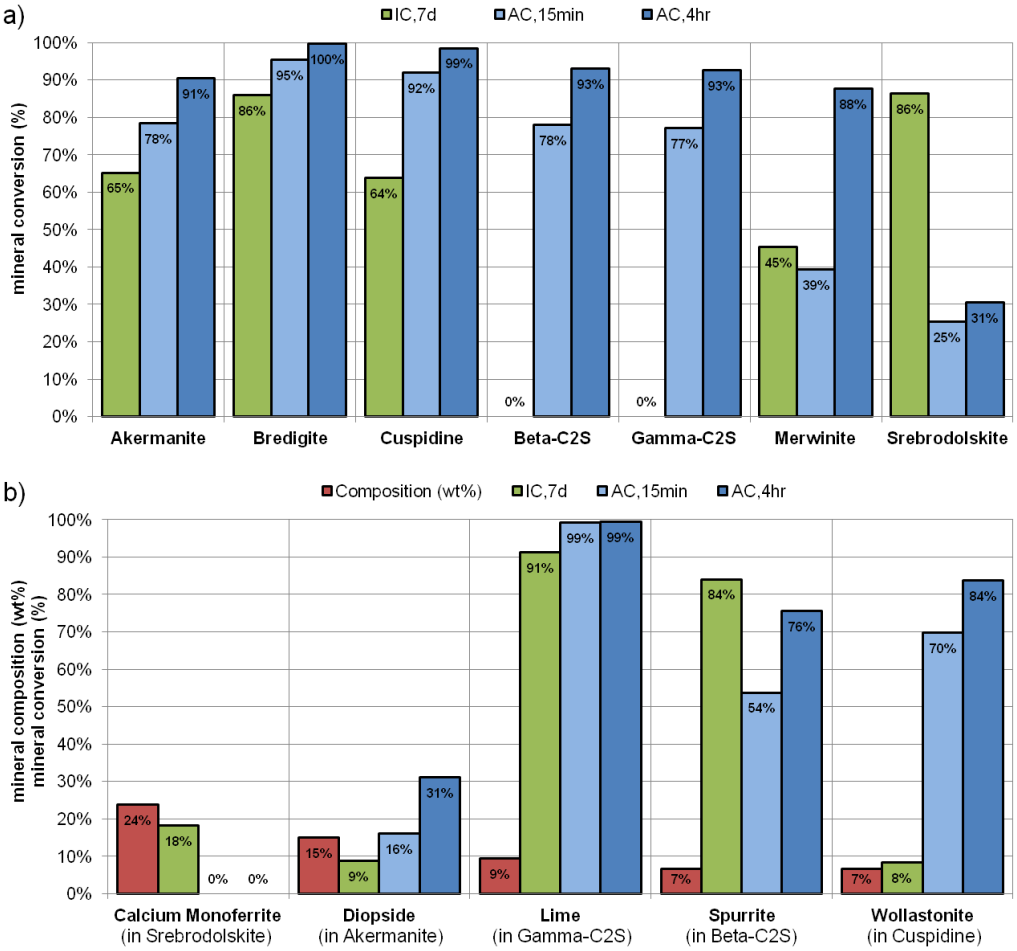

Fig. 8.4. Carbonation conversion of target (a) and secondary (b) mineral phases of synthetic minerals, determined by QXRD.

The results of Fig. 8.4a, for target minerals, are largely analogous to the CO_2 uptake results of Fig. 8.3a. That is, samples with greatest CO_2 uptake had the most complete target mineral conversion. For instance, bredigite is confirmed as the most converted mineral after carbonation, and srebrodolskite converts much more extensively in the incubator than in the autoclave. Doucet (2010) found the nitric acid solubility of brownmillerite (a mineral closely related in chemical composition to srebrodolskite, namely $Ca_2Fe_{1.4}Mg_{0.3}Si_{0.3}O_5$) to be much lower than that of β–C_2S; this may explain autoclave results, but does not explain the inverse behaviour in the incubator. Mineralogical analysis also uncovers the effect of some secondary minerals on the CO_2 uptake (either enhancing or hindering it). Åkermanite mineral conversion is significantly better than suggested by CO_2 uptake, because the secondary phase in this synthesized sample, 15 wt% of diopside ($CaMgSi_2O_6$), performs comparatively more poorly towards carbonation (Fig. 8.4b). On the other hand, the mineral conversions of β– and γ–C_2S in the incubator are found to be nil; the small CO_2 uptakes of these synthesized materials is caused by their free oxide contents, such as the 9 wt% of lime in γ–C_2S, which carbonates very well in the incubator (Fig. 8.4b). Goto *et al.* (1995) presented good reactivity of β– and γ–C_2S in a moist incubator over 48 hours. In that study, however, the solids were not initially wet, receiving all moisture from the wet gas. Ibanez *et al.* (2007) also did not moisten γ–C_2S for carbonation, but rather hydrated it for one month before CO_2 curing experiments for two months duration. In the present study the C_2S solids might have been flooded (i.e. too moist, see Fig. 8.5), and thus rendered unreactive (or became flooded due to low reactivity (i.e. low exothermic heat generation)). The other synthetic minerals did not experience

this detrimental effect, and were not flooded as seen in Fig. 8.5; therefore it is a mineral specific behaviour and not a process limitation. It is known that γ–C_2S has low hydration capacity (Saito *et al.*, 2010), which could explain its low reactivity in the mild incubator process conditions, but the similar poor result of β–C_2S, an important hydraulic component of OPC cement (Ibanez *et al.*, 2007), is less expected. Other notable results from these analyses are the confirmation that merwinite is the slowest mineral to carbonate in the autoclave, with conversion increasing by 49% after 4 hours compared to 15 minutes (Fig. 8.4a), and the better susceptibility of calcium monoferrite ($CaFe_2O_4$) to incubator carbonation (Fig. 8.4b), similar to the other calcium ferrite, srebrodolskite. The slow reactivity of merwinite can also explain the late loss of moisture and thus low final moisture content of the sample in the incubator (Fig. 8.5).

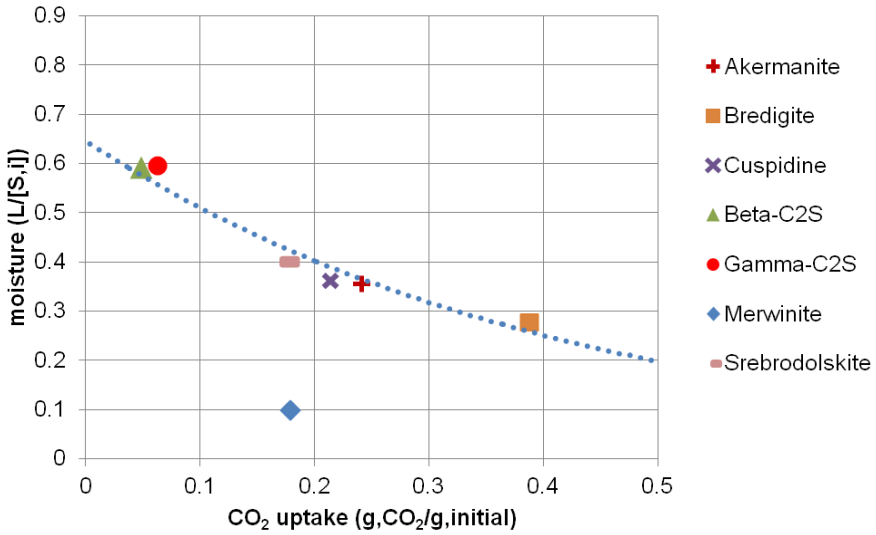

Fig. 8.5. Final moisture content of synthetic minerals carbonated in the CO_2 incubator (expressed based on initial solid mass [S,i]) versus CO_2 uptake determined by TGA.

8.3.3. Steel slags carbonation results

As with the synthetic minerals, Rietveld refinement was also used to assess carbonation conversion of alkaline mineral phases present in the steel slags. Fig. S8.3 (in the Supplementary Material) presents the mineral conversions of the seven main mineral phases of the steel slags, together with the already presented conversion values of the synthetic minerals for easier comparison. As stated earlier, the complex diffraction patterns of the slags increase the uncertainty in the quantification values, in particular for mineral phases present in small amounts (< 10 wt%); therefore these data should be interpreted in a more qualitative manner.

In the case of the stainless steel slags (AOD and CC), Fig. S8.3 suggests that the minor mineral phases, (åkermanite, cuspidine and β–C_2S) react more quickly and extensively than the major phases. As a result, the formation of carbonate products on the surface of the slag particles may hinder the carbonation conversion of the major mineral phases. While bredigite conversion is moderately good (this phase converted very well in the case of the synthetic mineral), the conversions of γ–C_2S and merwinite are much lower than expected based on the synthetic mineral results presented earlier. A distinction can also be made between results of AOD and CC slag, in that CC slag presents more contrasting results: bredigite and β–C_2S carbonated well in CC slag,

while γ–C_2S had poor conversion. The same minerals in AOD slag carbonated more moderately, achieving roughly 30–50% conversions. This may be caused by slag particle morphology.

Fig. 8.6 illustrates that CC slag particles resemble single mineral phases, like those pictured in Fig. 8.7, while AOD slag particles appear to have homogenous appearance, which suggests that these particles are composed of mixtures of mineral phases. These differences can be caused by differing cooling rates during slag production in the steelworks. Consequently, in CC slag, the mineral phases more susceptible to rapid carbonation can react to near completion more quickly, and their precipitated carbonate products can deposit on other mineral particles and hinder their reactivity. In contrast, mineral phases of AOD slag gradually and simultaneously react, and thus achieve more similar carbonation conversions over time. These interpretations are in agreement with carbonation kinetics results of Santos *et al*. (2012b). Compared to synthesized minerals, slag particles are also, on average, larger in diameter (approx. 20–30 μm versus < 10 μm), which can hinder carbonation conversion due to reduced reactive surface area and greater diffusion lengths.[XXVI]

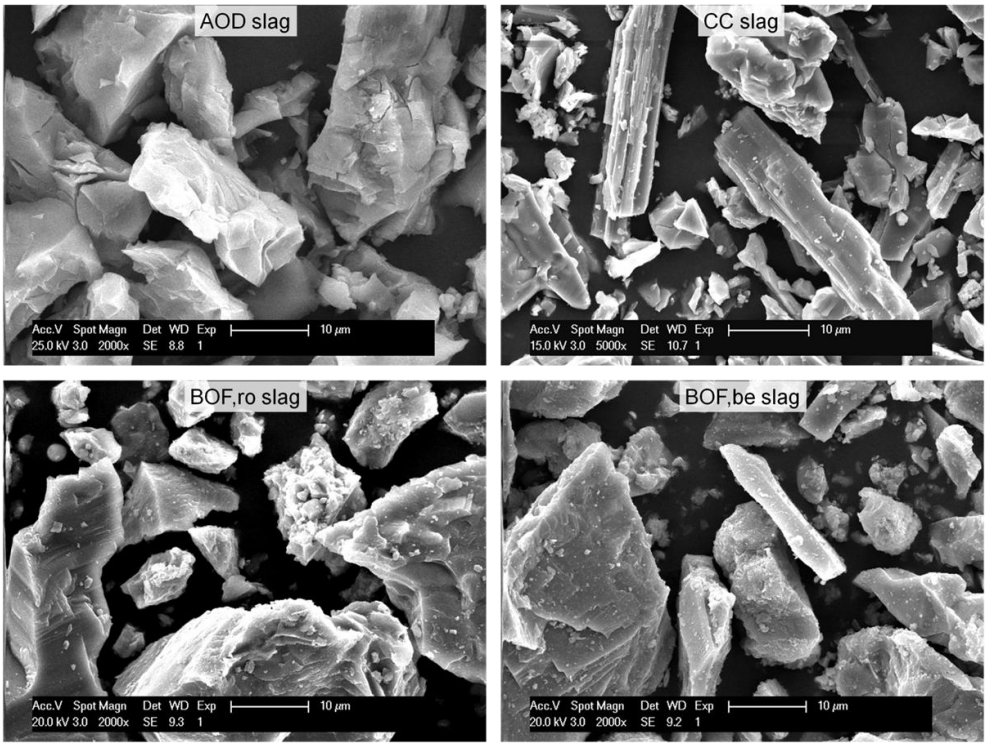

Fig. 8.6. Morphology of fresh steel slag particles, inspected by SEM.

[XXVI] Remark: it is also possible that the differences in reactivity between the synthetic minerals and those same minerals present in the slags may be due to solid solution effects in the slags. Namely, the incorporation of impurities in the mineral structures may affect the reactivity of those phases compared to the pure minerals. Detailed microstructural analysis of the slag phases is needed to find out which phases may suffer from this phenomenon, and to what extent this can play a role in their reactivity.

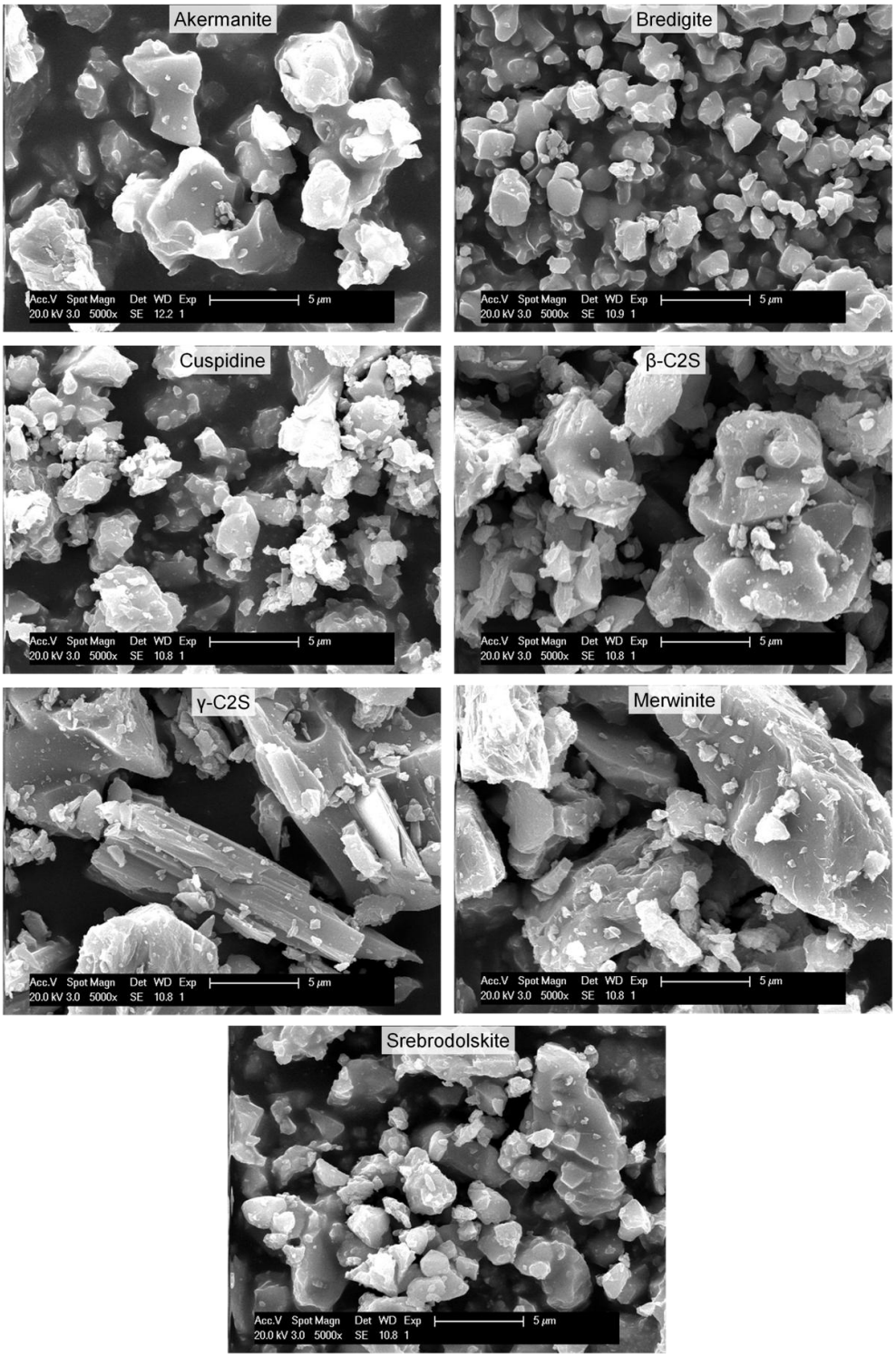

Fig. 8.7. Morphology of fresh synthetic mineral particles, inspected by SEM.

In the case of BOF slags, it is evident in Fig. S8.3 that srebrodolskite carbonation conversion differs from results of the synthesized mineral. The conversion of this mineral in BOF-ro slag is considerably higher in the autoclave than in the incubator, and is also higher than the synthesized mineral in the autoclave. In BOF-be slag this mineral also carbonates better in the autoclave, though conversion levels are lower than the other slag. It is unclear what may cause these differences, but location of the mineral in the slag particles, which contain several mineral phases unreactive to carbonation, particularly iron oxides and silicates, may play an important role (Doucet, 2010; Santos *et al.*, 2012c). On the other hand, the conversion of β–C_2S in both BOF slags follows similar

trend as the corresponding synthesized mineral: fast and high conversion in the autoclave, and low conversion in the incubator.

8.3.4. Carbonate mineral phases

Resulting mineral phases produced after carbonation experiments were different for each material. The formation of Ca–, Ca_xMg_y– and Mg–carbonates was found to be influenced by the alkaline earth metals contents of the materials.[XXVII] Fig. 8.8 shows the distribution of carbonate products formed from the synthetic materials (subfigure a) and the steel slags and pure oxides (subfigure b), determined by QXRD. It is evident that Ca–carbonates are the predominant product after carbonation, given the high calcium contents of the materials. It is also clear that two main polymorphs of $CaCO_3$ are formed: calcite and aragonite. Aragonite formation was dominant in samples containing magnesium (i.e. åkermanite, bredigite and merwinite). This is in agreement with reported literature on the aragonite promoting effect of Mg ions in solution (Santos *et al*., 2012a). Vaterite, the least geochemically stable crystalline $CaCO_3$ polymorph and thus rarely formed in nature (Railsback, 2006), was detected in incubator carbonated samples of C_2S. These were the same samples that had no carbonation conversion of its target minerals. Pure lime (CaO), which is present in small quantities in the C_2S samples and is likely responsible for their CO_2 uptakes in the incubator, formed similar carbonate products during incubator carbonation (Fig. 8.8b). Thus it appears that vaterite forms as an intermediate product of lime carbonation prior to conversion to one of the other more stable forms of $CaCO_3$.

[XXVII] Remark: Siderite formation was not detected, likely given the relatively low CO_2 pressures utilized, compared to the supercritical conditions used by Qafoku et al. (Chem. Geol. 332–333 (2012) 124–135), who obtained siderite from fayalite at 35-80 °C and 90 atm,CO_2 pressure.

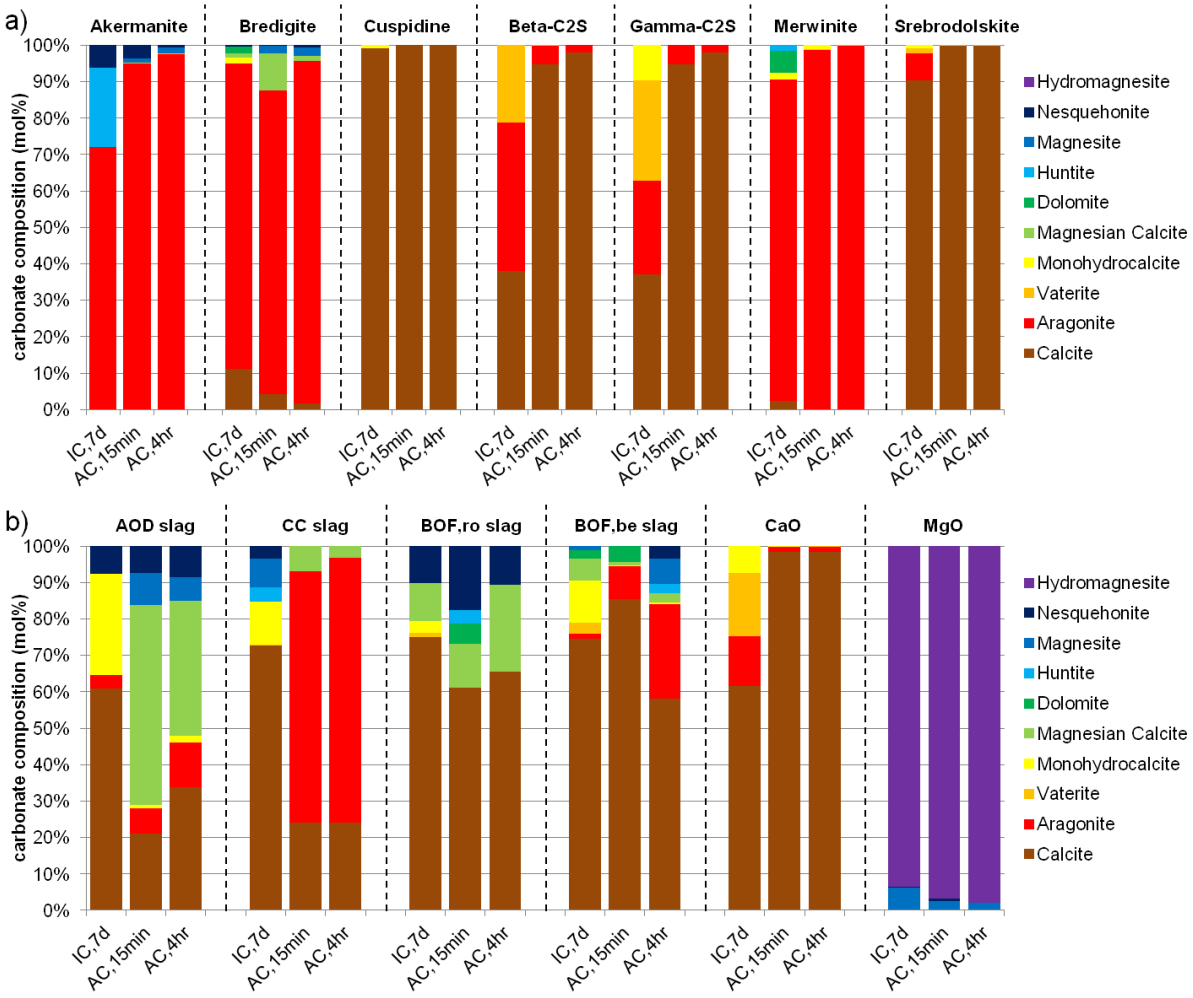

Fig. 8.8. Carbonate composition of synthetic minerals (a) steel slags and pure oxides (b) after carbonation experiments, expressed as molar percentage fractions of total carbonate content, determined by QXRD.

The presence of Mg-carbonates in the Mg-containing synthetic minerals can be considered rather small, relative to their Mg contents. The Ca:Mg molar ratios of åkermanite, bredigite and merwinite are 2:1, 7:1 and 3:1, respectively. As such, if Ca and Mg carbonation conversions maintained the same ratios, it would be expected that the molar fractions of Mg–carbonates would be, respectively, 33 %, 12.5 % and 25 %. None of the synthetic minerals approach these values. It can thus be concluded that a major reason for the CO_2 uptakes of these minerals falling short of their theoretical maximal values based on their chemical composition (Fig. 8.3), is that calcium is nearly solely responsible for CO_2 uptake. As such, the maximal values based only on calcium contents, plotted as horizontal bars in Fig. 8.3, are more realistic of the true CO_2 uptake capacities of these materials (with the exception of bredigite, which reacts nearly completely), at least under the carbonation process conditions herein tested.

Results for carbonate products of steel slags (Fig. 8.8b) somewhat differ from those for synthetic minerals. More varied carbonate products form, in particular significant amounts of monohydrocalcite ($CaCO_3 \cdot H_2O$) and magnesian calcite ($Ca_xMg_yCO_3$, where typically $0 < y < 15$ mol% (Kitano *et al.* (1979)) are detected. The former was found primarily in incubator carbonated samples, and thus may result from the milder and slower crystallization mechanisms that takes place in this process. The latter formed in all slags, with autoclaved AOD slag containing significant quantities. The formation of Mg–carbonates is also detected, of which nesquehonite

($MgCO_3 \cdot 3H_2O$) was the most common. The greater carbonation reactivity of Mg in the slags compared to the synthetic minerals may be due to its partial presence is the form of periclase (MgO) and brucite ($Mg(OH)_2$) (Table 8.2), free (hydr)oxides that may more readily react than Mg trapped in silicate matrices. This is confirmed by the conversion of pure MgO into nearly pure hydromagnesite ($Mg_5(CO_3)_4(OH)_2 \cdot 4H_2O$) under all process conditions (Fig. 8.8b). The carbonate to Mg molar ratio of this mineral, 4:5, suggests that maximal CO_2 uptake is limited to 80 %, in agreement with the CO_2 uptakes measured by TGA (Fig. 8.3b). The preferential formation of hydrated Mg–carbonates over the anhydrous magnesite ($MgCO_3$) is explained by its large ionic potential, which promotes hydration in solution (Railsback, 2006). It is possible that hydrated Mg-carbonates do not suffer from the same level of hardening and porosity reduction as calcite, which would explain why MgO carbonated more extensively than CaO in the incubator.

8.3.5. Non-carbonate mineral phases

Besides crystalline carbonates, mineral carbonation can produce other non-carbonate crystalline phases as well as amorphous matter. Non-carbonate mineral phases that may be produced from mineral carbonation mainly include structurally simpler components originating from the decomposition of complex silicates. These are hematite (Fe_2O_3), enstatite ($MgSiO_3$), wollastonite ($CaSiO_3$) and quartz (SiO_2). Fig. 8.9 shows that these components can be identified in small quantities (< 5 wt%) in both carbonated synthetic minerals and steel slags. Wollastonite formation in steel slags is most notable, indicating that its reactivity to mineral carbonation is slower than the native silicates. Formation of this mineral phase may thus hinder further carbonation of the slags, as its formation along the reactive front towards the shrinking particle core contributes to decreased ionic diffusivity.

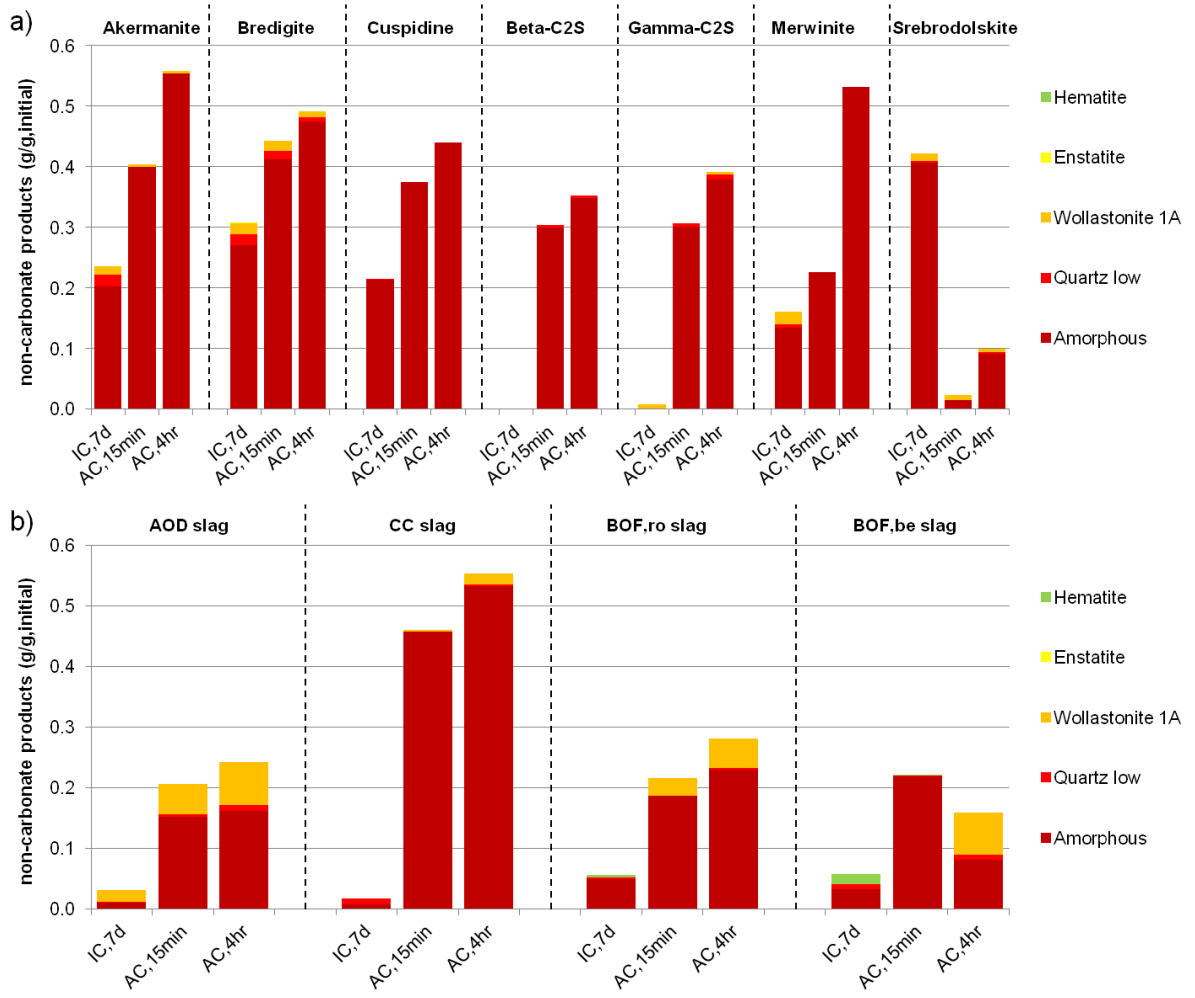

Fig. 8.9. Non-carbonate composition of synthetic minerals (a) and steel slags (b) after carbonation experiments, expressed as grams non-carbonate phase per gram initial material, determined by QXRD.

The vast majority of non-carbonate products, however, are amorphous. Comparing Fig. 8.9 with Fig. 8.3, it is evident that formation of amorphous matter is proportional to CO_2 uptake and thus mineral carbonation conversion. By elemental balance, seeing as most carbonation products are Ca- and Mg-rich and Si-poor, it can be concluded that the amorphous matter is composed mainly of amorphous silica (SiO_2). Baciocchi *et al.* (2010c) confirmed by geochemical modelling that the leaching of Si from carbonated AOD slag is controlled by amorphous silica, unlike in the case of fresh slag where the leaching mechanism is controlled by C-S-H (calcium silicate hydrate). Amorphous silica layers can also contribute to the passivation of mineral particles towards carbonation (Daval *et al.*, 2011), though present results suggest that pure minerals are less affected by this phenomenon since CO_2 uptakes reached near completion for several samples. It can be that, as commented by Daval *et al.* (2011), the properties of silica coatings may depend on the structure and composition of the parent mineral or on the experimental conditions, and thus may affect mineral carbonation to different extents.

8.3.6. Carbonated particle and crystal morphology

Morphological assessment of the carbonated synthetic minerals was performed by SEM, allowing for direct observation of the carbonation products formed and of any visibly identifiable

uncarbonated parent mineral. Fig. 8.10 illustrates the appearance of four samples carbonated in the autoclave for 4 hours (bredigite, γ–C_2S, merwinite and srebrodolskite) and of two samples carbonated in the incubator for 7 days (γ–C_2S and srebrodolskite). The first striking distinction between these samples pertains to the calcium carbonate polymorphs. Bredigite and merwinite were both identified by XRD to contain mainly the aragonite polymorph of $CaCO_3$; however the morphology of the aragonite crystals is strikingly different between the two samples. The crystals in bredigite resemble thin needles, some aggregated into larger crystal bundles and others freely dispersed, while the crystals in merwinite have much lower aspect ratios and are closely packed around particles shaped much like the parent mineral particles (Fig. 8.7). Possibly the slower reactivity of merwinite compared to bredigite, discussed in Sections 8.3.1 and 8.3.2 based on CO_2 uptake and mineral conversion results, promotes surface precipitation of the crystals and allows for more prominent growth of individual crystals.

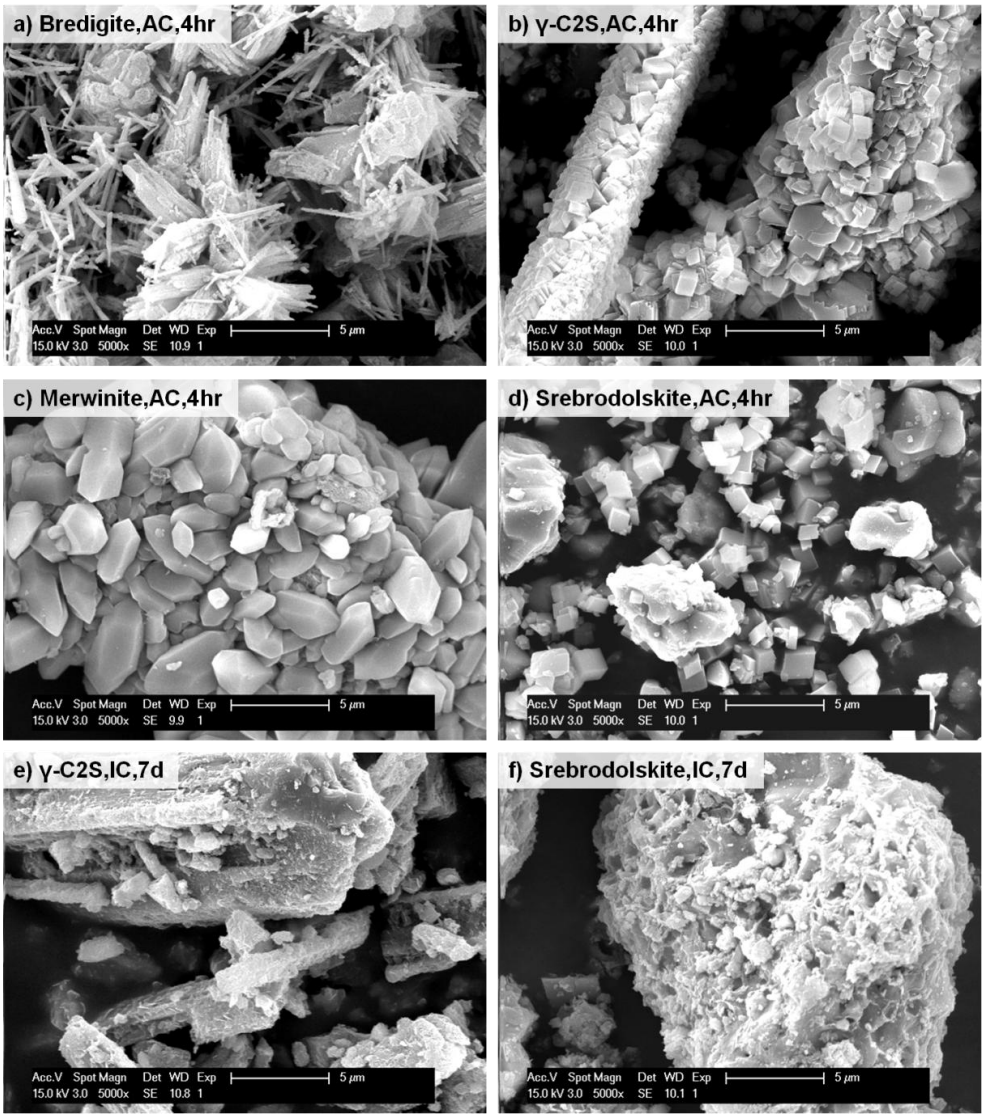

Fig. 8.10. SEM images of synthetic minerals carbonated in autoclave (a-d) and incubator (e-f) experiments.

Furthermore, the morphology of the $CaCO_3$ product layer, its crystals and their packing density, can affect mineral carbonation progression, in terms of both kinetics and terminal conversion. Aragonite crystals formed from bredigite had much lower packing density than those

formed from merwinite. These aspects can have implications for the access of the carbonate-containing aqueous medium to the reactive front and the consequent leaching and precipitation of alkaline species from the unreacted core.

Calcite crystals in autoclave carbonated γ–C_2S also collected on the surface of the parent particles, as can be seen by comparing the rod-like shapes in Fig. 8.10b with that on Fig. 8.10e, which represents γ–C_2S poorly carbonated in the incubator. Though carbonating more quickly than merwinite, mineral conversion of γ–C_2S was also slower and less complete than bredigite; although the smaller particle size of fresh bredigite (Fig. 8.7) may have played a role in this result. Rhombohedral calcite crystals similar to well carbonated γ–C_2S are also seen in poorly carbonated srebrodolskite (Fig. 8.10d). In the latter case, however, unreacted particles without any surface precipitation are clearly visible; these were confirmed by EDX to have the composition of Ca–ferrites. In contrast, well carbonated srebrodolskite, reacted in the incubator and illustrated in Fig. 8.10f, does not show clear presence of calcite crystals, despite confirmation by XRD of its presence in larger amounts (30 wt%). It appears as if the carbonate forms incongruently within the parent particles. This may be the case with γ–C_2S as well, by inspection of Fig. 8.10e. Therefore, besides chemical susceptibility, differing nanoporosity of particle grains may also play a role in the carbonation reactivity of these minerals, as it has been found to affect weathering rates of naturally occurring silicates (Brantley & Mellott, 2000).

8.3.7. Basicity

Carbonation is also responsible for basicity reduction of carbonated materials, an effect which is beneficial to highly basic materials, including steel slags, as it contributes to reducing the leaching of a variety of heavy metals and helps meet safe disposal or re-utilization requirements (Santos *et al.*, 2012b,c). Data in Fig. 8.11 represent the pH values of fresh and carbonated synthetic minerals and steel slags under the different carbonation conditions tested. These data are re-plotted on Fig. S8.4 (in the Supplementary Material) versus CO_2 uptake; the decreasing trends are proportional to CO_2 uptake results, and hence to mineral conversion, in the sense that less carbonated samples registered pH values closer to that from fresh samples, and more carbonated samples registered pH values that approach the value for pure $CaCO_3$ (9.91, unequilibrated with atmospheric CO_2 (Visual MINTEQ)).

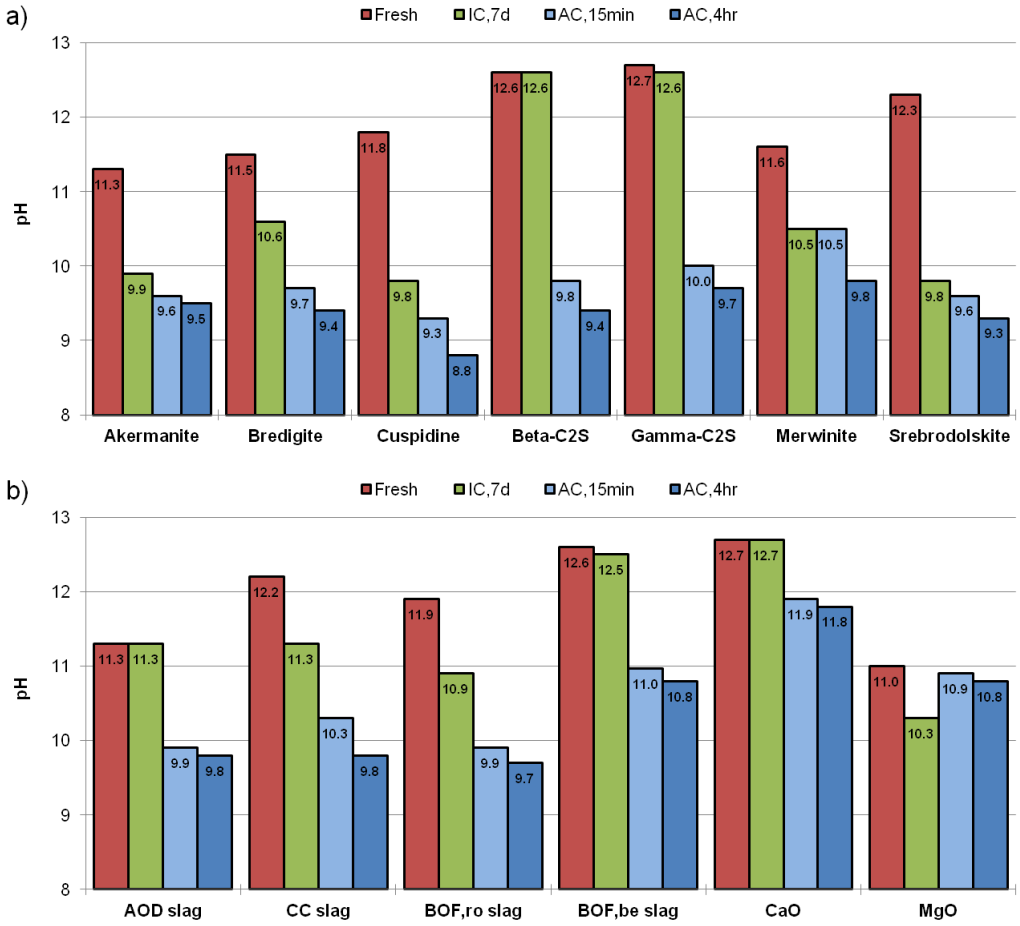

Fig. 8.11. Basicity of synthetic minerals (a) and steel slags (b) before and after carbonation experiments, expressed as pH value in aqueous solution.

It can be noted from Fig. 8.11a that β– and γ–C_2S had the highest initial pH values, consistent with the pH value of fresh CaO (Fig. 8.11b), meaning that lime is the mineral phase controlling the basicity of these materials. This is also the case with BOF-be slag (Fig. 8.11b), which has a substantial amount of free lime in its innate composition (Table 8.2). Just as lime did not carbonate extensively in the incubator (Fig. 8.3b), and hence its pH essentially did not change, neither did the pH of these mineral and slag samples change in the incubator. In contrast, in the autoclave, where pure lime carbonated extensively (Fig. 8.3b), the pH of both lime and the aforementioned materials reduced significantly. The fresh pH values of the other synthetic minerals and slags were notably lower, varying in the interval 11.3–11.9 (except for srebrodolskite and CC slag, which were around 12.2–12.3). These pH values are in agreement with values predicted by Chen *et al*. (2004) for C-S-H basicity through geochemical modelling, and thus represent the basicity of the constituent alkaline silicate minerals upon hydration.

Lastly, it is interesting to note that even though pure MgO had essentially complete mineral conversion towards predominantly hydromagnesite (Fig. 8.8b), its basicity did not change significantly as a function of CO_2 uptake (Fig. S8.4). This is due to the intrinsic chemical composition of hydromagnesite, which includes two hydroxyl groups that refrains it from achieving complete carbonation into $MgCO_3$, as well as the inherently greater solubility of Mg–carbonates relative to Ca–carbonates, which contributes to maintaining the pH of hydrated Mg–carbonates around 10.2–10.8 (Visual MINTEQ).

8.4. CONCLUSIONS

This study evaluated the susceptibility towards mineral carbonation of the individual alkaline mineral phases present in steel and stainless steel slags that still require sustainable valorisation routes (namely AOD, CC and BOF slags), one of which can be the carbonation of these residues leading to the stabilization of their leaching behaviour and lowering of their basicity. The study's objective was accomplished from two perspectives. First, the individual mineral phases were synthesized via solid state sintering of stoichiometric oxide mixtures, which were utilized in mineral carbonation experiments, with the resulting material being analyzed chemically and mineralogically. Second, the steel slags themselves were likewise carbonated and analyzed, to assess and compare their behaviour against the synthetic minerals. The advantage of the first approach is the high purity of the mineral phases of interest in the materials, which were produced at > 70 wt% target mineral and < 10 wt% residual free oxides. This level of purity increases the accuracy of mineralogical analyses (QXRD by Rietveld refinement) and reduces the effect of secondary minerals on the overall carbonation behaviour (CO_2 uptake and basicity reduction), compared to the study of the steel slags themselves, which contain a multitude of co-existing reactive mineral phases present in concentrations as low as 1 wt% and no higher than 35 wt%.

In this manner it was possible to conclude that bredigite ($Ca_7Mg(SiO_4)_4$) is the most reactive individual mineral phase towards carbonation, though all mineral phases tested reacted substantially to carbonation, with some variability observed regarding carbonation conversion, carbonation kinetics and utilized carbonation methodology (between the milder CO_2 incubator carbonation and the more intense pressurized slurry autoclave carbonation). Not all results from the synthetic minerals experiments, however, were directly correlated with the steel slag results. For instance, srebrodolskite and C_2S carbonation conversions were respectively higher in autoclaved BOF slag and incubated CC slag than their corresponding synthetic mineral samples in these respective processes. Bredigite and merwinite, on the other hand, did not reach the same levels of carbonation conversion in AOD slag than in their corresponding synthetic samples. These results, among others presented in this work, make it clear that mineralogical susceptibility towards mineral carbonation is not the only determining factor controlling carbonation reactivity and CO_2 uptake capacity of steel slags. Particle morphology, in particular grain size and location of the mineral phase components, is equally important, as reactive mineral phases dispersed within less reactive phases do not have the same opportunity to react with CO_2 as if they were directly exposed to the reactive medium. The precipitation of carbonate products on particle surfaces, coupled to the consequent formation of depleted silica layers around the shrinking unreacted core, are also more likely to impede the progression of carbonation in slag particles than in pure mineral particles, as the active area of the spheroidal reactive front will be smaller in the case of the former due to the presence of unreactive species (such as iron oxides and silicates).

The QXRD technique was also applied in this study to elucidate information on the carbonate and non-carbonate phases formed after carbonation. It was found, for instance, that Mg-containing minerals (åkermanite, bredigite and merwinite) promote the formation of aragonite, while calcite forms from those minerals containing only Ca as the alkaline species. In addition, magnesian calcite formed more significantly from slags than synthetic minerals. Amorphous matter, predominantly consisting of SiO_2 as suggested by elemental mass balance, was the predominant non-carbonate product. The morphology of the $CaCO_3$ crystals and their packing density, however, was not consistent amongst polymorphs, as observed from SEM inspection; aragonite crystals formed from

bredigite had much higher aspect ratio and lower packing density than those formed from merwinite. These aspects can have implication for the access of the carbonate-containing aqueous medium to the reactive front and the consequent leaching and precipitation of alkaline species from the unreacted core; that is, the morphology of the carbonate product layer can affect carbonation progression (kinetics and terminal conversion).

Understanding the mineralogical behaviour of alkaline materials towards mineral carbonation is one more step in advancing this scientific field and in inching closer to industrial implementation of this technology. The outcome is the facilitation of the optimal development of intensified carbonation technologies that: (i) overcome existing process barriers; (ii) better meet energy and economical demands of carbon sequestration technologies; and (iii) better meet materials valorisation requirements. It also aids in the selection of the most appropriate carbonation process technology for each particular application dealing with a distinct alkaline material. Furthermore, given that alkaline residues such as slags originate from high temperature processes, where these materials are molten, it can be of interest to tune the chemical composition of the slag (by additions to the molten phase) to produce a more desirable mineralogy of the cooled material that is more susceptible towards mineral carbonation. Finally, the results of the present study can also contribute to increasing confidence in the *a priori* predictability of carbonation effects such as the CO_2 uptake capacity of the material, and the properties of the carbonated product, such as its resulting basicity and, with the aid of geochemical models, its leaching behaviour.

8.5. REFERENCES

Baciocchi, R., Costa, G., Di Bartolomeo, E., Polettini, A., Pomi, R. (2010a): Carbonation of Stainless Steel Slag as a Process for CO_2 Storage and Slag Valorization. *Waste Biomass Valor.*, **1**, 467–477.

Baciocchi, R., Costa, G., Lategano, E., Marini, C., Polettini, A., Pomi, R., Postorino, P., Rocca, S. (2010b): Accelerated carbonation of different size fractions of bottom ash from RDF incineration. *Waste Manage.*, **30**, 1310–1317.

Baciocchi, R., Costa, G., Polettini, A., Pomi, R. (2009): Influence of particle size on the carbonation of stainless steel slag for CO_2 storage. *Energy Procedia*, **1**, 4859–4866.

Baciocchi, R., Costa, G., Polettini, A., Pomi, R., (2010c): The influence of carbonation on major and trace elements leaching from various types of stainless steel slag. *in*"Proceedings of the Third International Conference on Accelerated Carbonation for Environmental and Materials Engineering", Turku, Finland, 215–226.

Berliner, R., Ball, C., West, P.B. (1997): Neutron powder diffraction investigation of model cement compounds. *Cem. Concr. Res.*, **27**, 551–575.

Brantley, S.L. & Mellott, N.P. (2000): Surface area and porosity of primary silicate minerals. *Am. Mineral.*, **85**, 1767–1783.

Bukowski, J.M. & Berger, R.L. (1979): Reactivity and strength development of CO_2 activated non-hydraulic calcium silicates. *Cem. Concr. Res.*, **9**, 57–68.

Chaurand, P., Rose, J., Briois, V., Olivi, L., Hazemann, J.-L., Proux, O., Domas, J., Bottero, J.-Y. (2007): Environmental impacts of steel slag reused in road construction: A crystallographic and molecular (XANES) approach. *J. Hazard. Mater.*, **B139**, 537–542.

Chen, J.J., Thomas, J.J., Taylor, H.F.W., Jennings, H.M. (2004): Solubility and structure of calcium silicate hydrate. *Cem. Concr. Res.*, **34**, 1499–1519.

Das, B., Prakash, S., Reddy, P.S.R., Misra, V.N. (2007): An overview of utilization of slag and sludge from steel industries. *Resour. Conserv. Recycl.*, **50**, 40–57.

Daval, D., Sissmann, O., Menguy, N., Saldi, G.D., Guyot, F., Martinez, I., Corvisier, J., Garcia, B., Machouk, I., Knauss, K.G., Hellmann, R. (2011): Influence of amorphous silica layer formation on the dissolution rate of olivine at 90 °C and elevated pCO_2. *Chem. Geol.*, **284**, 193–209.

De Paula, M. & Francisco, R.H.P. (2008): Utilização da difração de raios-X por pó na caracterização de ferritas do tipo perovskitas. *Tchê Química*, **5**, 23–30.

Doucet, F.J. (2010): Effective CO_2-specific sequestration capacity of steel slags and variability in their leaching behaviour in view of industrial mineral carbonation. *Miner. Eng.*, **23**, 262–269.

Engström, F. (2010): Mineralogical Influence on Leaching Behaviour of Steelmaking Slags - A Laboratory Investigation. *Doctoral Thesis*, Luleå University of Technology.

Goto, S., Suenaga, K., Kado, T. (1995): Calcium Silicate Carbonation Products. *J. Am. Ceram. Soc.*, **78**, 2867–2872.

Huijgen, W.J.J., Witkamp, G.-J., Comans, R.N.J. (2005): Mineral CO_2 Sequestration by Steel Slag Carbonation. *Environ. Sci. Technol.*, **39**, 9676–9682.

Ibáñez, J., Artús, L., Cuscó, R., López, A., Menéndez, E., Andrade, M.C. (2007): Hydration and carbonation of monoclinic C_2S and C_3S studied by Raman spectroscopy. *J. Raman Spectrosc.*, **38**, 61–67.

IPCC (2005): Carbon Dioxide Capture and Storage. B. Metz, O. Davidson, H. de Coninck, M. Loos, L. Meyer, eds., Cambridge University Press, Cambridge, 442 pp.

Kitano, Y., Tokuyama, A., Arakaki, T. (1979): Magnesian calcite synthesis from calcium bicarbonate solution containing magnesium and barium ions. *Geochem. J.*, **13**, 181–185.

Laursen, K. & White, T. (2003): Rietveld refinement of 2-theta split ranges – a method for reducing analysis time. *Adv. X-Ray Anal.*, **46**, 220–225.

Lim, M., Han, G.-C., Ahn, J.W., You, K.-S. (2010): Environmental Remediation and Conversion of Carbon Dioxide (CO_2) into Useful Green Products by Accelerated Carbonation Technology. *Int. J. Environ. Res. Public Health*, **7**, 203–228.

Mahieux, P.-Y., Aubert, J.-E., Cyr, M., Coutand, M., Husson, B., (2010): Quantitative mineralogical composition of complex mineral wastes – Contribution of the Rietveld method. *Waste Manage.*, **30**, 378–388.

Mirhadi, S.M., Tavangarian, F., Emadi, R. (2012): Synthesis, characterization and formation mechanism of single-phase nanostructure bredigite powder. *Mater. Sci. Eng. C*, **32**, 133–139.

Oyamada, K., Tsukidate, M., Watanabe, K., Takahashi, T., Isoo, T., Terawaki, T. (2008): A field test of porous carbonated blocks used as artificial reef in seaweed beds of Ecklonia cava. *J. Appl. Phycol.*, **20**, 863–868.

Quaghebeur, M., Nielsen, P., Laenen, B., Nguyen, E., Van Mechelen, D. (2010): Carbstone: Sustainable Valorisation Technology for Fine Grained Steel Slags and CO_2. *Refract. Worldforum*, **2**, 75–79.

Railsback, L.B. (2006): Some Fundamentals of Mineralogy and Geochemistry. http://www.gly.uga.edu/railsback/FundamentalsIndex.html (Retrieved 20.09.2012).

Rietveld, H.M. (1969): A profile refinement method for nuclear and magnetic structures. *J. Appl. Crystallogr.*, **2**, 65–71.

Saito, T., Sakai, E., Morioka, M., Otsuki, N. (2010): Carbonation of γ-Ca_2SiO_4 and the Mechanism of Vaterite Formation. *J. Adv. Concr. Technol.*, **8**, 273–280.

Santos, R.M., Ceulemans, P., Gerven, T. (2012a): Synthesis of pure aragonite by sonochemical mineral carbonation. *Chem. Eng. Res. Des.*, **90**, 715–725.

Santos, R.M., François, D., Mertens, G., Elsen, J., Gerven, T. (2012b): Ultrasound-intensified mineral carbonation. *Appl. Therm. Eng.*, doi:10.1016/j.applthermaleng.2012.03.035.

Santos, R.M., Ling, D., Sarvaramini, A., Guo, M., Elsen, J., Larachi, F., Beaudoin, G., Blanpain, B., Gerven, T. (2012c): Stabilization of basic oxygen furnace slag by hot-stage carbonation treatment. *Chem. Eng. J.*, **203**, 239–250.

Snellings, R., Machiels, L., Mertens, G., Elsen, J. (2010): Rietveld refinement strategy for quantitative phase analysis of partially amorphous zeolitized tuffaceous rocks. *Geol. Belg.*, **13**, 183–196

Steinour, H.H. (1959): Some effects of carbon dioxide on mortars and concrete—discussion. *Concrete Briefs, J. Am. Concr. Inst.*, **55**, 905–907.

Teir, S., Eloneva, S., Fogelholm, C.-J., Zevenhoven, R. (2007): Dissolution of steelmaking slags in acetic acid for precipitated calcium carbonate production. *Energy*, **32**, 528–539.

Van Bouwel, J. (2012): Intensified aqueous mineral carbonation of alkaline industrial residues for CO_2 storage and waste remediation: effect of process parameters on carbonation conversion, leaching behavior and mineralogy. *Master's Thesis*, KU Leuven.

Vandevelde E. (2010): Mineral Carbonation of Stainless Steel Slag. *Master's Thesis*, KU Leuven.

Wang, G., Emery, J. (2004): Technology of slag utilization in highway construction, *in*"Proceedings of the Annual Conference of the Transportation Association of Canada", Quebec City, Canada.

8.6. SUPPLEMENTARY MATERIAL

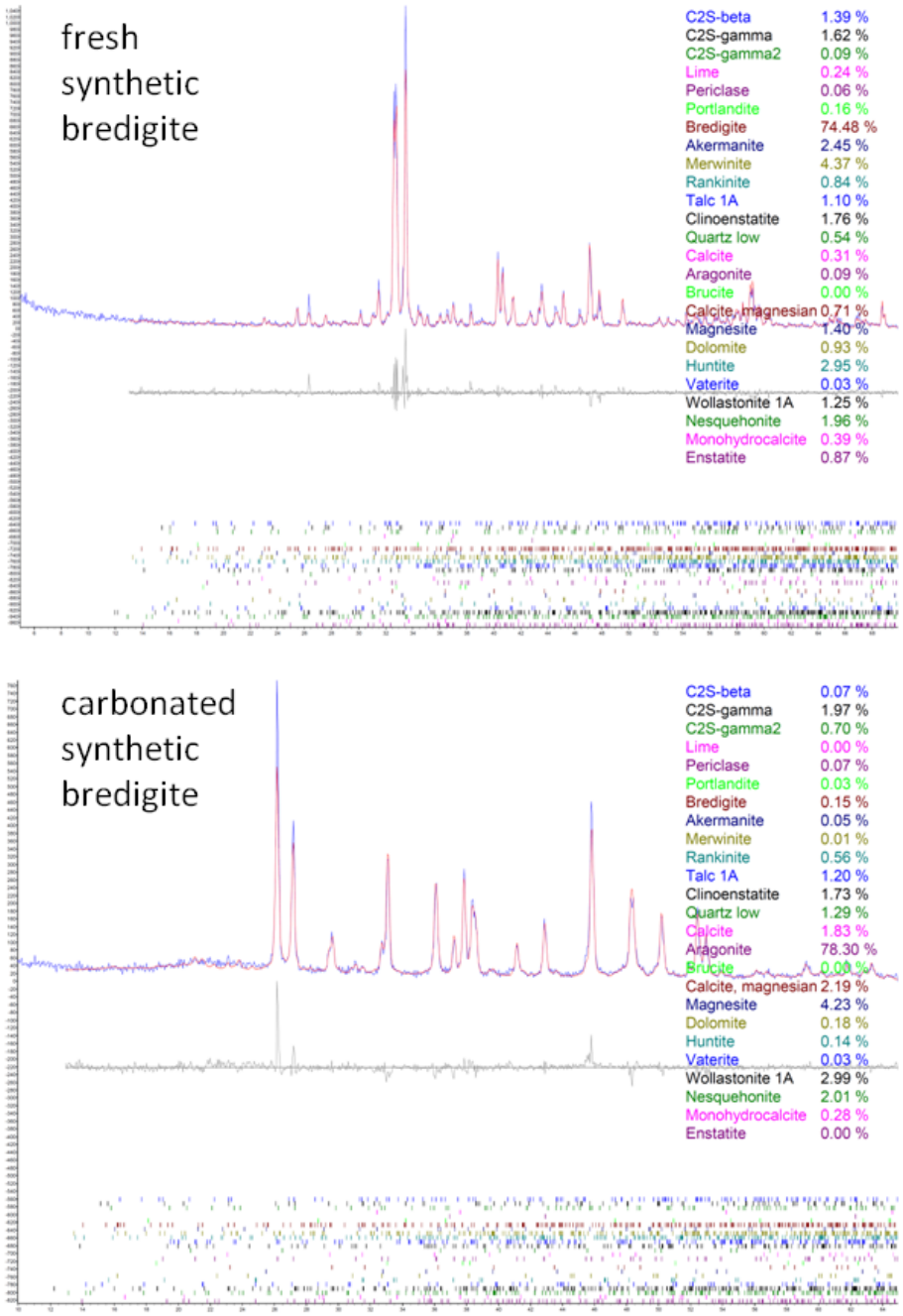

Fig. S8.1. Rietveld refinement of fresh and carbonated synthetic bredigite samples.

Table S8.1. Secondary mineral phases (excluding free oxides) of synthesized minerals, determined by QXRD, in wt%. Values for the secondary mineral phases present in greatest amounts in each synthetic sample are bolded. 'Target' and free oxide values are presented in Table 8.3 in the main text.

Secondary phases	Chemical formula	Synthetic Akermanite	Synthetic Bredigite	Synthetic Cuspidine	Synthetic β–C_2S	Synthetic γ–C_2S	Synthetic Merwinite	Synthetic Srebrodolskite
Akermanite	$Ca_2MgSi_2O_7$	target	2.7	–	–	–	8.4	–
Bredigite	$Ca_7MgSi_4O_{16}$	–	target	–	–	–	**9.0**	–
Calcium Monoferrite	$CaFe_2O_4$	–	–	–	–	–	–	**23.8**
$CaFe_3O_5$	$CaFe_3O_5$	–	–	–	–	–	–	1.0
Clinoenstatite	$Mg_2Si_2O_6$	6.5	1.0	–	–	–	–	–
Cristobalite	SiO_2	–	–	–	2.0	–	–	–
Cuspidine	$Ca_4Si_2O_7F_2$	–	–	target	–	–	–	–
β–C_2S	Ca_2SiO_4	–	1.5	2.3	target	**10.1**	–	–
γ–C_2S	Ca_2SiO_4	1.4	1.9	–	6.4	target	1.8	–
Diopside	$CaMgSi_2O_6$	**14.9**	–	–	–	–	–	–
Enstatite	$MgSiO_3$	–	1.9	–	–	–	–	–
Fluorite	CaF_2	–	–	5.4	–	–	–	–
Hematite	Fe_2O_3	–	–	–	–	–	–	2.1
Merwinite	$Ca_3MgSi_2O_8$	–	**4.8**	–	–	–	target	–
Quartz	SiO_2	2.0	–	–	–	–	2.5	–
Spurrite	$Ca_5(SiO_4)_2CO_3$	–	–	–	**6.5**	–	–	–
Srebrodolskite	$Ca_2Fe_2O_5$	–	–	–	–	–	–	target
Talc	$Mg_3Si_4O_{10}(OH)_2$	–	1.2	–	–	–	–	–
Wollastonite	$CaSiO_3$	–	1.4	**6.5**	5.1	–	2.8	–

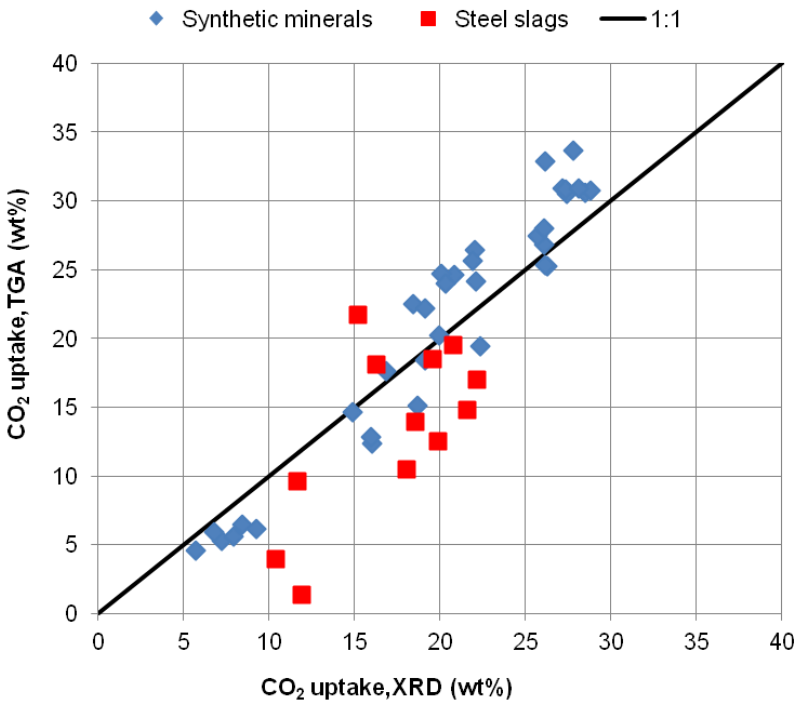

Fig. S8.2. Comparison of CO_2 uptake determination by QXRD versus TGA.

Table S8.2. Sample calculation of Rietveld refinement data handling (of hypothetical materials for simplicity purpose) to determine normalized phase composition, including amorphous content (bolded), of carbonated materials and mineral conversion values (bolded).

			(a)	(b)	(c)	(d)	(e)	(f)
		unit	β-C_2S	γ-C_2S	calcite	amorphous	CaO	Total
(1)	Fresh	wt%	50.0	50.0	0.0	0.0	0.0	100.0
(2)	Carbonated	wt	30.0	20.0	50.0	-	0.0	100.0
(3)	MW	g/mol	172.24	172.24	100.09	-	56.08	-
(4)	%Ca	wt%	46.54	46.54	40.04	-	71.47	-
(5)	%CO_2	wt%	0.00	0.00	43.96	-	0.00	-
(6)	%SiO_2	wt%	34.88	34.88	0.00	-	0.00	-
(7)	Fresh,mol	mol	0.290	0.290	-	-	-	-
(8)	Fresh,Ca	wt%	23.27	23.27	0.00	-	-	46.54
(9)	Fresh,SiO_2	wt%	17.44	17.44	0.00	-	-	34.88
(10)	Carb,Ca	wt	13.96	9.31	20.02	-	-	43.29
(11)	Carb,CO_2	wt	0.00	0.00	21.98	-	-	21.98
(12)	Carb,-CO_2	wt	-	-	-	-	-	78.02
(13)	Carb,-CO_2,Ca	wt	-	-	-	-	-	55.49
(14)	Carb,-CO_2,otherelem	wt	-	-	-	-	-	44.51
(15)	Carb,-CO_2,crystalline	wt	38.45	25.63	-	-	35.91	100.00
(16)	Carb,-CO_2,amorph	wt	-	-	-	-	-	**16.13**
(17)	Carb,cryst+amorph	wt	32.25	21.50	-	16.13	30.12	100.00
(18)	Carb,cryst+amorph,Ca	wt	15.01	10.01	-	-	21.53	46.54
(19)	Carb,cryst+amorph	mol	0.187	0.125	-	-	-	-
(20)	Conversion	%	**35%**	**57%**	-	-	-	-

Description of calculation steps:

(1) Mineral composition of fresh material (hypothetical), determined by XRD; amorphous fraction determined by internal standard methodology (20wt% Al_2O_3).

(2) Crystalline mineral composition of carbonated material (hypothetical), determined by XRD, without use of internal standard.

(3) Molecular weight of mineral phases.

(4) Percentage by mass of elemental calcium in each mineral phase.

(5) Percentage by mass of carbonate in each mineral phase.

(6) Percentage by mass of silica in each mineral phase.

(7) Mineral composition of fresh material expressed in mols; e.g. (7a) = (1a)/(3a) = 50.0/172.24 = 0.290.

(8) Crystalline calcium mass content of fresh material: individual phases (8a-c) and total (8f); e.g. (8a) = (1a)x(4a)/100 = 50.0x46.54/100 = 23.27.

(9) Crystalline silica mass content of fresh material: individual phases (9a-c) and total (9f); e.g. (9a) = (1a)x(6a)/100 = 50.0x34.88/100 = 17.44.

(10) Crystalline calcium mass content of carbonated material: individual phases (10a-c) and total (10f); e.g. (10a) = (2a)x(4a)/100 = 30.0x46.54/100 = 13.96.

(11) Crystalline carbonate mass content of carbonated material: individual phases (10a-c) and total (10f); e.g. (10c) = (2c)x(5c)/100 = 50.0x43.96/100 = 21.98; (10f) values are used to plot Fig. S8.2.

(12) Total crystalline mass content of 'carbonated material excluding crystalline carbonate': (12f) = 100-(11f) = 100-21.98 = 78.02.

(13) Crystalline calcium mass content of 'carbonated material excluding crystalline carbonate': (13f) = (10f)/(12f)x100 = 43.29/78.02x100 = 55.49.

(14) Crystalline mass content of elements other than calcium in 'carbonated material excluding crystalline carbonate': (14f) = 100-(13f) = 100-55.49 = 44.51.

(15) Crystalline mineral composition of 'carbonated material excluding crystalline carbonate': e.g. (15a) = (2a)/(12f)x100 = 30.0/78.02x100 = 38.45; note: (15c) not calculated because carbonates have been recalculated into alkaline oxides (e.g. CaO) due to removal of carbonate mass, and is therefore replaced by (15e) = ((2c)-(11f))/(12f)x100 = (50.0-21.98)/78.02x100 = 35.91.

(16) Amorphous content of 'carbonated material excluding crystalline carbonate': (16f) = 100-(8f)/(13f)x(14f)-(8f) = 100-(46.54/55.49)x44.51-46.54 = 16.13; this value can be compared directly with the amorphous content of the fresh material (1d) to calculate the g/g,initial values presented in Fig. 8.9.

(17) Normalized mineral composition of carbonated material, excluding carbonate mass and including amorphous mass: e.g. (17a) = (15a)x(1-(16f)/100) = 38.45x(1-16.13/100) = 32.25; except (17d) = (16f).

(18) Verification of calcium mass balance, individual phases (18a-e) and total (18f); e.g. (18a) = (17a)x(4a)/100 = 32.25x46.54/100 = 15.01; calcium mass balance verified, on the assumption that all calcium is crystalline, as (18f) = (8f).

(19) Mineral composition of normalized carbonated material expressed in mols; e.g. (19a) = (17a)/(3a) = 32.25/172.24 = 0.187; calculated only for alkaline (i.e. reactive) phases present in original material, and used to determine mineral conversion values.

(20) Mineral conversion of alkaline phases: e.g. (20a) = ((7a)-(19a))/(7a) = (0.290-0.187)/0.290 = 35.5%; values calculated in this manner are used to plot Fig. 8.4 and Fig. S8.3.

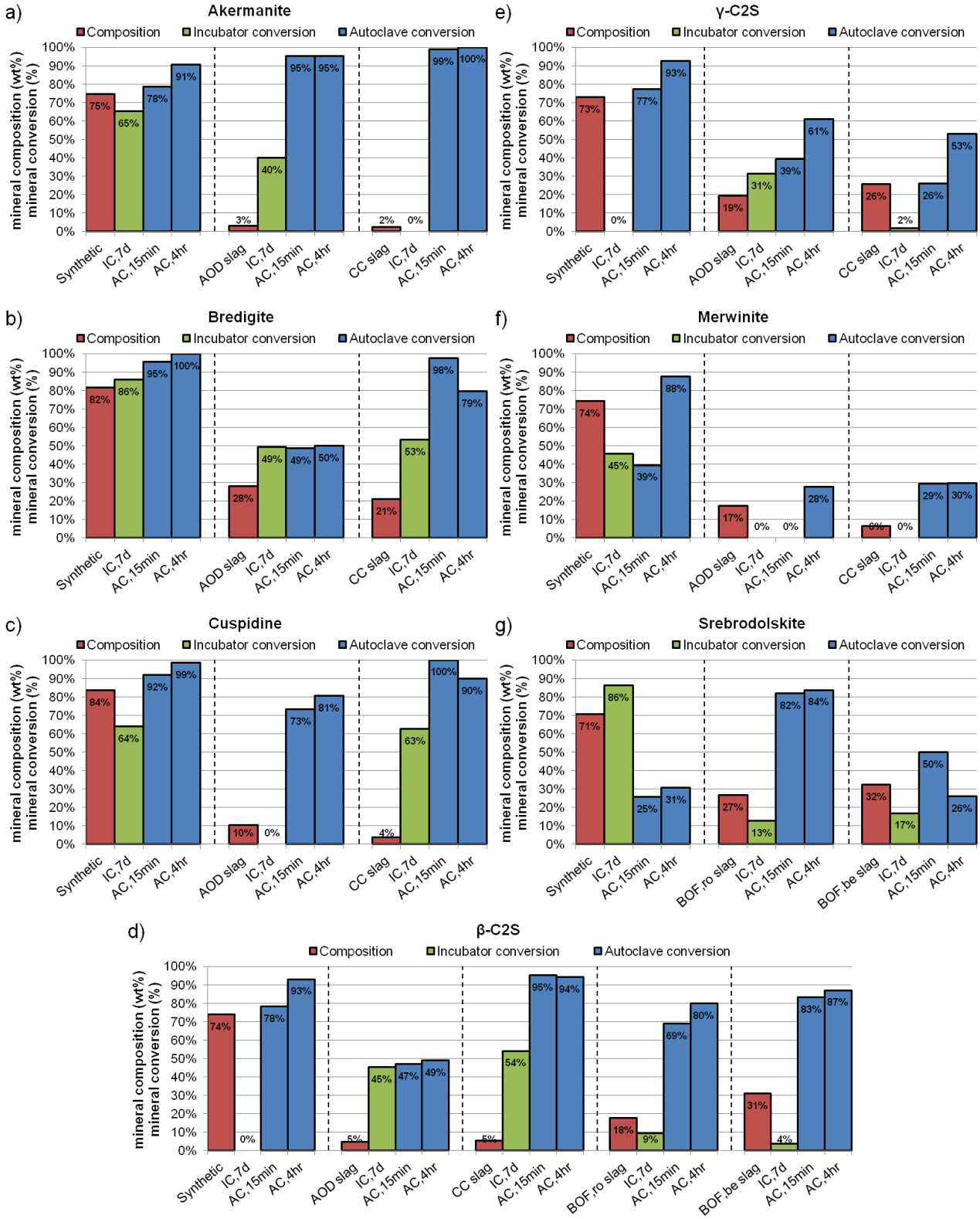

Fig. S8.3. Carbonation conversion of the seven target mineral phases of the synthetic samples and of the same mineral phases found in the steel slags, determined by QXRD.

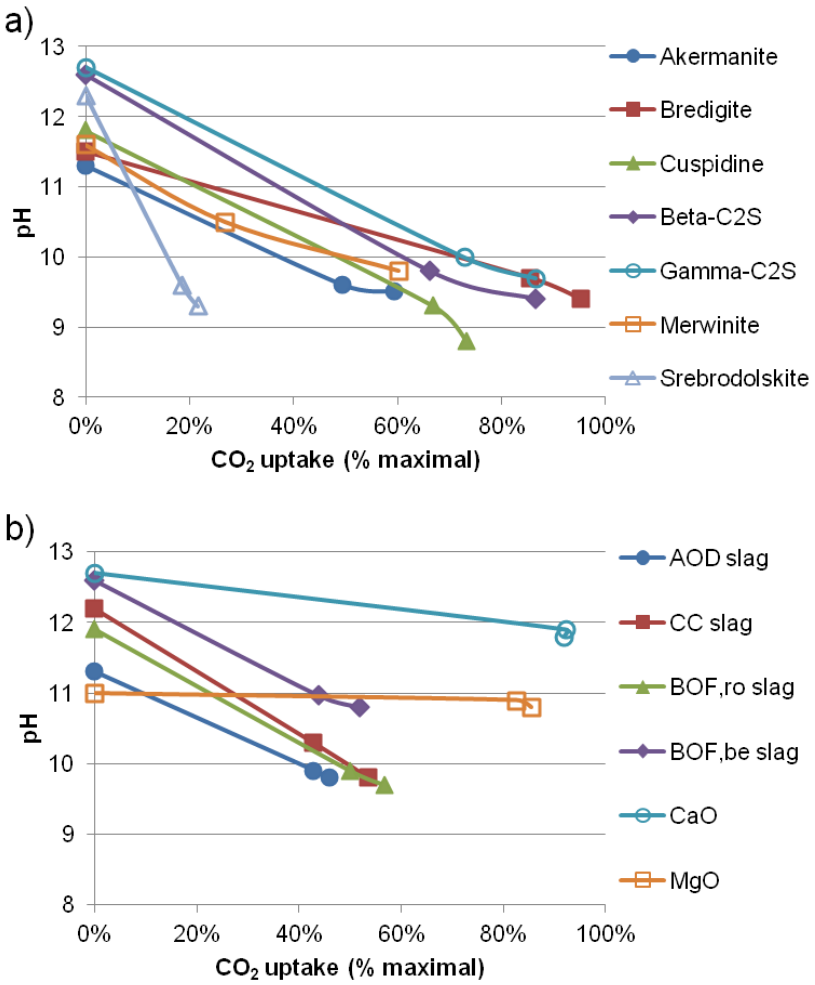

Fig. S8.4. Basicity of synthetic minerals (a) and steel slags (b) as a function of CO_2 uptake, expressed as pH value in aqueous solution.

9. Accelerated mineral carbonation of stainless steel slags for CO_2 storage and waste valorization: effect of process parameters on geochemical properties

ABSTRACT – This work explores the mineral carbonation of stainless steel slags in search for a technically and economically feasible treatment solution that steers these waste residues away from costly disposal in landfills and into valuable applications. Argon Oxygen Decarburization (AOD) and Continuous Casting (CC) slags prove ideal for mineral carbonation as their powdery morphology forgoes the need for milling and provides sufficient surface area for high reactivity towards direct aqueous carbonation. Experiments were undertaken using two methodologies: unpressurized thin-film carbonation, and pressurized slurry carbonation. The influence of process parameters (temperature, CO_2 partial pressure, time, solids loading) on the slag carbonation conversion are investigated, seeking the optimal conditions that maximize the potential of the slags as carbon sinks. It was found that CC slag carbonates more extensively than AOD slag at essentially every processing condition due to differences in particle microstructure; still, it was possible to reach up to 0.26 and 0.31 g,CO_2/g,slag uptake with AOD and CC slags, respectively, at optimal processing conditions via pressurized slurry carbonation. Mineral carbonation conversion was accompanied by significant reduction in basicity, as much as two pH units, and stabilization of heavy metals leaching, meeting regulatory limits (borderline for Cr) for safe waste materials re-use. Via quantitative mineralogical analyses, it was possible to differentiate the carbonation reactivity of several alkaline mineral phases, and to discern the preferential formation of certain Ca- and Mg-carbonates depending on the processing route and operating conditions. Slurry carbonation was found to deliver greater mineral carbonation conversion and optimal treatment homogeneity, which are required for commercial applications. However, thin-film carbonation may be a more feasible route for the utilization of slags solely as carbon sinks, particularly due to the elimination of several processing steps and reduction of energy demand.

GRAPHICAL ABSTRACT

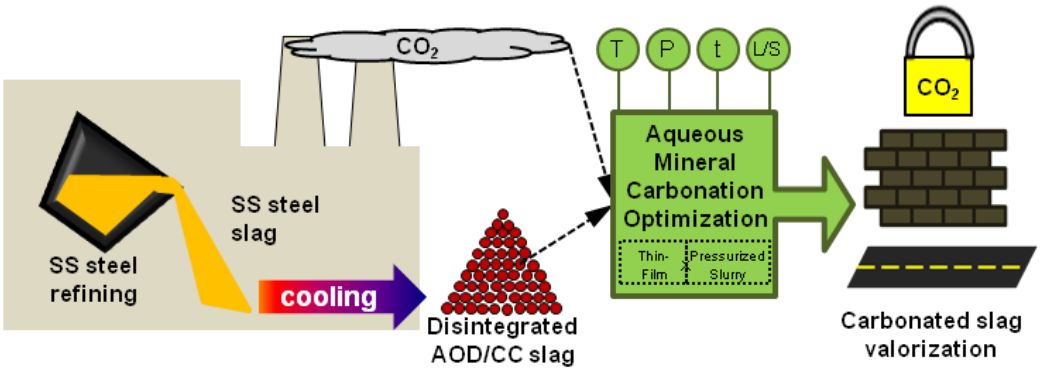

Published as
R.M. Santos, J. Van Bouwel, E. Vandevelde, G. Mertens, J. Elsen, and T. Van Gerven. "Accelerated mineral carbonation of stainless steel slags for CO_2 storage and waste valorization: effect of process parameters on geochemical properties".
International Journal of Greenhouse Gas Control 17, 2013, 32-45.

Author contributions
R.M.S. co-supervised Master's student E. Vandevelve, supervised Master's student J. Van Bouwel, performed part of the experimental and analytical work, and wrote the article.

9.1. INTRODUCTION

Mineral carbonation involves the capture of carbon dioxide in a mineral form by its reaction with alkaline materials, composed of calcium- and magnesium-rich oxides and silicates, leading to the formation of solid carbonate products (Lackner et al., 1997). The principal aims and advantages of this approach are the geochemical stability and storage safety of mineral carbonates, the opportunities for process integration presented by the technology, due to the exothermicity of the reaction, that enable energy efficiency gains, and the potential for valorisation of otherwise low-value resources (virgin or waste) into useful products. However, several barriers still limit the deployment of mineral carbonation in industry, which, apart from the lack of legislative mandates for carbon capture and a sustainable CO_2 pricing scheme, include: the high energy intensity, slow reaction kinetics and low reaction conversions of traditional processing routes; complexities of the production chain and process adaptability; and competition for attention with alternative carbon capture technologies (such as geological carbon capture and storage (CCS)). Matching the right alkaline materials with the right mineral carbonation processes is key to overcoming the barriers that prevent this technology from full-scale implementation (Santos and Van Gerven, 2011).

Steel slags, by-products of steel production processes, are a widely available class of industrial waste materials that can potentially benefit from mineral carbonation through the reduction in basicity (pH), swelling stabilization, and reduction of heavy metals leaching (Baciocchi et al., 2010; Huijgen and Comans, 2006; Santos et al., 2012b, 2012c). Moreover, their high CO_2 uptake capacities, coupled to the large on-site CO_2 emissions of steelworks, offers opportunities for carbon capture credit gains. To date, most research on single-step aqueous carbonation of steel slags have focussed on Basic Oxygen Furnace (BOF) slag, originating from the second processing step of carbon steel production and notably studied by Huijgen et al. (2005) Huijgen and Comans (2006) and Chang et al. (2011a, 2011b, 2012, 2013), and on Electric Arc Furnace (EAF) slag, originating from the first step of the stainless steel production, with results recently reported by Baciocchi et al. (2010, 2011). However, a main disadvantage to the carbonation of these residues is the milling requirement to generate sufficient reactive surface area, as these slags solidify upon cooling in the form of monoliths.

The present study focuses instead on two additional slags produced from the stainless steel process that possess powdery morphology and can benefit in a more energy efficient manner from mineral carbonation: Argon Oxygen Decarburization (AOD) slag, and Continuous Casting (CC) slag, also referred to as Ladle Metallurgy (LM) slag. These fine powders cause severe dusting issues during handling and storage in the steelworks; furthermore, the slag in this form cannot be readily re-utilized or valorised, and often must to be landfilled (Domínguez et al., 2010). Concerns regarding drainage from steel slag disposal sites, which can be extremely alkaline and a source of pollution to surface and ground waters (Mayes et al., 2008), add to the disposal costs. Treatment strategies, including the addition of stabilizing ions, silica and rapid cooling, which aim at preventing the disintegration of the slags by hindering the expansive β- to γ- transformation of dicalcium silicate (C2S), have been tested and, in some cases, implemented in industry (Durinck et al., 2008). However costly and energy intensive processes, hazardous additives (boron), and low-value final products still force the industry to search for more sustainable solutions.

Prior to the present study, we have reported in Santos et al. (2012b) findings on the carbonation of AOD and CC slags under atmospheric pressure bubbling slurry conditions, with and without the use of ultrasound for intensification of the reaction. Therein it was found that at 50 °C and for up to

4 h reaction time, sonication increased the reaction rate, achieving higher carbonation conversion and lower basicity. AOD slag Ca-conversion increased from 30% to 49%, and pH decreased from 10.6 to 10.1, while CC slag Ca-conversion increased from 61% to 73% and pH decreased from 10.8 to 9.9. The enhancement effect of ultrasound was attributed to the removal of passivating layers (precipitated calcium carbonate and depleted silica) that surround the unreacted particle core and inhibit mass transfer. However, an efficiency analysis pointed to significant challenges for scale-up of this technology, due to the high energy consumption of the ultrasound process, resulting in net negative CO_2 capture.

In search of more feasible processing conditions (technically and sustainably), this work explores two additional routes for the mineral carbonation of AOD and CC slags: (i) unpressurized thin-film carbonation, and (ii) pressurized slurry carbonation. Both methodologies are viewed as offering lower energy intensity compared to ultrasound carbonation, the former being performed under passive/mild conditions, while the latter has the potential to deliver reaction rate intensification in a more efficient manner. Herein, experiments are undertaken to investigate the influence of process parameters (temperature, CO_2 partial pressure, time, solids loading) on the slag carbonation kinetics, including CO_2 uptake and mineral conversion, seeking the optimal conditions that maximize the potential of the slags as carbon sinks. The heavy metal leaching and basicity behaviours are also evaluated to characterize the geochemical character of the carbonated materials, whose mineralogical composition, including the formed carbonate phases, are assessed and quantified.

9.2. MATERIALS AND METHODS

9.2.1. Materials characterization methodologies

The chemical composition of the slags was determined by X-ray Fluorescence (XRF) analysis, using a sequential wavelength dispersive spectrometer (PANalytical PW 2400) and SuperQ software for quantification; measurement uncertainty is approximately ± 2 units of the last significant figure reported, and verifiable detection limit is ~0.01 wt%. The volume-based particle size distributions and the average particle diameters, expressed as D[4,3] (volume moment mean diameter) and D[3,2] (surface area moment mean diameter) were determined by wet Laser Diffraction (LD, Malvern Mastersizer) in sonicated deionized water, with a measurement uncertainty of ± 5 %, determined by replicates, and detection range of 0.06–878.7 μm. The morphology of fresh and carbonated powders was observed by Scanning Electron Microscopy (SEM, Philips XL30) and inspected with Energy-dispersive X-ray Spectroscopy (EDX).

The mineralogical composition of the slags was determined by semi-quantitative X-Ray Diffraction (QXRD), adapting the methodology of Snellings et al. (2010). Measurements were performed on a Philips PW1830 equipped with a graphite monochromator and a gas proportional detector, using Cu Kα radiation at 30 mA and 45 kV, step size of 0.03° 2θ and counting time of 2 s per step, over 10–65° 2θ range. Mineral identification was done in Diffrac-Plus EVA (Bruker) and mineral quantification was performed by Rietveld refinement technique using Topas Academic v4.1 (Coelho Software). Mahieux et al. (2010) verified that QXRD of complex mineral wastes can be performed coherently and reliably, though it inherently carries a level of uncertainty. In this work the 'goodness of fit', calculated in Topas, for AOD and CC slag samples averaged to 1.45 ± 0.09 and 1.42 ± 0.13, respectively. Mineral composition and conversion values were calculated based on

the methodology detailed in our recent study reported in Bodor et al. (2013), whereby the mass fractions delivered by Rietveld analysis are translated into molar fractions normalized against the pre-carbonation mass of the materials (to discount the CO_2 uptake mass after carbonation, which artificially lowers the mass fractions of non-carbonate components) and the formation of amorphous materials during carbonation is taken into account (which, if ignored, causes overestimation of mineral mass fractions) by utilizing the calcium mass balance as a reference. This data handling procedure enhances the accuracy of mineral conversion values and allows for more precise comparison of the results, as opposed to the simple comparison of pre-carbonation composition to post-carbonation composition. Mean quantification accuracy, based on replicate analyses, has been estimated for steel slags in the present study at ± 2.3 wt% of the quantified amount.

The CO_2 uptake of carbonated materials was quantified by Thermal Gravimetric Analysis (TGA, Netzsch STA 409). An amount of ~100 mg sample was weighed in a sample pan heated from 25 to 900 °C under nitrogen flow at a heating rate of 15 °C/min. The weight loss was recorded by the TGA microbalance and the amount of CO_2 released was quantified by the weight loss between 300–800 °C. It was verified using pure Ca- and Mg-carbonates (Fig. S9.1 in the Supplementary Content) that this temperature range covers the CO_2 release region, and excludes the low temperature region where hydrates decompose. While this temperature range also overlaps with the dehydroxylation region of $Ca(OH)_2$ (~340–430 °C), the interference is assumed to be negligible due to the lack of evidence of the formation of hydroxylated products by XRD and Fourier transform-infrared (FTIR) analyses. The method reproducibility, caused by sample size and inhomogeneity and assessed by replicates, was ± 2 %. Carbonation conversion is then calculated as the ratio of CO_2 uptake experimentally determined to the theoretical CO_2 uptake capacity of the slag (given in Section 9.2.2). Loss on ignition (LOI) of fresh samples was also determined by TGA, and quantified by the weight loss between 25 and 800 °C. FTIR spectra of sample powders were recorded on a Perkin Elmer Frontier spectrometer with attenuated total reflection (ATR) accessory in the region of 4000–650 cm^{-1} at a resolution of 1 cm^{-1}.

Determination of aqueous elemental concentrations was performed by Inductively Coupled Plasma Mass Spectroscopy (ICP-MS, Thermo Electron X Series); measurement accuracy, determined using standard solutions (diluted from 1000 mg/L Merck CertiPUR elemental standards), was ± 2 %.

9.2.2. Stainless steel slags

The AOD and CC stainless steel slags were obtained from a Belgian steelworks. The materials were freshly collected from the production process, and were stored in sealed containers to avoid atmospheric weathering. It was verified by TGA that the CO_2 contents of the uncarbonated slags at the completion of the study were < 0.010 g,CO_2/g,slag. Prior to analyses or experimentation, the materials were sieved to < 500 μm particle size to remove a small portion of coarse particles (< 5 wt%). Particle size distributions, determined by LD, are presented in Fig. S9.2 in the Supplementary Content, and indicate bimodal distributions with maxima between 0.1 to 1 μm and 10 to 100 μm. AOD slag has D[4,3] = 46.1 μm and D[3,2] = 3.9 μm, and CC slag has D[4,3] = 39.3 μm and D [3,2] = 2.8 μm.

The chemical compositions of the slags, determined by XRF analysis, are presented in Table 9.1. Both slags contain high concentrations of calcium and moderate concentrations of magnesium, components which imparts these materials their alkaline properties and reactivity

towards mineral carbonation. These values are used for calculating the maximum theoretical CO_2 uptake capacities of the slags. AOD and CC slags have CO_2 uptake capacity of 0.528 and 0.520 g,CO_2/g,slag, respectively. Expressed as mass percentages, these values correspond to 34.2 and 34.6 wt%,CO_2, respectively. Trace elements detected by XRF, present in quantities of 0.1–0.01 wt%, are, in decreasing order: AOD: Sr, Nb, V, La, Cl, Zr; CC: V, K, Cl, Nb, Ni, Sr, Zn, Mo, Pb.

Table 9.1. Chemical composition of steel slags determined by XRF and expressed as elements (> 0.1 wt%) and oxides, and loss on ignition (LOI) determined by TGA.

Elements (wt%)	Al	Ca	Cr	Fe	Mg	Mn	S	Si	Ti	
AOD slag	0.74	39.2	0.52	0.17	5.4	0.32	0.24	15.2	0.24	
CC slag	0.57	35.8	3.4	1.1	6.6	0.39	0.25	12.8	0.51	
Oxides (wt%)	Al_2O_3	CaO	Cr_2O_3	Fe_2O_3	MgO	MnO	SO_3	SiO_2	TiO_2	LOI
AOD slag	1.4	54.8	0.76	0.25	9.0	0.42	0.24	32.5	0.40	0.10
CC slag	1.1	50.0	5.0	1.6	10.9	0.50	0.63	27.4	0.86	1.5

The mineralogical compositions of the slags, determined by QXRD, are presented in Table 9.2. The diffractograms of these materials are provided in Fig. S9.3 in the Supplementary Content. The main mineral phase of both AOD and CC slags is gamma-dicalcium-silicate (γ-C2S, Ca_2SiO_4), of which the latter contains significantly greater amount. AOD slag notably contains greater quantities of bredigite ($Ca_{14}Mg_2(SiO_4)_8$), cuspidine ($Ca_4Si_2O_7F_2$), β-C2S (Ca_2SiO_4),[XXVIII] and merwinite ($Ca_3Mg(SiO_4)_2$), while CC slag possesses significantly more periclase (MgO) and enstatite ($Mg_2Si_2O_6$).

[XXVIII] Remark: The greater amount of β-C2S in AOD slag suggest that this slag was cooled faster from its molten state than CC slag, since it is known that rapid cooling can stabilize the β polymorph. This is possible given that AOD slag was manually sampled by operators from the slag pot prior to boron addition, and thus it might have been quickly quenched, while CC slag was obtained from the slag yard, where cooling happens rather slowly (Pandelaers et al., ISIJ Int. 53(6) (2013) 1106–1111).

Table 9.2. Mineral composition (wt%) of stainless steel slags determined by QXRD with Rietveld refinement (three largest values bolded).

Mineral	Chemical formula	AOD slag wt%	CC slag wt%
Åkermanite	$Ca_2MgSi_2O_7$	3.3	1.8
Bredigite	$Ca_7Mg(SiO_4)_4$	**18.9**	**12.4**
Cuspidine	$Ca_4Si_2O_7F_2$	**13.9**	9.1
β-Dicalcium silicate	Ca_2SiO_4	10.2	3.9
γ-Dicalcium silicate	Ca_2SiO_4	**24.1**	**38.6**
Enstatite	$Mg_2Si_2O_6$	3.9	9.7
Fayalite	Fe_2SiO_4	0.8	1.9
Gehlenite	$Ca_2Al_2SiO_7$	1.1	0.2
Lime	CaO	0.1	0.6
Magnetite	Fe_3O_4	0.4	2.1
Merwinite	$Ca_3Mg(SiO_4)_2$	12.7	6.7
Periclase	MgO	7.4	**10.7**
Portlandite	$Ca(OH)_2$	0.4	1.4
Quartz	SiO_2	0.5	0.4
Wollastonite	$CaSiO_3$	2.4	0.4
Amorphous	-	nd	nd
Sum		100	100

nd = not detected, using internal standard (corundum) methodology of Snellings et al. (2010).

9.2.3. Thin-film carbonation methodology

Thin-film carbonation consists in reacting moist solids with a CO_2/air mixture within an incubator. The slag samples were initially wetted with ultrapure water to obtain 25 wt% moisture content: 100 g mixed with 33.3 ml H_2O. This moisture content was determined as optimal based on preliminary tests performed by Vandevelde (2010) and reported in Santos et al. (2010).[XXIX] These studies showed that it is necessary to maintain the moisture content between 10–35 wt% for the duration of the experiment to sustain the thin-film carbonation reaction, which was aided by maintaining near-saturation relative humidity. This serves to minimize sample dry-out that can occur due to the exothermic heat of reaction during carbonation, and to prevent flooding of the sample, which can hinder the diffusion of CO_2 towards the reaction front at the solid-liquid interface. Also reported were superior carbonation performances at 30 °C (versus 50 °C) and at 20 vol% CO_2 partial pressure at 1 atm total pressure (versus 10 vol%), as a result of improved CO_2 solubility under these conditions.

In the present study, the moist pastes were thinly spread on trays and placed in a CO_2–chamber (Sanyo CO_2 incubator MCO-17, pictured in Fig. S9.4 in the Supplementary Content) at 30 °C, under a CO_2 partial pressure of 0.2 atm (balance air) and ~95% relative humidity. The samples were rewetted during the experiment, at 26 h (addition of 13.3 ml H_2O, or 2/5 of initial moisture content) and at 94 h (addition of 20 ml H_2O, or 3/5 of initial moisture content). At the same time as re-wetting, samples were lightly deagglomerated using a pestle, as carbonation can lead to cementitious behaviour of the stationary material, thus decreasing powder surface area and

[XXIX] Results of Vandevelde (2010), published in Santos et al. (2010), are presented in Section 9.8.

hindering carbonation progression (Vandevelde, 2010). Intermediate samples were collected at these times and dried at 60 °C for 24 h. The remaining carbonated samples were removed from the CO_2–chamber after six days (144 h) of carbonation, and subsequently dried at 60 °C for 24 h. The weight change during drying was used to determine free moisture content of the collected samples.

9.2.4. Slurry carbonation methodology

Slurry carbonation of stainless steel slags was conducted in a Büchi Ecoclave 300 Type 3E autoclave reactor (Büchi Glas Uster AG, pictured in Fig. S9.5 in the Supplementary Content) of 1.1 litre internal volume, equipped with cyclone impeller stirrer (0 to 2000 rpm), electric-heating/water-cooling jacket, and capable of operating at pressures of 0 to 60 bar_g and temperatures of 20 to 250 ^oC. Experiments were conducted using 800 ml ultrapure water, 1000 rpm stirring speed and industrial grade (99.5 % purity) CO_2 (Praxair). Process parameters varied were: temperature (*T*, 30–180 °C), CO_2 partial pressure (*P*, 2–30 bar), reaction time (*t*, 5–120 min), and solids loading (*S*, 25–250 g/L). Parameters were varied individually, using the following median condition as a baseline: 90 °C, 6 bar,CO_2, 60 min, and 62.5 g/L. The carbonated slurry was vacuum filtered using Whatman 5 filter paper (2.5 μm nomimal pore size) and the recovered solids were oven dried at 105 °C for 4 h. Select experiments were performed in duplicate for data validation; average reproducibility of measured carbonation conversion, determined in similar manner as Huijgen and Comans (2006), was ± 2.9 % (reproducibility data is presented in Fig. S9.6 in the Supplementary Content). Geochemical modelling of aqueous carbonation equilibria was performed using Visual MINTEQ (ver. 3.0, KTH). The activity coefficients were calculated using the Davies equation, valid for the ionic strengths modelled here (< 1 M), and the gas solubilities were found to be in good agreement with the experimental and modeling data presented in Rosenqvist et al. (2012).

9.2.5. Batch leaching test methodology

Leaching tests were performed, in triplicates, on fresh and carbonated slag samples to determine the effect of carbonation on the mobility of regulated metals and on the material basicity. For each sample, an amount of 10 grams of solids was mixed with 100 ml ultrapure (18.2 MΩ·cm) water (*L/S* = 10) in a sealed PE bottle, and shaken on a vibration table (Gerhardt Laboshake) at 160 rpm and 25 °C for 24 hours. Solution pH was measured to determine basicity (± 0.1 pH units); basicity values were compared to the values of pure carbonates modelled using Visual MINTEQ. The leaching solution was filtered with 0.45 μm membrane filter prior to dilution for ICP-MS measurement; solution matrix was 0.3 M nitric acid. Elemental concentration reproducibility, based on replicates, averaged ± 15 %. Table 9.3 presents heavy metals and metalloids detected and their respective leaching limits (in milligrams metal leached per kilogram dry solid) according to Belgian Walloon regulations for secondary materials re-use in non-structural applications (Ministère de la Région Wallonne, 2001).

Table 9.3. Heavy metal leaching limits for waste material re-use in Belgium (Wallonia).

	As	Ba	Cd	Co	Cr[2]	Cu	Mo
Limit[1] (mg/kg)	1.0	N.R.	1.0	1.0	1.0	20	1.5
	Ni	Pb	Sb	Se	Ti	V	Zn
Limit[1] (mg/kg)	2.0	2.0	2.0	N.R.	20	N.R.	9.0

[1] Regulation: DIN 38414/EN 12457-4/CEN TC 292 (Ministere De La Region Wallonne, 2001)

[2] Limits prescribed for Cr(VI), whereas total Cr measured.

N.R.: not regulated.

9.3. RESULTS

9.3.1. CO_2 uptake

9.3.1.1. Thin-film carbonation CO_2 uptake

Thin-film carbonation experiments were conducted to assess the carbonation extent and the geochemical changes resulting from mineral exposure to CO_2 at mild operating conditions, in view of developing a technically and economically feasible process for industrial implementation of stainless steel slag carbonation. Results of the thin-film carbonation experiments on AOD and CC slags are presented in Fig. 9.1 in the form of thermogravimetrical curves. The mass loss upon heating is directly correlated to the decomposition of carbonates and hydrates, which occur at discrete temperature ranges, and thus can be used to estimate carbonation conversion as the ratio between actual CO_2 uptake and theoretical CO_2 uptake capacity.

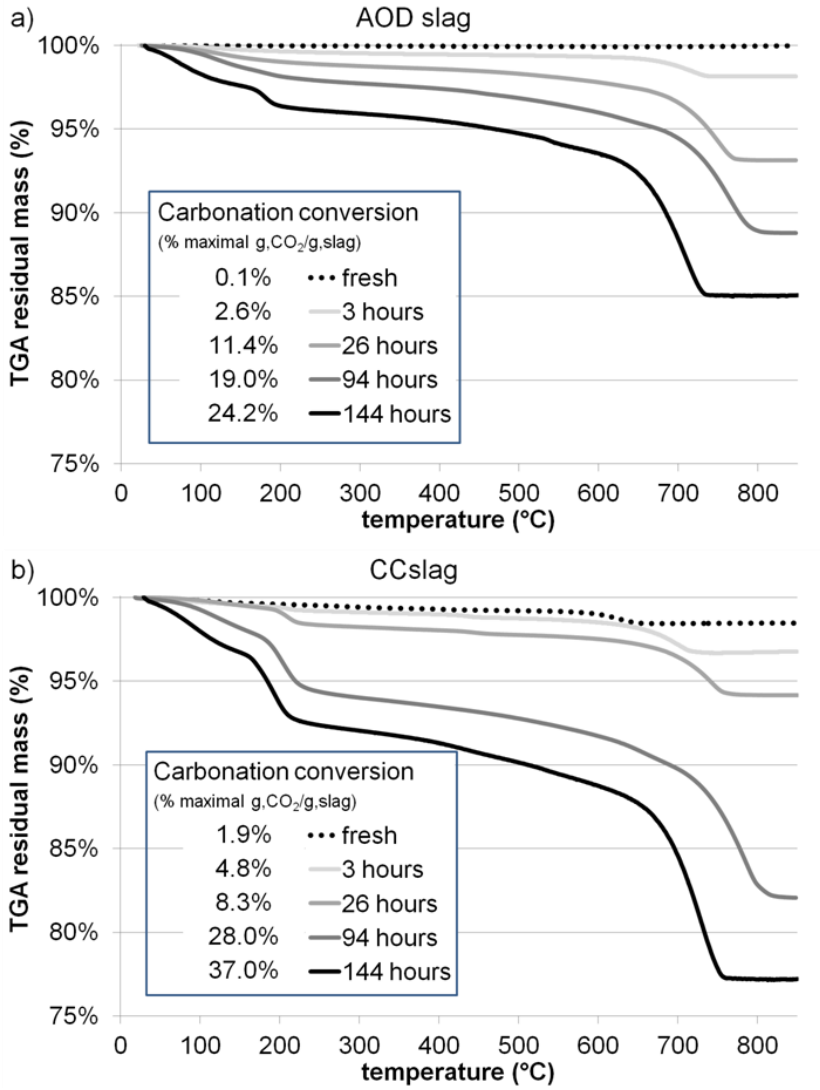

Fig. 9.1. Thin-film carbonation results: thermogravimetrical curves and carbonation conversion values for AOD (a) and CC (b) slags as a function of reaction time; $P(CO_2)$ = 0.2 atm, T = 30 °C, L/S = 25 wt%, 95% relative humidity.

Two distinct mass loss regions are observed, one below 250 °C, and another between 600–800 °C. The former can be attributed to loss of H_2O from chemically bonded water, while the latter belongs to the $CaCO_3$ decomposition reaction. Between 250–600 °C the curves display gradually declining slopes. This temperature range corresponds to a number of possible reactions, including dehydroxylation and magnesium-containing carbonate decompositions reactions, such as those indicated in Fig. S9.1 and reported by Hollingbery and Hull (2012), and the decomposition of amorphous or poorly crystalline carbonate species, reported by Cizer et al. (2012). In any case, the mass losses in this intermediary temperature range are significantly smaller than those at the comparatively high and low temperature ranges, meaning that small quantities of these species are formed.

It is observed by inspection of the trends in Fig. 9.1 that the reaction extent of CC slag is greater than that of AOD after 94 hours for all three temperature ranges, indicative of greater formation of all aforementioned species. This is quantified by the carbonation conversion values presented, where CC slag achieves 28.0 % conversion at 94 hours, compared to 19.0 % for AOD slag, and 37.0 % conversion after 144 hours, compared to 24.2 % for AOD slag. During the first 26 hours, however, the carbonation extents of both slags are comparable. This suggests that

carbonation kinetics of both slags are initially similar, just as their chemical and mineralogical compositions are also similar, but the progression of AOD slag carbonation becomes hindered earlier than in the case of CC slag.

Passivating layers composed of carbonate products, residual silica and unreactive minerals were shown in our previous study (Santos et al., 2012b) to form during mineral carbonation, restricting contact between the unreacted core and the dissolved CO_2 in the aqueous medium and thus slowing down or even stopping the reaction progress. In that study, performed using atmospheric pressure bubbling slurry conditions, carbonation conversion values (recalculated to account for the sum of Ca and Mg content of the slags) for AOD and CC slags reached plateaus at 25.8 % and 48.5 %, respectively, after four hours of reaction time (without using sonication for removal of passivating layers). The results in the present study, though reached only after extensively longer processing times, are comparable, suggesting that the reaction extent limitation mechanism may be similar. Additional thin-film carbonation processing time may still marginally increase conversion under the tested conditions, but this would be unattractive from an industrial application perspective.

In the present thin-film carbonation methodology, two additional factors can play a role in limiting reaction progression: (i) sample moisture, and (ii) cementitious behavior of the sample paste. The exothermic heat of the carbonation reactions partially evaporates water from the sample paste over time. Water can also be consumed in the carbonation reactions through the formation of hydrated mineral phases (e.g. calcium silicate hydrate (CSH), monohydrocalcite ($CaCO_3 \cdot H_2O$), hydromagnesite ($Mg_5(CO_3)_4(OH)_2 \cdot 4H_2O$), nesquehonite ($MgCO_3 \cdot 3H_2O$), etc.). Insufficient moisture can significantly reduce or even cease the rate of reaction (Vandevelde, 2010). Table 9.4 presents the moisture content of the slags as a function of time. The moisture content of CC slag drops significantly more than that of AOD slag. Between the 3 and 26 hour samplings, the moisture content of CC slag is reduced by 9.1 wt%, versus 4.3 wt% for AOD slag. At the 94 hour sampling, despite prior re-wetting, CC slag moisture is only 3.8 wt%, while AOD slag moisture is stabilized near 18 wt%. At the 144 hour sampling the moisture content of CC slag is again much lower than that of AOD slag, despite prior re-wetting at the 94 hour mark. Lowering of CC slag moisture content, however, does not appear to significantly hinder reactivity towards carbonation, as it achieves greater carbonation extent than AOD slag (as previously shown in Fig. 9.1). In fact, the moisture loss can be proportionally related to carbonation conversion, as well as to the formation of hydrated phases suggested by the mass loss measured by TGA at temperatures below 250 °C.

Table 9.4. Thin-film carbonation results: sample moisture (wt%) as a function of reaction time.

	AOD slag wt%	CC slag wt%
Initial	25.0	25.0
3 hours	22.1	23.2
26 hours[1]	17.8	14.1
26 hours re-wetted	25.9	22.9
94 hours[2]	17.6	3.8
94 hours re-wetted	29.3	19.3
144 hours	19.3	6.7

[1] Subsequently re-wetted with additional 2/5 of initial moisture content.

[2] Subsequently re-wetted with additional 3/5 of initial moisture content.

In terms of cementitious behavior, both slags presented hardening during carbonation. This phenomenon is caused by aggregation of precipitating carbonate crystals that bond individual particles and form a solid matrix. This behavior has led to the investigation of using stainless steel slags as binders in construction materials applications (Kriskova et al., 2012). However, for carbonation purposes, this behavior can potentially lead to reduced paste porosity and permeability, and thus hinder carbonation progression. Comparatively, as assessed during deagglomeration of the material by mortar and pestle during re-wetting, CC slag hardened more and continued to harden after each sampling, while AOD slag hardening decreased as a function of time. Therefore, it does not appear that the cementitious behavior is the principle reason for the inferior carbonation performance of AOD slag. Cizer et al. (2012) propose that the evaporation of water decreases the pore water content and allows better diffusion of gaseous CO_2 into the bulk volume of lime paste through the open paths formed along the sample depth, thus aiding carbonation progression. Additional possibilities for lower AOD slag reactivity are particle morphology and microstructure, and its mineralogical composition, which are assessed in Section 9.3.2.

9.3.1.2. Slurry carbonation CO_2 uptake

Slurry carbonation experiments were conducted to assess the carbonation extent and the geochemical changes resulting from mineral exposure to CO_2 at a range of process conditions, seeking to intensify the mineral carbonation reaction and thus achieve greater CO_2 uptake and carbonation conversion than the previously tested methods. Slurry carbonation also has the benefit, versus thin-film carbonation, of improved mass transfer and enhanced particle attrition, due to continuous mixing of the solids in suspension. Fig. 9.2 shows the results of the slurry carbonation experiments on AOD and CC slags, where the effect of four process variables (T, $P(CO_2)$, t, and S) on the carbonation conversion (expressed as percentage of the maximal CO_2 uptake), determined by TGA, is presented.

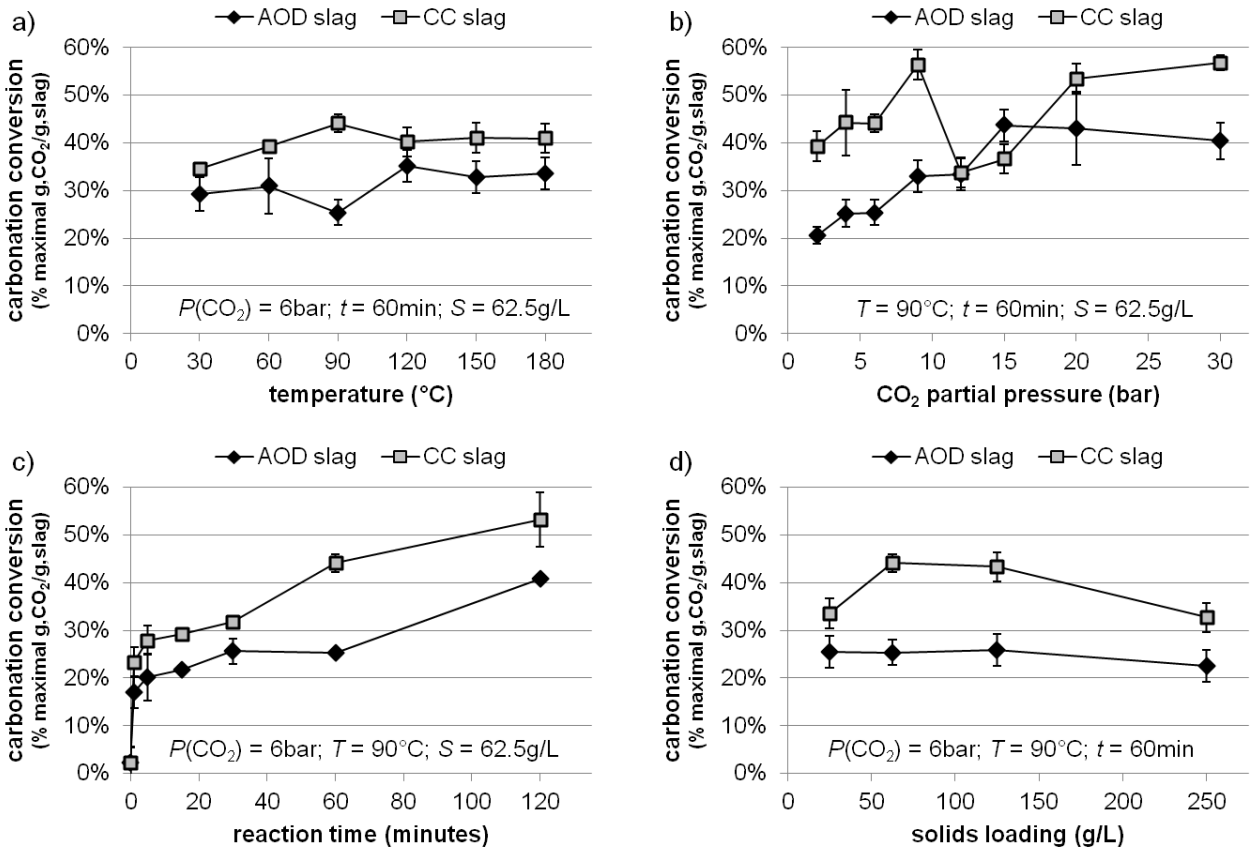

Fig. 9.2. Slurry carbonation results: effect of temperature (a), CO_2 partial pressure (b), reaction time (c) and solids loading (d) on the carbonation conversion of AOD and CC slags; error bars reflect reproducibility data presented in Fig. S9.6 in the Supplementary Content).

Under nearly all conditions tested, CC slag carbonation conversion surpassed that of AOD slag when exposed to identical process parameters, in agreement with previously tested methodologies. This reaffirms that slag mineralogy, morphology and microstructure are the likely causes for this discrepancy; more details on this investigation are given in Section 9.3.2. The effect of temperature on carbonation conversion of both slags appears to be small (Fig. 9.2a). However, it should be noted that experiments with temperatures above 100 °C required additional cooling time prior to depressurization, up to 60 minutes in the case of 180 °C. Since CO_2 remained in the reactor during cooling, carbonation reaction likely continued over time, and also at different temperatures until reaching 100 °C, when the reactor was opened. This may explain why the negative effect of high temperatures, namely reducing CO_2 solubility (depicted in Fig. 9.3), is not seen. Still, in the case of CC slag, carbonation conversion did not surpass those achieved at 90 °C and below, while in the case of AOD, slight improvement is seen, particularly comparing results at 90 °C and 120 °C. As the cooling time at 120 °C was only in the order of five minutes, the moderately higher temperature appears to have contributed to its carbonation conversion, though no further benefit is seen from higher temperature experiments. It should also be noted that this series of experiments was conducted using 6 bar,CO_2; the influence of temperature under different baseline partial pressures may differ. For instance, at lower pressures the CO_2 solubility is more significantly affected by temperature than at higher pressures (Fig. 9.3).

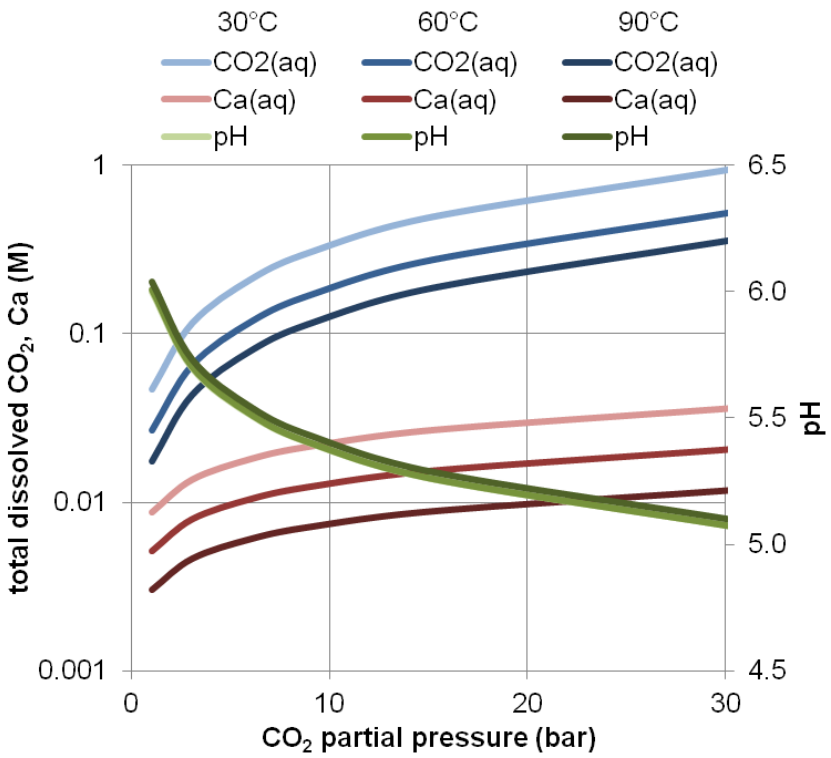

Fig. 9.3. Geochemical modeling of $CO_2/CaCO_3/H_2O$ equilibrium: effects of temperature and CO_2 partial pressure on total dissolved species and pH.

The CO_2 partial pressure resulted in more significant changes in carbonation conversion (Fig. 9.2b). Up to 9 bar, both slags responded well to increased pressure, displaying conversion improvements in the order of 15 %. After this point, CC slag displayed a peculiar reduction in conversion in the order of 20 %, which only recovered to previous levels at 20 bar; this trend was absent from AOD slag results. As such, maximal CC slag conversion occurred both at 9 and 30 bar, while AOD slag conversion peaked at 15 bar. Mechanistically, increased CO_2 pressure results in greater CO_2 solubility, but also in lower solution pH (Fig. 9.3), due to the formation and dissociation of carbonic acid. The complex equilibria result in increased $CaCO_3$ solubility at higher pressures, but even at 30 bar and 30 °C total dissolved Ca remains below 1.5 g/L (Fig. 9.3). This explains why increased pressure is not detrimental to carbonation conversion.

Prolonged reaction time proportionally increased carbonation conversion of both slags (Fig. 9.2c). Carbonation reactivity was found to be very fast; within one minute of carbonation time, conversion of AOD and CC slags reached 17.1 % and 23.3 %, respectively. Thereafter carbonation conversion continued to increase in approximately linear fashion up to 120 minutes. During the first 30 minutes the conversion difference between AOD and CC slags remained around 7 %, and widened to 12 % after 120 minutes. The slopes of the curves suggest that additional reaction time may further increase conversion, but that they would unlikely surpass roughly 50 and 60 % for AOD and CC slags, respectively. The values at 120 minutes, however, are similar to maximal conversion obtained in our previous study (Santos et al., 2012b) when using sonication. Hence the increased temperature, pressure and better mixing of the present study serve as efficient alternatives for the intensification of the mineral carbonation reaction compared to the energy intensive sonication applied at milder process conditions. On the other hand, sonication of the slurry at present intensified conditions could serve to speed reaction conversion, particularly after the 15

minute mark when diffusion through the passivating layers, pictured in Fig. 9.4, becomes rate limiting.

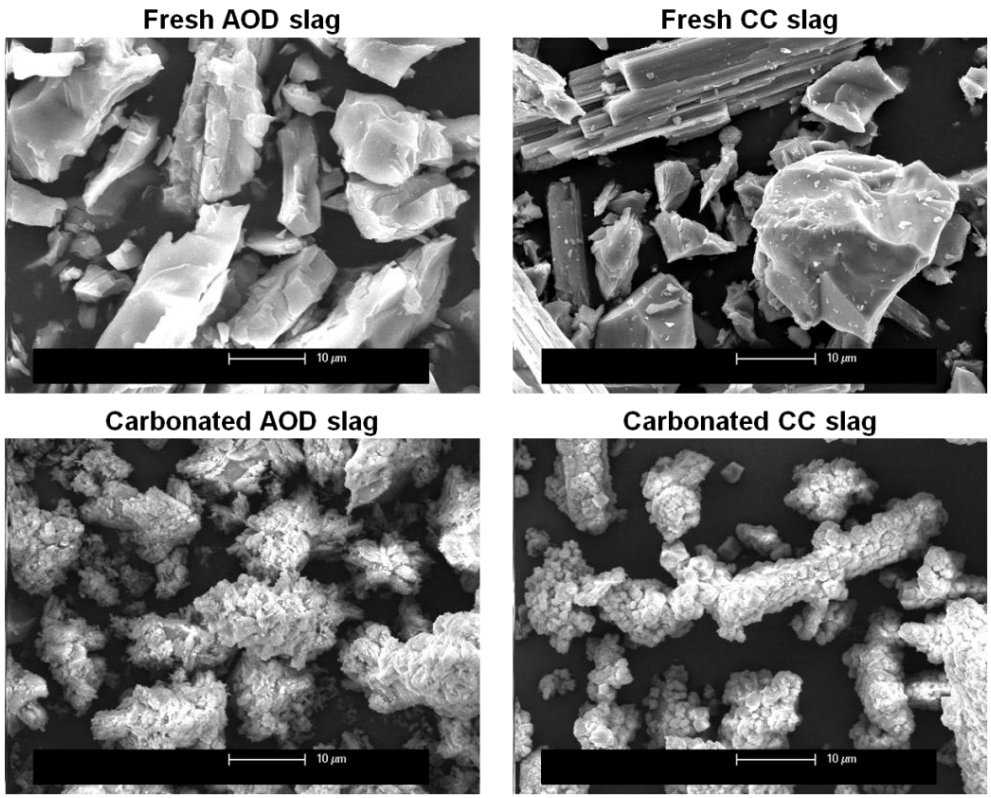

Fig. 9.4. Fresh and carbonated (120 minutes) slag particle morphology.

The last parameter changed during slurry carbonation was solids loading (Fig. 9.2d). It is not expected that solids loading should have a significant effect on carbonation conversion due to exhaustion of dissolved CO_2, especially at prolonged reaction times. Rather, solids loading can affect the rate and intensity of interparticle collisions, and the mixing efficiency. CC slag results suggest that diminished particle interaction, and consequently surface erosion, limits carbonation conversion. This effect, however, is not seen in the case of AOD slag. At high solids loading both slags exhibit a drop-off in carbonation conversion, which can be due to poorer mixing of the dense slurry, and consequently lower mass transfer rates as well as reduced particle collisions. This effect is also greater in the case of CC slag. The mild effect of solids loading on carbonation conversion bodes well for scale-up of this technology, as industrial implementation can benefit from the decreased reactor volume required for the treatment of dense slurries. Furthermore, better mixer, reactor geometry and baffle configuration designs can likely extend the carbonation conversion drop-off to higher solids loadings. To conclude, it can be said that the maximum achievable CO_2 uptake capacities of AOD and CC slags, assuming 50 % and 60 % maximal conversions, are 0.264 and 0.312 g,CO_2/g,slag (or 20.9 and 23.8 wt%), respectively.

9.3.2. Mineralogy

Stainless steel slags consist of a mixture of mineral phases, including several varieties of alkaline silicates (e.g. bredigite, cuspidine, β- and γ-dicalcium silicates (C_2S), and merwinite) and (hydr)oxides (e.g. brucite, lime, periclase and portlandite). It is likely that these different minerals

have different carbonation affinities and kinetics. Doucet (2010) showed that even in 0.5 M HNO_3, only 70–90% of Ca and 40–80% of Mg are leached from finely milled BOF and EAF slags. Moreover, different phases may respond differently to changes in mineral carbonation process conditions (i.e. temperature and pressure). Such behaviors may help explain why the maximal achievable carbonation conversions presented in the previous section are significantly lower than the theoretical capacities.

Additionally, the morphological configuration of the mineral phases can affect the exposure of different minerals to the reacting aqueous medium. Fig. 9.4 suggests that individual particles of fresh CC slag are primarily composed of specific minerals, as they display clear morphological differences (more images provided in Fig. S9.7 in the Supplementary Content). Inspection of individual particles by EDX (presented in Fig. S9.8 in the Supplementary Content) demonstrated that rod shaped particles consist of calcium silicate (recent studies by our group on pure synthetic minerals, reported in Bodor et al. (2013), confirmed such crystalline morphology belonging to γ-C_2S). The chemical composition of particles of apparent smooth surface corresponded well to periclase, while two chemistries of coarse particles were observed, correlating well with β-C_2S and calcium-magnesium silicates. AOD slag particles do not possess discernible morphological features, and EDX analysis did not distinguish particular mineral chemistries. It thus appears that the crystallization of these two slags upon cooling differs, either due to slight differences in chemical composition or due to differences in the cooling paths they undergo in the production process (e.g. quenching rates).

Carbonated slag samples were analyzed by QXRD to elucidate the behavior of the major alkaline mineral phases towards mineral carbonation. Time-dependent results of thin-film and slurry carbonation samples are presented in Figs. 9.5 and 9.6, respectively. Pressure- and temperature-dependent results of slurry carbonation samples can be found, respectively, in Figs. S9.9 and S9.10 in the Supplementary Content. Despite using the QXRD data handling procedure of Bodor et al. (2013) to enhance the accuracy of conversion values and allow for more precise comparison of the results, as opposed to the simple comparison of pre-carbonation composition to post-carbonation composition, the semi-quantitative nature of the Rietveld analysis of complex mineral samples is reflected in the magnitude of the error bars, which are intuitively larger for phases present in smaller quantities in the slags.

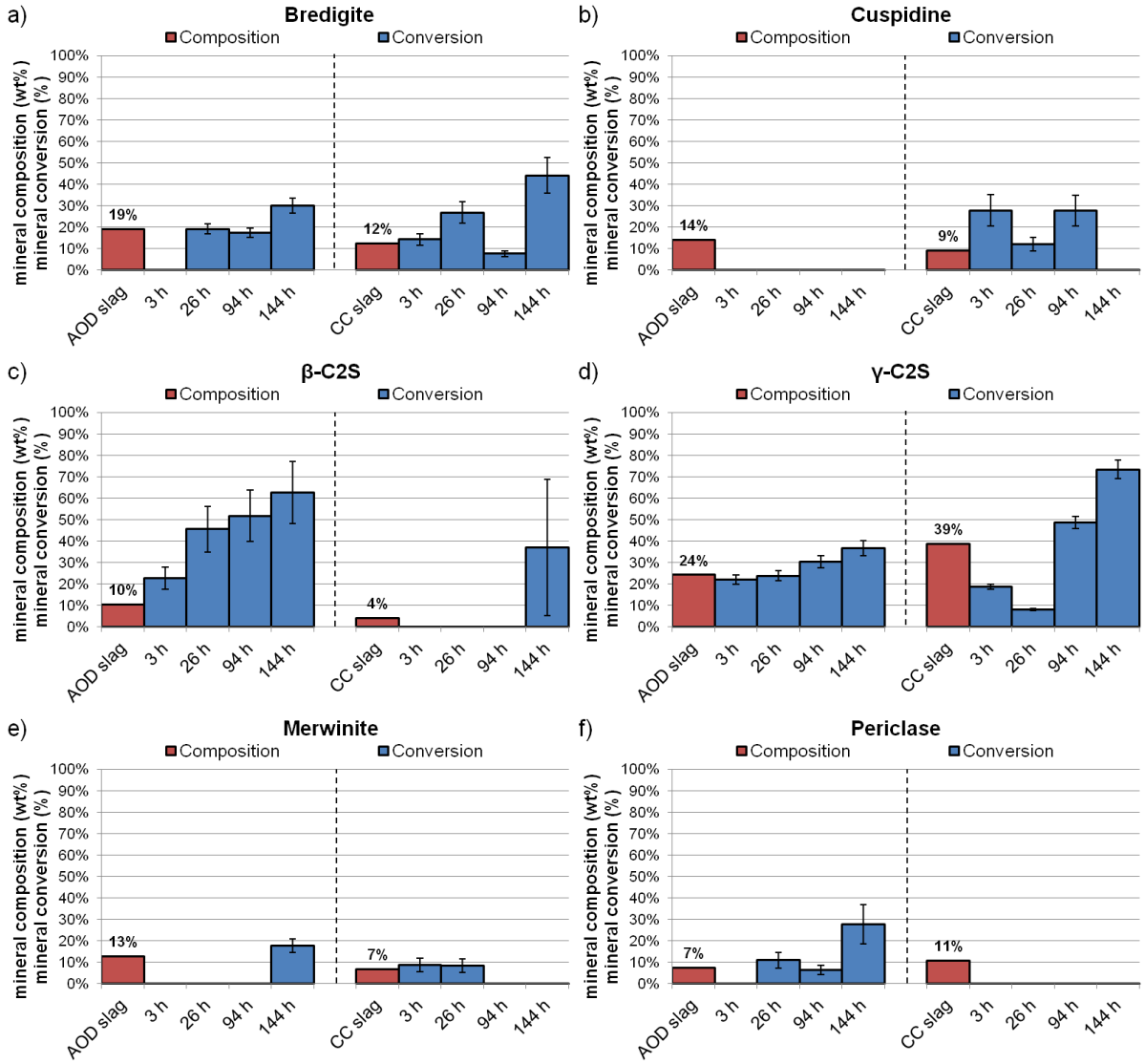

Fig. 9.5. Thin-film carbonation results: carbonation conversion of slag mineral phases (bredigite (a), cuspidine (b), β-C2S (c), γ-C2S (d), merwinite (e) and periclase (f)) as a function of reaction time; $P(CO_2)$ = 0.2 atm, T = 30 °C, L/S = 25 wt%, 95% relative humidity; error bars represent mean quantification accuracy, based on select replicate analyses, of ± 2.3 wt% of the quantified amount.

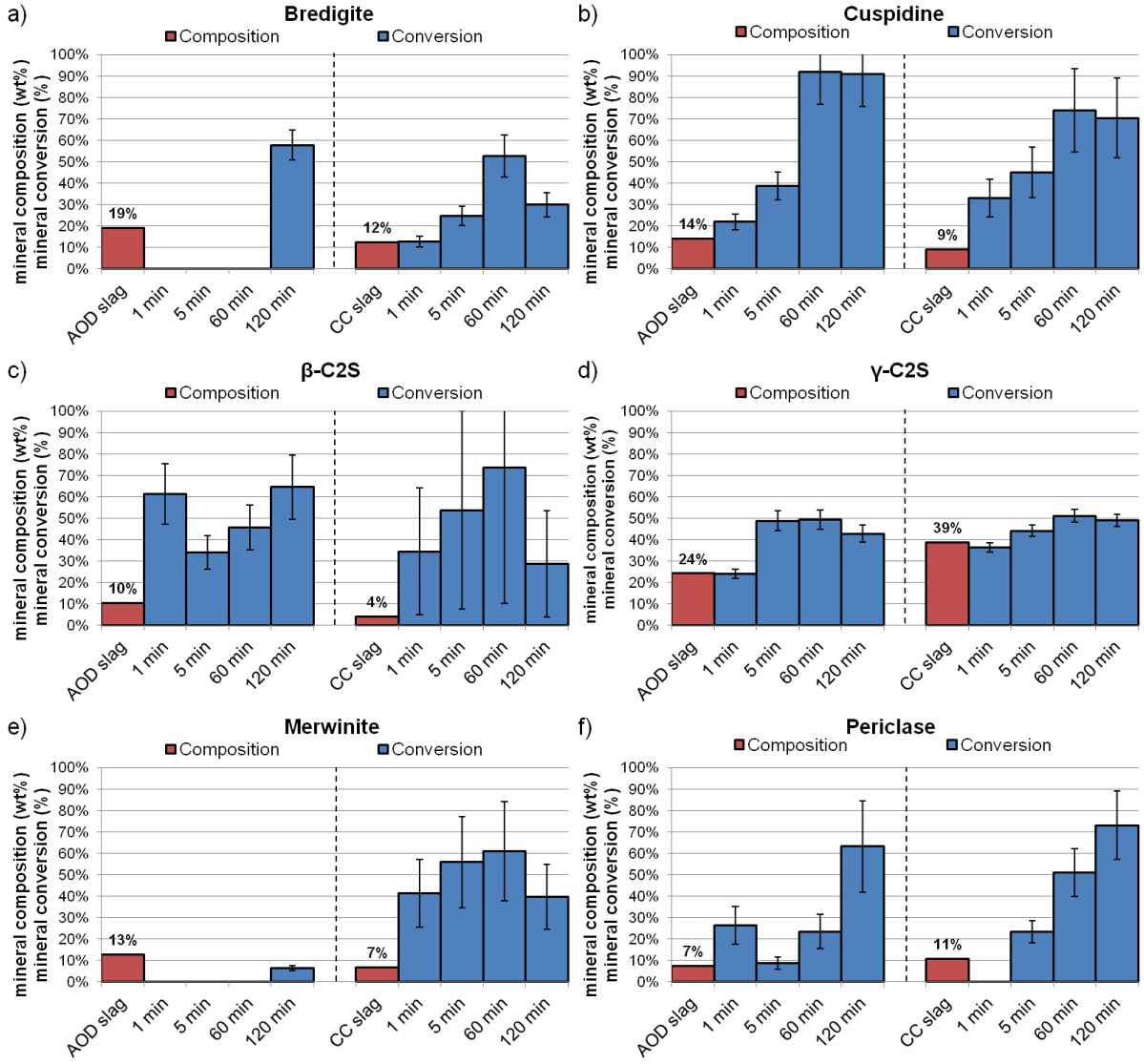

Fig. 9.6. Slurry carbonation results: carbonation conversion of slag mineral phases (bredigite (a), cuspidine (b), β-C2S (c), γ-C2S (d), merwinite (e) and periclase (f)) as a function of reaction time; $P(CO_2)$ = 6 bar, T = 90 °C, S = 62.5 g/L; error bars represent mean quantification accuracy, based on select replicate analyses, of ± 2.3 wt% of the quantified amount.

It is observed in Fig. 9.5 that the carbonation conversion of C2S polymorphs dominates the CO_2 uptake of both slags during thin-film carbonation. Bredigite conversion also reaches significant values, contributing well to AOD slag CO_2 uptake given its large content. Cuspidine, merwinite and periclase reactivities are comparatively poor in both slags; some low extent observed conversions of these minerals may be due to quantification variability caused by diffraction peak overlap, reducing confidence in these trends. It appears that the better carbonation conversion of γ-C2S in CC slag over AOD slag, and the greater content of this mineral phase in CC slag over AOD slag, largely accounts for the higher CO_2 uptake achieved by CC slag over the prolonged thin-film carbonation reaction times.

Mineral conversion is generally significantly improved in slurry carbonation, as observed in Fig. 9.6. Partial carbonation conversion is observed for nearly all reported phases in both slags. The conversion of β-C2S and γ-C2S appears to occur and stabilize faster, while the carbonation conversions of bredigite, cuspidine and periclase generally improve over time. The latter two phases were poorly reactive in thin-film carbonation; hence benefit most from the increased intensity of

slurry carbonation. Merwinite appears to react well in CC slag, but remained essentially unconverted in AOD slag; though uncertainty in the CC slag composition value (7 wt%) could contribute to overestimation of its conversion in this slag. It is otherwise difficult to identify mineralogical reasons for the better CO_2 uptake of CC slag over AOD slag, as quantification uncertainties can mask the differences of concurrently converting minerals.

Mineral conversion values as a function of temperature (see Fig. S9.9) did not display particularly conclusive trends, with the exception of improved γ-C2S carbonation from AOD slag at higher temperatures. As the overall CO_2 uptake values of these samples were quite similar (as previously presented in Fig. 9.2a), it can be said that temperature does not appear to promote the reactivity of any particular phase (at 6 bar CO_2 partial pressure). Carbonation pressure had a more noticeable effect on AOD slag mineralogy (see Fig. S9.10), with meaningful improvements in β-C2S, merwinite and periclase conversions at higher pressures. The noticeably lower CO_2 uptakes of CC slag at 12-15 bar (Fig. 9.2b), however, appear to be related to decreased reactivity of these same mineral phases under these intermediary conditions.

It was also possible to utilize QXRD analysis to assess the formation of different carbonate mineral phases. Time-dependent results of thin-film and slurry carbonation samples are presented in Fig. 9.7; pressure- and temperature-dependent results of slurry carbonation samples can be found in Fig. S9.11 in the Supplementary Content. A total of ten different carbonate phases were detected, ranging from pure Ca-carbonates (namely calcite ($CaCO_3$), aragonite ($CaCO_3$), vaterite ($CaCO_3$) and monohydrocalcite ($CaCO_3 \cdot H_2O$)), to Ca-Mg-carbonates (magnesian calcite ($Ca_{1-0.85}Mg_{0-0.15}CO_3$), dolomite ($CaMg(CO_3)_2$) and huntite ($Mg_3Ca(CO_3)_4$)), to pure Mg-carbonates (magnesite ($MgCO_3$), nesquehonite ($MgCO_3 \cdot 3H_2O$) and hydromagnesite ($Mg_5(CO_3)_4(OH)_2 \cdot 4H_2O$)).

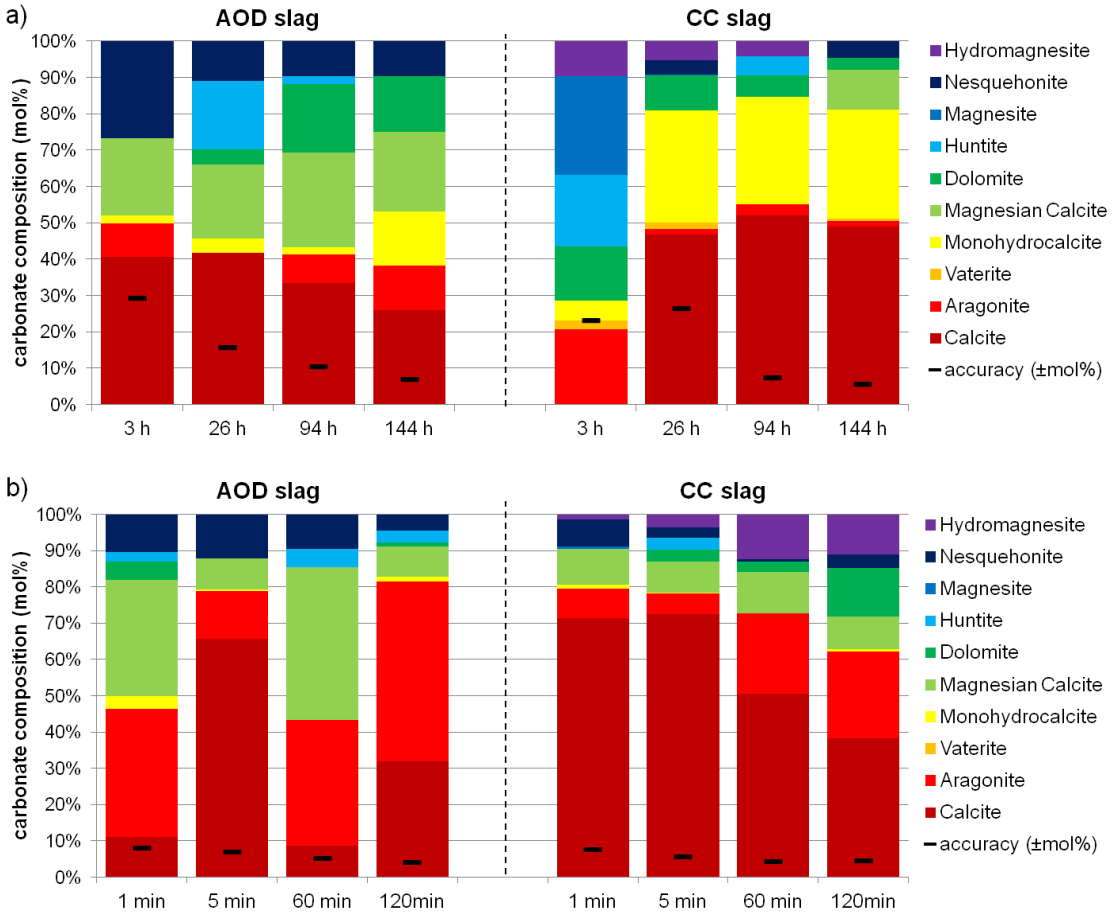

Fig. 9.7. Composition of carbonate mineral phases (normalized to 100 % of carbonate content) for thin-film carbonation (a) and slurry carbonation (b) as a function of reaction time; error bars represent mean quantification accuracy, based on select replicate analyses, of ± 2.3 wt% of the quantified amount.

Calcium-containing carbonates were the predominant products after carbonation, given the high calcium content of the slags. Calcite is generally the most common mineral variety, followed by aragonite and monohydrocalcite; no significant amount of vaterite was detected. Aragonite formation predominates in slurry carbonated samples, especially those treated to higher temperatures (see Fig. S9.11); its formation is known to be promoted under elevated temperatures (≥ 70 °C) and in the presence of Mg-ions (Santos et al., 2012a). Conversely, monohydrocalcite was observed almost exclusively in thin-film carbonated samples, where the milder process conditions, higher reaction pH and/or slower reaction kinetics may aid in its stability. Nishiyama et al. (2013) found a positive correlation between higher reacting solution pH and preferential formation of monohydrocalcite over anhydrous $CaCO_3$. In fact, the basicity of CC slag is higher than that of AOD slag (more details in Section 9.3.3), which may explain the greater monohydrocalcite content found in thin-film carbonated CC slags (Fig. 9.7a). In addition, Fukushi et al. (2011) have shown that monohydrocalcite is an intermediate product in the transition of amorphous calcium carbonate to stable calcite or aragonite. This may explain its time-dependent behavior, as it appears to form after prolonged periods (≥ 26 h) in the CO_2 chamber.

Substantial amounts of Ca-Mg-carbonates also form, especially magnesian calcite, followed by the more Mg-rich dolomite. Furthermore, their presence seems to occur in samples that contain less calcite and aragonite. This suggests that under certain conditions the Mg-ions that inhibit calcite

growth and promote aragonite formation become trapped in the forming crystal, and as the Mg substitution in the $CaCO_3$ matrix creates strains on the crystalline structure that increase its solubility (Railsback, 2006), mineralogical evolution towards magnesian calcite takes place. Carbonated slag samples that contain more magnesian calcite also tend to contain greater quantities of other Mg-containing carbonates, although there is no clear trend with regards to time, temperature or pressure dependency. Nesquehonite and hydromagnesite are the predominant Mg-carbonates formed, both in thin-film and slurry carbonation. However, nesquehonite is more commonly found in AOD slag samples, while hydromagnesite is almost exclusively seen in CC slag samples. Zhang et al. (2006) suggest that hydromagnesite is preferentially formed over nesquehonite at higher pH; the higher basicity of CC slag compared to AOD slag (discussed in Section 9.3.3) may explain this difference in Mg-carbonate mineralogy. Huntite and magnesite, though detected, are usually quantified under the margin of error attributed to each sample based on QXRD uncertainty (plotted on each figure). The preferential formation of hydrated Mg–carbonates over the anhydrous magnesite is explained by the large ionic potential of Mg, which promotes hydration in solution (Railsback, 2006).

9.3.3. Heavy metal leaching

Mineral carbonation of stainless steel slags not only serves to capture CO_2, but is also beneficial to improving geochemical properties of the material, thus helping to meet safe disposal or re-utilization requirements (Baciocchi et al., 2010; Huijgen and Comans, 2006; Santos et al., 2012c). Leaching tests were used to observe the effect of carbonation on the basicity of the solid samples, expressed by pH value in water, and on the heavy metals leached from these solids into solution. Carbonation can have an effect on these parameters due to three phenomena. Firstly, calcium and magnesium hydroxides, originating from the hydration of free oxides or silicates, convert to carbonates. The pH value of pure $Ca(OH)_2$ in solution is 12.4 at 25^oC (predicted by geochemical modelling); likewise the pH of $CaCO_3$ in solution is 8.2–9.9 (depending on CO_2 saturation in solution). As a result, it is expected that fully carbonated slags exhibit lower basicity. Secondly, the formation of a carbonate layer blocks access of inner unreacted alkaline minerals to the solution. This can also contribute to a gradual pH reduction as a function of carbonation progression (Santos et al., 2012b). Lastly, the conversion of some metal (hydr)oxides to metal carbonates changes the solubility of these metals (e.g. $BaCO_3$, $PbCO_3$, $ZnCO_3$ (Fernández-Bertos et al., 2004)).

Fig. 9.8 confirms the aforementioned hypotheses. Data of slurry carbonation performed at different times, temperatures and CO_2 partial pressures are plotted together to illustrate the trend as a function of CO_2 uptake. Thin-film carbonation data correspond to samples collected at varying treatment times. Samples with greater CO_2 uptake, and thus higher carbonation conversion, exhibited lower pH. Particularly, the greater reaction extents obtained by slurry carbonation resulted in better basicity improvement compared to thin-film carbonation. It was possible to reduce the pH of AOD/CC slags from 11.7/12.3 to as low as 9.4/9.7 after slurry carbonation, compared to 10.9/10.8 for the longest duration of thin-film carbonation. Compared to our previous study (Santos et al., 2012b), performed under atmospheric pressure bubbling slurry conditions and yielding maximal basicity reductions to pH of 9.9/10.1, the pH values from pressurized slurry carbonation have been improved due to greater carbonation conversions, entering the range of $CaCO_3$ basicity control. Basicity reduction as a function of CO_2 uptake progresses approximately linearly. It is

likely that pH is initially controlled by silicate hydrates (above pH 11 (Chen et al., 2004)), followed by hydrated carbonates (below pH 10.8, assessed by geochemical modelling), and finally by $CaCO_3$ polymorphs below pH 10. It is also notable that AOD slag basicity is lower than that of CC slag initially, and remains so for comparable levels of CO_2 uptake. This may be due to, other than mineralogical differences, greater exposure of the slag's different alkaline minerals (which have different solubilities and reactivities towards hydration and carbonation) to the aqueous medium, given the observed differences in particle morphology (Fig. 9.4 and Fig. S9.7). As carbonate precipitation is accelerated at high pH, the differing slag basicities, potentially buffering the carbonating medium to slightly different pH levels, could play a role in the greater CO_2 uptakes achieved by CC slag at comparable pH values (as inferred on Fig. 9.8).

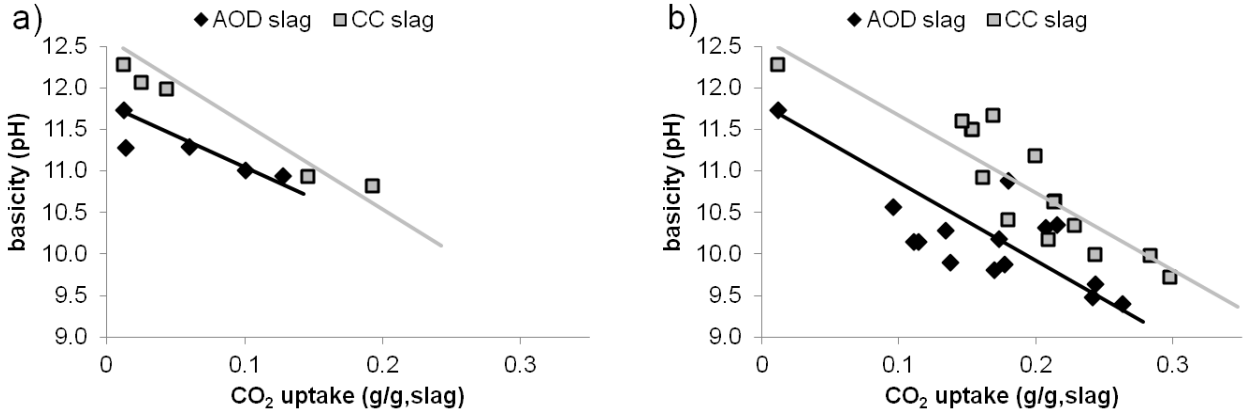

Fig. 9.8. Basicity of stainless steel slag samples from thin-film carbonation (a) and slurry carbonation (b) as a function of CO_2 uptake.

The heavy metal leaching values of the solutions for which pH was measured are presented in Fig. 9.9 for slurry carbonation, and in Fig. S9.12 in the Supplementary Content for thin-film carbonation. The heavy metals measured correspond to those presented in Table 9.3, eleven of which are currently regulated in Wallonia (Belgium) for materials re-use. The concentrations of As in all solutions were below the detection limit of ICP-MS, and are therefore not reported. Horizontal dashed lines in the figures indicate the regulatory limits of respective elements; where no line is seen, the limit is greater than all measured values and the plotted y-axis scale. Accordingly, only four elements present significant leaching risk: Cr, Mo, Pb and Zn.

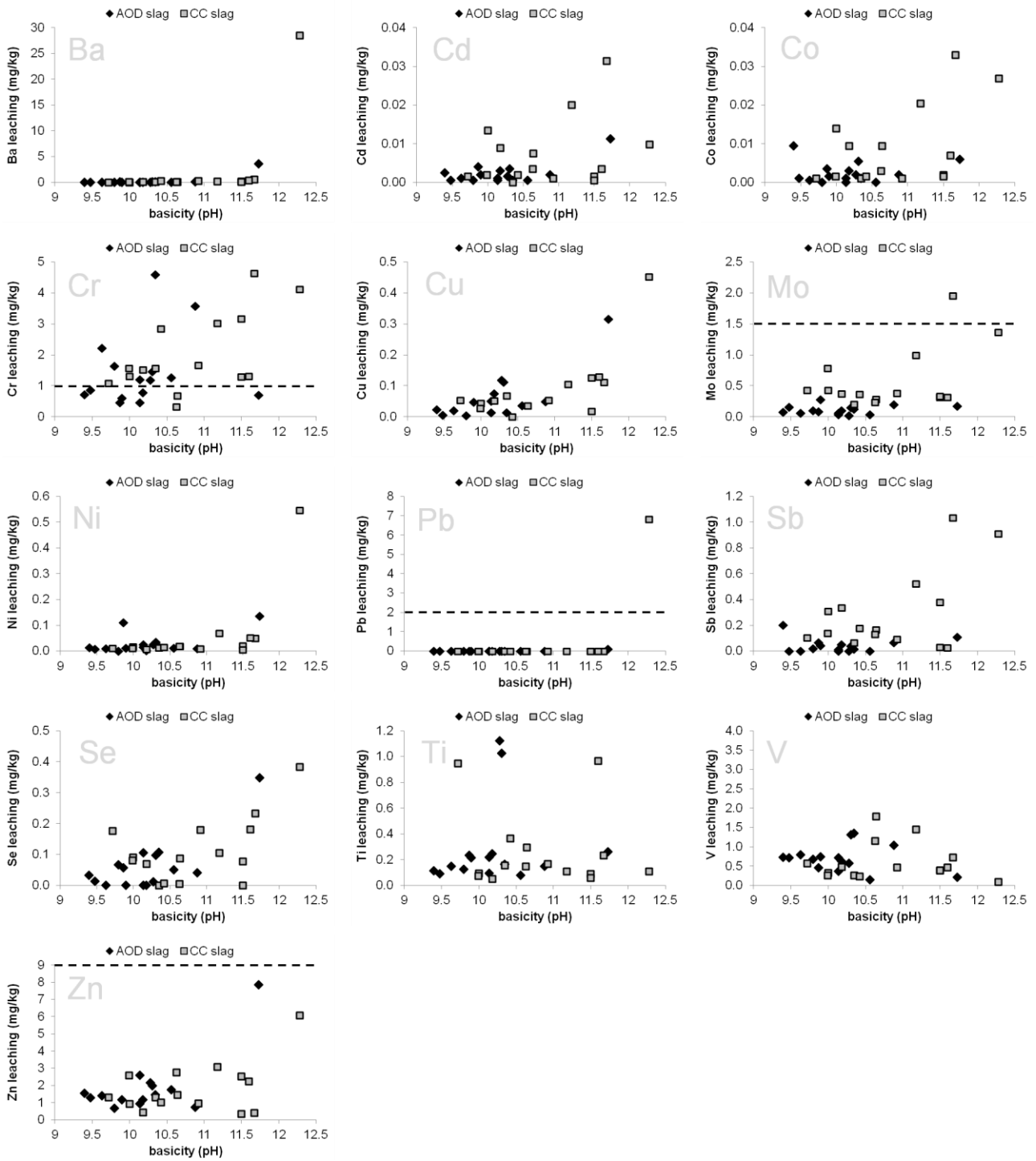

Fig. 9.9. Slurry carbonation results: leaching of heavy metals from stainless steel slags as a function of pH. Horizontal dashed lines indicate Belgian (Wallonia) regulatory limits; where no line is seen, the limit is greater than the y-axis shown.

The rightmost data point of each data series on the graphs, at the highest pH, corresponds to the fresh slag; all other points are carbonated samples. Fresh AOD slag does not exceed any limit, though it comes close for Cr and Zn. Fresh CC slag exceeds limits for Cr and Pb, and approaches those for Mo and Zn. Carbonation successfully decreases leaching of Mo, Pb and Zn, where slurry carbonated samples (Fig. 9.9) generally fall farther below leaching limits than thin-film carbonated samples (Fig. S9.12). Results for Pb and Zn meet the expectations based on the review of Fernández-Bertos et al. (2004). It was reported in Santos et al. (2012c) that Mo leaching increased

slightly after direct hot-stage carbonation of BOF slag. Cornelis et al. (2008) suggests that Mo leaching can slightly increase, remain constant or decrease as the pH lowers, depending on the speciation of Mo. Decreased Mo leaching is attributed in that study to the formation of $PbMoO_4$. As CC slag contains more Pb than AOD and BOF slags, it is possible that this mechanism explains the observed behavior from slurry carbonated samples.

In the case of Cr, the heavy metal present by far in greatest quantities in the slags (Table 9.1), some samples fall or remain under the limit while others remain or go above (leaching from fresh CC slag being higher than from AOD slag). Nevertheless, there appears to be some convergence to low leaching values once the sample pH reaches ~10 or lower; accordingly, this only occurs for the better carbonated slurry samples. The variability in Cr leaching could have its roots in the array of uptake mechanisms described by Fernández-Bertos et al. (2004). They report the possibility of Cr associating with calcium silicate hydrate (CSH) as a silicon substitute at higher pH values; but this mineral phase can undergo solubilisation at lower pH, re-releasing Cr. At lower pH values still, calcite and neoformed double metal salts can take up Cr and again reduce leaching. Cornelis et al. (2008) geochemically modelled several Cr-containing species that may be responsible for its pH-dependent behavior, the three of which most likely participate being: $Ca_2Cr_2O_5 \cdot 6H_2O$ (i.e. substituted CSH), $Cr(OH)_3$, and $PbCrO_4$. While carbonation-induced reduction of Cr leaching appears to be mild, if not debatable, Van Gerven et al. (2005) showed that Cr-containing untreated bottom ashes brought to the same lower pH as carbonated ashes, by acidification, show much higher Cr leaching, meaning that Cr speciation in carbonated samples at least offers a buffer that hinders drastic solubilisation.

It is also possible to make some useful observations from the leaching results of the nine remaining heavy metals that do not pose a threat to exceeding regulatory limits. Positive correlations of leaching reduction with carbonation extent can be made for Ba, Cd, Co*, Cu, Ni*, Sb* and Se. The starred elements correspond to those for which improvement was substantial only in slurry carbonation. Leaching of Ti was generally low compared to the regulatory limit, even for the highest outliers. Leaching of V increased by roughly one order of magnitude compared to fresh sample values, with greater increase observed from thin-film carbonated samples (Fig. S9.12). Leaching of V is not currently regulated, but if its future leaching value is similar to those of other currently regulated metalloids (i.e. 1–2 mg/kg), its leaching could become a concern. Still, the risk of V leaching from stainless steel slags appears to be milder than from BOF slag, where carbonation induced solubilisation can reach upwards of 10 mg/kg (Santos et al., 2012c).

It should also be noted that the encapsulating carbonate layer that forms during aqueous carbonation (Fig. 9.4) is not observed in direct hot-stage carbonation. This passivating layer, though detrimental for carbonation reaction progression, may play an important role in limiting heavy metal leaching by reducing exposure of the unreacted or unreactive phases in the particle core to the aqueous medium. The good homogeneity of slurry carbonation may explain beyond its better CO_2 uptake the reason for its generally superior leaching performance compared to thin-film carbonation. This can be particularly ascribed to the V leaching behavior from thin-film carbonated slags (Fig. S9.12), where the lower pH of the overall sample may exacerbate V leaching from some less carbonated particles.

9.4. DISCUSSION

The slags herein tested (freshly produced AOD slag absent of boron additives, and as-produced CC slag) proved ideal for mineral carbonation as their powdery morphology forgoes the need for costly milling (required for EAF and BOF slag carbonation) and provides sufficient surface area to impart high reactivity towards direct aqueous carbonation. The stainless steel slags were also verified to capture more CO_2 than BOF slag as reported by Huijgen et al. (2005) and EAF slag as reported by Baciocchi et al. (2011); it was possible to reach 21–24 wt%,CO_2 with AOD and CC slags compared to reported maxima of ~15 wt%,CO_2 with finely milled BOF and EAF slags.

It was also made apparent that high temperatures and pressures are not required for extensive carbonation of AOD and CC slags, which can have a positive impact on processing costs recently reported in literature. Kelly et al. (2011) assumed 35.5 bar, 200 ^{o}C, and no heat recovery, to model a carbonation process based on the data of Huijgen et al. (2005), and concluded that the energy penalty is too high. On the contrary, slurry carbonation makes it possible to harvest the exothermic heat generated by the carbonation reaction (Santos et al., 2013), and present results show that 90 °C and 9 bar,CO_2 suffice for rapid reaction. Even milder conditions can be used to further reduce processing costs, if necessary, with small loss of CO_2 uptake if well optimized.

Mineral carbonation conversion was accompanied by significant reduction in basicity, as much as two pH units after slurry carbonation. The stabilization of heavy metals leaching was also assessed. It was shown that these slags do not pose significant leaching risks compared to Belgian (Wallonia) regulatory limits for waste materials re-use, and that carbonation serves to further reduce the leaching of most heavy metals, especially with slurry carbonation. The only metal that approached limiting values was Cr, which is present in significant quantities in the slags and thus warrants observation as to its behavior, although several carbonated samples remained below the limit. Durinck et al. (2008) reviewed several methods by which Cr can be better stabilized through alterations to the hot-stage molten slag and its cooling trajectory. The recovery of Cr, a valuable metal, from stainless steel slags could also circumvent this issue, and is being investigated (Adamczyk et al., 2010).

Slurry carbonation was found to deliver greater mineral carbonation conversion and optimal treatment homogeneity, which are required to achieve high levels of CO_2 uptake, basicity reduction and heavy metal stabilization. However, these features are only required when the carbonated product is to be valorized beyond a carbon sink, for example as soil conditioner (pH control), as fine aggregate (sand substitute) in construction materials (e.g. concrete) or as mineral filler in chemical products (e.g. paints). In this manner, valorization applications can potentially afford the additional processing costs associated with slurry carbonation. However, as Zingaretti et al. (2013) correctly suggest, thin-film carbonation may be a more feasible route for the utilization of slags as carbon sinks, particularly due to the elimination of CO_2 separation and compression and of liquid-solid separation, and the reduction of heating and mixing demands. Prolonged treatment times (herein reported as long as 6 days under stationary conditions with intermittent de-agglomeration and re-wetting) may be reduced if the carbonating paste is more often de-agglomerated (to counter cementitious behavior) and re-wetted (to maintain required moisture content), for example with the application of a rotary drum as proposed by Zingaretti et al. (2013). In addition, the aforementioned valorization options envision direct use of the carbonated slags in commercial applications; however industrial symbiosis (Brent et al., 2012) and inter-industry solid residue utilization as blended materials (Mäkelä et al., 2012) should also be explored, as they can open new valorization

routes, enable better energy/exergy efficiencies, and potentially diminish material property requirements commonly associated with commercial reagents and products.

The present study also elucidated the mineralogical response of the stainless steel slags towards carbonation by applying Rietveld refinement for the quantification of the mineral phases in the fresh and carbonated samples. Although the quantification uncertainty of this technique for complex mineral samples including slags does not allow for precise measurement of carbonation kinetics, it was possible to qualitatively differentiate mineral phases that react more substantially than others over time, to observe noticeable differences in reactivity at varying process conditions (*T* and *P*), and to discern the preferential formation of certain Ca- and Mg-carbonates (mainly calcite, aragonite, magnesian calcite, monohydrocalcite, nesquehonite and hydromagnesite) depending on the processing route and operating conditions.

In a recent work of our research group, reported in Bodor et al. (2013), it was assessed if the carbonation conversion limitations could be attributable to differences in the susceptibility towards carbonation of individual alkaline mineral phases present in steel and stainless steel slags. To this end, seven high-purity minerals were synthesized by solid-state sintering and carbonated individually. The results suggest that mineralogical susceptibility towards carbonation is not the only determining factor controlling carbonation reactivity and CO_2 uptake. Particle morphology, in particular grain size and location of the mineral phase components, appears to be equally important, as reactive mineral phases dispersed within less reactive phases do not have the same opportunity to react with CO_2 as if they were directly exposed to the reactive medium. Such distinctions may also affect basicity and pH buffering levels, which can potentially influence carbonation rate and conversion.

These points can be related to the fact that CC slag clearly carbonated more extensively than AOD slag at essentially every processing condition, despite the two slags having very similar chemical compositions and sharing essentially the same mineral phases, though in differing proportions. Unequal cooling trajectories during slag production may be responsible for controlling particle microstructure. In a way this is inopportune, as substantially more AOD slag is produced during steelmaking. On the other hand, it suggests that AOD slag mineralogy and particle morphology should be tuned to resemble more closely that of CC slag, either via chemical/mineral additions to the hot-stage molten slag, or via precise control of the slag cooling path (i.e. the quenching rate). Durinck et al. (2008) describe this as 'slag engineering', by which the links between process parameters, slag microstructure and product properties are leveraged to turn secondary materials into tailored resources.

9.5. CONCLUSION

The metallurgical industry is in need of novel valorization routes to steer slags away from traditional storage in landfills and into valuable applications. At the same time, the technological field of mineral carbonation is in need of a process that is economical and scalable, to serve as a platform for its dissemination and uptake by several industrial activities that can benefit from it but are still skeptical of its merit. The results herein presented are promising for the valorization of carbonated AOD and CC stainless steel slags as secondary raw materials, or at least for their utilization solely as carbon sinks, while at the same time reducing their disposal costs and environmental impact.

9.6. REFERENCES

Adamczyk, B., Brenneis, R., Adam, C., Mudersbach, D., 2010. Recovery of Chromium from AOD-Converter Slags. Steel Research International 81, 1078–1083.

Baciocchi, R., Costa, G., Di Bartolomeo, E., Polettini, A., Pomi, R., 2010. Carbonation of Stainless Steel Slag as a Process for CO_2 Storage and Slag Valorization. Waste and Biomass Valorization 1, 467–477.

Baciocchi, R., Costa, G., Di Bartolomeo, E., Polettini, A., Pomi, R., 2011. Wet versus slurry carbonation of EAF steel slag. Greenhouse Gases: Science and Technology 1, 312–319.

Bodor, M., Santos, R.M., Kriskova, L., Elsen, J., Vlad, M., Van Gerven, T., 2013. Susceptibility of mineral phases of steel slags towards mineral carbonation: mineralogical, morphological and chemical assessment. European Journal of Mineralogy, in press, http://dx.doi.org/10.1127/0935-1221/2013/0025-2300.

Brent, G.F., Allen, D.J., Eichler, B.R., Petrie, J.G., Mann, J.P., Haynes, B.S., 2012. Mineral Carbonation as the Core of an Industrial Symbiosis for Energy-Intensive Minerals Conversion. Journal of Industrial Ecology 16, 94–104.

Chang, E.-E., Chen., C.-H., Chen, Y.-H., Pan, S.-Y., Chiang, P.-C., 2011a. Performance evaluation for carbonation of steel-making slags in a slurry reactor. Journal of Hazardous Materials 186, 558–564.

Chang, E.-E., Chiu, A.-C., Pan, S.-Y., Chen, Y.-H., Tan, C.-S., Chiang, P.-C., 2013. Carbonation of basic oxygen furnace slag with metalworking wastewater in a slurry reactor. International Journal of Greenhouse Gas Control 12, 382–389.

Chang, E.-E., Pan, S.-Y., Chen, Y.-H., Chu, H.-W., Wang, C.-F., Chiang, P.-C., 2011b. CO_2 sequestration by carbonation of steelmaking slags in an autoclave reactor. Journal of Hazardous Materials 195, 107–114.

Chang, E.-E., Pan, S.-Y., Chen, Y.-H., Tan, C.-S., Chiang, P.-C., 2012. Accelerated carbonation of steelmaking slags in a high-gravity rotating packed bed. Journal of Hazardous Materials 227–228, 97–106.

Chen, J.J., Thomas, J.J., Taylor, H.F.W., Jennings, H.M., 2004. Solubility and structure of calcium silicate hydrate. Cement and Concrete Research 34, 1499–1519.

Cizer, Ö., Van Balen, K., Elsen, J., Van Gemert, D., 2012. Real-time investigation of reaction rate and mineral phase modifications of lime carbonation. Construction and Building Materials 35, 741–751.

Cornelis, G., Johnson, A., Van Gerven, T., Vandecasteele, C., 2008. Leaching mechanisms of oxyanionic metalloid and metal species in alkaline solid wastes: A review. Applied Geochemistry 23, 955–976.

Domínguez, M.I., Romero-Sarria, F., Centeno, M.A., Odriozola, J.A., 2010. Physicochemical Characterization and Use of Wastes from Stainless Steel Mill. Environmental Progress & Sustainable Energy 29, 471–480.

Doucet, F.J., 2010. Effective CO_2-specific sequestration capacity of steel slags and variability in their leaching behaviour in view of industrial mineral carbonation. Minerals Engineering 23, 262–269.

Durinck, D., Engström, F., Arnout, S., Heulens, J., Jones, P.T., Björkman, B., Blanpain, B., Wollants, P., 2008. Hot stage processing of metallurgical slags. Resources, Conservation and Recycling 52, 1121–1131.

Fernández-Bertos, M., Simons, S.J.R., Hills, C.D., Carey, P.J., 2004. A review of accelerated carbonation technology in the treatment of cement-based materials and sequestration of CO_2. Journal of Hazardous Materials B112, 193–205.

Fukushi, K., Munemoto, T., Sakai, M., Yagi, S., 2011. Monohydrocalcite: a promising remediation material for hazardous anions. Science and Technology of Advanced Materials 12, 064702.

Hollingbery, L.A., Hull, T.R. 2012. The thermal decomposition of natural mixtures of huntite and hydromagnesite. Thermochimica Acta 528, 45– 52.

Huijgen, W.J.J., Comans, R.N.J., 2006. Carbonation of Steel Slag for CO_2 Sequestration: Leaching of Products and Reaction Mechanisms. Environmental Science & Technology 40, 2790–2796.

Huijgen, W.J.J., Witkamp, G.-J., Comans, R.N.J., 2005. Mineral CO_2 Sequestration by Steel Slag Carbonation. Environmental Science & Technology 39, 9676–9682.

Kelly, K.E., Silcox, G.D., Sarofim, A.F., Pershing, D.W., 2011. An evaluation of ex situ, industrial-scale, aqueous CO_2 mineralization. International Journal of Greenhouse Gas Control 5, 1587–1595.

Kriskova, L., Pontikes, Y., Cizer, Ö, Mertens, G., Veulemans, W., Geysen, D., Jones, P.T., Vandewalle L., Van Balen K., Bart Blanpain, B., 2012. Effect of mechanical activation on the hydraulic properties of stainless steel slags. Cement and Concrete Research 42, 778–788.

Lackner, K.S., Butt, D.P., Wendt, C.H., 1997. Progress on binding CO_2 in mineral substrates. Energy Conversion and Management 38, S259–S264.

Mahieux, P.-Y., Aubert, J.-E., Cyr, M., Coutand, M., Husson, B., 2010. Quantitative mineralogical composition of complex mineral wastes – Contribution of the Rietveld method. Waste Management 30, 378–388.

Mäkelä, M., Harju-Oksanen, M.-L., Watkins, G., Ekroos, A., Dahl, O., 2012. Feasibility assessment of inter-industry solid residue utilization for soil amendment—Trace element availability and legislative issues. Resources, Conservation and Recycling 67, 1–8.

Mayes, W.M., Younger, P.L., Aumônier, J., 2008. Hydrogeochemistry of Alkaline Steel Slag Leachates in the UK. Water, Air & Soil Pollution 195, 35–50.

Ministère de la Région Wallonne, 2001. Arrêté du Gouvernement wallon favorisant la valorisation de certains déchets. Moniteur Belge 2, 23859–23883.

Nishiyama, R., Munemoto, T., Fukushi, K., 2013. Formation condition of monohydrocalcite from $CaCl_2$–$MgCl_2$–Na_2CO_3 solutions. Geochimica et Cosmochimica Acta 100, 217–231.

Railsback, L.B., 2006. Some Fundamentals of Mineralogy and Geochemistry. http://www.gly.uga.edu/railsback/FundamentalsIndex.html (Retrieved 15.12.2012).

Rosenqvist, J., Kilpatrick, A.D., Yardley, B.W.D., 2012. Solubility of carbon dioxide in aqueous fluids and mineral suspensions at 294 K and subcritical pressures. Applied Geochemistry 27, 1610–1614.

Santos R., François D., Vandevelde, E., Mertens, G., Elsen J., Van Gerven, T., 2010. Process intensification routes for mineral carbonation. Proceedings of the Third International Conference on Accelerated Carbonation for Environmental and Materials Engineering, (ACEME10), November 29–December 1, 2010, Turku, pp. 13–22.

Santos, R.M., Ceulemans, P., Van Gerven, T., 2012a. Synthesis of pure aragonite by sonochemical mineral carbonation. Chemical Engineering Research and Design 90, 715–725.

Santos, R.M., François, D., Mertens, G., Elsen, J., Van Gerven, T., 2012b. Ultrasound-intensified mineral carbonation. Applied Thermal Engineering, doi: 10.1016/j.applthermaleng.2012.03.035.

Santos, R.M., Ling, D., Sarvaramini, A., Guo, M., Elsen, J., Larachi, F., Beaudoin, G., Blanpain, B., Van Gerven, T., 2012c. Stabilization of basic oxygen furnace slag by hot-stage carbonation treatment. Chemical Engineering Journal 203, 239–250.

Santos, R.M., Van Gerven, T., 2011. Process intensification routes for mineral carbonation. Greenhouse Gases: Science and Technology 1, 287–293.

Santos, R.M., Verbeeck, W., Knops, P., Rijnsburger, K., Pontikes, Y., Van Gerven, T., 2013. Integrated mineral carbonation reactor technology for sustainable carbon dioxide sequestration: 'CO_2 Energy Reactor'. Energy Procedia, in press, https://www4.eventsinteractive.com/iea/viewpdf.esp?id=270035&file=\\DCFILE01\EP11%24\Eventwin\Pool\office27\docs\pdf\ghgt-11Final00715.pdf.

Snellings, R., Machiels, L., Mertens, G., Elsen, J., 2010. Rietveld refinement strategy for quantitative phase analysis of partially amorphous zeolitized tuffaceous rocks. Geologica Belgica 13, 183–196.

Van Gerven, T., Van Keer, E., Arickx, S., Jaspers, M., Wauters, G., Vandecasteele, C. 2005. Carbonation of MSWI-bottom ash to decrease heavy metal leaching, in view of recycling. Waste Management 25, 291–300.

Vandevelde, E. 2010. Mineral Carbonation of Stainless Steel Slag. Master's Thesis, KU Leuven.

Zhang, Z., Zheng, Y., Ni, Y., Liu, Z., Chen, J., Liang, X., 2006. Temperature- and pH-Dependent Morphology and FT-IR Analysis of Magnesium Carbonate Hydrates. The Journal of Physical Chemistry B, 110, 12969–12973.

Zingaretti, D., Costa, G., Baciocchi, R., 2013. Assessment of the energy requirements for CO_2 storage by carbonation of industrial residues. Part 1: Definition of the process layout. Energy Procedia, in press, https://www4.eventsinteractive.com/iea/viewpdf.esp?id=270035&file=\\DCFILE01\EP11%24\Eventwin\Pool\office27\docs\pdf\ghgt-11Final01055.pdf

9.7. SUPPLEMENTARY CONTENT

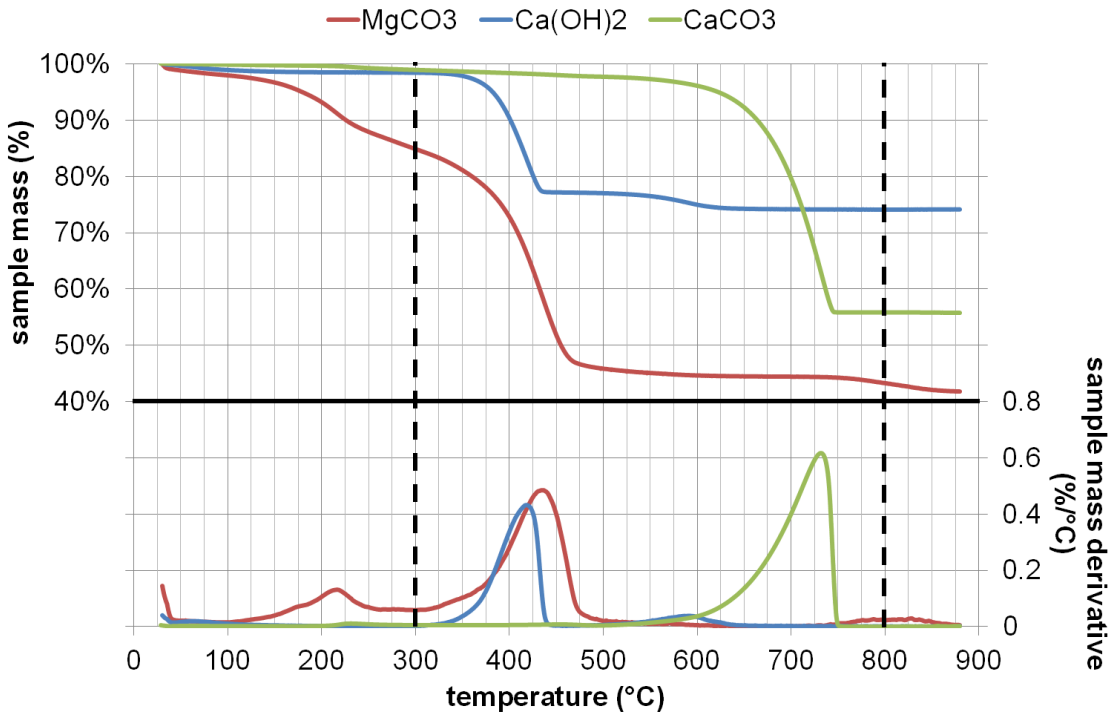

Fig. S9.1. Thermal gravimetric analysis of analytical grade $MgCO_3$, $Ca(OH)_2$ and $CaCO_3$; secondary mass losses are likely due to small quantities of hydrates (in the case of the carbonates) or carbonates (in the case of $Ca(OH)_2$) formed due to air exposure in storage.

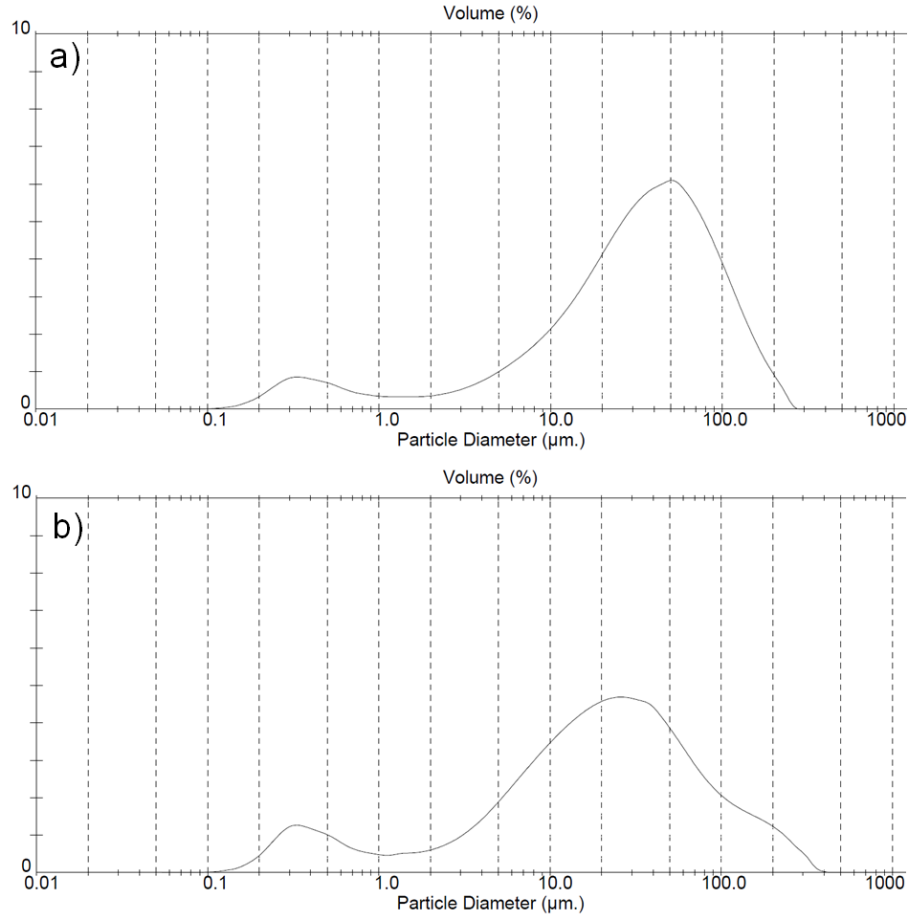

Fig. S9.2. Particle size distributions by volume of fresh AOD (a) and CC (b) slags, determined by laser diffraction.

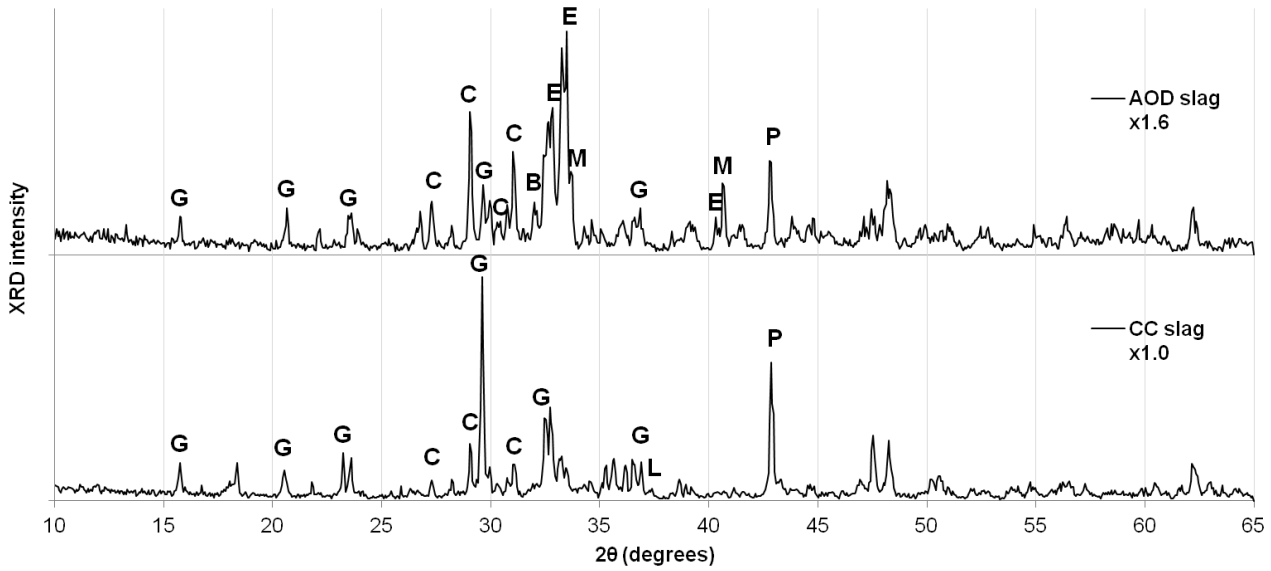

Fig. S9.3. X-ray diffractograms of fresh AOD and CC slags. Intensities have been normalized for better viewing; multipliers are indicated on figure below sample labels. Main visually distinguishable mineral peaks are indicated: B = β-C2S; C = cuspidine; E = bredigite; G = γ-C2S; L = lime; M = merwinite; P = periclase.

Fig. S9.4. Thin-film carbonation experimental apparatus: Sanyo CO_2 incubator MCO-17.

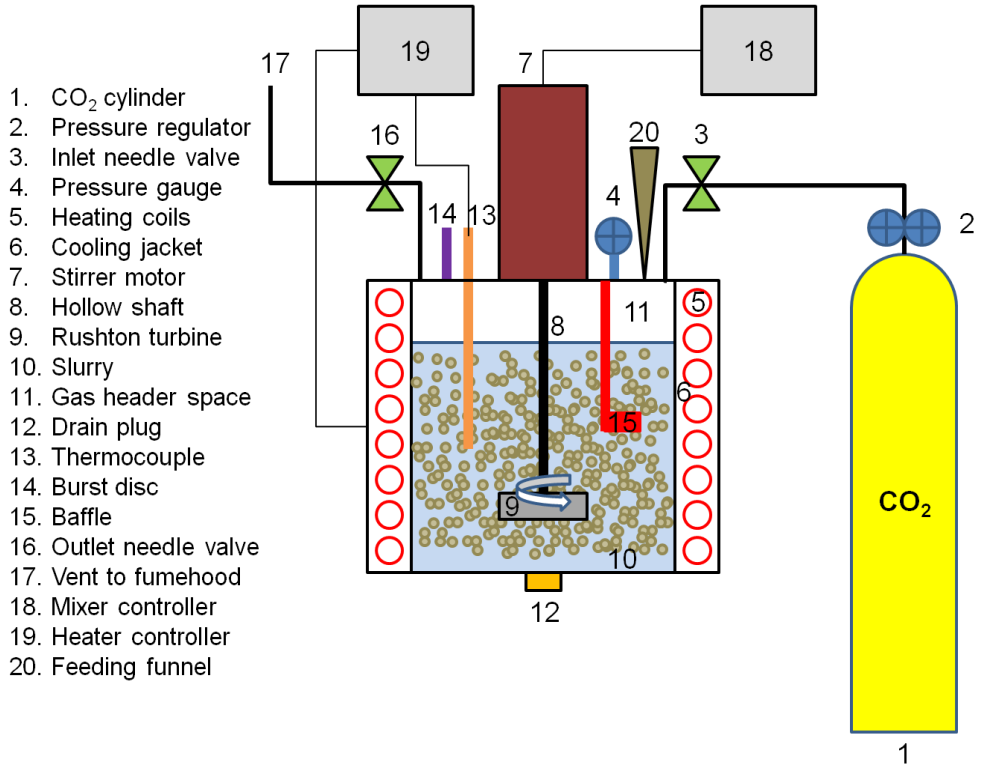

Fig. S9.5. Slurry carbonation experimental apparatus (Büchi Ecoclave autoclave reactor and CO_2 cylinder) and schematic.

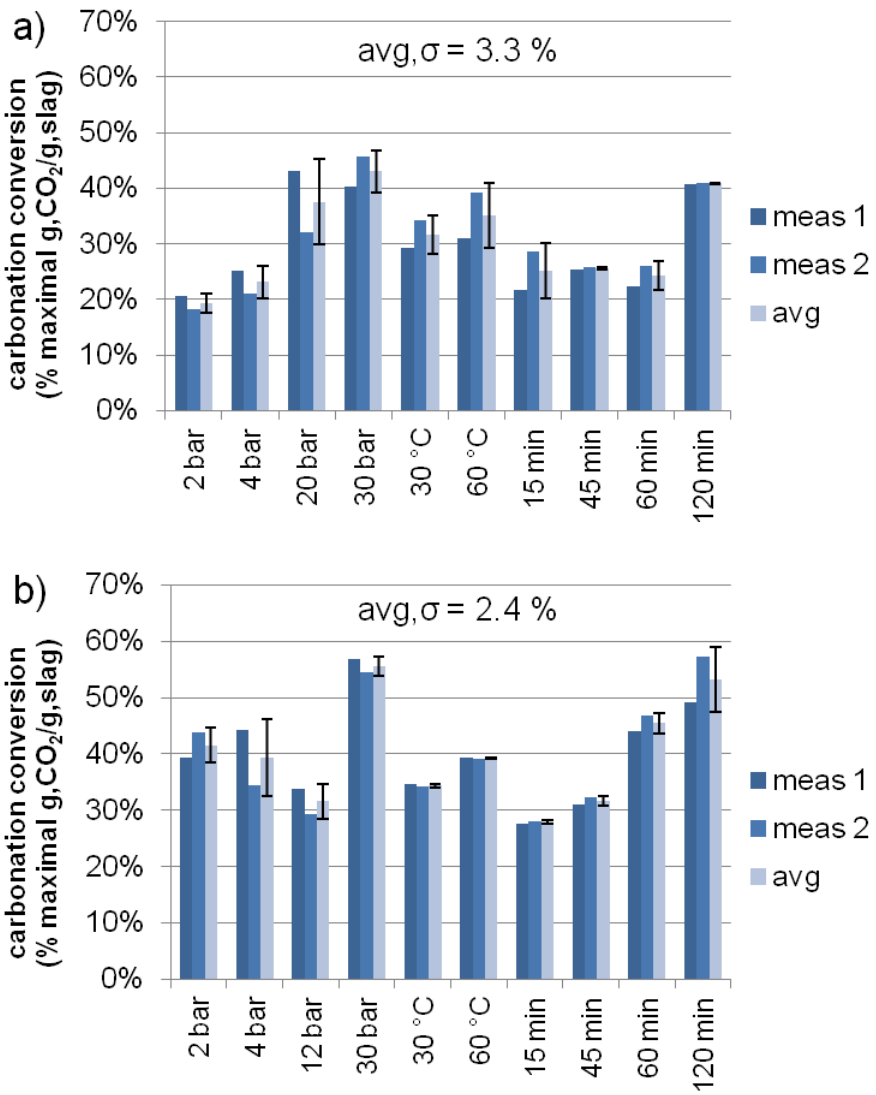

Fig. S9.6. Slurry carbonation reproducibility testing for AOD (a) and CC (a) slags; σ is the standard deviation, expressed as % maximal uptake.

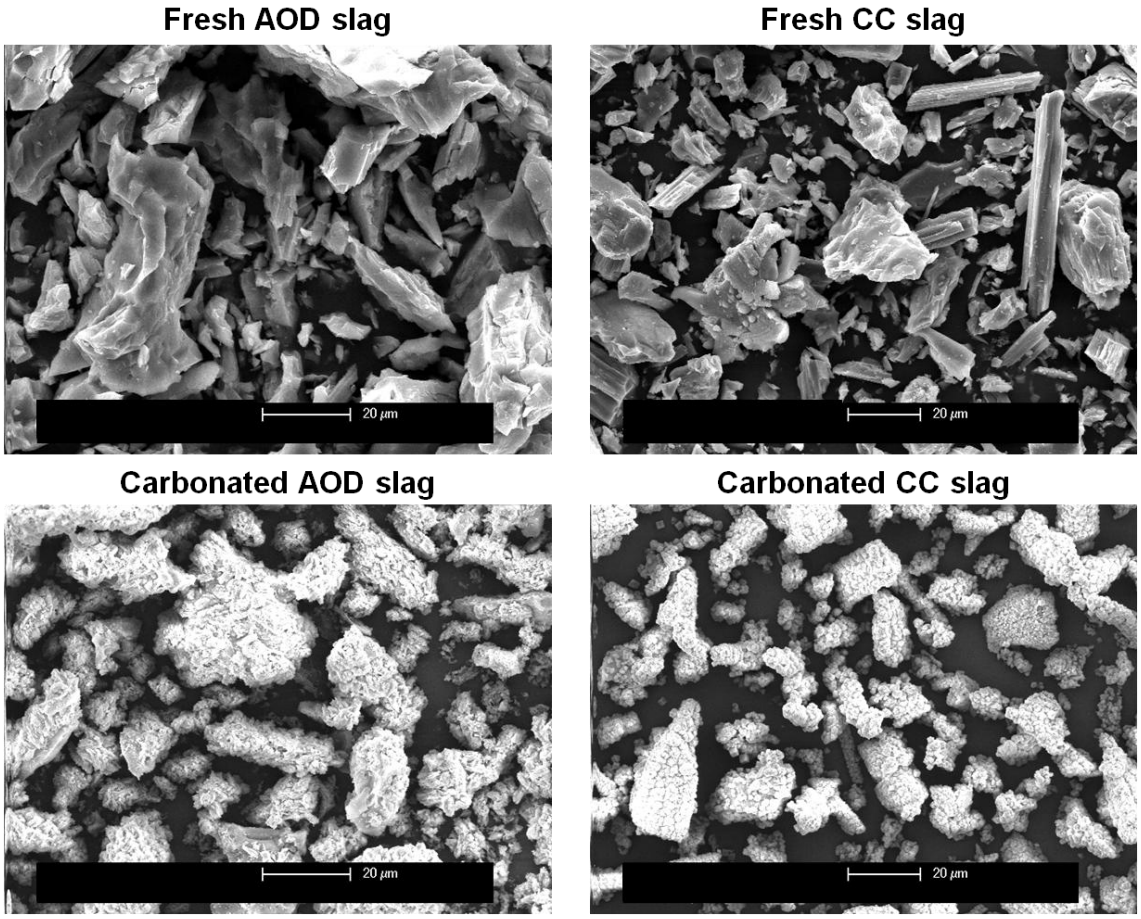

Fig. S9.7. Fresh and carbonated (120 minutes) slag particle morphology.

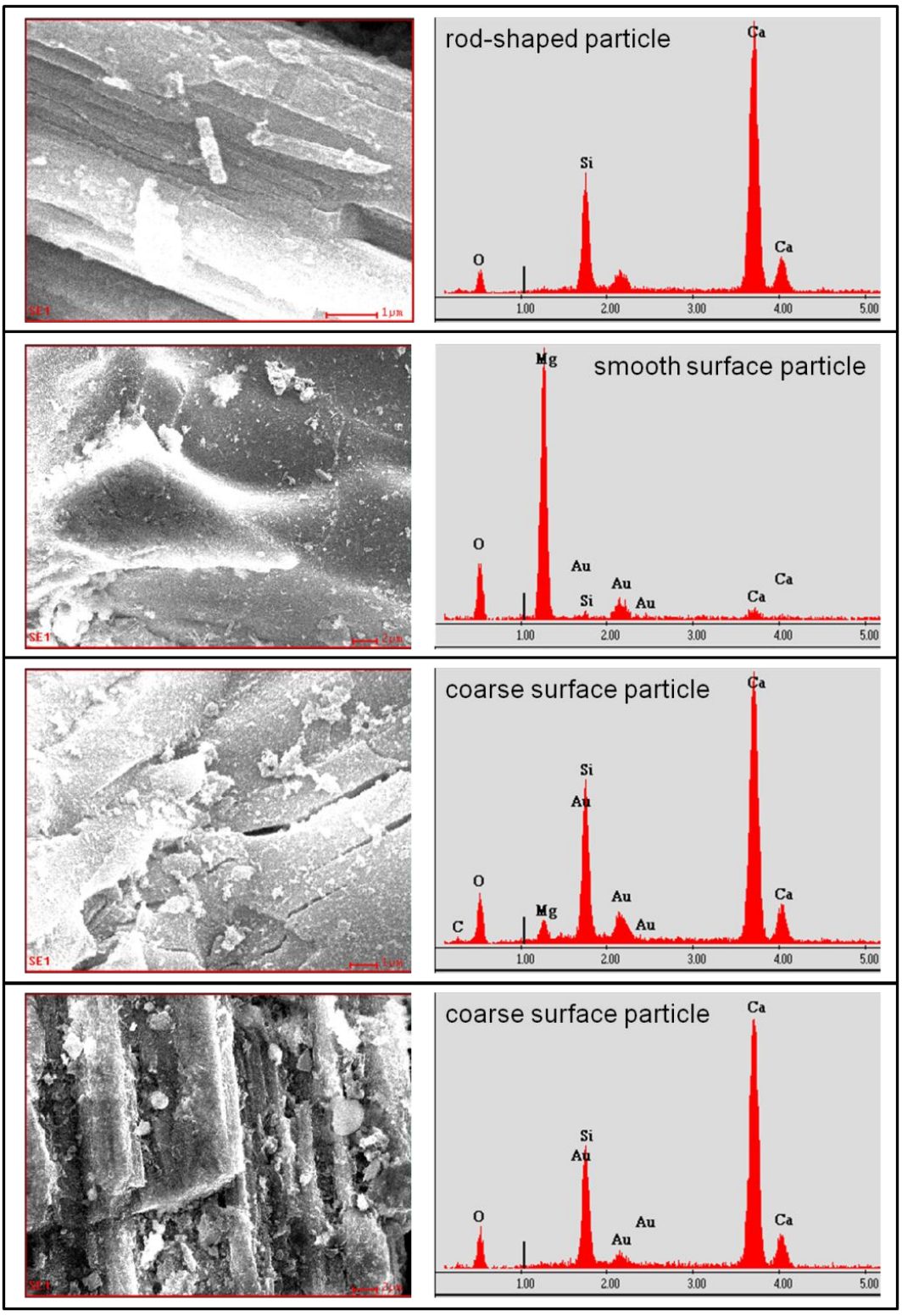

Fig. S9.8. EDX analysis of individual CC slag particles of different morphologies.

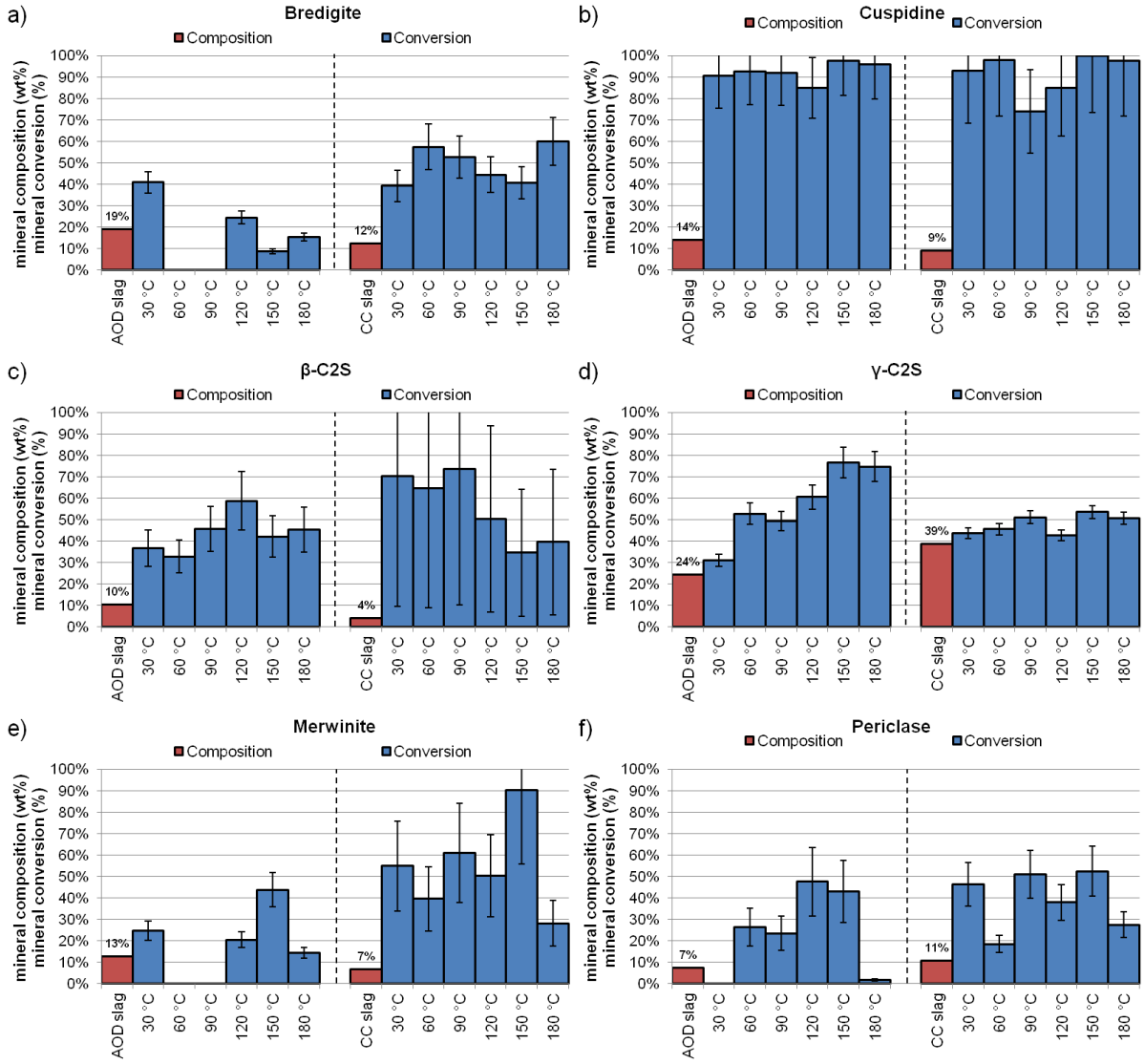

Fig. S9.9. Slurry carbonation results: carbonation conversion of slag mineral phases (bredigite (a), cuspidine (b), β-C2S (c), γ-C2S (d), merwinite (e) and periclase (f)) as a function of temperature; $P(CO_2)$ = 6 bar, t = 60 min, S = 62.5 g/L.

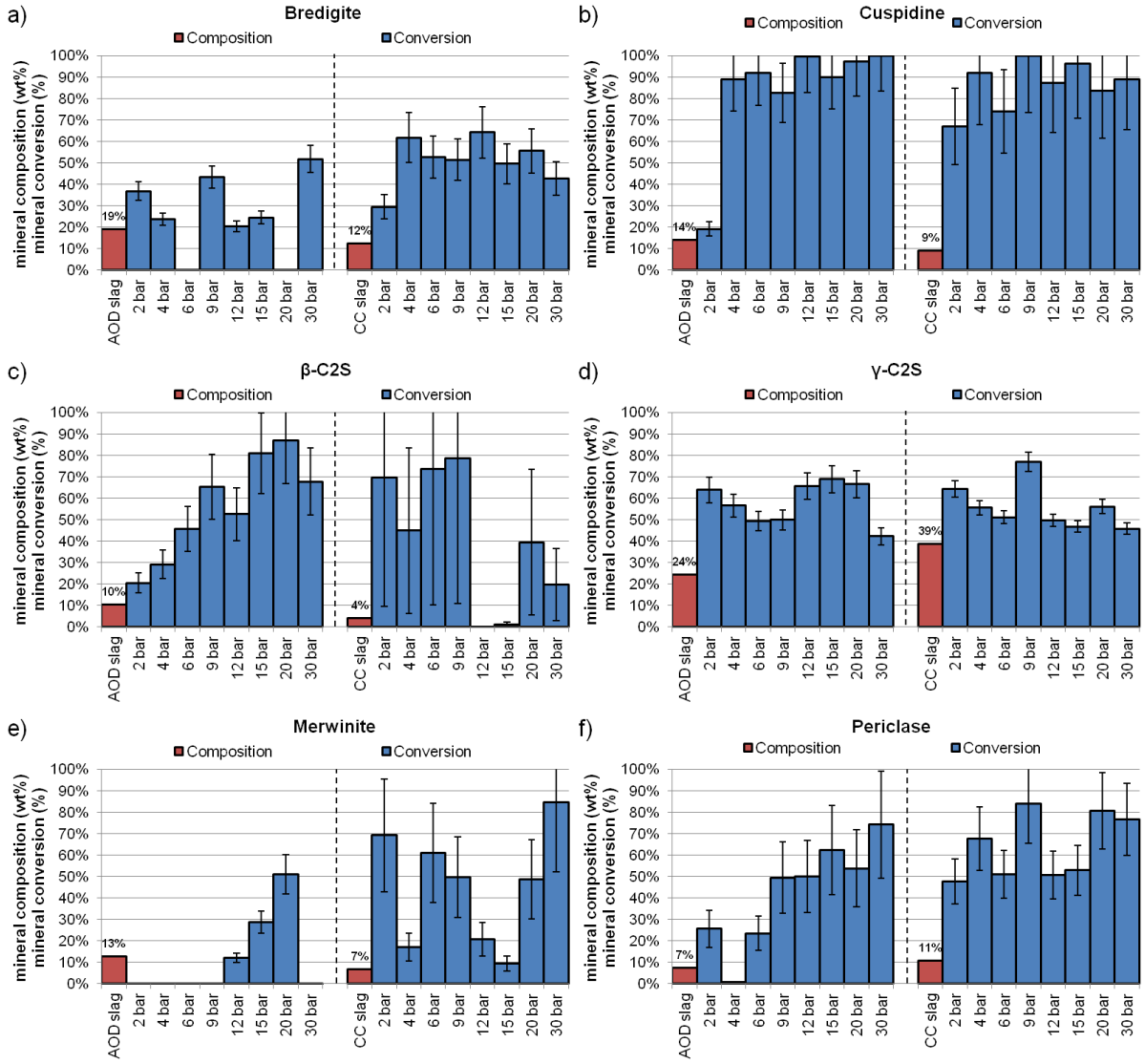

Fig. S9.10. Slurry carbonation results: carbonation conversion of slag mineral phases (bredigite (a), cuspidine (b), β-C2S (c), γ-C2S (d), merwinite (e) and periclase (f)) as a function of CO_2 partial pressure; T = 90 °C, t = 60 min, S = 62.5 g/L.

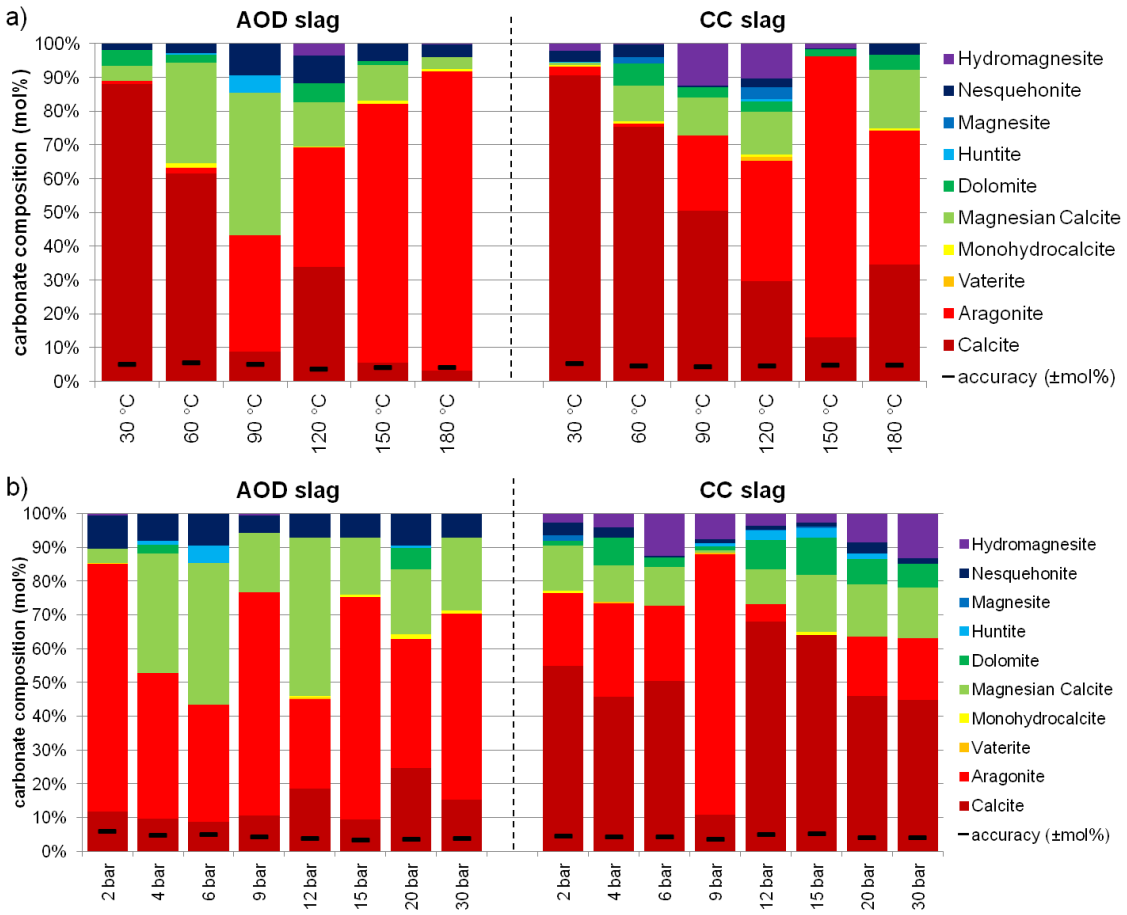

Fig. S9.11. Composition of carbonate mineral phases (normalized to 100 % of carbonate content) for slurry carbonation as a function of temperature (a) and CO_2 partial pressure (b).

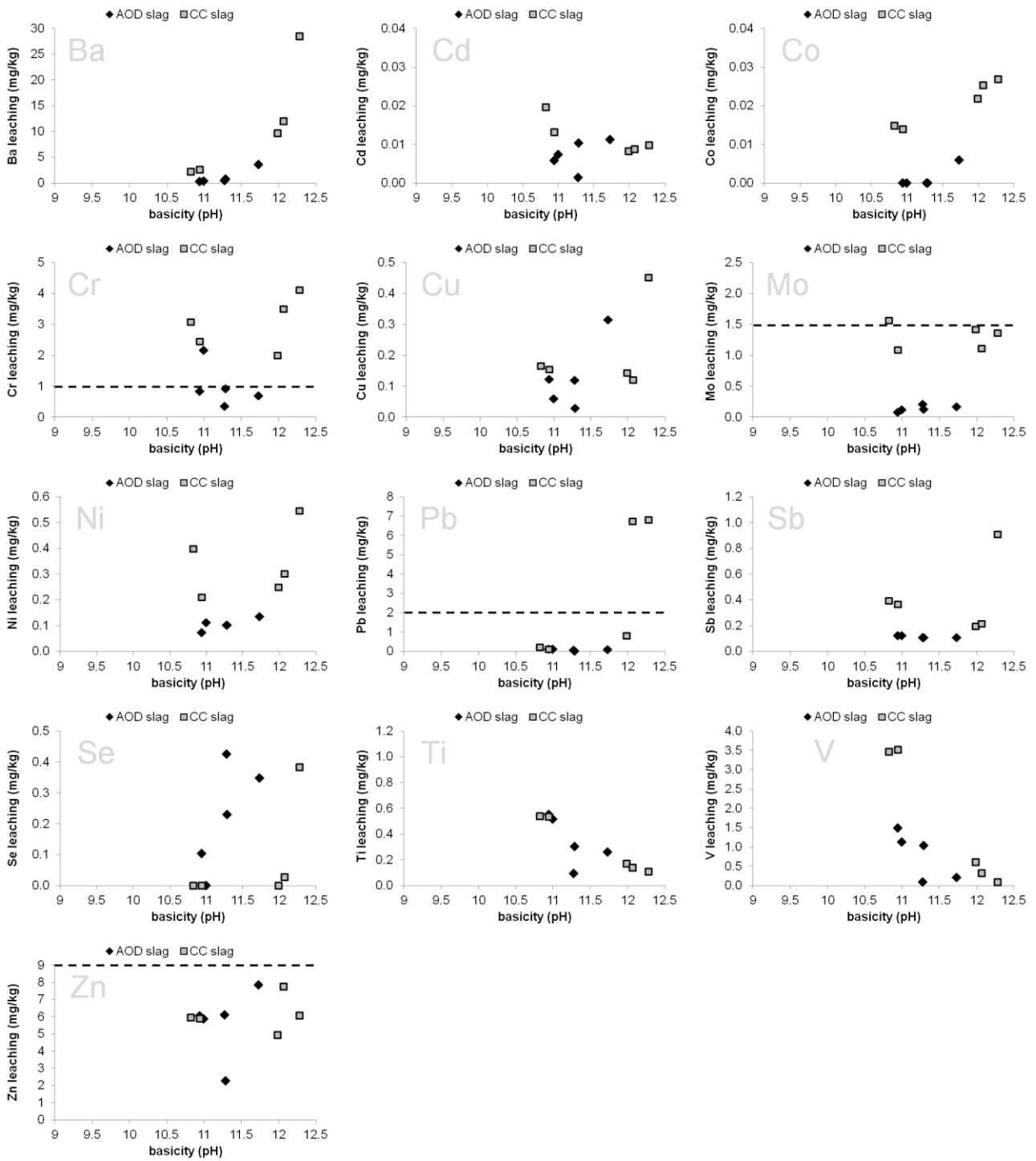

Fig. S9.12. Thin-film carbonation results: leaching of heavy metals from stainless steel slags as a function of pH. Horizontal dashed lines indicate Belgian (Wallonia) regulatory limits; where no line is seen, the limit is greater than the y-axis shown.

9.8. ADDENDUM

(not in publication)

9.8.1. Thin-film carbonation preliminary data

Figs. A9.1, A9.2 and A9.3 present results from Santos et al. (2010) on the effect of moisture content and temperature on the CO_2 uptake of AOD slag under thin film carbonation.

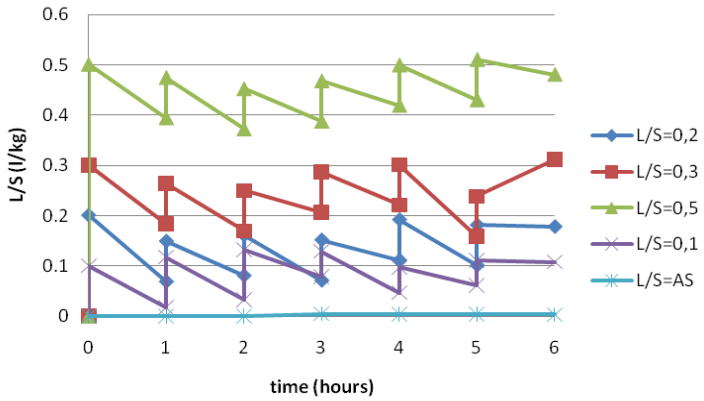

Fig. A9.1. Moisture content during carbonation of AOD slag; water added hourly; T=50°C, 20% CO_2, L/S ratios: AS=0.0004 l/kg, 0.1, 0.2, 0.3 and 0.5 l/kg.

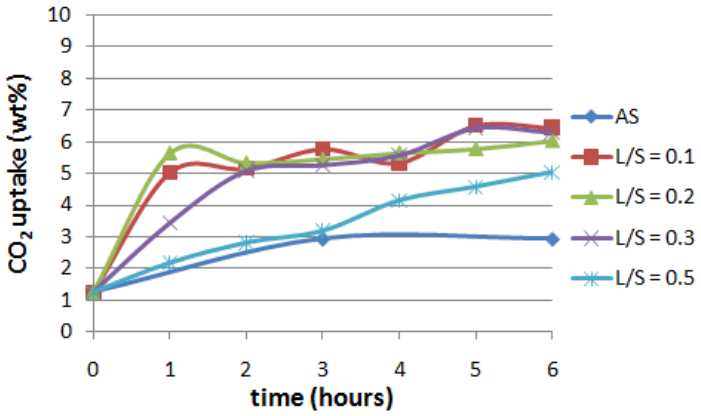

Fig. A9.2. CO_2 uptake of AOD slag; water added hourly; T=50°C, 20% CO_2, L/S ratios: AS=0.0004 l/kg, 0.1, 0.2, 0.3 and 0.5 l/kg.

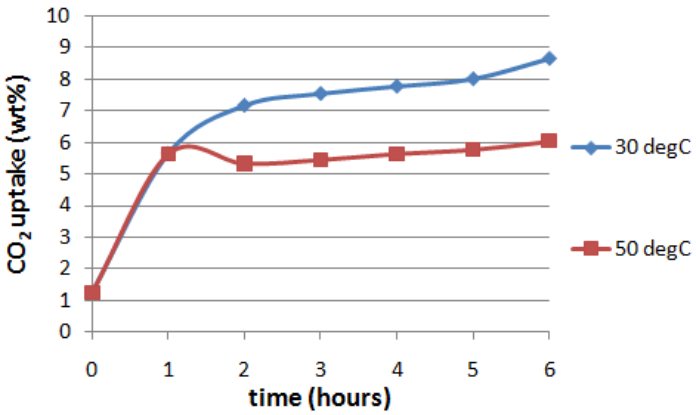

Fig. A9.3. Influence of temperature on carbonation of AOD slag. Process conditions: 30°C or 50°C, 20% CO_2 and initial L/S ratio of 0.2 l/kg.

9.8.2. Theoretical analysis of carbonated shell effect on passivation

One of the strategies to enhance mineral carbonation that was not investigated in depth in this project was the reduction of particle size to counter the shrinking core limitations of the reation. Prior studies have looked at this effect. For example, Baciocchi et al.[XXX] studied the effect of particle size on the carbonation of stainless steel slag and found a positive correlation between CO_2 uptake and particle size reduction. The main mechanism of this effect was linked to the reduction of the specific surface area of the slag with increasing particle size, which decreased the slag reactivity towards CO_2. The main issue, however, is that the milling required to decrease slag particle size to the point that it significantly improves carbonation extent is costly and energy intensive, therefore being detrimental to the goals of net CO_2 sequestration and slag valorization. That is why in this project, the main focus was on the mineral carbonation of slags fine enough to achieve substantial carbonation without the need for milling.

One interesting aspect that was not discussed in detail in the published works herein presented, but that can give an indication for slag engineering, is the thickness of the carbonation reaction front. It would be valuable to know what maximum slag particle size achieves full carbonation, and starting from which particle size is only partial carbonation achievable. Fig. A9.4 illustrates these two theoretical cases. The first two particles from the left reach full carbonation since, according to Eq. (A9.1), the particle radius (r_x) is less than or equal to the converted thickness (t_{carb}). The last two particles on the right are only partially carbonated since, according to the second part of Eq. (A9.1), the particle radius is greater than the converted thickness. In this case, it is possible to estimate the particle conversion degree (*%carb*) using the given formula, which simply equals the ratio between the volume of the carbonated hollow sphere, over the volume of the entire particle sphere. It should be noted that this model has two important assumptions: first, it assumes all mineral phases carbonate equally and, second, it does not take into account the increasing particle size due to accumulation of carbonate crystals on the surface of the particle (i.e. t_{carb} is expected to be larger than the calculated value, although this simplification does not significantly affect the estimated radius of the unconverted particle core ($r_x - t_{carb}$)).

[XXX] Baciocchi, R., Costa, G., Polettini, A., Pomi, R. (2009). Influence of particle size on the carbonation of stainless steel slag for CO_2 storage. Energy Procedia 1, 4859-4866.

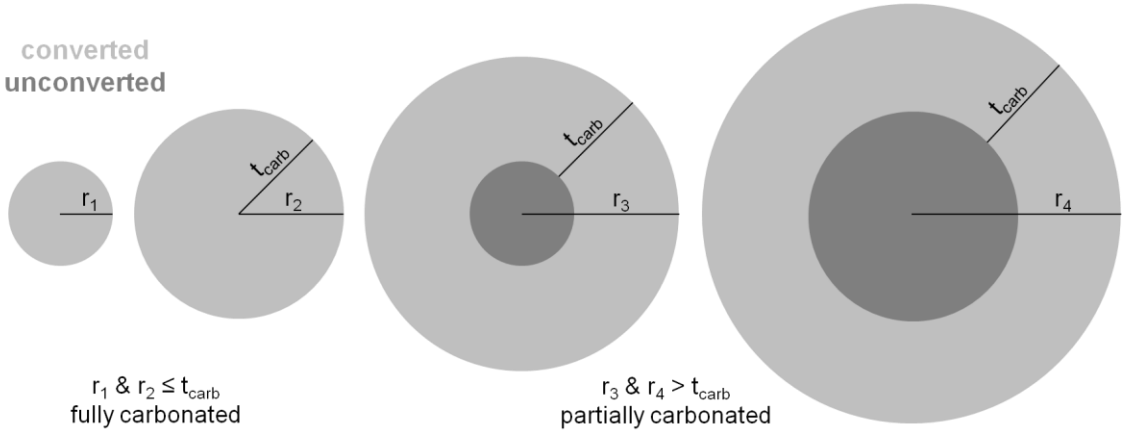

Fig. A9.4. Theoretical model of physical carbonation conversion extent for particles of different size (see text for description of assumptions made).

$$\%carb = \begin{cases} if\left[r_x \leq t_{carb}\right], = 100\% \\ if\left[r_x > t_{carb}\right], = \dfrac{\frac{4}{3}\pi r_x^3 - \frac{4}{3}\pi\left(r_x - t_{carb}\right)^3}{\frac{4}{3}\pi r_x^3} \end{cases} \quad \text{(A9.1)}$$

Using Eq. (A9.1) together with the particle size distributions of AOD and CC slag obtained by laser diffraction, it is possible to estimate the particle size below which full carbonation may occur, and above which only partial carbonation occurs. Furthermore, it is possible to estimate carbonation conversion degree as a continuous function of particle size. The maximal carbonation degrees of AOD and CC slags presented earlier in Chapter 9, 50% and 60%, respectively, are used in the calculation. The modelling results together with particle size distributions are presented in Fig. A9.5. It is found that the estimated particle size for full carbonation conversion is very similar for the two slags, 5.5 and 5.3 μm for AOD and CC slags, respectively. Taking into account that CC slag possessed 20.3 vol% of particles below 5.3 μm, while AOD slag possessed only 13.2 vol% of particles below 5.5 μm, this helps explain why the overall carbonation degree of CC slag is greater than AOD slag. Beyond these particle diameter values, the conversion degree of both slags drops as the particle diameter increases, crossing the 50% mark at around 26 μm, and the 25% mark at around 60 μm. Interestingly, despite slightly different particle size distributions, the *%carb* curves overlap each other almost precisely. This is an indication that this model has good validity, despite the assumptions previously discussed. What this model shows is that, if a certain carbonation extent is desired for all particles, in view of slag stabilization or valorization, it may be possible to physically separate the greater proportion of well carbonated (and thus likely stabilized) particles from the poorly carbonated particles (or alternatively sieve the slag prior to carbonation). This approach would result in a valorizable fine product batch, and a smaller batch containing coarse unstabilized slag that may be disposed of at reduced cost, or be more easily valorizable due to the removal of fines.

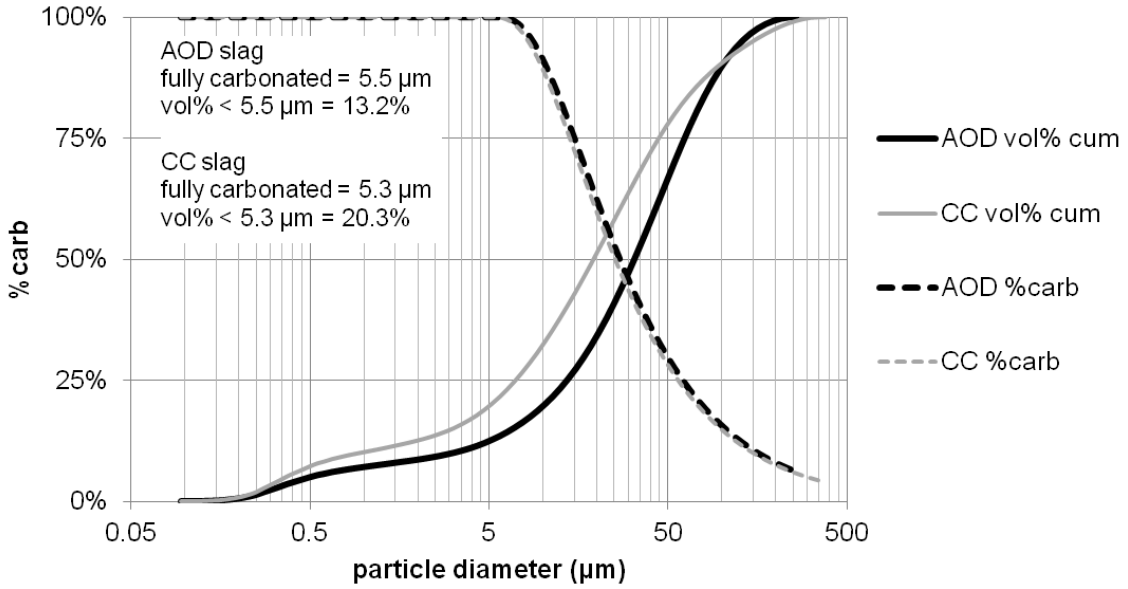

Fig. A9.5. Particle size distribution of fresh AOD and CC slags (vol% cum), determined by laser diffraction, and modelling results of particle carbonation conversion degrees (%carb).

In order to confirm if particle size is a more important factor in limiting carbonation degree versus mineralogy, a carbonation test was performed on finely milled CC slag, prepared using a McCrone Micronizing Mill. The particle size distribution of this material is presented in Fig. A9.6. The D_{50} value of this material is about one third that of the original slag (20.2 µm), the surface specific D[3,2] value is 42% smaller, and >99.9 vol% of the material is below 60 µm (the value previously estimated for 25% conversion).

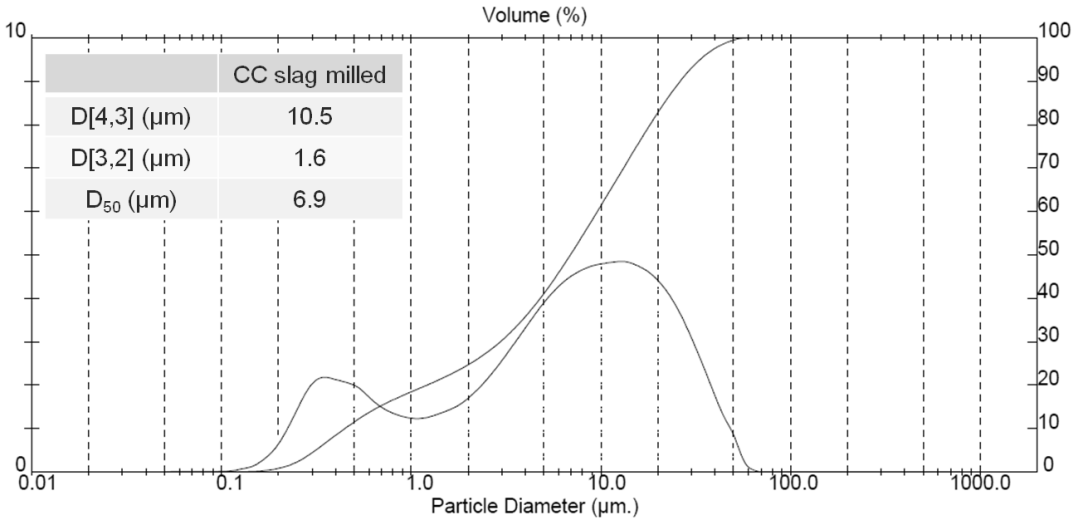

Fig. A9.6. Particle size distribution of micronized CC slag, determined by laser diffraction.

Pressurized slurry carbonation tests were conducted with original and milled CC slags for determination of the particle size reduction effect on carbonation conversion. The processing conditions used were mild (60 °C, 3 bar,CO_2, 20 g solids in 800 ml DI water, 1000 rpm stirring), while reaction durations were comparatively long (6 and 24 hours). Thermogravimetric analysis curves and calculated conversions are presented in Fig. A9.7. Milling improved carbonation conversion by 3.4%, both after 6 and 24 hours. Still, conversion evidently did not reach full extent. Even considering only the calcium content of CC slag to calculate conversion (seeing that

carbonation conditions might have been too mild to fully react the magnesium content), the conversion obtained after 24 hours using the milled material is still limited to 75%. This emphasizes that mineralogical and microstructual effects also play an important role in limiting conversion, as already discussed in detail in preceding sections of this thesis. This is therefore an important conclusion in view of possible future efforts to engineer slags and other thermal residues for high reactivity as carbon sinks.

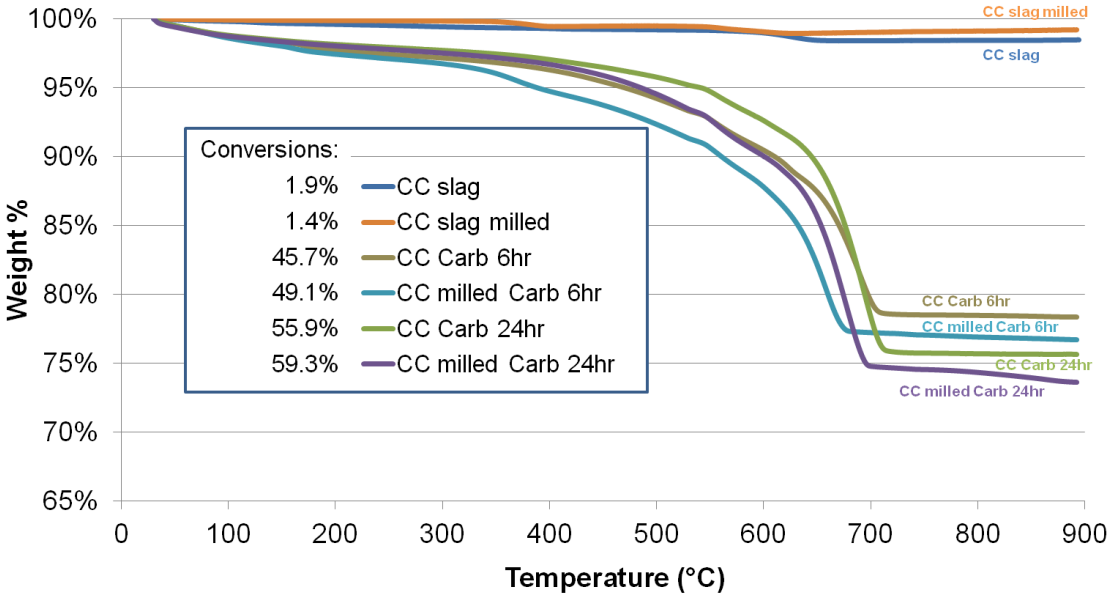

Fig. A9.7. Pressurized slurry carbonation results of original and milled CC slag, determined by thermogravimetric analysis; CO_2 uptake calculated as weight loss between 300 and 750 °C.

10. Conclusions and future perspectives

10.1. General conclusions and findings

As part of the CCS concept, mineral carbonation (sequestration) of CO_2 was initially applied to natural minerals. Once the proof of concept was established and the technology mechanisms reasonably well understood, the focus also turned to the utilization of alkaline industrial wastes, which were found, in large part, to be not only more reactive (compared to serpentine and olivine, for example), but also easily and (geographically) widely available. Even if available in smaller quantities compared to resources of natural silicate minerals, alkaline wastes can still sequester meaningful quantities of CO_2, especially as many of these residues are generated near large point sources of CO_2.[XXXI] Mineral carbonation can thus constitute a truly end-of-pipe approach to CCS, as environmentally worrisome transportation or pipelining can be eliminated. Mineral carbonation also overcomes the lack of permanency of underground CCS (with the exception of in-situ geological mineral carbonation) that is counter to sustainability, since important concerns over leakage risks and long-term stewardship of the stored CO_2 are eliminated. A further benefit identified when utilizing waste materials for mineral carbonation, besides serving as carbon sinks, has been the possibility of stabilizing some of the detrimental properties of these materials (e.g. leaching/toxicity), and valorizing them, either by reducing treatment, disposal and storage costs, or producing materials that can be safely re-utilized commercially.

However, the chemical, mineralogical and morphological properties of these materials also vary widely, impacting their behavior towards carbonation and the resulting effects of carbonation. As such, only recently has a large enough body of research formed to investigate the many opportunities available and develop the necessary material-specific intensified carbonation processes. This thesis focused on three types of steel slags that are rich in calcium and calcium-magnesium silicates and ferrites, free lime and magnesia: Argon Oxygen Decarburization (AOD) slag, Continuous Casting (CC) slag, and Basic Oxygen Furnace (BOF) slag. Two of these slags, AOD and CC, possessed powdery morphology, which is ideal for high carbonation yield and low processing costs. BOF slag, which is traditionally cooled into monolith-shaped, low-surface area material, is envisioned to be a prime candidate for hot-stage granulation, which can impart the necessary material exposure for sufficient reactivity towards hot-stage carbonation.

[XXXI] Kirchofer, A., Becker, A., Brandt, A., Wilcox, J. (2013). CO_2 Mitigation Potential of Mineral Carbonation with Industrial Alkalinity Sources in the United States. Environmental Science & Technology 47, 7548-7554.

Several challenges still remain to enable large-scale and widespread adoption of mineral carbonation as an industrial process. Processing costs still need to be reduced, especially in view of reducing external energy input and maximizing the utilization of the exothermic carbonation heat of reaction. To this end, efforts were made during this doctoral project to find sustainable routes to the materialization of residues from thermal processes into carbon sinks via novel process intensification routes [Chapter 3]. To qualify as sustainable, mineral carbonation processes should aim to match the rate of CO_2 emissions from industrial sources, and to achieve carbonation in an economical and net-positive sequestration manner. In particular, it was identified that matching the right alkaline materials with the right mineral carbonation processes is key to overcoming the barriers that have prevented this technology from reaching the market; this is the essence of π^2, process intensification (π_1) combined with process integration (π_2).

The application of ultrasound for particle abrasion and removal of passivating layers [Chapter 4], and for the promotion of the acicular aragonite polymorph of calcium carbonate, which yielded potentially valuable products [Chapter 5] and helped to improve calcium leaching and carbonation extent [Chapter 6], has been shown. The proof-of-concept on the application of ultrasound for overcoming the shrinking core barrier of mineral carbonation processes due to the abrasion of particles in suspension was achieved, but it was found that the energy demand of the technology is prohibitively high in its present form. In view of energy conservation, several approaches can be further investigated to improve the feasibility of the process. These include the use of renewable electricity, increasing the solids loeading in slurry, changing or adjusting the liquid medium, the optimization of ultrasound application (sonication frequency, probe dimensions, reactor dimensions, flow configuration, and transducer geometrical arrangement), or the utilization of other cavitation generating technologies. The combination of all these factors may allow ultrasound-intensified mineral carbonation to become an industrially feasible technology. The approach utilized here may also be extended to other chemical reactions that require intensification. In those cases, more favourable process conditions (e.g. material properties, reaction kinetics, and required intensification extent) and economical incentives (e.g. product value, high cost competing technology, etc.) may permit more immediate application of this technology.

The combination of ultrasound with soluble magnesium chloride allowed for the formation of pure aragonite precipitates at lower bulk temperatures than previously reported, including close to ambient temperature at optimized conditions. Evidence was collected on the mechanisms at play for several process parameters, including: the symbiotic relationship between ultrasound and $MgCl_2$, the precipitation/dissolution cycle of magnesium ions, the control of particle morphology, and the influences of sonication amplitude and cycle, of pre-sonication, of CO_2 flow rate, and of solids concentration. One of the main findings was the mechanism that promotes aragonite formation

under sonication, which consists of two effects: (i) imploding cavities generate localized regions of high temperature that lead to the nucleation of aragonite seeds, given aragonite formation is promoted at higher temperatures; and (ii) the nucleation rate is enhanced by sonication, thus maintaining stochastically preferable aragonite formation over calcite even at low crystal growth bulk temperatures. Thus, the smaller aragonite crystals formed at low bulk temperatures appear to be a product of slower aragonite crystal growth at these temperatures, combined with increased aragonite nucleation in the presence of ultrasound. With the mechanism of $MgCl_2$ regenerability well understood, having confirmed the efficacy of reutilized $MgCl_2$ in a fed-batch process, this substance was then tested as a self-regenerative additive for enhancement of calcium leaching and carbonation conversion. Magnesium chloride proved to be atom-efficient for the calcium leaching from CaO, but was inefficient in the leaching of wollastonite, and partially efficient for the thermal residues tested. This indicates that mineralogy plays an important role in the extractability of calcium from different alkaline minerals, such as oxides, silicates, ferrites, sulphates and aluminates. This is analogous to the differences in reactivity towards mineral carbonation of different alkaline materials (e.g. wollastonite requires more aggressive conditions (i.e. higher T and P) than steel slags). Further work is required to better exploit $MgCl_2$ as a carbonation additive.

Hot-stage processing was found to be an attractive route to the treatment of BOF slag in view of applications of the residue in building materials and civil works (e.g. road construction) [Chapter 7]. The desire to attempt BOF slag carbonation at high temperature stems from the fact that the carbonation thermodynamics of the alkaline components of the slag are favourable up to high temperatures. Furthermore, the granulation processing of the slag while molten can potentially reduce the cost of generating surface area needed for carbonation (compared to milling of cooled and hardened slag). It is envisioned that the freshly granulated and still hot (200-1000 °C) slag can be exposed to CO_2-containing flue gases generated in the steelworks, constituting an integrated and intensified approach to slag carbonation. Favourable thermodynamics, however, do not guarantee that these carbonation reactions will occur fast enough, as reaction kinetics also play an important role. Therefore research on this topic aimed at confirming the susceptibility of BOF slag carbonation at high temperature, both with regards to carbonation kinetics and CO_2 uptake. Carbonation extent was found to be directly proportional to the free lime content. In contrast, the other two oxides tested (MgO and Fe_2O_3) did not carbonate in the temperature range tested. Stainless steel slag samples containing mainly calcium silicates and negligible free lime content also did not exhibit reactivity to direct carbonation at these temperatures. Therefore it was concluded that CaO is the principal mineral in BOF slag responsible for CO_2 uptake during direct high temperature carbonation. This is an important finding, as it shows that hot-stage carbonation is a material specific process, and cannot necessarily be applied to other thermal residues such as

stainless steel slags and incineration bottom ashes. The necessary level of free lime conversion needed to satisfactory stabilize BOF slag swelling in construction material applications remains to be investigated. In particular, it should be understood if near-surface carbonation, which is enough to reduce basicity and alter leaching behaviour, suffices, or if complete free lime volumetric conversion is required to enable valorization.

Geochemical and mineralogical mechanisms were also investigated in greater depth, making use of the Rietveld refinement mineral quantification method applied to X-ray diffraction data, which has seldom been used for complex waste materials in prior works. This has enabled clarification on the relationships between carbonation conditions, mineral composition, basicity and leaching [Chapter 9], and on the susceptibility of individual mineral phases to hydration and mineral carbonation [Chapter 8]. The synthesis of pure alkaline mineral phases found in steel slags enabled unique insight on the reactivity of individual phases towards mineral carbonation at different processing conditions (milder thin-film carbonation and more intense pressurized slurry carbonation). Understanding the mineralogical behaviour of alkaline materials towards mineral carbonation is one more step in advancing this scientific field and in inching closer to industrial implementation of this technology. The outcome is the facilitation of the optimal development of intensified carbonation technologies and the selection of the most appropriate carbonation process technology for each particular application dealing with a distinct alkaline material.

The results of the present study can also contribute to increasing confidence in the *a priori* predictability of carbonation effects such as the CO_2 uptake capacity of the material, and the properties of the carbonated product, such as its resulting basicity and, with the aid of geochemical models, its leaching behaviour. Based on all findings, however, it was concluded that mineralogical susceptibility towards carbonation is not the only determining factor controlling carbonation reactivity and CO_2 uptake. For instance, some difference in behaviour of individual minerals was observed between the synthetic materials and the slags. Solid solutions in the slags may alter the reactivity of its mineral phases. Particle morphology, in particular grain size and physical distribution of the mineral phase components (liberation), also appears to be important, as reactive mineral phases dispersed within less reactive phases do not have the same opportunity to react with CO_2 as if they were directly exposed to the reactive medium. This was evident from the hot-stage carbonation work, where CaO dispersed in an unreactive matrix in BOF slags particles did not fully carbonate even at optimal conditions and with reduced particle sizes. As such, given that thermal residues such as slags originate from high temperature processes where these materials are in the molten state, it can be of interest to tune their chemical composition, and to control their cooling trajectory, as a means of slag engineering. This can enable the production of residues having more

desirable mineralogy, morphology and microstructure, and that are more susceptible towards mineral carbonation.

Under nearly all conditions tested, CC slag carbonation conversion surpassed that of AOD slag when exposed to identical process parameters despite the two slags having very similar chemical compositions and sharing essentially the same mineral phases, though in differing proportions. This reaffirms that slag mineralogy, morphology and microstructure are the likely causes for this discrepancy. Unequal cooling trajectories during slag production may be responsible for controlling particle microstructure. In a way this is inopportune, as substantially more AOD slag is produced during steelmaking. On the other hand, it suggests that AOD slag mineralogy and particle morphology should be tuned to resemble more closely that of CC slag, using the aforementioned slag engineering strategies, thus transforming low value secondary waste materials into tailored resources. This is approach is appealing, as the metallurgical industry is in need of novel valorisation routes to steer slags away from traditional storage in landfills and into valuable applications. At the same time, the technological field of mineral carbonation is in need of a process that is economical and scalable, to serve as a platform for its dissemination and uptake by several industrial activities that can benefit from it but are still skeptical of its merit. The results herein presented are promising for the valorisation of carbonated AOD and CC stainless steel slags, either as commerciable materials, or at least for their utilization solely as carbon sinks, while at the same time reducing their disposal costs and environmental impact.

Besides sonochemical and hot-stage carbonation, two further processing routes were extensively experimented: thin-film and pressurized slurry carbonation. It was found that increased temperature, pressure and better mixing during pressurized continuously stirred autoclave carbonation serve as efficient alternatives for the intensification of the mineral carbonation reaction compared to the energy intensive sonication applied at milder process conditions. However, it remains to be seen if sonication of the slurry at intensified conditions could serve to speed reaction conversion, particularly after the initial reaction period when diffusion through the passivating layers becomes rate limiting. Slurry carbonation, both at atmospheric and pressurized conditions, was also found to deliver optimal treatment homogeneity. This resulted in improved basicity reduction and heavy metal stabilization, compared to the heterogeneous treatment resulting from stagnant thin-film carbonation. Still, it should be emphasized that these characteristics are only required when the carbonated product is to be valorised beyond a carbon sink, for example as soil conditioner (pH control), as fine aggregate (sand substitute) in construction materials (e.g. concrete), or as mineral filler in chemical products (e.g. paints and polymers). In this manner, valorisation applications can potentially afford the additional processing costs associated with slurry carbonation. Conversely, thin-film carbonation may be a more feasible route for the utilization of

slags as carbon sinks, particularly due to the elimination of CO_2 separation and compression and of liquid-solid separation, and the reduction of heating and mixing demands. This is an example of optimization via reduction in 'surplus of severity'. In addition, the aforementioned valorization options envision direct use of the carbonated slags in commercial applications; however, industrial symbiosis and inter-industry solid residue utilization as blended materials should also be explored, as they can open new valorisation routes, enable better energy/exergy efficiencies, and potentially diminish material property requirements commonly associated with commercial reagents and products.

Several findings of fundamental nature realized during this thesis work are also worth highlighting. Many of these findings were made by utilizing specific experimental or analytical methods under-utilized in other mineral carbonation works and that were given particular focus in this thesis. These range from the simple measurement of basicity to elucidate more complex geochemical behaviours, to the utilization of advanced in-situ characterization techniques to follow reaction progress. Other important techniques extensively applied included particle size characterization using laser diffraction, mineralogical composition determined by quantitative X-ray diffraction via Rietveld refinement, and utilization of regulatory leaching limits for assessment of treatment performance. The following paragraphs detail the main findings made using these techniques.

It was possible to follow particle size growth or reduction by laser diffraction, which elucidate effects of carbonation (precipitated layer and microstructure) and sonication (particle attrition and fragmentation). It was also realized that of the three average particle diameters obtained by laser diffraction, the Sauter mean diameter (D[3,2]), being surface area sensitive, is the most important when it comes to the susceptibility towards mineral carbonation of powdery materials, since mineral carbonation reactivity is proportional to exposed surface area. This mean diameter was also found to be the most sensitive to sonication effects, as it best detects the formation of micron- to sub-micron sized fragments. The volume-moment mean diameter (D[4,3]), on the other hand, is useful in indicating the degree of erosion of larger particles. Laser diffraction results were particularly useful in assessing the performance of sonication as a means of process intensification. It was interesting to note that slag particle size reduces after only 30 minutes of sonicated carbonation, when in the case of non-reacting sonication the particle size did not change. This is suggestive that sonication not only removes the precipitated calcium carbonate layer, but also the depleted silica layer that once constituted the original slag particle material, and that this depleted silica layer is weaker than the original silicate material. This was further substantiated by comparing SEM images to the laser diffraction results and observing that two particle size modes form: flaky sub-micron particles and rounded particles roughly 2-10 μm in size, which appears to be remnants of larger

particles that have been significantly eroded over time. It is also worth noting that, while SEM provides direct visualization of particles, it is a semi-quantitative method for assessing particle size distribution, while laser diffraction is a quantitative method for doing so, and thus offers added insight not realizable by SEM. Laser diffraction also provided a window into the mechanism that controls the particle size of sonochemically synthesized aragonite precipitates. The larger particle modes are thought to represent needle-shaped particles, while the smaller modes may be fragmented particles, due to sonication, and/or particles that formed near the end of the experiments when crystal growth became hindered by diminishing calcium concentration in solution. Samples from low temperature synthesis (24 ^{o}C and 30 ^{o}C) were found to have unimodal distributions below 3 μm. The low temperatures, which may hinder crystal growth throughout the experiment, can be attributed to the smaller particle sizes. When $MgCl_2$ was used as an additive during slag slurry carbonation, laser diffraction helped to provide an explanation as to why $MgCl_2$ addition was only beneficial in the presence of sonication. Particle size reduction was linked to the formation of acicular aragonitic crystals, whose morphology and arrangement appeared to be more easily cleaved off the surface of the carbonated particles due to sonication than the more closely packed calcitic layers formed in the absence of $MgCl_2$.

The measurement of basicity couples with other more advanced geochemical analyses to yield useful understanding about reaction progress and efficiency, and even provides hints about the relationship between microstructural and macro-scale properties. For instance, comparing the trends in decreasing basicity as a function of CO_2 uptake between AOD and CC slags, it was observed that in the case of AOD slag, under stirred carbonation conditions, it reached lower values of pH at lower carbonation conversions, suggesting that its passivating layers are effective in shielding the unreacted core. In contrast, in the case of CC slag, the calcium carbonate layer that forms on carbonated slag under mechanical mixing alone did not prove sufficient to completely shell the unreacted particle core, since the stirred and sonicated basicity trends overlaped. This also demonstrates that the removal of the rate/conversion limiting layers (calcium carbonate and depleted silica) upon sonication is not necessarily detrimental to basicity. The differences seen between AOD and CC slag basicity behaviour were combined with SEM observations to draw further conclusions about the effect of microstructural characteristics on product properties. CC slag particles were seen to possess heterogeneous morphology, indicative of different mineralogical compositions between individual particles. On the other hand, AOD slag particles appeared to be more homogenous. Consequently, in CC slag, the mineral phases more susceptible to rapid carbonation can react to near completion more quickly, and their precipitated carbonate products can deposit on other mineral particles and hinder their reactivity. In contrast, mineral phases of AOD slag gradually and simultaneously react, and thus achieve more similar carbonation

conversions over time, although at a slower rate. In the work conducted on the carbonation of pure synthetic minerals, basicity measurement allowed understanding about which mineral phases control solution pH. Basicity reduction was found to be a function of CO_2 uptake, and progressed approximately linearly. Lime is the most likely phase to control basicity at high pH values (>~12); next are silicate hydrates (pH ~11–12), followed by hydrated carbonates (pH < 10.8), and finally by $CaCO_3$ polymorphs (pH < 10). It was also notable that AOD slag basicity is lower than that of CC slag initially, and remains so for comparable levels of CO_2 uptake. This may be due to, other than mineralogical differences, greater exposure of the slag's different alkaline minerals (which have different solubilities and reactivities towards hydration and carbonation) to the aqueous medium, given the observed differences in particle morphology. As carbonate precipitation is accelerated at high pH, the differing slag basicities, potentially buffering the reaction medium to slightly different pH levels, could play a role in the greater CO_2 uptakes achieved by CC slag at comparable pH values. Finally, in the hot-stage carbonation work with BOF slag, it was found that reduction in basicity of the coarser samples was very similar to the reduction obtained with the finer samples. This is explained by the fact that carbonation primarily occurs near the particle surface, which contacts the liquid phase and controls pH. Therefore reduction in basicity is not always directly proportional to CO_2 uptake, but rather depends on particle size and most importantly on exposed surface area. Only for a specific slag particle size fraction are CO_2 uptake and basicity reduction proportionally linked.

The use of Rietveld refinement for the quantification of mineral phases from X-ray diffractograms is a technique that deserves more attention in the mineral carbonation community, since it provides an unparalleled level of insight not realizable by more commonly used microstructural techniques such as EDX (similar to the comparison between LD and SEM). In the study on the utilization of $MgCl_2$ as a leaching additive, QXRD was used to understand the mechanisms behind differences in leaching efficacy from different materials. It was possible to observe the transformation of lime into portlandite, the precipitation of brucite, the enrichment of anhydrite, and the dissolution of portlandite, calcium chloride hydroxide, innate soluble salts, and to a lesser extent alkaline silicate phases. Rietveld analysis also allows for detailed assessment of the behaviour of the constituent minerals of carbonated materials tested when exposed to CO_2, allowing for determination of the susceptibility to carbonation of each mineral phase. To improve the accuracy of the analysis, rather than simply comparing the pre-carbonation composition to the post-carbonation composition, a new data handling procedure was developed [Chapter 8]. Mass fractions delivered by Rietveld analysis were translated into molar fractions normalized against the pre-carbonation mass of the materials (to discount the CO_2 mass uptake after carbonation, which artificially lowers the mass fractions of non-carbonate components) and taking into account the

formation of amorphous materials during carbonation (which, if ignored, causes overestimation of mineral mass fractions). Still, even applying this method, the semi-quantitative nature of the Rietveld analysis of complex mineral samples was reflected in the magnitude of the error bars for sample replicates, which were intuitively larger for phases present in smaller quantities in the slags. For simpler minerals, however, such as the carbonate precipitates synthesized from pure $Ca(OH)_2$, and the carbonated synthetic silicates and ferrites, the quantification accuracy was found to be high. QXRD results showed that different alkaline mineral phases convert more or less under different carbonation conditions and routes, and that different carbonates form under different processing conditions and routes, and from different minerals or slags. Incomplete conversion of synthetic minerals was linked to limited magnesium carbonation conversion, since the amount of magnesium carbonates detected was lower than that expected based on Ca:Mg ratio; thus it was concluded that the calcium content is nearly solely responsible for CO_2 uptake. In case of slags, however, Mg is present in larger extent as periclase and brucite, thus more reactivity and greater formation of magnesium-containing carbonates was detected. In terms of non-carbonate post-carbonation products, QXRD showed that wollastonite formation in steel slags is notable, indicating that its reactivity to mineral carbonation is slower than the native silicates. Formation of this mineral phase may thus hinder further carbonation of the slags, as its formation along the reactive front towards the shrinking particle core contributes to decreased ionic diffusivity. The vast majority of non-carbonate products, however, were found to be amorphous. The developed data handling procedure allowed quantification of the amorphous fraction in addition to the crystalline fraction. Performing elemental balances, seeing as most carbonation products are Ca- and Mg-rich and Si-poor, it was concluded that the amorphous matter is composed mainly of amorphous silica.

It was possible to make unique observations by following the carbonation of CaO and BOF slags in real-time using in-situ TGA. First, during CaO carbonation two distinct carbonation regimes were observed, one kinetically controlled and a second diffusion-controlled, while for the slag samples a single diffusion-controlled regime dominated. In the case of slag samples, these effects can be explained by the necessity of CO_2 to diffuse across a native inert layer into slag particles from the start of carbonation to achieve further uptake, and a second regime does not occur since emerging carbonates form a dispersed patchwork within the particle, rather than a dense shell. In the case of pure CaO, significant carbonation at the exposed outer surface occurs immediately, only later to be followed by diffusion through the reacted carbonate layer into the particle core. Because of this, temperature-controlled CO_2 diffusivity appears to be a greater limiting factor for slag carbonation than reaction kinetics. This was reaffirmed by the greater effect of temperature on BOF slag carbonation extent than for CaO. Another unique possibility explored with is-situ TGA was to track CO_2 uptake during the hot-to-cold path that BOF slag is expected to undertake in the

industrial setting when being reacted immediately after slag granulation from the molten stage. In this manner, the exact temperature at which carbonation commences, as a function of CO_2 partial pressure, was identified. Real-time monitoring of CO_2 uptake also allowed determination of carbonation kinetics, which showed that hot-stage carbonation may be fast enough to be conducted in the short period of time the cooling slag is expected to remain at the required temperature window for efficient carbonation.

By comparing leaching results to regulatory limits, it was possible to have a better sense of the valorization potential of carbonated heavy metal and metalloid containing thermal residues. Carbonation of BOF slag was found to have a noticeable positive effect on reducing leaching of barium, nickel and cobalt; while chromium, molybdenum and vanadium leaching increased after carbonation. Comparing leaching results to regulatory limits, it was found that V exceeds its limit, while Cr and Mo remain below their limits. Under more moderate carbonation extent (10 minutes reaction time), the extent of solubility increase of these metals was lower, conforming to regulatory limits. These results advise that, in view of industrial implementation of BOF slag carbonation, it should be considered whether a higher or lower carbonation extent is more interesting for commercialization of carbonated BOF slag. In the case of stainless steel slags, four elements were found to present significant leaching risk from the untreated slags: Cr, Mo, Pb and Zn. Carbonation successfully decreased leaching of Mo, Pb and Zn. Leaching of V increased, but unlike in the case of BOF slag, here it remained well below the regulatory limit. Compared to hot-stage carbonation, it was realized that slurry and thin-film carbonation routes have a particular advantage: the encapsulating carbonate layer, though detrimental for carbonation reaction progression, may play an important role in limiting heavy metal leaching by reducing exposure of the unreacted or unreactive phases in the particle core to the aqueous medium. Another insight made from leaching results was that the good homogeneity of slurry carbonation may explain beyond its better CO_2 uptake the reason for its generally superior leaching performance compared to thin-film carbonation. This can be particularly ascribed to the V leaching behaviour from thin-film carbonated slags, where the lower pH of the overall sample may exacerbate V leaching from some less carbonated particles.

The findings of this doctoral work contribute to the advancement of accelerated mineral carbonation for the purposes of carbon capture and industrial alkaline solid waste remediation. However, besides technical challenges, practical issues also need to be overcome. One such barrier is the lack of economical reward for the capture of CO_2, as well as for the valorization of waste materials. The industrial mindset focuses on maximizing profit, and thus most attention is given to increasing the production efficiency of the principal products (e.g. steel), rather than applying large efforts to waste treatment and management. Legislative directives are likely needed to compel

industry to change its attitude,[XXXII] though greater awareness by the industry and young engineers of sustainable green technologies, including mineral carbonation, may slowly buck the trend.

Another challenge faced by mineral carbonation technologies is the competition for attention with alternative CCS technologies, especially underground storage. Mineral carbonation does have the possibility to capture all anthropogenic CO_2 emissions, given the amount of suitable minerals present in the Earth's crust.[XXXIII] Mineral carbonation also presents additional benefits, including geochemically permanent CO_2 storage without leakage risk, energy generation from the exothermic reaction, as well as valorization opportunities through the commercialization of the formed carbonate materials. Still, underground storage, presently, presents lower costs and more scalable opportunities, so it is understandable that it remains as the lead option for CCS. This should not mean that mineral carbonation research is not important; in fact the opposite holds true: more investment should be directed towards mineral carbonation so that it eventually can become the preferred CCS route, capitalizing on its evident advantages. As such, a greater level of industrial cooperation and governmental support is needed. Two such examples are the KU Leuven's Knowledge Platform on Sustainable Materialization of Residues from Thermal Processes into Products (SMaRT-Pro^2), under which this doctoral project was performed, and the Research Consortium on Sustainable Inorganic Materials Management (SIM^2), which aims to carry forward the momentum generated by SMaRT-Pro^2.

10.2. RELATED AND ONGOING WORKS

During my doctoral project, within the framework of SMaRT-Pro^2, I had the opportunity to work with colleagues on several other research topics related to the valorization of residues from thermal processes into products, and to accelerated mineral carbonation more generally (i.e. including natural minerals and for purposes other than carbon sinks). On certain topics, research work has already led to the publication of findings, while on other topics work is still ongoing. In the next subsections the objectives, the methods and available principal findings of these works are summarized.

[XXXII] Dubois, M. (2013). Economic instruments for European waste management. PhD Thesis, KU Leuven.
[XXXIII] Lackner, K.S. (2003). A Guide to CO_2 Sequestration. Science 300(5626), 1677-1678.

10.2.1. Remediation of municipal solid waste incineration bottom ashes

This study, reported in Santos et al.[XXXIV], compared the performance of four different approaches for stabilization of regulated heavy metal and metalloid leaching from municipal solid waste incineration bottom ash (MSWI-BA): (i) short term (three months) heap ageing, (ii) heat treatment, (iii) accelerated moist carbonation, and (iv) accelerated pressurized slurry carbonation. These treatments were performed on identical materials, methodologically sampled and split to ensure similarity of material properties. This makes the comparison of treatment performance more reliable than comparing studies available in literature performed by different research groups on differing materials. To better elucidate the effect of material characteristics and the geochemical effects of the treatment methods on the treated ash properties, two distinct types of MSWI-BA were tested in this study: one originating from a moving-grate furnace incineration operation treating exclusively household refuse (sample B), and another originating from a fluid-bed furnace incineration operation that treats a mixture of household and light industrial wastes (sample F). The leaching values of all samples were compared to the Flemish (NEN 7343) and the Walloon (EN 12457-4/DIN 38414-S4) Belgian regulations.

Batch leaching of the fresh ashes at natural pH showed that seven elements exceeded at least one regulatory limit (Ba, Cr, Cu, Mo, Pb, Se and Zn), and that both ashes had excess basicity (pH > 12). Accelerated carbonation achieved significant reduction in ash basicity (9.3-9.9); lower than ageing (10.5-12.2) and heat treatment (11.1-12.1). For sample B, there was little distinction between the leaching results of ageing and accelerated carbonation with respect to regulatory limits; however carbonation achieved comparatively lower leaching levels. Heat treatment was especially detrimental to the leaching of Cr. For sample F, ageing was ineffective and heat treatment had marginally better results, while accelerated carbonation delivered the most effective performance, with slurry carbonation meeting all DIN limits. For NEN limits, Mo and Sb consistently exceeded the (proposed) leaching limits. Tests conducted with varying pH, by acid addition, point to the leaching enhancement of these elements at lower pH (<approx. 11). For the samples tested, Sb was the only element present in sufficient quantities to pose a risk, but this is an issue that should not be overlooked when it comes to the effect of carbonation. For heavy metals and metalloids that cannot be stabilized by accelerated treatment processes or short term ageing, it appears that only long-term

[XXXIV] Santos, R.M., Mertens, G., Salman, M., Cizer, Ö., Van Gerven, T. (2013). Comparative study of ageing, heat treatment and accelerated carbonation for stabilization of municipal solid waste incineration bottom ash in view of reducing regulated heavy metal/metalloid leaching. Journal of Environmental Management, 128, 807-821.

(order of decades) mineral alterations, such as the formation of Al- and Fe-hydrates that permanently bind such elements,[XXXV] can provide definitive stability.

Lowered basicity due to mineral carbonation of alkaline oxides was deemed the dominant stabilization mechanism. Slurry carbonation is able to reach greater carbonation conversion due to its intense mixing, which improves mass and heat transfer and increases the homogeneity of the treatment compared to the stationary and hardening solids in moist carbonation. The higher temperature of the treatment is also useful for enhancing carbonation kinetics (leaching and $CaCO_3$ precipitation), and pressurization assists in maintaining sufficient CO_2 solubility. Furthermore, appreciable quantities of aragonite, a polymorph of $CaCO_3$ that is beneficial to Ba and Pb uptake, were detected in the slurry carbonated samples due to the higher temperature carbonation conditions (90 °C). Slurry carbonation is also effective in washing out Cl ions, which may permit utilization of the treated samples in construction applications that required low chloride leaching.

From a practical application point of view, slurry carbonation also avoids two limitations of the other two accelerated treatment methods. For instance, the heat treatment process would require holding the incinerated material in the primary furnace for longer periods, to ensure complete combustion, or introducing a secondary heating step after the primary process (e.g. rotary kiln). In either case, this type of processing would inherently introduce additional expenses and inefficiencies in the incineration process, and are thus less preferable than accelerated ageing/carbonation. Moist carbonation, on the other hand, requires substantially longer treatment times (7 days used in this study) to achieve satisfactory carbonation conversion and hence leaching stabilization; from an industrial perspective, holding and processing 7 days worth of bottom ashes, which must be spread thinly, regularly turned over, and kept moist, would require large processing facilities and extensive energy expenditure. Slurry carbonation also poses some uncertainties of its own, such as determining if flue gases could be directly used as a CO_2 source, or if purification or concentration of the gases (to reduce compression costs) would be required.

It would be ideal to develop treatment technologies for particular MSWI-BA compositions, since it would likely achieve better results (e.g. lower leaching) than methods developed more generally (i.e. for an array of composition ranges). The preference of the industry, however, is for the development of treatment technologies that can be applied 'off-the-shelf', that is, that can be adapted to a variety of plants and that will work with a wide range of feed inputs into the incinerator. In this manner, detailed monitoring of feed input and excessively burdensome process control can be avoided, thus allowing incinerators the flexibility to change feed as the market or

[XXXV] Saffarzadeh, A., Shimaoka, T., Wei, Y., Gardner, K.H., Musselman, C.N. (2011). Impacts of natural weathering on the transformation/neoformation processes in landfilled MSWI bottom ash: a geoenvironmental perspective. Waste Management 31, 2440-2454.

process economics dictate. A necessary next step in developing bottom ash treatment technologies should be the investigation of process design options and the determination of processing costs.

10.2.2. Bioleaching of natural and waste-derived alkaline materials

Bioleaching is a potential route for the valorisation of low value natural and waste alkaline materials. It may serve as a pre-treatment stage to mineral carbonation and sorbent synthesis processes by increasing the surface area and altering the mineralogy of the solid material and by generating an alkaline rich (Ca and Mg) aqueous stream. It may also aid the extraction of high value metals from these materials (e.g. Ni), transforming them into valuable ore reserves. In this study, reported in Chiang et al.[XXXVI], the bioleaching potential of several chemoorganoheterotrophic bacteria (*Bacillus circulans*, *Bacillus licheniformis*, *Bacillus mucilaginosus*, *Sporosarcina ureae*) and fungi (*Aspergillus niger*, *Humicola grisea*, *Penicillium chrysogenum*) towards the alteration of chemical, mineralogical and morphological properties of pure alkaline materials (wollastonite and olivine) and alkaline waste residues (AOD and BOF steel slags, and MSWI boiler fly ash) at natural pH (neutral to basic) was assessed. Bioleaching was conducted using two methodologies: one-step (microorganisms inoculated into nutrient broth containing alkaline solids) and two-step (alkaline solids added to autoclaved broth culture).

Bioleaching induced positive results with respect to increased solubilisation of alkaline earth metals and nickel, and the alteration of basicity, mineralogy and morphology of solid materials. AOD slag experienced solubilisation–precipitation mechanism, as evidenced by the decline of primary phases (such as dicalcium-silicate, bredigite and periclase) and the augmentation of secondary phases (e.g. merwinite and calcite). Nickel-bearing minerals of olivine (clinochlore, lizardite, nimite and willemseite) significantly diminished in quantity after bioleaching. Altered mineralogy resulted in morphological changes of the solid materials and, in particular, in increased specific surface areas.

The bioleaching effect can be attributed to the production of organic acids (principally gluconic acid) and exopolysaccharides (EPSs) by the microorganisms. The similarities between fungal and bacterial mediated bioleaching suggest that biogenic substances contribute mostly to its effects, as opposed to bioaccumulation or other direct action of living cells. This aspect supports the use of two-step bioleaching as opposed to one-step, since the biogenic substances can be produced under optimal conditions prior to the introduction of potentially hazardous solid materials.

[XXXVI] Chiang, Y.W., Santos, R.M., Monballiu, A., Ghyselbrecht, K., Martens, J.A., Mattos, M.L.T., Van Gerven, T., Meesschaert, B. (2013). Effects of bioleaching on the chemical, mineralogical and morphological properties of natural and waste-derived alkaline materials. Minerals Engineering, 48, 116-125.

Further work is required to better understand the bioleaching mechanisms. Routes for optimisation of the biochemical processes include: (i) adoption of continuous leaching (e.g. heap or column) to overcome solubility limits; (ii) genetic amelioration of the utilised microorganisms, to produce strains more resistant to alkaline environments and to the presence of heavy metals, and that generate greater quantities of the key lixiviant biogenic substances; and (iii) identification of other suitable strains isolated from alkaline environments (e.g. mining and metallurgical waste sites and biodeteriorated cementitious and stony structures).

10.2.3. Integrated mineral carbonation reactor technology: the gravity pressure vessel

To overcome the limitations of mineral carbonation that thus far have prevented it from becoming an industrially feasible and economicall acceptable route to sustainable CO_2 sequestration, a novel reactor technology that makes use of a Gravity Pressure Vessel is being developed in collaboration with Innovation Concepts B.V., holders of the proprietary patent (WO2011/155830A1). The 'CO_2 Energy Reactor' applies the principles of process integration and process intensification to achieve the technological leap needed to make mineral carbonation industrially feasible. The key advances of the 'CO_2 Energy Reactor' over previous reactor designs are its autothermicity (dispensing the need for external heating), hydrostatic pressurization (reducing pumping and compression requirements), vertical plug flow design (ensuring slurry homogeneity), and underground installation (minimizing heat losses, safety risks and pressurized vessel construction specifications). Residence time is controlled by the reactor length that can reach up to 2400 m, resulting in hydrostatic built pressures that can reach 120 bar. By continuously recycling exothermic reaction heat (-89, -87, and -64 kJ/mol,CO_2 respectively for olivine, wollastonite and serpentine carbonation), even for relatively low exothermic reactions it is still possible to achieve high end temperatures (e.g. up to 220 °C) without external energy input. The three-phase slurry flow (water carrier, CO_2 gas and solid minerals) also generates sufficient turbulence to promote particle-particle interaction, leading to removal of passivating layers (carbonate precipitates and amorphous silica matrix) and autogenous milling of the reacting material, permitting post-processing separation of the various phases into valuable product streams. These products include calcium and magnesium carbonate precipitates with potential application as paper and polymer fillers, amorphous silica powder with potential application in the glass making, tyre manufacturing and concrete industries, and enriched metal residues (containing, for example, iron, nickel and chromium from olivine).

The work reported in Santos et al.[XXXVII], based on the Master's thesis of Wouter Verbeeck (KU Leuven, 2012), presents the technical details of the conceptual design, mathematical modelling results on the effect of process parameters on reaction characteristics (kinetics and conversion) and on energy balances. Olivine ($(Mg,Fe)_2SiO_4$), which has CO_2 binding capacity of ~460 g/kg, was used as the target feedstock. The parameter sets (particle size, solids loading, pumping rate, and reactor dimensions) that ensure autothermic behavior, maximize carbonation efficiency and enable recoverable heat generation were identified on a preliminary scoping basis. The results obtained suggest that the 'CO_2 Energy Reactor' is chemically and thermodynamically capable of sequestering carbon dioxide in an autothermic and efficient manner when the process conditions are suitably chosen. Some factors not considered in the model could further enhance the process performance, such as the use of additives that promote Mg and Si leaching (e.g. weak acids, salts, chelating ligands and enzymatic catalysts)[XXXVIII], and the three phase fluid turbulence that may significantly aid in removal of passivating layers from the particle surfaces due to enhanced particle-particle or particle-wall interactions.[XXXIX]

The 'CO_2 Energy Reactor' can be an important component of the multi-array of CCS technologies needed to substantially reduce greenhouse gas emissions and stabilize, if not reduce, atmospheric levels. As Butt et al.[XL] put it, from a sustainability philosophy, 'prevention is better than cure', climate change mitigation is better than adaptation, and thus "having CCS technology is better than not having it at all".

10.2.4. Two-way valorization of blast furnace slag

The utilization of industrial alkaline waste materials such as steel slags for CO_2 capture could be more appealing to the industry if the benefits of mineral carbonation and waste stabilization/valorization could be combined symbiotically. Indirect carbonation is especially interesting due to the production of high-purity products, particularly precipitated calcium carbonate (PCC); however, the generation of a destabilized solid residue which contains minor but hazardous

[XXXVII] Santos, R.M., Verbeeck, W., Knops, P., Rijnsburger, K., Pontikes, Y., Van Gerven, T. (2013). Integrated mineral carbonation reactor technology for sustainable carbon dioxide sequestration: 'CO_2 Energy Reactor'. Energy Procedia 37, 5884-5891.

[XXXVIII] Zhao, H., Park, A.-H.A. Microbial and chemical enhancement of carbon mineralization. In: Proceedings of the 3rd International Conference on Accelerated Carbonation for Environmental and Materials Engineering, Turku, Finland, 29 Nov - 1 Dec 2010 (pp. 51).

[XXXIX] Penner, L., O'Connor, W.K., Dahlin, D.C., Gerdemann, S., Rush, G.E. Mineral Carbonation: Energy Costs of Pretreatment Options and Insights Gained from Flow Loop Reaction Studies. In: Proceedings of the Third Annual Conference on Carbon Capture & Sequestration, Alexandria, VA, USA, 3-6 May 2004 (OSTI ID: 899009).

[XL] Butt, T.E., Giddings, R.D., Jones, K.G. (2012). Environmental Sustainability and Climate Change Mitigation—CCS technology, better having it than not having it at all!. Environmental Progress & Sustainable Energy 31(4), 642-649.

heavy metals and metalloids hinders this approach. This study investigates the potential of two-way valorization of blast furnace slag (BFS) via: 1) production of PCC from the initial-stage extraction step; and 2) utilization of the solid residue for the production of microporous and mesoporous materials that have the potential to be applied as sorbents, and that at the same time can act to stabilize the intrinsically contained hazardous components. Blast furnace slag is chosen (as opposed to the other slags studied in this thesis) due to its large and global production, and its rather consistent chemical and mineralogical composition, which have allowed it to be commercialized in applications such as cement feedstock, and its aluminium content, an essential component of aluminosilicate-based zeolites.

A two-stage process has been devised to transform BFS symbiotically into two valuable products: precipitated calcium carbonate (PCC) and zeolitic sorbents. Calcium is first selectively extracted by leaching with organic acids, followed by carbonation of the leachate to precipitate $CaCO_3$. In parallel, the hydrothermal conversion of the extracted solid residues in alkaline solution induces the dissolution/precipitation mechanism that leads to the formation of micro- and meso-porous materials. In the work reported in preliminary form by Chiang et al.[XLI], two organic acids were trialled: succinic and acetic acids. Both acids satisfactorily prevented the leaching of aluminium, required for the subsequent synthesis of zeolites. However, while the leaching performance of succinic acid was superior, carbonation of its leachate did not result in the production of PCC, but rather the precipitation of calcium succinate, and only with the addition of pH buffers. In contrast, carbonation of the acetic acid leachate resulted in the production of PCC of mainly calcite mineralogy with trace amounts of magnesian-calcite. The hydrothermal conversion stage successfully resulted in the formation of zeolitic phases; however undesirable tobermorite ($Ca_5(OH)_2Si_6O_{16}\cdot 4H_2O$) formation was also observed, due to the incomplete removal of calcium in the leaching stage.

With the proof-of-concept confirmed, efforts are underway on improving the leaching extension in the first stage, by tuning acid concentration, temperature and time, reducing and narrowing the particle size distribution of the produced PCC, enhancing the synthesis of zeolitic materials that impart high microporosity in the hydrothermal conversion stage, and testing the produced sorbent materials in adsorption applications.

[XLI] Chiang, Y.W., Santos, R.M., Elsen, J., Meesschaert, B., Martens, J.A., Van Gerven, T. (2013). Two-way valorization of blast furnace slag into precipitated calcium carbonate and sorbent materials. In: Proceedings of the 4th International Conference on Accelerated Carbonation for Environmental and Materials Engineering. Leuven, Belgium, 9-12 April 2013 (pp. 357-367).

10.2.5. In-situ high-pressure X-ray diffraction investigation of mineral carbonation kinetics of steel slags and synthetic constituent phases

Individual mineral phases that make up steelmaking slags have varying degrees of susceptibility to mineral carbonation. In this research a unique X-ray diffractometer is utilized, which allows monitoring of the mineral conversion progress in-situ, at wide range of processing conditions (e.g. pressure, temperature and water content) suitable for carbonation. The principal objective is to quantify the reaction kinetics (mineral conversion and carbonate formation) and maximal conversion of the various alkaline mineral phases present in AOD, CC and BOF slags.

Using ex-situ analysis techniques, it has been possible to understand the general trends and limitations of carbonation reactivity, such as qualitatively differentiating mineral phases that react more substantially than others over time, observing noticeable differences in reactivity at varying process conditions (T and P), and discerning the preferential formation of certain Ca- and Mg-carbonates depending on the processing route. However, precise data on the reaction kinetics of individual mineral phases is still lacking. This is largely due to the following constraints:

(i) only a finite number of experiments can be performed when varying each process condition (e.g. 15, 30, 60, 120 minutes duration) while still having enough difference between the samples to attribute the differences to the process conditions rather than to analytical variability;

(ii) the reaction kinetics are fast (approx. 50% of the maximal CO_2 uptake takes place in the first 5 minutes of reaction time in pressurized slurry carbonation), and it is difficult to control experimental duration accuracy down to seconds or few minutes (since, for example, there is a finite time between turning off CO_2 gas flow, cooling the sample, filtering the solution, etc.); and

(iii) the complex diffraction patterns of steelmaking slags add uncertainty to mineral phase identification and quantification accuracy.

Better understanding and predictability of the effects of mineral carbonation conditions on steelmaking slags can be obtained by following the carbonation reaction progress in-situ by X-ray diffraction (XRD). This technique can allow for detailed and accurate analysis of reaction kinetics and maximal mineral conversions. This research is conducted at the laboratories of Todd Schaef at the Pacific Northwest National Laboratory (PNNL), who developed the in-situ high-pressure X-ray diffraction technique.[XLII] The unique reaction cell is made of >99% beryllium, being transparent to

[XLII] Schaef, H.T., Windisch Jr., C.F., McGrail, B.P., Martin, P.F., Rosso, K.M. (2011). Brucite [$Mg(OH_2)$] carbonation in wet supercritical CO_2: An in situ high pressure X-ray diffraction study. Geochimica et Cosmochimica Acta 75, 7458–7471.

X-rays, is compatible with water-bearing supercritical CO_2 fluids, and can be operated at geologically relevant combinations of temperature and pressure suitable for carbonation reactions. The reactor is contained within a diffractometer (Bruker-AXS Discover D8) fitted with a two-dimensional General Area Detector Diffraction System (GADDS), which allows collection of complete diffraction patterns (10-46° 2θ range) in short period of time (200 seconds typical). Wet supercritical and moist gaseous carbonation methods are employed. Moist gas carbonation allows for better signal strength and reduced carbonation kinetics compared to supercritical carbonation, thus allowing more precise assessment of the mineral conversion and carbonate formation over time.

Figure 10.1 shows a pattern collected during moist gas carbonation of synthetic cuspidine at 70 °C and 6 bar-CO_2 for 20 hours. The cuspidine phase reacts to near completion over the first 8 hours. During this period, the formation of an intermediary vaterite phase can be seen. Vaterite disappears at later stages of the reaction, leading to the formation of mainly calcite carbonate with traces of aragonite. The fluorite phase originally present in the synthetic sample remains unreacted.

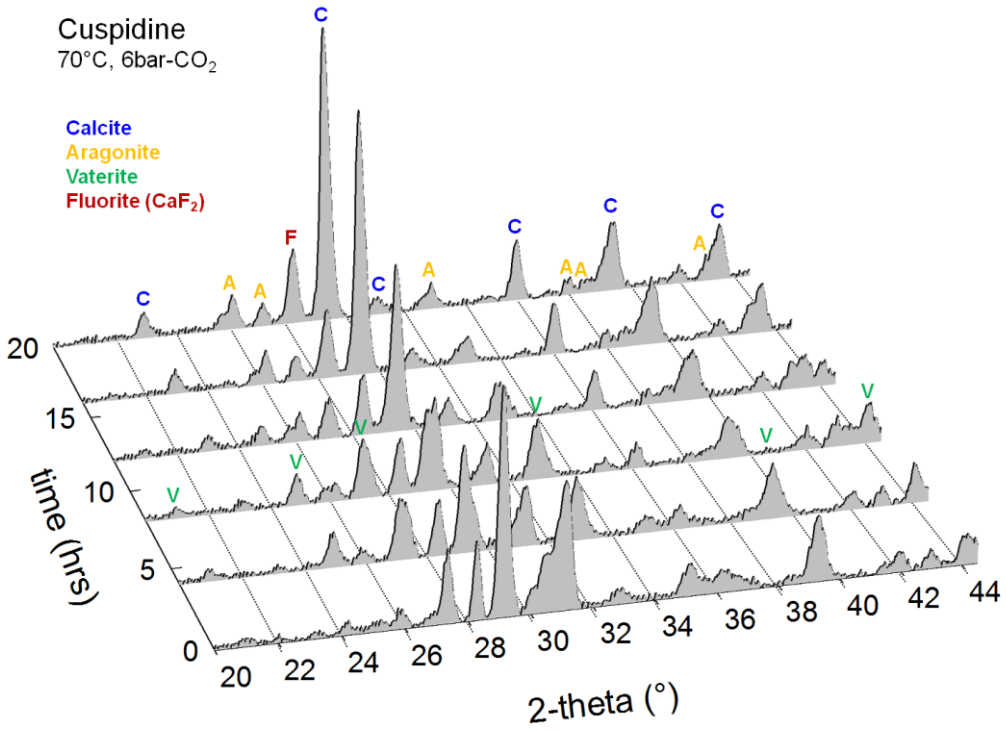

Figure 10.1. In-situ XRD results of synthetic cuspidine carbonation in moist gas. C = calcite; A = aragonite; V = vaterite; F = fluorite.

10.3. FUTURE PERSPECTIVES

The various research lines investigated in the doctoral thesis and the findings reported point to the directions that can lead to widespread adoption of mineral carbonation as a CO_2 sequestration solution as well as an industrial waste treatment and valorisation technology. Work still lies ahead to make the transition from the laboratory bench to the industrial setting. This includes engineering scale-up strategies, but also acquiring further fundamental understanding of mineral carbonation mechanisms. The following paragraphs describe lines of work that are being pursued.

The hot-stage carbonation treatment of BOF slag appears to be a potentially feasible route for the valorisation of BOF slag as a construction material, as it reduces free lime content, basicity and leaching of some hazardous elements. Investigation is still warranted on finding the necessary level of free lime conversion needed to satisfactory stabilize the BOF slag. The following relations should be further studied: swelling vs. total carbonation/hydration degree; and swelling vs. surface carbonation/hydration degree. It should thus be assessed whether 50% conversion or more is required for complete stabilization, or if near-surface carbonation, which has been found sufficient to reduce basicity, may be enough to improve material properties and enable its valorisation. The role that other minerals may play in the hydration and volume expansion of BOF slag should also be investigated. Marius Bodor and Geanina Cristea, visiting researchers at the KU Leuven, have found that slurry carbonated BOF slag leads to reduced swelling upon application of the material in cement mortar as a sand replacement aggregate. The study in this thesis and that of Bodor and Cristea (2013) used crushed samples of BOF slag; however, it is envisioned that the slag will be granulated prior to carbonation. It is thus essential to study the effect of granulation on the reactivity of the slag to hot-stage carbonation. That is, it should be found if the slag crystallinity is reduced, if the slag mineral composition is modified, if the free lime distribution within the slag particle changes, and if the particle size range achievable by granulation is sufficiently fine to impart high specific surface area. Detailed investigation is also required to elucidate the fundamental rate-reducing mechanisms (porosity, diffusivity, mineralogy) and how hot-stage tuning of the slag (chemistry and cooling path) can affect these.

Calcium carbonate is a typical product of the mineralization of carbon dioxide via aqueous precipitation in alkaline rich solutions, given the abundance of natural and residual calcium sources and its high reactivity towards mineral carbonation. One of the main applications of precipitated calcium carbonate (PCC) is in papermaking, mainly as filler or pigment. A major advantage of PCC over the more traditional ground calcium carbonate (GCC) is that it can take more varied morphological forms that influence paper properties, including light scattering coefficient, brightness, opacity, apparent density, tensile strength, stiffness, folding endurance, porosity and

printability, in different manners.[XLIII,XLIV,XLV] The novel *hubbard squash-like* particle morphology achieved within this doctoral research may offer new and advantageous applications, due to its altered particle size distribution and surface texture compared to the more common acicular crystals, that are yet to be examined. Its application in papermaking is a route that deserves investigation. Furthermore, the properties that make certain PCC's attractive for papermaking applications should be studied in order to elucidate how to achieve these properties using the novel sonochemical route. Knowledge on the effects of PCC properties on paper qualities is important in view of informing researchers working on PCC production for the purposes of carbon capture and waste valorisation on the product requirements for industrial applications. In particular, the effect of impurities originating from the calcium source material, sometimes waste-derived, or from additives used during calcium extraction or precipitation on the properties of paper products should be looked at. This can be useful as currently most researchers are focusing on production yield rather than properties, and as a result many produced PCC's are not suitable for their intended applications.

The increasing demand and diminishing availability of raw materials requires us to look beyond conventional sources. In the future, the importance of low-grade ores and waste residues as a source for raw materials is expected to increase. For instance, the world's nickel reserves are about 75 million tonnes.[XLVI] Despite this apparent abundance, the processing of less desirable silicate minerals will become increasingly important. The escalating depletion of high-grade sulphidic ores will make it necessary to obtain metals from the more abundant but lower grade ores and mineral processing wastes. An approach that has started being investigated, by the Master's thesis of Aldo Van Audenaerde from the KU Leuven, is to use mineral carbonation as a pre-treatment stage for Ni extraction from alkaline materials. The precept is that by altering the mineralogy the separation of mineral phases can be made easier. Furthermore, carbonation pre-treatment may make it easier to extract valuable metals trapped in the carbonate phase (compared to the original silicate phases) and/or may concentrate valuable metals in separable phases. This is an example of CO_2 utilization, a concept that is gaining favour over CO_2 storage due to the higher value generation. Van Audenaerde (2013) found that nickel recovery from carbonated olivine could be improved by 43-63% using inorganic and organic acids. Other by-products of the carbonation

[XLIII] Hubbe, M.A. (2004). Filler Particle Shape vs. Paper Properties – A Review. TAPPI 2004 Spring Technical Conference, 7-3.

[XLIV] Hu, Z., Shao, M., Li, H., Cai, Q., Zhong, C., Xianming, Z., Deng, Y. (2009). Synthesis of Needle-Like Aragonite Crystals in the Presence of Magnesium Chloride and Their Application in Papermaking. Advanced Composite Materials 18(4), 315-326.

[XLV] Koivunen, K., Paulapuro, H. (2010). Papermaking potential of novel structured PCC fillers with enhanced refractive index. TAPPI Journal (01/2010), 4-12.

[XLVI] U.S. Geological Survey, Mineral Commodity Summaries, January 2013 [Online], Available at: http://minerals.usgs.gov/minerals/pubs/commodity/nickel/mcs-2013-nicke.pdf [accessed October 18, 2013].

reaction included amorphous silica, chromium-rich metallic particles and iron-substituted magnesium carbonate (Figure 10.2). The mineral carbonation pre-treatment approach may also be applicable to lateritic ores. Another approach that should be investigated is performing mineral separation and elemental recovery during mineral carbonation, rather than afterwards as done in the aforementioned thesis. During carbonation, magnesium and the trace metals dissolve in the acidic aqueous solution (due to carbonic acid). At this stage, the mobile metals and residual solids could be separated more easily, prior to precipitation of the carbonates. This process is presently under development by partners Innovation Concepts B.V.

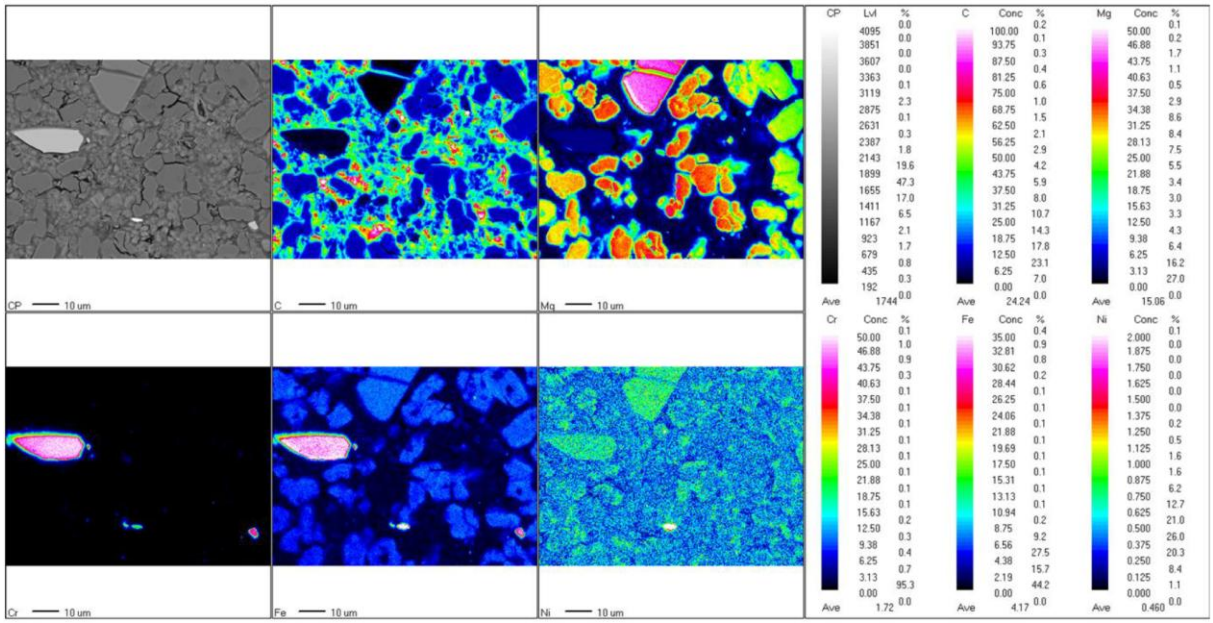

Figure 10.2. Elemental mapping of carbonated olivine obtained by electron probe microanalysis (EPMA).[XLVII]

As a final point, the acceleration of mineral carbonation can potentially benefit greatly from the adoption of intensified processing technologies. To date, most research has focused on the fundamentals of the carbonation reaction, including thermodynamic, kinetic, geochemical and mineralogical aspects. Much less work has been done on the process engineering side, with few exceptions (e.g. Pan et al.[XLVIII]; Zevenhoven et al.[XLIX]). In this thesis, Chapter 3 briefly introduced

[XLVII] Van Audenaerde, A. (2013). Sustainable nickel extraction from olivine via carbonation and bioleaching treatments. M.Sc. Thesis, KU Leuven

[XLVIII] Pan, S.-Y., Chiang, P.-C., Chen, Y.-H., Tan, C.-S., Chang, E.-E. (2013). Ex Situ CO_2 Capture by Carbonation of Steelmaking Slag Coupled with Metalworking Wastewater in a Rotating Packed Bed. Environmental Science & Technology 47, 3308-3315.

[XLIX] Zevenhoven, R. Fagerlund, J., Nduagu, E., Romão, I., Highfield, J. (2013). Stepwise serpentinite carbonation using the Åbo Akademi route – status and latest developments. In: Proceedings of the 4th International Conference on Accelerated Carbonation for Environmental and Materials Engineering. Leuven, Belgium, 9-12 April 2013 (pp. 389-398).

the concept of process intensification in view of mineral carbonation. In Chapters 4 and 7 and in Section 10.2.3, processing routes that make use of the four domains of process intensification (structure, energy, time and synergy) to accelerate mineral carbonation and improve net CO_2 sequestration (i.e. reduce energy consumption) were explored. Still, this is just the tip of the iceberg. More leading edge research is warranted on developing clever intensified processes for accelerating mineral carbonation in sustainable ways.

Curriculum Vitae

Rafael Mattos dos SANTOS
Born: January 7, 1982 in Curitiba, Brazil
Nationality: Brazilian/Canadian
Contact: rafael.santos@cit.kuleuven.be; rafael.santos@alumni.utoronto.ca

Academic background:

01/2010 – 12/2013: Doctoral Studies in Chemical Engineering, KU Leuven, Leuven, Belgium.
01/2006 – 09/2007: Master of Applied Science in Chemical Engineering, University of Toronto, Toronto, Canada.
09/2000 – 05/2004: Bachelor of Applied Science in Chemical Engineering, University of Toronto, Toronto, Canada.

Professional experience:

09/2007 – 01/2010: Vale Inco, Mississauga/Port Colborne/Sudbury, Canada.
05/2004 – 01/2006: Zenon Environmental, Oakville, Canada.
05/2002 – 09/2002: Braskem Petrochemicals, Porto Alegre, Brazil.

Grants and fellowships:

Doctoral Studies (KU Leuven):
2013: FWO Travel Grant for short stay abroad at the Pacific Northwest National Laboratories, Richland, Washington, USA.
2012: FWO Travel Grant to attend GHGT-11, Kyoto, Japan.
2011: FWO Travel Grant for short stay abroad at Laval University, Quebec City, Canada.
2011: CIM MetSoc Travel Grant to attend COM 2011, Montreal, Canada.
2010 – 2013: NSERC Postgraduate Scholarship.
2010 – 2013: KU Leuven Scholarship – Industrial Research Fund / Industrieel Onderzoeksfonds.